Deciphering Effector Protein Functions of *Ustilago maydis* involved in gall formation

Dissertation zur Erlangung des Doktorgrades

(Dr. rer. nat.)

der

Mathematisch-Naturwissenschaftlichen Fakultät

der

Rheinischen Friedrichs-Wilhelms-Universität Bonn

vorgelegt von

Pouria Bahrami

aus

Ramsar, Iran

Bonn, 2023

Angefertigt mit der Genehmigung der Mathematisch-Naturwissenschaftlichen

Fakultät der Rheinischen Friedrichs-Wilhelms-Universität Bonn

1. Gutachter: Prof. Dr. Armin Djamei

2. Gutachter: Prof. Dr. Peter Dörmann

Tag der Promotion: 22.03.2024

Erscheinungsjahr: 2024

ACKNOWLEDGMENT:

I would like to extend my heartfelt gratitude to my PhD supervisor, **Prof. Armin Djamei**, for granting me the opportunity to pursue my doctoral studies under his guidance. It has been a great honor and a source of pride for me to work under your supervision, Armin.

I would like to express my sincere thanks to **Prof. Peter Dörmann**, my co-supervisor and the second reviewer of my thesis, for dedicating his valuable time.

I also appreciate **Prof. Andreas Meyer** and **Prof. Claudia Knief** for their presence on my PhD committee.

A special thanks go to **Mamoona**, **Maxim**, **Kishor**, and **Nathalia** for their generous support and scientific advice throughout my entire PhD project, I learned a lot from you and will never forget any single moment that we had in the last years. **Mamoona**, my kind-hearted colleague, your kind support at the beginning of my career will never be forgotten. **Maxim**, my multi-tasking bench-mate, I have enjoyed our daily discussions about science, technology, and politics, as well as your p20 Eppendorf pipette. **Kishor**, my supportive friend, your positive outlook is truly infectious; it brightens up everyone's day. **Natalia**, my amazing colleague, you brought a significant amount of energy, smile, and science to our lab.

Daniela, our great lab manager, you were always available and supportive. I sincerely thank **Caro**, **Kerstin, Nicole,** and **George** for their assistance and technical support in the laboratory throughout these years.

I extend my heartfelt thanks to all my dear Ph.D. colleagues I have had the privilege of working with and learning during my Ph.D. journey: **Nithya**, my kind-hearted and long-time colleague since IPK with amazing cooking. **Tomas**, my cheerful friend, with your marvelous recipes and exclusive quality control methods. **Kim**, my kind colleague and office mate, your self-assured display has truly left a lasting impression on me. **Komal**, my kind-hearted colleague, your children will have a strong mother on their back. **Angeline**, my nice colleague, it was a pleasure working with you.

I would like to express special thanks and heartfelt gratitude to **Dr. Med. Aram Ramezanzadeh**, who has always supported me even from afar in the last two years.

Last but not least, I sincerely thank my best friend and wife, **Mona**. Thank you for your unwavering support, love, and kindness, and for being the driving force behind my achievements. Without you, I couldn't have made it.

Learning is the beginning of wealth: searching and learning is where the miracle process all begins.

"Jim Rohn"

ABSTRACT:

Plants are location-bound organisms and thus directly exposed to their environmental conditions. Unlike mammals, plants lack a somatic adaptive immune system and therefore need to rely on their innate immune system and the activation of diverse signaling pathways emerging from the infected region. Plants have developed intricate defense mechanisms to identify and respond to invaders. To achieve a successful infection, plant invaders pathogens, require strategies to suppress defense responses and manipulate metabolic processes. For this purpose, pathogens secrete molecules called effectors in order to loot nutrients necessary for their growth and reproduction. This ongoing competition between the pathogen and the host revolves around gaining new effectors and defense proteins, respectively.

Cereal grains meet nearly half of humankind's caloric requirement. Wheat, maize, and rice are humans' most common food resources. Maize is the most preferred grain in southern and Eastern Africa, Central America, and Mexico. The biotrophic fungus *Ustilago maydis* causes smut disease in maize (*Z. mays*) and teosinte *(Z. mays ssp. parviglumis). U. maydis* is an outstanding model organism for studying various aspects of plant-pathogen interactions. *U. maydis* promotes the formation of galls in all aerial parts of the host plant, in contrast to other smut fungi such as *Ustilago hordei, Tilletia caries, Tilletia laevis*.

In the presented study, I mostly worked on a *U. maydis* effector that was genetically located in cluster 5A. The effector called cabbage-like phenotype 1 (Cab1) is based on the observed phenotype of over-expression in the non-host system, *A. thaliana*. I could demonstrate that Cab1 targets BIN2 (Shaggy-like kinase 3) at the C-terminal domain and re-localizes BIN2 from the cytosol to the nucleus. In the results of Cab1-Bin2 interaction in the non-host system, I showed 10 times more phosphorylation of AtBIN2 Tyrosine Y^{200}, and five times less ubiquitination of AtBIN2-Lysine35 than the control. Respectively, these post-translation modifications correlate to higher activity and less degradation of AtBin2 in the presence of Cab1. The results of total RNA sequencing showed that Cab1 induction downregulates *Samll Auxin Up-regulated RNAs (SAURs)* and *Expansins (EXPs)*-mediated cell wall expansion which also aligns with our phenotypic observations and

molecular studies. I showed the Cab1 mechanism to promote the AtBin2 active state *in planta.* The appendix contains my contributions to other unpublished studies in the lab during my Ph.D. career at Djamei lab.

ZUSAMMENFASSUNG

Pflanzen sind ortsgebundene Organismen und daher direkt den Umweltbedingungen ausgesetzt. Im Gegensatz zu Säugetieren fehlt Pflanzen ein adaptives Immunsystem im Körper und sie müssen sich daher auf ihr angeborenes Immunsystem und die Aktivierung verschiedener Signalwege in der infizierten Region verlassen. Pflanzen haben komplexe Abwehrmechanismen entwickelt, um Eindringlinge zu erkennen und darauf zu reagieren. Um eine erfolgreiche Infektion zu erreichen, müssen pflanzliche Krankheitserreger Strategien entwickeln, um Abwehrreaktionen zu unterdrücken und Stoffwechselprozesse zu manipulieren. Zu diesem Zweck scheiden Krankheitserreger Moleküle aus, die sogenannten Effektoren, aus, um Nährstoffe zu nehmen, die für ihr Wachstum und ihre Vermehrung notwendig sind. Dieser andauernde Wettbewerb zwischen dem Krankheitserreger und dem Wirt dreht sich um die Gewinnung neuer Effektoren und Abwehrproteine, jeweils.

Getreide deckt fast die Hälfte des Kalorienbedarfs der Menschheit. Weizen, Mais und Reis sind die häufigsten Nahrungsmittelressourcen für Menschen. Mais ist das bevorzugte Getreide in Süd- und Ostafrika, Zentralamerika und Mexiko. Der biotrophe Pilz *Ustilago maydis* verursacht Brandkrankheiten im Mais (*Zea mays*) und Teosinte (*Zea mays ssp. parviglumis*). *U. maydis* ist ein herausragender Modellorganismus zur Erforschung verschiedener Aspekte der Wechselwirkungen zwischen Pflanzen und Krankheitserregern. *U. maydis* fördert die Bildung von Gallen in allen oberirdischen Teilen der Wirtspflanze, im Gegensatz zu anderen Brandpilzen wie *Ustilago hordei, Tilletia caries, Tilletia laevis.*

In der vorliegenden Studie habe ich hauptsächlich an einem *U. maydis*-Effektor gearbeitet, der genetisch im Cluster 5A lokalisiert war. Der Effektor namens "Cabbage-like phenotype 1" (Cab1) basiert auf dem beobachteten Phänotyp einer Überexpression im nicht-wirtlichen System *A. thaliana*. Ich konnte zeigen, dass Cab1 das BIN2 (Shaggy-ähnliche Kinase 3) in der C-terminalen Domäne anzielt und BIN2 aus dem Cytosol in den Zellkern umlagert. In den Ergebnissen der Cab1-Bin2-Interaktion im nicht-wirtlichen System habe ich gezeigt, dass die Phosphorylierung von AtBIN2-Tyrosin 200 zehnmal stärker ist und die Ubiquitinierung von AtBIN2-Lysin 35 fünfmal schwächer ist als bei der

Kontrolle. Diese posttranslationellen Modifikationen korrelieren entsprechend mit einer höheren Aktivität und weniger Abbau von AtBin2 in Gegenwart von Cab1. Die Ergebnisse der total-RNA-sequencing zeigten, dass die Induktion von Cab1 die Zellwandexpansion durch *SAURs* und *Expansine* unterdrückt, was auch mit unseren phänotypischen Beobachtungen und molekularen Studien übereinstimmt. Ich habe den Mechanismus von Cab1 zur Förderung des aktiven Zustands von AtBin2 in Pflanzen aufgezeigt. Im Anhang finden Sie meine Beiträge zu anderen unveröffentlichten Studien im Labor während meiner Promotion in der Djamei-Forschungsgruppe.

ABBREVATIONS

AFB: Auxin Signaling F-Box

AFP1/2: Antifungal Maize Proteins 1/2

APS: Ammonium Persulfate

ARFs: Auxin Response Factors

AtPRP38: A. thaliana Pre-Mrna Splicing Factor 38

AtUBL5: A. thaliana Ubiquitin-Like Protein

Aux/IAA: Auxin/Indole-3-Acetic Acid

AUXRes: Auxin Response Elements

BAK1: BRI1-Associated Kinase 1

bE: Locus b Allele East

BES1: Brassinosteroid Insensitive 1-Ems-Suppressor 1

BIL1: Bin2-Like1

BIL2: Bin2-Like2

BIN2: Gsk3-Like Kinase Brassinosteroid Insensitive2

bin2/dwarf12/ucu1: A. thaliana Mutants at TREE Motif of Bin2, Shows Dwarf Phenotype

BRI1: Brassinosteroid-Insensitive 1

BRL1: Bri1-Like1

BRL3: Bri1-Like3

BRRE/E-Box: BR Response Element/Enhancer Box

BR: Brassinosteroid

BSKs: BR-Signaling Kinases

BSU1: BRI1 Suppressor 1

bW: Locus B Allele West

BZR1: Brassinazole Resistant 1

Cab1: Cabbage-Like Phenotype 1

Cmu1: Chorismate Mutase

Co-IP MS: Co-Immunoprecipitation Mass Spectrometry

CW: Plant Cell Wall

det2: A. Thaliana de-etiolated2 mutant

DMSO: Dimethyl Sulfoxide

dpg: Days Post Germination

dpi: Days Post-Induction

DTT: Dithiothreitol

E263k: Substitution of Amino Acid E With K At Tree Motif Of BIN2

EGB: Early Golden Bantam

ETI: Effector-Triggered Immunity

ETS: Effector-Triggered Susceptibility

EXPs: Expansins

GR: Glucocorticoid Receptor

GSK3: Glycogen Synthase Kinase3/Shaggy Like Kinases

GSK3α/B: Homo sapiens Shaggy-Like Kinases A/B

HsBrca2: Breast Cancer Type2 Susceptibility Protein Brca2

JA: Jasmonic Acid

Jsi1: Jasmonate/Ethylene Signaling Inducer 1

Lys: Lysin

mfa1/2: Lipopeptide Pheromone Components 1/2

NaOh: Sodium Hydroxide

NB-LRR: Nucleotide-Binding-Leucine-Rich Repeats

NBs: Nuclear Bodies

NGS: Next Generation of Sequencing

P35s-XVE: 35s β–Estradiol Inducible Promoter

P35s: 35s Cauliflower Mosaic Virus Promoter

PAMPs: Pathogen-Associated Molecular Patterns

PEG: Polyethylene Glycol

Pep1: U. Maydis Effector Protein Essential During Penetration-1

Pit2: Protein Important For Tumors 2

PLCPs: Papain-Like Cysteine Proteases

PP2A: Protein Phosphatase 2a

pra1/2: Lipopeptide Pheromone Receptors 1/2

PRRs: Pattern Recognition Receptors

PTI: PAMP-Triggered Immunity

PTM: Post-Translational Modification

Rsp3: Repetitive Secreted Protein 3

SA: Salicylic Acid

SAUR15: Small Auxin-Up Rna 15

SAUR19: Small Auxin Up Rna19

SAURs: Small Auxin Up-Regulated Rnas,

SDS: Sodium Dodecyl Sulfate

See1: Seedling Efficient Effector 1

SnRnps: Small Nuclear Ribonucleoproteins

SOB3: Suppressor Of Phytochrome B4-3

TEMED: N,N,N',N'-Tetramethylethylenediamine

TRET: Telomerase Reverse Transcriptase

TIR1: Transport Inhibitor Response 1

Tyr: Tyrosine

USPL1: Ubiquitin-Specific Peptidase-Like1

Wrap53: WD Repeat-Containing Antisense to Tp53

Y2H: Yeast 2 Hybrid

1 INTRODUCTION

1.1 Plant-Pathogen Interactions

Plants are location-bound organisms and thus directly exposed to their environmental conditions. Unlike mammals, plants lack a somatic adaptive immune system and therefore need to rely on their innate immune system and the activation of diverse signaling pathways emerging from the infected region (Jones & Dangl, 2006). The continuous co-evolutionary struggle between plants and pathogens has led to the development of complex interactions. These interactions involve the production of diverse molecules by both the pathogens and the plants (Singh et al., 2023).

1.1.1 Plant Immunity System

Plants have developed intricate defense mechanisms to identify and respond to invaders. The initial defense takes place on the plant cell surface, where pathogen-associated molecular patterns (PAMPs), such as fungal chitins and bacterial flagellins, are recognized by pattern recognition receptors (PRRs). This recognition triggers PAMP-triggered immunity (PTI). In the second stage, successful pathogens spread effectors that disrupt PTI, resulting in Effector-triggered susceptibility (ETS). ETS allows the pathogen to obtain nutrients and spread within the host. In the third stage, the host's NB-LRR proteins recognize the pathogen's secreted effectors, leading to the activation of effector-triggered immunity (ETI). ETI induces hypersensitivity responses, which suppress the pathogen's proliferation within the host. To achieve a successful infection, the pathogen must acquire new effectors to counteract ETI. This ongoing competition between the pathogen and the host revolves around gaining new effectors and NB-LRR proteins, respectively (Jones & Dangl, 2006; Stotz et al., 2014; S. Zhang et al., 2022; J. M. Zhou & Zhang, 2020).

1.1.1 The lifestyle of plant-pathogenic fungi

The plant pathogen overcame barriers in the plant cell, allowing it to extract nutrients for its growth and reproduction. Plant pathogens were classified into three groups based on their nutrition types. Necrotrophs acquire nutrients from dead cells (saprophytes), *Botrytis cinerea* and *Pythium ultimum* are representative of this group. Hemibiotrophic fungi such

as *Magnaporthe oryzae* and *Phytophthora infestans*, exhibit biotrophic behavior only in the early stage of development then switching to necrotrophy (Fei & Liu, 2023). Biotrophs such as *Ustilago maydis* and *Blumeria graminis* extract nutrients from living cells. Among them, pathogens with a biotrophic lifestyle depend on establishing a long-term feeding relationship with their living host cell. The Biotrophic fungi also secrete lytic enzymes, carbohydrates, and protein-rich interfacial layers and long-term suppression of the host defense as part of their survival strategy. Additionally, biotrophic fungi employ various mechanisms to protect their effector molecules from host-defense receptor molecules. 1. *B. graminis* causes powdery mildew in wheat and barley grows with filamentous hyphae on the leaf surface and penetrates the epidermal cell wall and forms haustoria (a specific feeding structure) surrounded by plant plasma membrane during the infection (Fei & Liu, 2023). 2. *U. maydis* enters the plant cell wall and develops hyphae that are encased by the host plasma membrane for nutrient uptake and signal communication (Presti & Kahmann, 2017). Some specific genes of the pathogen were upregulated during infection for the suppression of the host defense mechanism (Djamei et al., 2011; Scott et al., 2022). 3. *Colletotrichum fulvum* is a biotrophic fungal pathogen that causes leaf mould in tomatoes. The infection, colonization, and inhibition of host defenses by *C. fulvum* are mediated by a number of effector proteins. An example of the escape mechanism from the host PRRs, *C. fulvum* secretes Ecp6 effector proteins that contain LysM chitin-binding domain and helps the pathogen to protect the host defense mechanism (Fei & Liu, 2023; Penninckx et al., 1998).

1.2 Plant growth and development

Plant growth and development is a complex interaction between physiological and molecular processes that shapes the structure, size, and function of plants. On one side, environmental factor including temperature, light, water, and nutrition availability influence plant growth and development. On the other side, biotic stresses can hinder plant growth and development by disrupting physiological processes and causing structural damage. Plants respond to these factors at both physiological and molecular levels (Cheng et al., 2019; Johnson & Lenhard, 2011; Kaur et al., 2022).

Plant hormones such as auxins, gibberellins, cytokinins, abscisic acid, and ethylene, regulate various aspects of plant growth and development. These hormones also control processes like cell division, elongation, and differentiation. The balance between cell division and elongation, governed by hormonal regulation and genetic factors, determines organ growth and overall plant architecture (Depuydt & Hardtke, 2011; Ortíz-Castro et al., 2009).

1.3 Auxin

U. maydis induces hypertrophy and hyperplasia, resulting in the formation of galls in various aerial parts of maize (Matei et al., 2018). Auxin is a key phytohormone, the molecular mechanism of auxin signaling involves auxin binding to Transport Inhibitor Response 1 (TIR1) and Auxin Signaling F-Box (AFB) proteins, triggering the degradation of auxin/Indole-3-Acetic Acid (Aux/IAA) proteins, de-repression of auxin response factors (ARFs), binding to auxin response elements (AuxREs) in target gene promoters, and subsequent modulation of gene expression (Du et al., 2020; Z. Yu et al., 2022). Noteworthy, ARFs are divided into two main groups: in Arabidopsis, activator ARFs, including ARF5, ARF6, ARF7, ARF8, and ARF19 are rich in glutamine, while repressor ARFs are abundant in serine, threonine, and proline. Certain repressor ARFs, such as ARF2, ARF3, ARF9, and ARF18, inhibit auxin-responsive gene expression by enlisting TPL/TPRs in Arabidopsis. The Aux/IAA-ARF module is better suited for activator ARFs than repressor ARFs. Although there is little evidence supporting the activation of repressor ARFs by Aux/IAA degradation, they remain significant members of the Arabidopsis ARF family (Chandler, 2016; Kuhn et al., 2020; Vernoux et al., 2011). Through its influence on various cellular processes, auxin controls cell elongation, division, and differentiation, ultimately impacting overall plant growth and development (Ai et al., 2023; Gallavotti, 2013).

Plant growth is a complex and highly regulated process influenced by different factors, including environmental conditions, genetics, and hormonal signals. One aspect of plant growth is the role of the plant cell wall, a dynamic structure that plays a fundamental role in determining the shape and rigidity of plant cells (Novaković et al., 2018). The plant cell wall (CW) consists of polysaccharides like hemicellulose, cellulose, and pectin, along with

lignin and glycoproteins. It envelops plant cells, providing diverse shapes, sizes, and physicochemical properties for various roles during development (Carpita et al., 2001). CW plays vital roles in morphogenesis, mechanical support, water and nutrient conduction, and defense against stresses (B. Zhang et al., 2021). One of the primary effects of auxin is its ability to promote cell elongation by regulating the expression of cell wall-related genes and the activity of cell wall-loosening enzymes. These lead to the relaxation of the cell wall, enabling cell expansion and subsequent changes in the cell shape and architecture (Ai et al., 2023; Gallavotti, 2013; Majda & Robert, 2018). Additionally, auxin impacts cell division and differentiation, further influencing plant cell shape and architecture (L. Wang & Ruan, 2013).

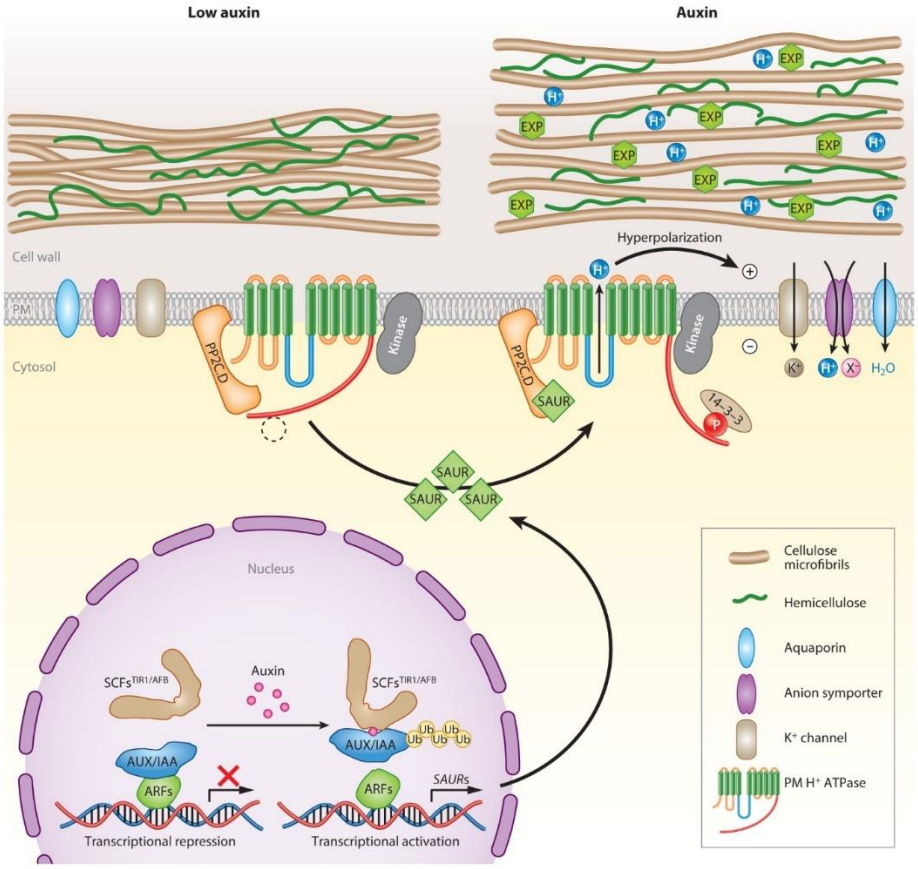

Figure 1-1 A model for auxin-mediated acid growth.

"In conditions with low auxin (left side), a protein kinase and PP2C.D protein phosphatases work together to control the activity of plasma membrane (PM) H+-ATPase. In response to auxin (right), primary SCF $^{TIR1/AFB}$ interacts with AUX/IAA and consequently promotes *SAURs* signaling. The transcripts got translated to SAUR proteins and directly interact and inhibit PM-localized

PP2C.D2/PP2C.D5/PP2C.D6, preventing these phosphatases from dephosphorylating Thr947 and perhaps additional residues of PM H+-ATPases, thus keeping these proton pumps in the phosphorylated, activated state. Consequently, the increase in PM H+-ATPase activity leads to the acidification of the apoplast, which activates expansins (EXPs) and enzymes that remodel the cell wall. The proton pumping also causes the plasma membrane to become more negative (hyperpolarized). This activates inward-rectifying K+ channels and energizes H+-coupled anion symporters (X−). These transport processes are essential for continuing the uptake of solutes, which is necessary for sustained water absorption and maintaining turgor pressure (Du et al., 2020)."

Small Auxin Up-regulated RNAs (*SAURs*), show rapid induction in response to auxin treatment, and both transcripts and protein have a high turnover upon induction (Stortenbeker & Bemer, 2019). SAURs interact with the PM-localized PP2C.D family and inhibit their function (Du et al., 2020). The inhibition of PP2C.D keeps the PM localized H+-ATPases pumps phosphorylated and activated. This increase in PM H+-ATPase activity, acidifies the apoplast, and promotes Expansins (EXPs) activity and cell wall loosening enzymes in *A. thaliana* (van Mourik et al., 2017). Transgenic lines of *A. thaliana* with overexpressed SAUR19 and the triple mutant of PP2C.D (*d2d5d6*) displayed a similar phenotype, including elongated cells in seedlings, leaves, stems, and floral organs (Ren et al., 2018). EXPs are small and non-enzymatic proteins found in all plants and enable the local sliding of wall polymers by reducing adhesion between wall polysaccharides in the apoplast (Marowa et al., 2016). EXPs promote the spillage between microfibrils by cutting non-covalent bonds between cellulose and Hemicellulose and increase cell wall plasticity and extensibility, enabling cell growth and development (J. Cosgrove, 2000; Mu et al., 2021; Sampedro & Cosgrove, 2005). In summary, according to the auxin-mediated acidic growth model, the downregulation of *SAURs* and *EXPs* hinders the plant cell wall loosening and consequently suppresses cell growth and development (Du et al., 2020; Sampedro & Cosgrove, 2005; van Mourik et al., 2017; Wieczorek & Grundler, 2006).

Hormone signaling pathways frequently crosstalk and act either synergistically or antagonistically to each other as part of the systemic decision-making processes that shape plant responses to internal and external cues. Auxin signaling modulates plant immunity as it crosstalks with well-established defense hormone signaling pathways, including the Salicylic acid (SA) and Jasmonic acid (JA) pathways (C. Han et al., 2023;

Ruan et al., 2019). In growth and developmental processes, auxin signaling frequently interacts with other growth hormone signaling pathways including those regulated by Cytokinins, Gibberellins, and Brassinosteroids (BRs) (Jing & Strader, 2019; Yang et al., 2018).

1.4 Brassinostroides

BRs are steroid phytohormones playing a key role in different aspects of plant growth and development, such as cell division and elongation, photomorphogenesis, and reproduction (Z. Li & He, 2020; Nolan et al., 2020). Besides, BRs are also important for fine-tuning the responses to both biotic and abiotic stressors (W. Song et al., 2022). To give an impression, in *A. thaliana* between 5000 to 8000 genes are on the transcriptional level modulated by Brassinosteroids (BRs) (Guo et al., 2013; Nolan et al., 2017a; X. Wang et al., 2014).

At the core of the BR signaling pathway is the perception of BRs by the membrane-localized receptor kinase, BRASSINOSTEROID-INSENSITIVE 1 (BRI1), and its paralogs (Friedrichsen et al., 2000; Z. He et al., 2000), BRI1-LIKE1 (BRL1) and BRI1-LIKE3 (BRL3) (Caño-Delgado et al., 2004; Kinoshita et al., 2005; Nolan et al., 2020). BRI1 was identified through molecular studies of *A. thaliana* BR mutants (Clouse et al., 1996; J. Li & Chory, 1997; Nolan et al., 2020). Upon binding to BRs, BRI1 forms a complex with its co-receptor BRI1-Associated Kinase 1 (BAK1) and undergoes autophosphorylation, and initiates a phosphorylation cascade of its downstream signaling components (T. W. Kim et al., 2011; J. Li & Chory, 1997; W. Song et al., 2022; Tang et al., 2008). One of the major mechanisms of BR action is the phosphorylation and activation of the serine-threonine phosphatase BRI1 SUPPRESSOR 1 (BSU1) via receptor-like cytoplasmic kinases, the BR-Signaling Kinases (BSKs), leading to dephosphorylation and inhibition of glycogen synthase kinase3 (GSK3)-like kinase BRASSINOSTEROID INSENSITIVE2 (BIN2). BIN2 acts as a negative regulator in BR signaling by phosphorylating and thereby inhibiting BR-regulated transcription factors BRASSINOSTEROID INSENSITIVE 1-EMS-SUPPRESSOR 1 (BES1) and BRASSINAZOLE RESISTANT 1 (BZR1) (J. X. He et al., 2002; J. Li et al., 2001; J. Li & Nam, 2002; Youn & Kim, 2015). BIN2-induced phosphorylation inactivates BES1 and BZR1 by promoting their cytoplasmic retention via

14-3-3 proteins (Gampala et al., 2007; J. X. He et al., 2002; J. Li et al., 2001; J. Li & Nam, 2002; Ryu et al., 2007; Youn & Kim, 2015), inhibiting their DNA binding activity (Vert & Chory, 2006), and stimulating their degradation (J. X. He et al., 2002; E. J. Kim et al., 2019; Yin et al., 2002). The presence of BRs triggers a feedback mechanism that inhibits BIN2 activity. The inactivation of BIN2 by BRs along with the dephosphorylation of the atypical basic helix–loop–helix (bHLH) transcription factors BES1 and BZR1 by PROTEIN PHOSPHATASE 2A (PP2A) (Tang et al., 2011) allows these transcription factors to become active in the nucleus to control BR-responsive gene expression again (J. X. He et al., 2002; Nolan et al., 2017; Tang et al., 2008; Yin et al., 2002; X. Yu et al., 2011).

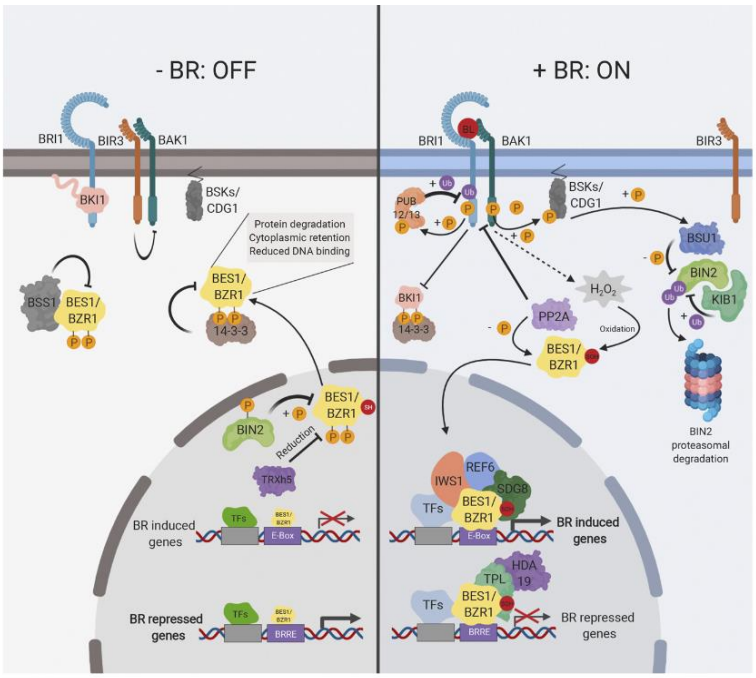

Figure 1-2 an overview of BR signaling pathway.

“When BRs are absent (left), PM-localized receptors BRI1 and BAK1 are inhibited by several factors, including BKI1 and BIR3. Additionally, BIN2 kinase functions as a negative regulator and phosphorylates BES1 and BZR1 TFs to inhibit their activity through multiple mechanisms. BSS1 forms a complex with BES1 and BZR1 in the cytoplasm, and THXh5 reduces BZR1 in the nucleus, further inactivating these TFs. This leads to relatively low expression of BR-induced genes and higher expression of BR-repressed genes. When BRs such as BL are present, they bind to the receptor BRI1 and coreceptor BAK1 to initiate BR signaling (right). BKI1 and BIR3 dissociate from the receptor complex, allowing BRI1 and BAK1 to become phosphorylated and activated. BSKs/CDGs are phosphorylated and activate BSU1 phosphatase to inhibit BIN2. Dephosphorylation by PP2A allows BES1 and BZR1 to function with other TFs and cofactors to promote BR-induced gene expression and inhibit BR-repressed gene expression. Figure was

created with the software BioRender (BioRender.com). BRRE, BR Response Element; BSU1, BRI1 SUPPRESSOR1; P, phosphorylation; PUB12/13, PLANT U-BOX12/13; SDG8, SET DOMAINGROUP8; SH, reduced Cys residue; SOH, oxidized Cys residue; TPL, TOPLESS; TRXh5, THIOREDOXIN H-TYPE5; Ub, ubiquitination.(Nolan et al., 2020)"

1.5 Auxin BR cross-talk

The interconnection between the auxin and BR pathways in plants is a complex and dynamic network that plays a crucial role in coordinating growth and development. Both auxin and BR are essential hormones involved in regulating various aspects of plant physiology, including cell elongation, division, and differentiation (Ai et al., 2023; Devi et al., 2022; Tian et al., 2017). This interconnection can be categorized into three groups: 1) Auxin influences BR signaling. 2) BR influences Auxin signaling. 3) Synergy between BR and Auxin signaling (Tian et al., 2017).

Auxin can regulate the BR signal pathway. DWARF4 is a key enzyme in BR production and controlling the BR level within the plant. Researches conducted on *DWF4pro::GUS A. thaliana* lines revealed that GUS activity commenced one hour after being stimulated with 10nM Auxin. Subsequent analysis of *DWF4pro::GUS* in auxin- and BR- mutant backgrounds demonstrated that the auxin-signaling pathway is essential for the induction of GUS activity, while the BR pathway is not involved. This discovery suggests a direct control of BR biosynthesis by the auxin signaling pathway. Moreover, chromatin immunoprecipitation assays provided further evidence by confirming that auxin inhibits the binding of the transcriptional repressor, BZR1, to the DWF4 promoter (Chung et al., 2011; Yoshimitsu et al., 2011). The impact of auxin on BR is further studied in rice, in the results, auxin treatment can increase the expression of the BR receptor gene, *OsBRI1* (Sakamoto & Fujioka, 2013). Auxin treatment in Arabidopsis, enhances the binding of BES1 to the promoter of SMALL AUXIN-UP RNA 15 (SAUR15) and mediates the early response of BR genes (Walcher & Nemhauser, 2012).

Conversely, BR also influences Auxin signaling at different levels. The expression of auxin-responsive genes like IAA5, IAA17, and IAA19 increases in response to BL treatment (Nakamura et al., 2003). Research indicates that the *de-etiolated2* (*det2*) mutant, which affects BR biosynthesis, reduces the expression of IAA5, IAA17, and IAA19 (H. Kim et al., 2006). The interaction between BZR1 and ARF proteins directly controls

the transport and signaling of Auxin through components such as PINs, AUX/IAA, TIR1, ARFs (Sun et al., 2010). Additionally, studies have demonstrated the interaction between BIN2 and ARF2 in the Y2H assay. BIN2 phosphorylates ARF2, inhibiting its DNA binding ability and repressing target genes. ARF2 is a target of BZR1, and its expression is reduced by BR treatment (Walcher et al., 2008).

The interaction between BR and auxin signaling has been categorized into primary and secondary levels (Ackerman-Lavert et al., 2021). The primary crosstalk happens when genes in the promoter region are activated by both BRRE/E-box and AuxRE, allowing direct regulation of transcription by both signaling pathways. While Secondary crosstalk occurs when genes that respond to either auxin or BR are expressed. The function of these proteins controls the expression of the other hormone-responsive genes (Tian et al., 2017).

Studies on BR-insensitive mutant *bri1-116* showed the active BZR1 or BR is required for Auxin-induced hypocotyl elongation. Additionally, the SUPPRESSOR OF PHYTOCHROME B4-3 (SOB3) mediated response to BR signaling, acts via regulation of SMALL AUXIN UP RNA19 (SAUR19) expression (Favero et al., 2017). Conversely, Auxin-related mutants including *iaa3* and *arf6/arf8* are another example of synergic interaction between Auxin and BR. These mutants are less sensitive to BR-induced hypocotyl elongation (T.-W. Kim et al., 2009; Tian et al., 2017).

1.6 Shaggy-like kinases family *in planta*

Plant GSK3-like family kinases are multifunctional and highly conserved non-receptor Ser/Thr kinases. They are involved in various developmental and stress-response pathways as light stress signaling networks or are required for growth and development (Hou et al., 2022; T. Li et al., 2020; Saidi et al., 2012; Wei & Li, 2016). *A. thaliana* GSK3 family contains 10 members, Maize has 11 and Rice encodes 12 isoforms of GSK3 (Dornelas et al., 1998; Yoo et al., 2006). Mammalian cells have only two isoforms GSK3α and GSK3β (Beurel et al., 2015). GSK3 genes in maize are distributed in different chromosomes. Chromosomes 3, 5, and 8 contain 2 GSK3 genes, while chromosomes 2 and 7 have no GSK3, and the rest of the Maize chromosomes, each encode only for 1

GSK3 (H. Li et al., 2022). AtGSK3s have been grouped into four clades and distributed in all 5 chromosomes. BIN2, BIN2 Like1 (BIL1), and BIN2-like2 (BIL2) are grouped in clade II and mainly function in the BR signaling pathway in *A. thaliana* (Nolan et al., 2022; Youn & Kim, 2015).

Protein phosphorylation is a common post-translational modification by kinases. This process typically entails adding a phosphate group to specific amino acid residues like serine, threonine, or tyrosine. Phosphorylation can profoundly influence the protein's structure and function. The reversible nature of protein phosphorylation allows for dynamic regulation of cellular processes, including signal transduction, gene expression, cell cycle regulation, and various other biological functions. This post-translational modification plays a central role in cellular communication and adaptation to changing environmental conditions (Ardito et al., 2017). Protein ubiquitination is another important post-translational modification. It attaches the small protein called ubiquitin to another protein, typically a target protein. Ubiquitination comprises a series of enzymatic reactions involving ubiquitin-activating enzymes (E1), ubiquitin-conjugating enzymes (E2), and ubiquitin ligases (E3s). Ubiquitination plays a significant role in regulating various cellular processes, including protein degradation, signal transduction, and protein localization (Callis, 2014).

Crystallography revealed two conserved domains in AtBIN2: an ATP binding site spanning amino acids 46-70, and a phosphate transfer motif spanning amino acids 120-367. AtGSK3 activity is regulated through various post-translational modifications. AtBSU1 inhibits AtBIN2 activity by removing phosphorylation from Tyr^{200}, while KIB1 facilitates ubiquitination of AtBIN2-Lys^{35}, leading to its degradation via the proteasome (Y. Song et al., 2023; Zhu et al., 2017). The E263K mutation in the AtBIN2-$TREE^{261-264}$ motif leads to a dwarf phenotype in *bin2/dwarf12/ucu1* (J. Li et al., 2001; Yan et al., 2009). The N-terminal region of GSKs contributes to the sub-cellular localization of GSKs, while the C-terminal region mostly interacts with other proteins (Youn et al., 2013).

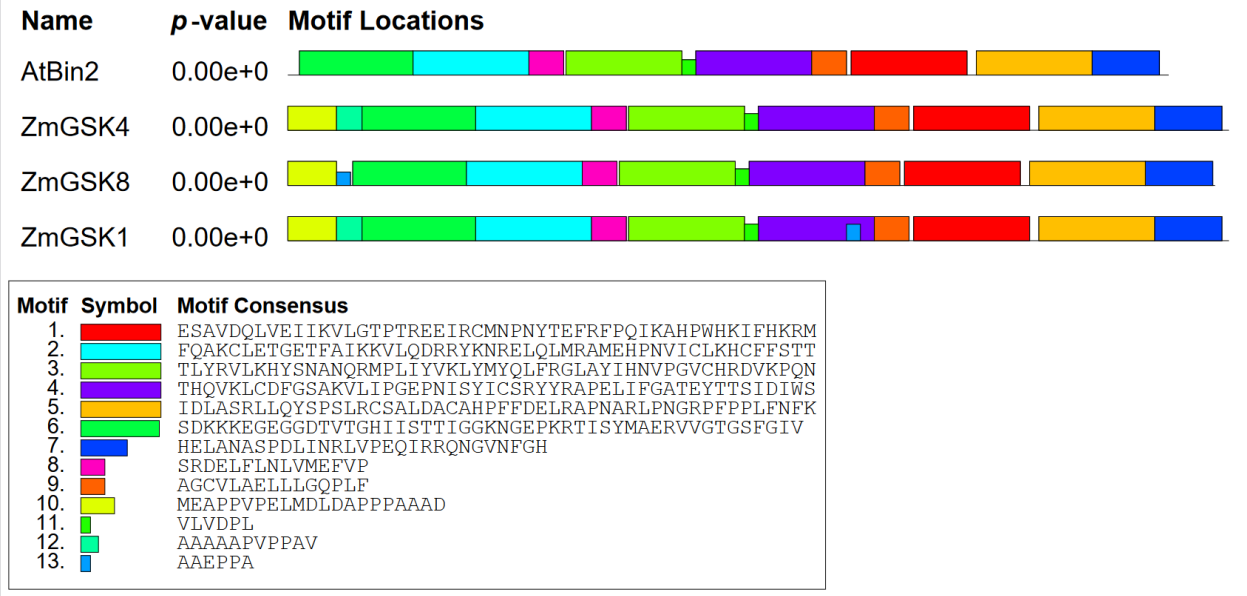

Figure 1-3 the conserved motifs of AtBIN2 and ZmGSKs

Using Paraline, the amino-acid sequence of AtBIN2 and three AtBIN2 orthologs in Maize were determined. ZmGSK3 and AtBIN2 contain 13 conserved motifs, with lengths ranging from 6 to 50 amino acids (E-values < 2.9 x 10^{-29}). The C-termini of GSKs contain highly conserved motifs while the N-termini show more variation.

1.7 Shaggy-like kinases in the mammalian system

GSK3α/β function as key regulators in a wide range of cellular processes including metabolic homeostasis, embryo development, neuronal growth, and differentiation. Dysfunction of GSK3 in mammalian cells causes different diseases such as cancer, neurodegenerative, Parkinson, Alzheimer, and bipolar disorders (Hur & Zhou, 2010; Kaidanovich-Beilin & Woodgett, 2011; Sutherland, 2011). While mammalian GSK3 was mostly characterized as a cytosolic protein, it was also found in other cellular compartments, such as the nucleus and mitochondria. The knockout of GSK3α/β had a different impact on cell survival. GSK3β knockout mice died at the embryonic stage, while GSK3α knockout mice survived. It seems GSK3α is unable to compensate for the absence of GSK3β (L. Wang et al., 2022). Like plant GSKs, post-translational modifications (PTMs) play an important role in the activity of mammal GSKs too. For instance, N-terminal Ser phosphorylation (Ser9 of GSK3β, Ser21 of GSK3α) inhibits and the Tyr phosphorylation (Tyr 216 of GSK3β, Tyr 279 of GSK3α) increases GSKs activity (Youn et al., 2013). GSK3α/β are widely expressed in different cell types and tissues,

such as the liver, pancreas, neurons, adipocytes, and myoblasts, and are associated with the regulation of energy metabolism and homeostasis (L. Wang et al., 2022).

1.8 Nuclear Bodies

Nuclear bodies (NBs) play crucial roles in the biogenesis of specific ribonucleoprotein complexes and the processing of key mRNAs in the nucleus (Staněk & Fox, 2017). NBs have three shared characteristics: 1- they are visible under the microscope 2- they consist of proteins and RNAs 3- in specific conditions like amyloid plaques, NBs continuously interchange their components with the surrounding nucleoplasm. NBs form in different structures from round balls to irregular shapes (Meyer, 2020). NBs function in the processing of specific RNAs, promote and control maturation of multi-factor complexes, sequester specific proteins and RNAs, and stress and antiviral responses (Machyna et al., 2015; Q. Wang et al., 2016).

Nuclear bodies (NBs) can be categorized into various groups. while Cajal bodies, nucleoli, and paraspeckles exhibit sub-compartmentalization, others have uniform structures. NBs have three shared characteristics: they are visible through a microscope, they consist of proteins and RNAs, and exhibit continuous exchange of components with the surrounding nucleoplasm under specific conditions such as amyloid plaques. NBs form varies from spherical shapes to irregular structures (Meyer, 2020).

The spliceosome is a multi-megadalton RNA-protein complex that carries out the splicing of eukaryotic precursor messenger RNA (pre-mRNA) by removing noncoding introns. It functions through four sequential stages: assembly, activation, catalysis, and disassembly (Wan et al., 2019).

Cajal bodies are the main organizers of short non-coding RNA biogenesis (snRNA) including spliceosomal snRNAs and snoRNA during RNA biogenesis. Studies have indicated that Cajal bodies are involved in the processing and modifications of snRNAs, as well as the assembly of functional small nuclear ribonucleoproteins (snRNPs). It is speculated that Cajal bodies may stimulate or coordinate the transcription of various spliceosomal snRNAs. Disruption of Cajal bodies by WRAP53 and USPL1 knockdowns reduces the expression of several snRNAs (Q. Wang et al., 2016).

In addition to spliceosomal snRNAs, hundreds of short non-coding RNAs accumulate in Cajal bodies, but the role of Cajal bodies in their metabolism remains unclear. Cajal bodies have been found to transiently associate with telomerase through Telomerase Reverse Transcriptase (TRET) RNA (Machyna et al., 2014).

Pre-mRNA splicing factor 38 (AtPRP38) is a crucial component of the spliceosome complex located in the nucleus. It plays a role upstream in regulating the RNA metabolic process, gene expression, and multicellular organismal development. A study by Machyna et al. (2014) demonstrated that AtPRP38 directly splices IAA1 in collaboration with AtUBL5. AtPRP38 is essential for the initial cleavage reaction of pre-mRNA, which is catalyzed by the spliceosome B-complex. Moreover, it is vital for the later maturation of the spliceosome. If AtPRP38 activity is absent, the formed spliceosome will become arrested in a catalytically impaired state (Plaschka et al., 2017; Xie et al., 1998).

1.9 The plant-pathosystem Zea mays/Ustilago maydis

Cereal grains meet nearly half of humankind's caloric requirement. Wheat, maize, and rice are humans' most common food resources. Maize is the most preferred grain in southern and Eastern Africa, Central America, and Mexico (Sandhu et al., 2007). The genus Zea consists of four species, with *Zea mays* L. being economically important. It is widely acknowledged that the Mexican annual teosinte serves as the wild ancestor of maize (*Zea mays L.*). *Zea mays* has 2n = 20 chromosomes (Díaz et al., 2020).

The biotrophic fungus *Ustilago maydis* causes smut disease in maize (*Z. mays*) and teosinte *(Z. mays ssp. parviglumis) and belongs to the group of basidiomycetes.* Smut pathogens have mostly a narrow host range and can cause severe damage to important crops like sorghum, sugarcane, barley, wheat, and maize (Scott et al., 2022). *U. maydis* is an outstanding model organism for studying various aspects of plant-pathogen interactions. *U. maydis* promotes the formation of galls in all aerial parts of the host plant, in contrast to other smut fungi such as *Ustilago hordei, Tilletia caries, Tilletia laevis* (Christoph & Gero, 2004).

The life cycle of *U. maydis* begins when airborne teliospores land on the host leaf and germinate. Under suitable environmental conditions, teliospores germinate and release

haploid cells (sporidia). The infection process of maize by *U. maydis* starts with the mating of two compatible sporidia. The mating initiates pathogenicity and sexual reproduction during the invasion of host cells. It should be mentioned, that the infectious filaments of the smut are regulated by a tetra-polar mating system. The tetra-polar system involves an a and b mating type loci with at least four alleles. The locus a contains genes that encode lipopeptide pheromone components (mfa1 and mfa2) and receptors (pra1 and pra2). The locus b, which has multiple alleles, encodes for two homeodomain proteins, bEast (bE) and bWest (bW). These proteins play a major role in determining pathogenicity (Banuett & Herskowitz, 1994; Brachmann et al., 2001). In the initial stage, once two compatible sporidia fuse due to pheromone stimuli, conjugation tubes form. After cell fusion, a dikaryotic mycelium is formed, which is the infectious form of the fungus. This phase marks the transition from a saprophytic to a biotrophic lifestyle for *U. maydis* (Lanver et al., 2017).

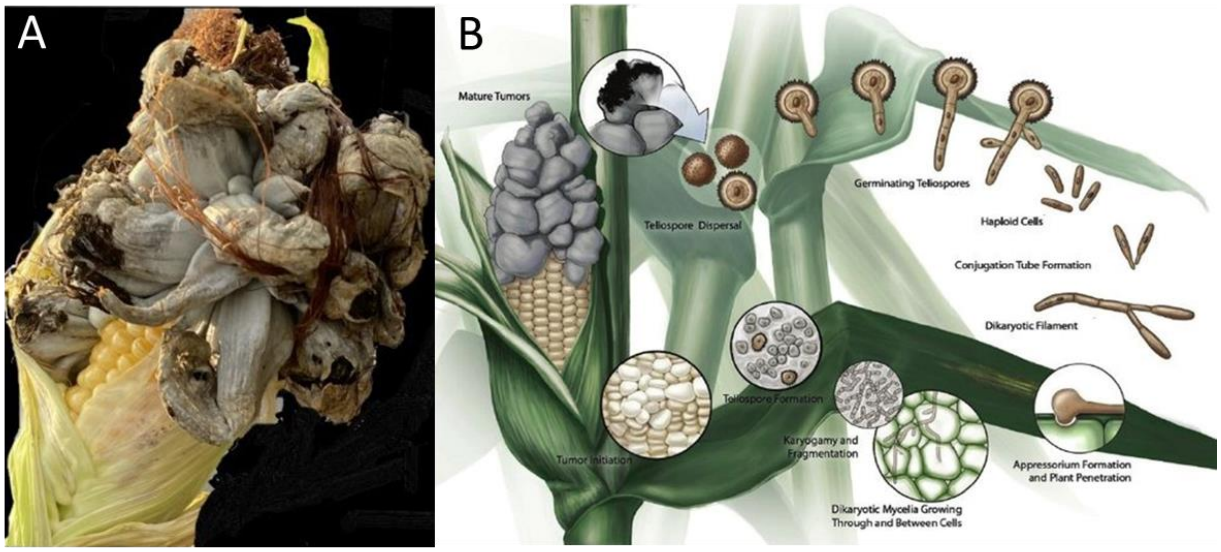

Photo by @Armin Djamei Saville and et al. 2012

Figure 1-4 The life cycle of U. maydis.

A. maize cob infected in the field by *U. maydis* exhibits certain symptoms including raptured galls and black teliospores dispersion into the environment.
B. The disease cycle of *U. maydis* begins with the spreading of mature teliospores into the environment (panel A). Teliospores produce four haploid cells after germination. When they land on a leaf surface, they perceive chemical and physical cues, which stimulate filamentous growth. Upon successful detection of a compatible mating partner, cells form conjugation tubes. These tubes facilitate cell-cell fusion, resulting in the formation of a

dikaryotic filament. The growing tip of the filament forms an appressorium, a penetration structure that enables the fungus to enter plant cells. Subsequently, the fungal hyphae spread intracellularly, reprogramming the host and inducing the formation of galls. Towards the end of the cycle, the hyphae fragment within the galls and create black teliospores, giving the galls a smutted appearance.

After successfully establishing a dikaryon, the penetration structure, also known as appressoria, penetrates into the host cells, and by secretion of the apoplastic effectors, avoids recognition events by the plant. In contrast to other fungi, *U. maydis* does not have a melanized appressorium. Instead, it relies on a combination of secreted cell wall-degrading enzymes and osmotic pressure at the penetration peg to penetrate the cell wall (Lanver et al., 2014).

After the penetration, the cell cycle block is removed and mitotic division and growth of the dikaryotic filaments start. The fungus grows inside the cell, completely surrounded by the host plasma membrane. Unlike many other fungi, *U. maydis* does not form haustoria. Instead, the hyphal surface is encased by the host plasma membrane, which serves as an interface for nutrient acquisition, signal exchange, and delivery of host-modifying molecules to the plant cell (Djamei & Kahmann, 2012). The metabolic and transcriptional reprogramming of the host cells at 2 dpi leads to hyperplasia (cell division) in leaf bundle sheet cells and hypertrophy (cell enlargement) in leaf mesophyll cells (Matei et al., 2018). The hypertrophy and hyperplasia in the infected tissue form galls, which are prominent symptoms linked to *U. maydis* infection.

The establishment of a successful infection by *U. maydis* is supported by the help of an arsenal of effector proteins that are secreted during host colonization. It was predicted that the *U. maydis* genome encodes 467 of these secreted effectors, some of which are arranged in clusters (Lanver et al., 2017). Effectors play essential roles in promoting pathogen establishment and progression, suppressing host immunity, and modifying the host's metabolism to facilitate the completion of the pathogen's life cycle (Scott et al., 2022; Y. Song et al., 2021). It has been shown that *U. maydis* secretes also small molecules (effectors) with phytohormone activities e.g., auxins, cytokinins, and abscisic acid during plant colonization (Bruce et al., 2011; Nagarajan et al., 2023; Reineke et al., 2008).

According to their place of action, effectors can have their role in the plant/pathogen interface, the apoplastic space, those are termed apoplastic effectors, or effectors that are translocated into the host cell are termed cytoplasmic effectors (Lanver et al., 2018; Uhse & Djamei, 2018). Studies have shown that some of the effectors suppress the plant's PTI responses to enable fungal colonization. Additionally, some effectors deactivate plant enzymes that can harm the pathogen or change the pathogen's physiology (Scott et al., 2022).

Several apoplastic effectors have been characterized that help the fungus in enhancing its virulence. For instance, *U. maydis* effector Protein important for tumors 2 (Pit2) was shown to suppress a group of maize papain-like cysteine proteases (PLCPs). Another functionally characterized apoplastic *U. maydis* effector Protein essential during penetration-1 (Pep1), which suppresses the generation of ROS molecules associated with plant defense by inhibiting plant peroxidases. The Repetitive secreted protein 3 (Rsp3) effector protects fungal hyphae by binding to at least two antifungal maize proteins AFP1 and AFP2. These maize proteins, called AFPs, are mannose-binding proteins that attack fungal hyphae, thereby limiting fungal growth (Doehlemann et al., 2009; Ma et al., 2018; Mueller et al., 2013).

Translocated effectors play a crucial role in fungal growth because of changing host physiology to favor *U. maydis*. For instance, Tin2, targets components of the phenylpropanoid pathway and binds to a maize protein kinase ZmTTK1. This binding increases the expression of genes involved in anthocyanin biosynthesis while reducing lignin biosynthesis (Tanaka et al., 2014). Translocated effectors can also be specific to certain organs. For example, the See1 effector of *U. maydis* interacts with the maize SGT1 protein, reactivating DNA synthesis in infected leaf tissue (Redkar et al., 2015). Plant hormones actively participate in plant immune responses, the experimental findings have provided evidence for the ability of *U. maydis* to manipulate host hormone signaling through diverse effectors. For instance, the secreted chorismate mutase (Cmu1) was shown to suppress the biosynthesis of salicylic acid (SA), while the Jasmonate/Ethylene signaling inducer 1 (Jsi1) induces signalling pathways involving JA (Jasmonic acid) and Ethylene (Djamei et al., 2011; Scott et al., 2022).

Previous studies have demonstrated the complex interaction between SA-signaling and Auxin-signaling during the plant defense responses against biotrophic pathogens (Čarná et al., 2014). Considering the importance of Auxin-SA crosstalk in plant immunity, it is not surprising that *U. maydis* secretes multiple effectors manipulating the Auxin signaling in the host. For example, the effectors Nkd1 and Tip1 to 5 have been identified as interactors of the transcriptional co-repressors TOPLESS/TOPLESS-related (TPL/TPRs) and were shown to de-repress the auxin signalling in plants. This interaction in the end promotes the susceptibility of the host to *U. maydis* (Navarrete et al., 2022; Navarrete et al., 2021). Recently, additional TPL interactors of *U. maydis* including Tips 6-8 have been reported. These findings indicate that the TPL class of corepressors and auxin signaling serves as a significant hub for *U. maydis* effector proteins (L. Huang et al., 2023; Khan et al., 2023).

1.10 Interdisciplinary studies on *U. maydis*

A lot of molecular mechanisms and proteins such as TOR signaling and GSK3s are highly conserved in plants and humans (Díaz-Troya et al., 2008). On the other hand, *U. maydis* is more closely related to humans than to budding yeast, and it shares numerous protein similarities with *Homo sapiens*. Growing evidence suggests that basic principles of long-distance transport, mitosis, and motor-based microtubule organization are conserved between *U. maydis* and humans. The mechanism of homologous recombination, involving the ‘Holliday junction’ was initially proposed on the basis of pioneering work in the 1960s by Robin Holliday in *U. maydis* (Steinberg & Perez-Martin, 2008). On the other hand, recent studies on Breast Cancer Type2 susceptibility protein BRCA2 (HsBRCA2), and its homologue, Brh2, was discovered in *U. maydis*. The smaller size of Brh2 in comparison with HsBRCA2 enabled the characterization of its activities in vitro and created a new opportunity for breast cancer studies. These studies experimentally supported a longstanding hypothesis regarding the function of BRCA2 in mammals (Duda et al., 2020). Juárez-Montiel et al. (2018) proposed utilizing heterologous expression and characterization of the aspartic endoprotease Pep4um-rec protein to test inhibitors targeting human cathepsin D, a crucial therapeutic target for breast cancer (Juárez-Montiel et al., 2018).

2 Aims of the thesis

This study aims to identify a putative *U. maydis* effector of the biotrophic smut fungus *U. maydis* that target conserved host proteins by using a heterologous plant expression system.

This thesis focused on the functional characterization of an *U. maydis* effector overexpressing in *A. thaliana* that exhibited a distinct dwarfed growth phenotype with dark green cabbage-like leaves. This effector was named *U. maydis* Cabbage 1 (Cab1). Various approaches, such as subcellular localization, disease symptom assessment, and secretion assays, were employed to characterize the function of Cab1. The host target of Cab1 was identified through Co-IP and mass spectrometry, as well as Y2H. The consequences of Cab1 expression were studied using the SplitTurboID assay and NGS. Furthermore, the potential induction of cell apoptosis by Cab1 was examined by transiently expressing it in the human cell lines.

3 Materials

3.1 Chemicals, enzymes, and antibodies

The chemicals used for this thesis were primarily obtained from the following companies: Carl-Roth, Merck, Roche, PanReac AppliChem, Qiagen, Jena Biosceince, Sigma-Aldrich, and Life technologies. The Glucanex enzyme purchased from Sigma-Aldrich. Cloning reagents (restriction enzymes, polymerases, ligases etc.) were primarily obtained from Thermo, and New England Biolabs. For SDS poly-acrylamide gel electrophoresis the size standard Page Ruler Prestained Protein Ladder (BioRad) was used. Primary antibodies used are mouse-anti HA, and Myc (Sigma-Aldrich), GFP, mCherry, V5 (VBC); as secondary antibodies Goat anti-Mouse and anti-Rabbit, and conjugated Streptavidin-HRP (Thermo-Scientific) were bought.

3.2 Buffers and solutions

Most buffers and solutions in this thesis were prepared as described previously (Ausubel et al., 2003; R. Green & Sambrook, 2012). Special buffers and solutions were made based on the reference papers. Where necessary, solutions got autoclaved or filter sterilized.

3.3 Kits

3.3.1 Kits were used in this thesis.

	Name	purpose	manufacturer
1	plasmid isolation	DNA isolation from *E. coli*	Qiagene/Thermo
2	RNA isolation	total RNA isolation from plants	M&N
3	DNA removal Jena	erase gDNA contamination of RNA	Jena Bioscience
4	cDNA	cDNA synthesis	ABI

Table 3-1 list of kits used in this study

3.4 Bacterial strains

	The following bacterial strain were used:		
1	GV3101/pMP90	pSOUP C58C1: pGv3101 RifR; pTiC58 ΔTDNA GentR; pSoup TetR	Used for plant infection Koncz & Schell, 1986; Hellens et al., 2000
2	Mach1	F– Φ80lacZΔM15 ΔlacX74 hsdR(rK–, mK+)ΔrecA1398 endA1 tonA	Invitrogen
3	BL21	F– ompT hsdSB (rB–, mB–) gal dcm (DE3)	Thermo

Table 3-2 Bacterial strains were used for this study

3.5 *U. maydis* strains:

Different *U. maydis* strains were used for this study.

SG200	a1 mfa2 bE1 bW2	Kämper et. Al. 2006
AB33	a1 Pnar:bW2, bE1	Brachmann et. Al., 2001
FB1	a1 b1	Banuett & Herskowitz, 1989
FB2	a2 b2	Banuett & Herskowitz, 1989

Table 3-3 U. maydis strains were used for this study

3.6 S. cerevisiae strains:

The following *S. cerevisiae* strains had been used in this thesis.

1	AH109	*MATa, ura3-52, trp1-901, leu2-3, 112, his3-200, gal4Δ, gal80Δ, LYS2::GAL1UAS-GAL1TATA-HIS3, MEL1, GAL2UAS-GAL2TATA-ADE2, URA3::MEL1UASMEL1TATA-lacZ*	Clontech
2	Y187	*MATα, ura3-52, trp1-901, leu2-3,112, his3-200, ade2-101, gal4Δ, gal80Δ, met–, URA3::GAL1UAS–Gal1TATA–lacZ, MEL1*	Clontech

Table 3-4 S. cerevisiae strains used in this study

3.7 Mammalian cell lines:

In this research, the *HeLa* and *Hek293T* human cell lines were utilized to investigate the effects of Cab1 exogenous expression on HsGSK3 activity.

3.8 Plant materials for the phenotyping and Cab1 project:

Several different plant species were used in this study. Araffector (*$P_{35S\text{-}XVE}$::Alpha amylase signal peptide-Effector-HA-P2A-Myc-Effector*) lines were dipped in Col-0-DR5 background and selection was done on Kanamycin.

	name	description
1	*Arabidopsis thaliana Columbia 0*	used for transgenic lines, gDNA, cDNA, NGS
2	*Arabidopsis thaliana Wassilewskija*	background of BIN2 triple knockout
3	*Zea mays* EGB	used for virulance assay
4	*Zea mays* B73	used for virulance assay and microscopy, sequenced genome
5	*Nicotiana benthamiana*	used for transient expression assay

Table 3-5 List of plant materials that were used in this study

4 Methods

4.1 Phenotyping

Phenotyping of *A. thaliana* Cab1 transgenic lines was performed in the following steps:

4.1.1 Selection of transgenic plants:

I selected and sterilized homozygous transgenic *A. thaliana* lines for cab1 effector using 70% ethanol. The lines were then transferred to $^1/_2$MS plates with antibiotics (Kanamycin). After 3 days of vernalization at 4°C, the plates were placed in growth chambers (MLR-352H-PE) with short-day conditions for 7 days. Phenotyping was conducted on seedlings 5 days after germination.

4.1.2 Transfer to induction plates

The induction and control plates were prepared using 1/2MS media with 10µM β–Estradiol and the appropriate amount of DMSO as the solvent, respectively. Five seedlings from each line were transferred to both, the induction and control plates. The plates also included control lines expressing GFP and mCherry fluorescent proteins as controls, and they were placed on the same induction and control plates. The plates were then vertically positioned in growth chambers, following short-day conditions.

4.1.3 phenotyping

the plant's phenotype was monitored at 5, 10, and 15 days after induction to capture both early and late phenotypes.

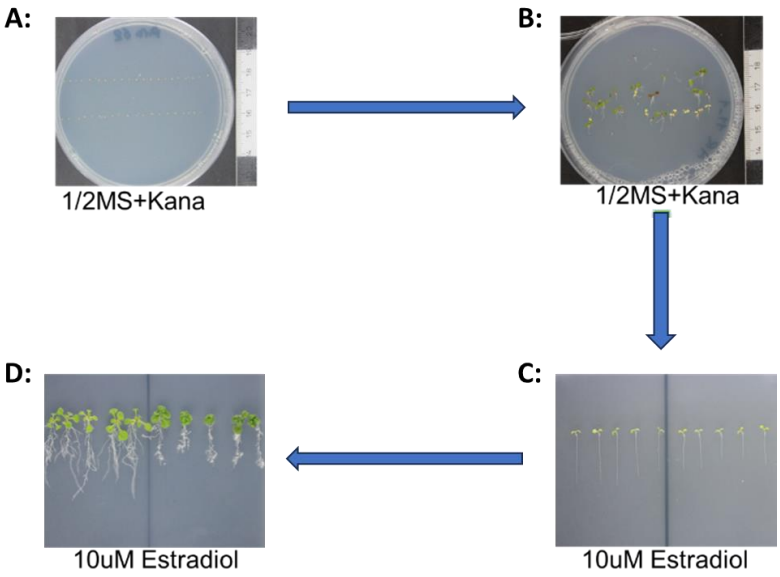

Figure 4-1 Phenotyping steps of A. thaliana Cab1 transgenic lines

A. Transgenic Arabidopsis thaliana lines were placed on $^{1}/_{2}$MS media containing Kanamycin (50 µg/ml) selection markers. The plates were stored in a vernalization chamber for 3 days.
B. The non-transformed plants start turning yellowish and die 3-5 days after germination.
C. The well-grown and uniform seedlings were transferred to induction and control plates and incubated vertically in growth chambers. The induction and control plates were prepared using 1/2MS media with 10µM β-Estradiol and the appropriate amount of DMSO as the solvent, respectively.
D. The images were captured 5-, 10- and 15-days post induction. Many lines did not show a clear phenotype. In almost 40 lines, the wide range of phenotypes, including impaired growth and development, anthocyanin accumulation and leaves bleaching, hypersensitive reaction and cell death were observed.

4.2 Cultivation of Bacteria

Bacteria were grown under aerobic conditions at 28°C (*A. tumefaciens* pSoup)/37°C (*E. coli*) in dYT broth (tubes) or on dYT agar (plates) at 200 rpm. To stop growing of the non-transformed bacteria, selection pressure was kept with antibiotics.

4.2.1 Overnight culture

The cultivation of bacteria in liquid media was done using dYT liquid containing the proper antibiotics. To re-grow bacteria, stored at -80°C as a glycerol stock, small amounts of the

glycerol culture were streaked onto dYT plates containing appropriate antibiotics and cultivated overnight (ON) at 28°C *(A. tumefaciens*) or 37°C (*E. coli*).

4.2.2 Bacterial glycerol stocks

To prepare transgenic strain stocks, 1 ml overnight cultures of bacterial strains combined with an equal amount of sterile 80% v/v glycerol in screw cap tubes, incubated at 4°C for a few hours and stored at -80°C.

4.3 Transformation of *A. tumefaciens*

A. tumefaciens strain GV3101 (pSoup) electro-competent cells were prepared with the following protocol and transformation was performed by Bio-Rad Gene Pulser Xcell Electroporation systems preset program.

4.3.1 Preparation of *Agrobacterium tumefaciens* electro-competent cells

1. Inoculate 5 mL of dYT (including antibiotics) with 10 µL liquid culture or a large colony of *A. tumefaciens*. Shake at 28 °C to prepare ON culture.
2. Inoculate two flasks containing 50 mL of LB media with 5 ml of *A. tumefaciens* ON culture and shake at 28 °C with 200 rpm for 4-6 hours.
3. Measure the bacterial density. Adjust OD600 to 0.5.
4. Pour the suspension into falcon tubes. Centrifuge the suspensions for 10 min at 3500 rpm at 4 °C. Discard the supernatant.
5. Re-suspend the bacteria gently with 25 mL cold sterile water.
6. Centrifuge for 15 min (5000 rpm, 4°C). Discard the supernatant.
7. Repeat steps 5.-6. four more times. It is very important to wash the cells with excess water to remove salts.
8. Discard supernatant and re-suspend in 2.5 mL cold-sterile 10% glycerol. Combine the solution of all tubes into one cold centrifuge tube. Centrifuge for 10 min (3500 rpm, 4°C).
9. Discard the supernatant and finally re-suspend cells completely but gently in 4 mL cold 10% glycerol.
10. Divide the solution into 50 µL aliquots by pipetting the cells into pre-cooled microcentrifuge tubes. Put them into liquid nitrogen immediately and store them at

-80 °C.

4.4 Transformation of *E. coli*:

Mach1 (Thermo Fisher Scientific, Waltham, MS, USA) chemo-competent cells transformed via heat shock 42°C for 60 sec, incubated on ice for 10 min, and recovered by adding 800µL dYT liquid at 37°C for 60 min 800rpm.

4.4.1 Preparation of chemo-competent *Escherichia coli* cells

1. Inoculate 5 mL of dYT (including antibiotics) with a large colony of *E. coli*. Shake at 37°C to prepare ON culture.
2. Inoculate 100 mL of dYT media supplemented with 10 mM MgCl2 and 10 mM MgSO4.
3. with 2 mL of the *E. coli* ON culture and shake at 37 °C at 200 rpm until OD600 0.4-0.6 is reached.
4. Transfer the cells to cold centrifuge bottles and incubate them on ice for 30 min.
5. Centrifuge the suspensions for 10 min at 3000 rpm at 4 °C. Discard the supernatant.
6. Re-suspend the cells gently in 33 mL cold RFI solution. Incubate on ice for 30 min.
7. Centrifuge for 10 min (3000 rpm, 4°C). Discard the supernatant.
8. Re-suspend the bacteria gently in 5-8 mL cold RFII solution and chill the cells on ice for at least 30 min.
9. Divide the solution into 50 µL aliquots by pipetting the cells into pre-cooled microcentrifuge tubes. Freeze aliquots in liquid nitrogen and store them at -80 °C.

RF I solution:

100 mM RbCl, 50 mM MnCl2 x 4 H2O, 30 mM potassium acetate, 10 mM $CaCl_2$ x 2 H_2O, 15% glycerol (w/v), pH5.8, 0.2M acetic acid, filter sterilize and store at 4°C

RF I solution:

10 mM MOPS, 10 mM RbCl, 75 mM CaCl2 x 2H_2O, 15 % glycerol (w/v), pH6.8 NaOH, filter sterilize and store at 4°C.

4.5 Cultivation of *U. maydis*

U. maydis strains were grown under aerobic conditions at 28°C in YEPS light (yeast extract peptone sucrose) broth or on YPD and PDA plates. To avoid the growth of untransformed bacteria, proper antibiotics were added.

4.5.1 *U. maydis* glycerol stocks

To prepare transgenic strains stocks, 1ml overnight culture of *U. maydis* strains combined with an equal amount of sterile 80% v/v glycerol in screw tubes, incubated at 4°C for a few hours and stored at -80°C.

4.5.2 Preparation of *U. maydis* protoplasts for transformation:

Transformation of *U. maydis* was performed using protoplasts obtained following a protocol modified from Schulz et al., 1990 and Gillissen et al., 1992 (Gillissen et al., 1992; Schulz et al., 1990).

1. Inoculate 4 mL YEPS light with fungal material from a plate and grow the culture ON at 28°C and 200 rpm.
2. In the afternoon of the next day inoculate the main culture by diluting the pre-culture 1:3000 in 100 mL YEPS light.
3. The next morning measures the OD600 (should be between 0.6-1.0) and pellet the cells in falcon tubes by centrifugation (10 min, 3500 rpm at RT). Discard the supernatant.
4. Re-suspend the cells in 20 mL SCS and spin for 10 min at 3500 rpm (RT). In the meantime, prepare the enzyme solution that will degrade the fungal cell wall. To do so, dissolve 10 mg/mL glucanex in 4 mL SCS buffer and filter sterilize the solution.
5. Discard the supernatant and re-suspend the pellet in the SCS-Glucanex solution (2mL per falcon). After 7-10 min observe the cells under the microscope. If 2/3 of the cells are round, add 10 mL SCS buffer and pellet the cells (10 min, 2000 rpm, cool down to 4°C while spinning). From now on store the cells on ice. Also, cool down the SCS buffer and the STC buffer.
6. Discard the supernatant and wash the pellet three times with 10 mL SCS. Make sure to always re-suspend the pellet carefully.
7. Discard the supernatant and wash the pellet once with 10 mL STC.

8. Discard the supernatant and carefully re-suspend the pellet in 1 mL cold STC.
9. Aliquot the protoplasts (100 µL) in microcentrifuge tubes. Store on ice until use or put in -80°C freezer for long-term storage.

4.5.3 Transformation of *U. maydis* protoplasts

Transformation of *U. maydis* is achieved by making use of homologous recombination in a PEG (polyethylene glycol) based protocol. Therefore, the used plasmid DNA has to be linearized and purified before starting the procedure described below. Transformed colonies were streaked out on selection plates and single colonies were used for further experiments.

1. Boil Regeneration agar (Reg. Agar) and let it cool to 50-60°C. Add the needed antibiotic agent and pour a 10mL bottom layer into a petri dish. Store the Reg. Agar bottle in 55°C incubator. In parallel cool down STC-PEG to 4°C.
2. Thaw protoplasts on ice. After thawing, add linear DNA (5 µg in max. 20 µL) and 1 µL Heparin (15 mg/mL). Incubate on ice for 15 min. While waiting pour the top layer of Reg. Agar (10 mL).
3. Add 500 µL precooled STC-PEG to the DNA/protoplast mix and carefully pipette up and down several times. Incubate the solution on ice for exactly 15 min.
4. Carefully plate the protoplasts on the poured Reg. Agar plate. Incubate the plate a minimum of four days at 28°C to get colonies.

Regeneration Agar:

1.0% (w/v) yeast extract, 2.0% (w/v) bacto peptone, 2.0 % (w/v) sucrose, 18.22% (w/v) sorbitol, 1.5 % (w/v) Agar, autoclave

STC PEG:

40% (v/v) PEG in STC buffer, filter sterilize

4.6 Cultivation of Saccharomyces cerevisiae

S. cerevisiae was grown under aerobic conditions at 28°C in YPD (yeast extract peptone dextrose) or SD (synthetic dextrose) broth (tubes) or on YPD agar (plates). To prohibit the growth of untransformed yeast, certain amino acids were not added to the medium,

allowing only those yeast strains to grow that express the corresponding auxotrophy marker genes.

YPD medium:

1 % yeast extract (w/v), 2 % bacto-peptone (w/v), [optional for plates: 2% bacto agar], Autoclave, add glucose (2%)

SD medium:

0.67 % yeast nitrogen base without amino acids (w/v), 0.06 % dropout amino acids (leu –trp –his –ade) (w/v), [optional for plates: 2% bacto agar], Autoclave, add glucose (2%).

To generate the different dropout combinations certain amino acids were added after autoclaving (e.g. 0.02 g/L adenine, 0.02g tryptophan, 0.02g histidine, 0.04g leucine)

4.6.1 *S. cerevisiae* glycerol stocks

To prepare transgenic strains stocks, 1ml overnight culture of *S. cerevisiae* combined with an equal amount of sterile 80% v/v glycerol in screw tubes, incubated at 4°C for a few hours and stored at -80°C.

4.6.2 Preparation of competent *S. cerevisiae* cells

The generation of competent yeast cells was done using the protocol described below.

1. Start the pre-culture by inoculating 5 mL YPD with yeast material from a plate and growing the culture ON at 28°C and 200 rpm.
2. Inoculate 50 mL YEPD with 1 mL of your ON culture to start the main culture.
3. Grow at 30ºC to an OD600 = 0.5-0.7 (ca. 4-6h).
4. Pellet the cells in falcon tubes by centrifuging them for 3 min at 500g. Discard the supernatant.
5. Wash the cells first with 15 mL ddH2O and then with 10mL SORB.
6. In parallel, boil the carrier DNA (10mg/mL denatured salmon sperm DNA; Invitrogen) for 10 min and then snap cool it on ice.
7. Dissolve the cells in 360 µL SORB and add 40 µL carrier DNA. From this step on, the cells are kept on ice. Dispense cells into 50 µL aliquots in microcentrifuge tubes, freeze them using liquid nitrogen, and then store them at -80°C.

4.7 Transformation of *S. cerevisiae*

S. cerevisiae was transformed using a PEG based protocol described below.

1. Thaw competent yeast cells on ice.
2. Add 5-10 µL plasmid DNA and mix the components by flicking.
3. Add 300 µL sterile PEG solution and mix again.
4. Incubate the cells for 30 min at 30°C while shaking (800rpm):
5. Perform a heat shock by incubating the cells for 15 min at 42°C.
6. Add 800 µL YPD medium to reaction and mix carefully.
7. Centrifuge the tubes for 3 min at 500g and discard the supernatant.
8. Wash the cells once with 1mL YEPD and then re-suspend the cells in 1 mL YEPD.
9. Incubate the reaction in a shaker for 30 min at 30°C.
10. Centrifuge the cells for 3 min at 500g, discard the supernatant and resolve pellet in 100µL ddH2O. Spread the cells on selective plates and incubate them at 28°C for 2-3 days.

SORB:

100 mM lithium acetate, 10 mM Tris HCl, pH8, 1 mM EDTA pH8, 1 M sorbitol, pH8 acetic acid, Filter sterilize.

PEG solution:

100 mM Lithium Acetate, 10 mM Tris HCl pH8, 1 mM EDTA pH8, 40% PEG 3350, Filter sterilizes

4.8 Extraction, purification, and analysis of nucleic acids

4.8.1 Common procedures

Basic procedures including restriction digestion, ligation, DNA amplification by PCR, and purification of DNA from PCR reactions/agarose gels were conducted using the supplied manuals (New England Biolabs, Qiagen). Sequencing of DNA was done by the LGC-Group.

4.8.2 Isolation of plasmid DNA from *Escherichia coli*

Isolation of plasmid DNA from bacteria was performed with Qiagen plasmid mini kit, midi prep was done by GeneJET Plasmid Midiprep Kit by Thermo Sceitific.

4.8.3 Isolation of genomic DNA from *U. maydis*

Genomic DNA from *U. maydis* had to be isolated for various purposes and was done as described below.

1. Inoculate 4 mL YEPS-light with fungal material from a plate and grow the culture ON at 28°C and 200 rpm.
2. Transfer 1 mL of culture into a prepared microcentrifuge tube (with one spoon of glass beads) and spin for 1 min at full speed. Discard supernatant. Freeze pellets at -20°C for long-term storage but at least for a few hours to ease cell disruption.
3. Add 500 µL Phenol-Chloroform and 400 µL *Ustilago* lysis buffer and shake tubes for 15 min vigorously.
4. Spin the tubes for 30 min at full speed. In the meanwhile, prepare new microcentrifuge tubes with 1 mL of 100% ethanol.
5. After centrifugation add 400 µL of the upper, aqueous layer and transfer it to the prepared tubes. Mix by inverting the tubes several times.
6. Spin the tubes for 5 min at full speed and discard the supernatant.
7. Wash the pellet with 1 mL 80% ethanol to remove residual salts. Spin 2 min at full speed and remove the supernatant carefully.
8. Add 20-30 µL TE-RNase and re-suspend the pellet. Incubate the tubes for 15 min at 55°C on a Thermo block with open lids to remove residual ethanol. Store DNA at -20°C.

***Ustilago* lysis buffer:**

2.0 % Triton X, 1.0 % SDS, 10 mM Tris HCl pH 8, 100mM NaCl, 1 mM EDTA

4.9 RNA extraction

Total RNA was extracted from 14-day-old Arabidopsis mCherry-Cab1$_{28\text{-}113}$ (*P$_{35S\text{-}XVE}$::mCherry-Cab1$_{28\text{-}113}$*) seedlings treated with 10µM β–Estradiol, 100µM SA, 50 nM Brassinolide (BL) and similar concentration of DMSO as mock. The extraction was

performed using a plant total RNA extraction kit (Macherey-Nagel Bioanalysis Dueren, Germany Cat:740949) according to the manufacturer's instructions.

4.10 DNase treatment of RNA and cDNA generation

Residual gDNA contamination after isolation of total RNA was removed by gDNA Removal Kit (Jena Bioscience PP-219). Per reaction, approximately 2µg of RNA was used.

1- Add 0.1 vol 10x Reaction buffer and 1µl of gDNA Remover
2- Mix gently and incubate the samples at 37°C for 10 min
3- 5 min 58°C to inactive of gDNA Remover enzyme (Jena Bioscience)
4- Spin down the samples and load 1ul of reaction on 2% freshly made Agarose gel to check the integrity of RNA.
5- Store total RNA at -20°C for short-term storage and -80°C for long-term storage.

1µg of total RNA was to obtain cDNA by reverse transcription. cDNA was synthesized from total RNA by using High-capacity cDNA reverse transcription kit (Applied Biosystems).

4.11 Real-time PCR

Real-time PCR allows for the quantification of cDNA-transcribed from mRNA. RT-qPCR was performed using GoTaq qPCR Master-Mix (Promega) under thermal cycling conditions (95^{o}C for 2min, 40 cycles of 95^{o}C for 15 s, and 60^{o}C C for 60s). The expression level of each gene was normalized by that of the reference gene PP2A.

4.12 RNA-Sequencing and data analysis

Total RNA was extracted from 14-days-old *A. thaliana* mCherry-Cab1$_{28\text{-}113}$ ($P_{35S\text{-}XVE}$::mCherry-Cab1$_{28\text{-}113}$) seedlings treated with mock, 10µM β–Estradiol, 100mM SA and 50 nM Brassinolide (BL). The extraction was performed using a plant total RNA extraction kit (Macherey-Nagel Bioanalysis Dueren, Germany Cat:740949) according to the manufacturer's instructions. The RNA-seq was performed at Novagen, UK and raw fastq files were analysed in-house. The Illumina reads were trimmed and quality filtered using

trimmomatic-0.39 (Bolger, A. M., Lohse, M., & Usadel, B. (2014). Trimmomatic: A flexible trimmer for Illumina Sequence Data. Bioinformatics, btu170) with standard settings (LEADING:3 TRAILING:3 SLIDINGWINDOW:4:15 MINLEN:36). Quality trimmed and filtered reads were aligned to *A. thaliana* reference transcripts using Hisat2 (https://www.nature.com/articles/s41587-019-0201-4) and quantified with Stringtie (ref 10.1186/s13059-019-1910-1) or directly analyzed with Salmon (Patro, R., Duggal, G., Love, M. I., Irizarry, R. A., & Kingsford, C. (2017). Salmon provides fast and bias-aware quantification of transcript expression. Nature Methods.) The read counts were further analyzed with DESeq2 (10.1186/s13059-014-0550-8.) and the differentially expressed genes were assigned with at least 10 read coverage, more than 1.5-fold change, and with adjusted p-value <0.05. GO enrichment was analyzed by shinyGO 0.80 (10.1093/bioinformatics/btz931).

4.13 Yeast two-hybrid screen

All yeast work has been conducted following the yeast protocols handbook (Clontech, 196 Mountainview, CA) and the previously described protocol (Navarrete, Grujic, Stirnberg, Saado, et al., 2021). Briefly, the Y187 strain (MAT α) was transformed with bait vectors (pGBKT7), while the AH109 strain (MAT a) was transformed with prey vectors (pGAD, pADGG – a modified version of pGADT7), using the LiAc/PEG method. For the yeast two-hybrid (Y2H) assay, the GAL4 activation domain from the prey vector pADGG was fused to the open reading frame of *U. maydis* Cab1 effector without the signal peptide ($Cab1_{28\text{-}113}$), and the GAL4 binding domain from the bait vector pGBKT7 was fused to the genes AtBin2, ZmGSK1, ZmGSK4, and ZmGSK8. The presence of the respective plasmids in the transformants was confirmed by PCR analysis. Positive interactions were determined by the growth of mated yeasts on intermediate or high stringency media five days after inoculation in spotting assays. All experiments were repeated three times to ensure the reliability and reproducibility of the results.

4.14 Yeast Competition Assay

For the yeast competition assay, two proteins were expressed under two independent promoters and terminators. ZmGSK4 (P_{ADH1}*::Gal4BD-Myc-ZmGSK4*) and Cab1

(P_{TDH3}::*GFP-Cab1*$_{28-113}$) were amplified as two independent constructs with compatible overhangs and cloned in pGBKT7 final vector. AtBin2 and mCherry are also cloned by the same method. The Gal4 activation domain of the prey vector pGG446 was fused to the AtPRP38. Yeast transformation and mating were performed based on the Y2H method.

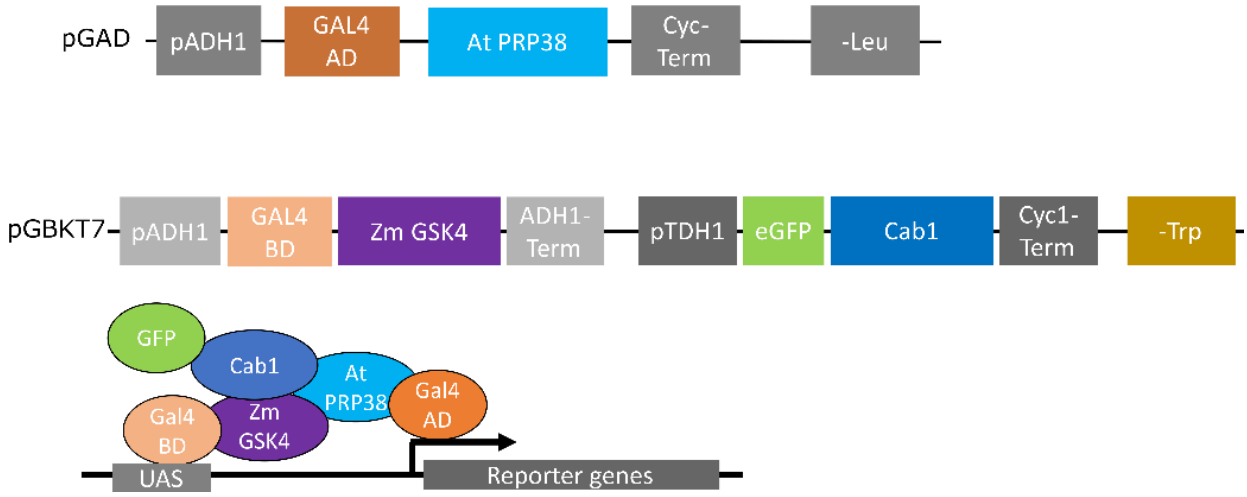

Figure 4-2 The schematic representation of the Y3H method

to investigate the direct interaction of Gal4DB-ZmGSK4 and Gal4AD-AtPRP38 in presence of Cab1, Gal4BD-ZmGSK4-GFP-Cab1 (P_{ADH1}::Gal4BD-Myc-ZmGSK4-P_{TDH3}::GFP-Cab1$_{28-113}$) construct was cloned in pBGKT7 bait vector Y187, whereas AtPRP38 was cloned into pGADT7 (P_{ADH1}::Gal4AD-HA-AtPRP38) activation vector and transformed into the yeast strain AH109 and transformed into the yeast strain. Diploid yeast after mating, containing both plasmids, were used for further investigation.

4.15 Biochemical Methods

4.15.1 Processing of yeast cells for Western blot

For western blot analysis of the yeast cells, mated yeast cells were processed via the following protocol, and after blotting, the membrane was subjected to proper antibodies to confirm the expression of proteins.

1. The cells were grown on 2ml -SD -LT liquid culture overnight

2. Pellet the cells 1min centrifuge full speed and remove the media
3. Incubate the cell in 200 ul 0.4M NaOH and add 20-30 glass beads per tube
4. Shake the tubes 2min 1500 rpm at room temperature
5. Pellet the cells 1min centrifuge full speed and remove the supernatant
6. Resuspend the pellet in 20 µl 4x SDS sample buffer + 50mM DTT + 26µl/ml β–mercaptoethanol 14.3 M + 60 µl 6M urea
7. Boil the samples 5min 95 °C
8. Pellet 1min full speed
9. Collect supernatant in new tube and store them on ice
10. The samples were separated on the acrylamide gel

10ml 4x SDS sample buffer: 2.5 ml 1 M Tris-HCl pH 6.8, 0.5 ml of ddH20, 1.0 g SDS, 0.8 ml 0.1% Bromophenol Blue, 4 ml 100% glycerol, 2 ml 14.3 M β-mercaptoethanol (add fresh from 100% stock)

4.15.2 Processing of plant materials for Western blot

To confirm the expression of induced proteins in *A. thaliana* transgenic lines and infected *N. benthamiana* leaves via *A. tumefaciens*, the samples were prepared in the following steps:

1- 50mg of plant materials were collected in 1.5 Epi
2- Add 120µl of 6M Urea RT
3- Grind the samples with the tissue grinder
4- 40µl of 4x SDS sample buffer and mix gently
5- Boil the samples 95°C 10min
6- Leave the samples at room temperature 5min
7- Spin down the samples 10 min full speed

10ml 4x SDS sample buffer: 2.5 ml 1 M Tris-HCl pH 6.8, 0.5 ml of ddH20, 1.0 g SDS, 0.8 ml 0.1% Bromophenol Blue, 4 ml 100% glycerol, 2 ml 14.3 M β-mercaptoethanol (add fresh from 100% stock)

4.16 SDS PAGE

To separate protein extracts according to their molecular weight SDS PAGE (sodium dodecyl sulfate-polyacrylamide gel electrophoresis) was conducted (Laemmli, 1970). Here, the separation of proteins takes place in vertical bis-acrylamide gels. To prepare the protein samples, they were denatured by adding SDS loading dye and boiling them for 10 min. The ionic detergent SDS unfolds proteins and binds to them with its hydrophobic domains. Thereby the whole protein becomes negatively charged and can be separated in an electric field according to its size. The loading dye contains DTT and β-mercaptoethanol as reducing agents.

Electrophoresis was performed with a constant current of 20-25 mA per gel immersed in SDS running buffer. As a size standard, the PageRuler, Protein Ladder (Bio-Rad) was used.

Resolving Gel: 10.0% (w/v) Acrylamide/Bisacrylamide, 300 mM Tris/HCl pH 8.8, 0.08% (w/v) sodium dodecyl sulfate (SDS), 0.03% (v/v) N,N,N',N'-Tetramethylethylenediamine (TEMED), 0.02% (w/v) ammonium persulfate (APS)

Stacking Gel: 4.00% (w/v) Acrylamide/Bisacrylamide, 125 mM Tris HCl, pH6.8, 0.10% (w/v) SDS, 0.08% (v/v) TEMED, 0.03% (w/v) APS

SDS running buffer: 192 mM Glycine, 25 mM Tris HCl pH8.3, 4.0 mM SDS

4.17 Western Blot Analysis

Protein mixtures can be qualitatively analyzed with the help of specific protein-ligand interactions. To do so proteins separated by SDS PAGE were transferred onto the Nitrocellulose membrane by Western blot (Towbin et al., 1979). Afterward, the proteins were analyzed using specific antibodies.

4.17.1 Western blot:

In the following the blotting procedure is explained. After SDS PAGE, the Nitrocellulose membrane was placed on four filter papers. The acrylamide gels were placed on the equilibrated filter paper. On top of the gel, 4 filter papers were placed and the cassette

got closed. Afterward, the cassette was placed into a machine, and the preset program was selected based on protein's molecular weight.

Blotting buffer: 200ml 5x Bio-Rad transfer buffer, 200ml absolute Ethanol, 600ml ddH_2O

4.17.2 Immunodetection of proteins

To identify specific proteins in complex protein extracts, they can be transferred onto Nitrocellulose membranes and detected by specific antibodies. Before detection, however, areas on the membrane not carrying proteins have to be blocked with an unspecific protein that will not be detected by the antibody. Therefore, the membrane is immersed in a blocking buffer and put on a rocking tray for at least one hour at room temperature. Superfluous blocking buffer is removed by washing the membrane three times with 1x TBST for five minutes.

Next, the primary antibody solution is added to the membrane and left for incubation at 4°C ON. Before the addition of the secondary antibody, the membrane is washed three times for five minutes with TBST to remove unbound primary antibodies. After incubation with the secondary antibody for at least one hour, the membrane was washed three more times using TBST and then developed using the Bio-Rad ChemiDoc system.

TBST, pH 7.5: 150mM sodium chloride, 50mM Tris, 0.1% (v/v) Tween 20

Blocking buffer: 1x TBST, 5% Milk (or Bovine Serum Albumin)

4.18 Methods involving plants:

4.18.1.1 Plant and pathogen material and growth conditions

The maize varieties EGB (Early Golden Bantam) and B73 were used in this study. The sequenced maize line B73 was chosen for making cDNA and cloning, while maize EGB line plants were used for the secretion assay, bombardment, and virulence assays with *U. maydis* knockout (KO) strains followed by disease scoring (Kämper et al., 2006). The plants were grown under controlled glasshouse conditions with a photoperiod of 16 hours of light at 28 °C and 8 hours of darkness at 22 °C and watered every 5 days. Specific methods will be further described below.

A. thaliana (ecotype Columbia-0), all *A. thaliana* transgenic lines, and *Nicotiana benthamiana* was grown in a growth chamber under 8 h: 16 h, light: dark cycle at 21 °C and 60% humidity. *A. thaliana* and *N. benthamiana* plants were watered by flooding every 3 days.

The solopathogenic *U. maydis* strain SG200 (Kämper et al., 2006) was the progenitor strain used to generate all the gene-replacement mutants and knockout strains by homologous recombination. All the strains were grown in YPD plates or broth supplemented with 100 µg/mL Ampicillin and appropriate selective agent at 28 °C, liquid cultures were shaken at 180 rpm.

4.18.1.2 Cab1 secretion assay

To visualize Cab1 secretion *in planta,* the predicted signal peptide (first 27 amino acids (Krogh et al., 2001)) was fused with the C-terminal mCherry. Expression was driven by a strong biotrophy-induced *cmu1* promoter (Djamei et al., 2011) and transgene was integrated into the *ip* locus of the solopathogenic *U. maydis* strain SG200 (Kämper et al., 2006). Three independent transgenic SG200 strains carrying the secretion construct (P_{cmu1}::Cab1$_{1-27}$-mCherry) were implemented for infection of 7-day-old *Z. mays* EGB plants and were grown under controlled conditions. At 4 dpi, plant leaf slices were collected and confocal microscopy was used to visualize the secretion. The mCherry without the attached signal peptide (P_{cmu1}::mCherry) was used as a negative control.

4.18.1.3 *U. maydis* knockout strains and mutants

To create cluster 5A knockout strains (Kämper, 2004). The flanking regions of the cluster, encompassing approximately 1 kb upstream of UMAG_02192 and 1 kb downstream of UMAG_02196, were cloned into the plasmid pGAM1311. In a similar manner, a knockout mutant of Cab1 was produced. This involved cloning regions approximately 600 bp before and 600 bp after Cab1 into the plasmid puko. This strategy allowed us to create the desired genetic modifications. For the Cab1 overexpression strain, full-length Cab1 was cloned under the *Pit2* strong biotrophic promoter (Doehlemann et al., 2011) and the Cab1 (P_{Pit2}::Cab1-3xHA) fusion construct was integrated into the *ip* locus *U. maydis* solopathogenic strain SG200 (Kämper et al., 2006).

4.18.1.4 Maize infection assay and scoring

Three independent biological replicates were performed for each transgenic strain. *U. maydis* strains were grown in YEPSL (0.4% yeast extract, 0.4% peptone, 2% sucrose). Cell suspensions in H_2O were adjusted to OD600=1.0. These suspensions were then injected into the stems of 7-day-old EGB maize seedlings using a syringe, as described by Kämper et al. (2006). The scoring was performed at 12 dpi. The infection symptoms were classified based on the disease rating proposed by Kämper et al. (2006) with slight modifications in the different gall categories. Additionally, the categories of "no symptoms," "stunted," and "dead" were included along with the five previous categories of "chlorosis," "small galls," "normal galls," "big galls," and "heavy galls" (Kämper et al., 2006). The disease index was calculated using Wilcoxon test analysis in R, with the *U. maydis* strain SG200 applied as the reference (Navarrete et al., 2022; Navarrete, Grujic, Stirnberg, Saado, et al., 2021; Saado et al., 2022; Stirnberg & Djamei, 2016) .

4.18.1.5 Molecular cloning

All gene models and the corresponding accession number employed in this study are documented in Table 5-1. All the plant and yeast expression plasmid constructs were generated via standard molecular procedures (R. Green & Sambrook, 2012) by using either Greengate (Lampropoulos et al., 2013) or Gateway cloning (Katzen, 2007). All the employed plasmids were cloned in Mach1 (Thermo Fisher Scientific, Waltham, MS, USA) cells and grown in dYT liquid medium or on YT agar plates supplemented with the appropriate antibiotic.

row	Gene Model	name	MaizeGDB name	B73 RefGen_v3	Aminoacid length	Clade	Plant
1	Zm00001d009055	ZmGSK2	gsk10 - glycogen synthase kinase10	M2G075992, GRMZM6G7	407 aa	I	Zea mays
2	Zm00001d024729	ZmGSK5	gsk7 - glycogen synthase kinase7	GRMZM2G155836	410 aa		
3	Zm00001d040263	ZmGSK9	gsk6 - glycogen synthase kinase6	GRMZM5G835235	377 aa		
4	Zm00001d008357	ZmGSK???-M1	gsk5 - glycogen synthase kinase5	GRMZM2G024151	422 ss		
5	Zm00001d016188	ZmGSK4	gsk3 - glycogen synthase kinase3	GRMZM2G151916	409 aa	II	
6	Zm00001d008893	ZmGSK1	gsk2 - glycogen synthase kinase2	GRMZM2G472625	406 aa		
7	Zm00001d039407	ZmGSK8	gsk1 - glycogen synthase kinase1	GRMZM2G045330	429 aa		
8	Zm00001d037010	ZmGSK7	bak3 - brassinosteroid insensitive1-associated receptor kinase like3	GRMZM2G043350	357 aa		
9	Zm00001d053548	ZmGSK11	gsk4 - glycogen synthase kinase4	GRMZM2G121790	423 aa		
10	Zm00001d029664	ZmGSK6	gsk8 - glycogen synthase kinase8	GRMZM2G131853	422 aa	III	
11	Zm00001d048564	ZmGSK10	gsk9 - glycogen synthase kinase9	GRMZM2G109624	470 aa		
12	Zm00001d012869	ZmGSK3	gsk11 - glycogen synthase kinase11	GRMZM2G138676	466	IV	
13	At5g26751	AtSK11	SHAGGY-RELATED KINASE 11		405 aa	I	Arabidopsis thaliana
14	At3g05840	AtSK12	SHAGGY-LIKE KINASE 12		409		
15	AT5G14640	AtSK13	SHAGGY-LIKE KINASE 13		410		
16	AT4G18710	AtSK21/BIN2	BRASSINOSTEROID-INSENSITIVE 2		380	II	
17	AT1G06390	AtSK22/BIL2	SHAGGY-LIKE PROTEIN KINASE 22		407		
18	AT2G30980	AtSK23/BIL1	SHAGGY-LIKE PROTEIN KINASE 23		412		
19	At3g61160	AtSK31	SHAGGY-LIKE PROTEIN KINASE 31		438	III	
20	At4g00720	AtSK32	SHAGGY-LIKE PROTEIN KINASE 32		472		
21	At1g09840	AtSK41	SHAGGY-LIKE PROTEIN KINASE 41		421	IV	
22	At1g57870	AtSK42	SHAGGY-LIKE PROTEIN KINASE 42		443		
23	At2G40650	PRP38	PRP38 family protein		355 aa		
24	Umag02193	UmCab1	uncharacterized protein		113 aa	Ustilago maydis	

Table 4-1 The accession numbers of the genes mentioned in this study

4.19 Biolistic transformation of maize

Leaves of 12-d-old maize were transiently transformed using 1.0 µm gold particles coated with 7 µg of each plasmid DNA delivered with the biolistic particle system (BioRad) and the details were described previously in (Djamei et al., 2011). Fluorescence emission was captured 1 day after transformation by confocal microscopy.

Biolistic bombardment materials:

1- $Ca(NO_3)_2$ 23.61gr/100ml H_2O, pH=10 (KOH), autoclave, store at 4°C

2- Gold particles prepared in 80% glycerol and stored in -20°C (for long-term storage).

3- Biolistic rupture disks (Cat: 1652328) 900 PSI

4- Biolistic Microcarriers (Cat: 1652335) (it should be washed in 100% Ethanol and dry on tissue paper)

Coating the gold particles with plasmid DNA:

The gold particles will get mixed with plasmid DNA in the following amounts:

7µl DNA (1µg/ul) + 87.5 µl Gold suspension + 94.5µl Ca $(NO_3)_2$

- $Ca(NO_3)_2$volume = DNA + Gold volume

1- mix DNA and gold in 1.5 Epi and mixed by tapping
2- Put the tube on the vortex and drop the proper amount of Ca $(No_3)_2$
3- Leave the samples at RT for 10 min (tap the tubes every 2 min)
4- Centrifuge 15sec 14000rpm
5- remove the supernatant
6- add 500ul 70% ethanol and invert at least 3 times
7- Centrifuge 15sec 14000rpm
8- Remove the Ethanol
1- add 500µl 99.6% Ethanol and invert the tubes 3x
2- Centrifuge 15sec 14000rpm
3- Remove the Ethanol
4- Add 30µl Ethanol 99.6% and perform the bombardment based on manufacturer protocol.

4.20 Agrobacterium-mediated transient expression of tobacco

For localization experiments *N. benthamiana* plants were transiently transformed using *A. tumefaciens* GV3101 (pSoup) mediated transformation. This was done using the protocol below:

1. Inoculate your Agrobacterium cultures in 8 mL liquid dYT containing the appropriate antibiotics.
2. Measure the cultures' optical density and pellet your cells by centrifugation (3000g, 10 min, RT). Discard the supernatant. Re-suspend the cells to an OD of 0.4 in

Agrobacterium resuspension medium (ARM). If you want to co-transform your tobacco plants using several Agrobacterium strains, optical density has to be adjusted so that in the final culture each strain has an OD of 0.4.

3. Incubate the cultures at RT for 3-24h.
4. Mix the cultures and infiltrate the suspension into *N. benthamiana* plants grown under short-day conditions at 22°C. Young plants at the 4-6 leaf stage are ideal.
5. Harvest infiltrated tissue three days post infiltration for microscopy or protein expression 2-3 days post induction.

ARM buffer: 10 mM MES NaOH pH5.6, 10mM $MgCl_2$, 0.15 mM Acetosyringone

4.20.1 Subcellular localization

To elucidate the subcellular localization of Cab1 in different plant overexpression systems. $Cab1_{28\text{-}113}$ was N-terminally tagged with mCherry under the strong 35S cauliflower mosaic virus (CaMV) promoter (*P_{35S}::mCherry-$Cab1_{28\text{-}113}$*). The construct were expressed in the *N. benthamiana* leaves via *Agrobacterium tumefaciens* strain GV3101 transformation. The samples were subjected for confocal microscopy 3 days-post infection. We have overexpressed the same cab1-mcherry fusions construct in *Z. mays* cells using biolistic transient expression and microscopy was performed 1 day post infection.

4.21 Bimolecular fluorescence complementation assay

AtBIN2 or ZmGSK4, and $Cab_{28\text{-}113}$, were fused either the C-terminal half of Venus (cVenus) or the N-terminal half of Venus (nVenus) fluorescent proteins, respectively, as previously described (Gookin & Assmann, 2014; Navarrete et al., 2022). Protein expression was driven by the constitutive 35S promoter and co-infiltration of these constructs was performed in the epidermal cells of *N. benthamiana*. Confocal microscopy was carried out three days post-infiltration. As negative control, NLS-luciferase-nVenus was co-expressed with ZmGSK4-cVenus, and microscopy was performed under the same experimental conditions.

4.22 SplitTurboID

4.22.1 SplitTurboID proof of concept

TurboID string splits into two low-efficiency fragments (Cho et al., 2020). N-terminal fragment tagged to Cab1-N-SplitTrubo (*P_{35S}::Cab1$_{28-113}$-V5-N-SplitTurbo$_{1-72}$*) while the c-terminal fragment tagged to AtBin2-C-SplitTrubo (*P_{35S}::AtBin2-HA-C-SplitTurbo$_{73-319}$*) .

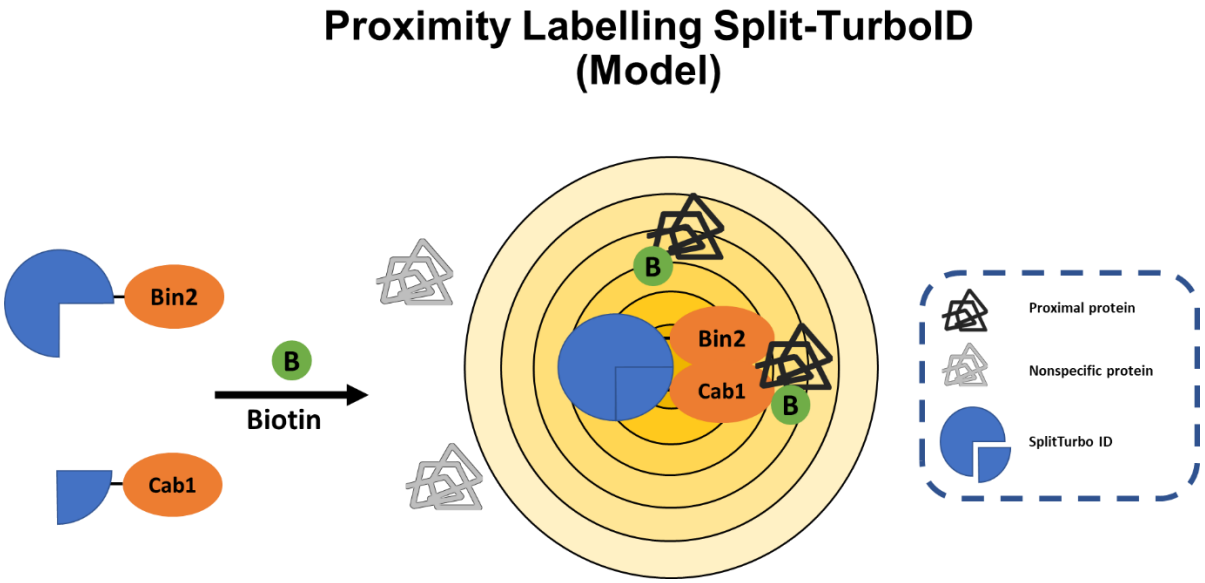

Figure 4-3 SplitTurboID proximity labeling

Based on the publication, TurboID string splits into two low-efficiency fragments. The N-terminal fragment tagged to Cab1-N-SplitTrubo (*P_{35S}::Cab1$_{28-113}$-V5-N-SplitTurbo$_{1-72}$*) and the C-terminal fragment tagged to AtBin2-C-SplitTrubo (*P_{35S}::AtBin2-HA-C-SplitTurbo$_{73-319}$*). In this methode, when two bait proteins are physically interacted with each other in the cell, the TurboID complex will form and become activated, in the results of forming the fuctional complex, the neighboring proteins get biotinylated.

Both constructs were transformed in Agrobacterium GV3101 and co-infiltrated in *N. benthamiana* epidermal cells. Biotin (25 µM) infiltrated in epidermal cells 36 hours post-Agrobacterium infiltration and samples were collected at 6hpi in liquid nitrogen. Total protein extracted in SDT-lysis buffer (100 mM Tris pH 7.5, 4% SDS, 0.1M DTT), total protein concentration adjusted 1 mg/ml in all samples by Bradford and precipitated with Phenol/chloroform method. After the methanol washing step, the samples were resuspended in binding buffer (0.1 M phosphate, 0.15 M NaCl, 0.5 % SDS, pH 7.2) and

incubated with Streptavidin Mag Sepharose beads (Cytiva 28985799) overnight. Magnetic beads were washed with buffer I (0.1 M phosphate, 0.15 M NaCl, 2 % SDS, pH 7.2) three times and buffer II (: 0.1 M phosphate, 0.15 M NaCl, pH 7.2) one time, then processed with MS. mCherry-SplitTurboID and AtBin2-UltraID samples were processed in parallel and subtracted from Cab1-SplitTurboID samples.

4.22.2 Pull down and biotinylation Assay

Agrobacterium tumefaciens GV3101 contains Myc-PRP38 (*P_{35S}::3xMyc-AtPRP38*) with Cab1-N-SplitTurbo (*P_{35S}::Cab1$_{28-113}$-V5-N-SplitTurbo$_{1-72}$*) and AtBin2-C-SplitTurbo (*P_{35S}::AtBin2-HA-C-SplitTurbo$_{73-319}$*) infiltrated in *N. benthamiana* leaves.

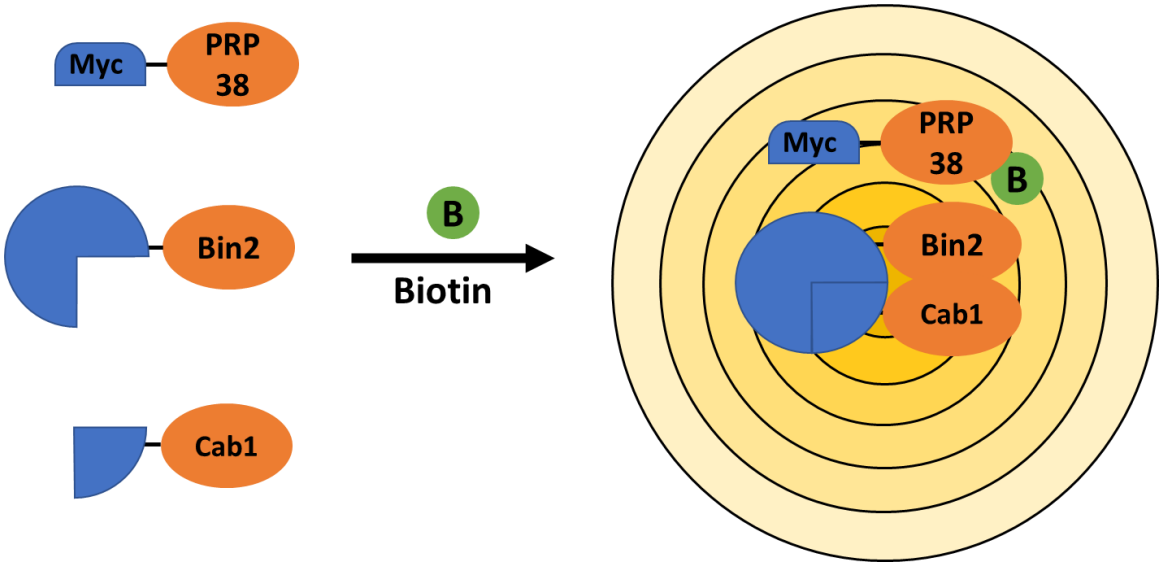

Figure 4-4 AtPRP38 got biotinylated by AtBin2 in the presence of Cab1

TurboID string splits into two low-efficiency fragments and tagged to Cab1-N-SplitTrubo (*P_{35S}::Cab1$_{28-113}$-V5-N-SplitTurbo$_{1-72}$*) and AtBin2-C-SplitTrubo (*P_{35S}::AtBin2-HA-C-SplitTurbo$_{73-319}$*), AtPRP38 (*P_{35S}::3xMyc-AtPRP38*) tagged with 3xMy and 3 three constructs were co-expressed transiently in *N. benthamiana*. Bait proteins physically interact with each other, the complex will become activated and biotinylate AtPRP38 when it is in neighboring of the bait proteins.

Biotin (25uM) infiltrated in epidermal cells 36 hours post-Agrobacterium infiltration and samples were collected at 6hpi in liquid nitrogen. mCherry-N-SplitTrubo (*P_{35S}::mCherry-V5-N-SplitTurb*) replaced with Cab1-N-SplitTrubo (*P_{35S}::Cab1$_{28-113}$-V5-N-SplitTurbo*) in the control. IP on biotinylated samples was performed using µMACS™ Micro Beads

system from Miltenyi Biotech (Bergisch Gladbach, Germany) according to the manufacturer protocol. The elution run on the gel, the blot was blocked with 5% BSA in 1X TBST buffer solution and developed with Myc and Streptavidin-HRP antibodies separately.

4.23 Immunoprecipitation assay in *N. benthamiana*

Agroinfiltration of GFP-Bin2 (P_{35S}::GFP-AtBin2) and mCherry-Cab1 (P_{35S}::mCherry-$Cab1_{28-113}$) constructs under the control of the strong 35S cauliflower mosaic virus (CaMV) promoter was performed for co-immunoprecipitation experiments. The constructs were infiltrated into *N. benthamiana* leaves. The leaves were harvested 3 days post-infiltration (dpi) and frozen directly in liquid nitrogen prior to further processing. Co-IP was conducted using μMACS™ Micro Beads system from Miltenyi Biotech (Bergisch Gladbach, Germany) following the manufacturer's protocol. The immunoprecipitated proteins were detected with anti-GFP and mCherry rabbit antibodies according to the manufacturer's protocol. The experiments were repeated independently at least two times.

4.24 Standard operating procedure for *H. schachtii* infection assays:

The cyst-forming assay was conducted following a standard protocol (M. Huang et al., 2021). Briefly, surface-sterilized mCherry-$Cab1_{28-113}$ ($P_{35S\text{-}XVE}$::mCherry-$Cab1_{28-113}$) *A. thaliana* seeds were subjected to vernalization on KNOP-medium at 4°C. The plates were then transferred to the climate chamber under a red/blue light source, maintaining the 16-h/8-h light/dark photoperiod at 24 °C. After 12 days of growth, mCherry-$Cab1_{28-113}$ were transferred on induction plates containing 10 μM β–Estradiol, 12 days post germination. For nematode propagation, *Sinapis alba* was used, and each plant was subjected to 60 active freshly hatched second-stage juveniles (J2s) nematodes. The infection rate was measured by the number of syncytia formed 14 day-post infection.

1- Maximum plants per petri dish: 2 plants
2- Minimum number of petri dishes per genotype: 5 i.e. n=10
3- Inoculation rate: 60 per plant – minimum: 50 (count active ones)
4- Number of females in Col-0 for reliable analysis: 5-15/plant

5- Age of plants for inoculation: 10-12 days
6- Counting of nematodes: 12 dpi
7- Measuring female size and syncytium size: 14 dpi
8- Optional: measure final size at 28 dpi
9- Minimum number of females and syncytium for reliable size measurement: 30 per repetition
10- Please always sterilize nematodes with 0.05% $HgCl_2$ for a maximum 5 min
11- Please wash the nematodes vigorously with autoclave ed water (not necessarily dH_2O) at least 4 times

Statistics:

1- Experiment conducted with a minimum of three independent repetitions.
2- A significance level of p-value < 0.05 should be used.
3- If there is only one treatment, the Student t-test should be employed. If there are multiple treatments, analysis of variance (ANOVA) or Fisher's LSD test should be utilized.
4- Statistical analyses should be conducted separately for each individual experiment.

4.25 BES1- phosphorylation

BES1-GFP (*P_{35S}::GFP-BES1*) was co-infiltrated with GR-Cab1$_{28\text{-}113}$ (*$P_{35S\text{-}XVE}$::GR-V5-Cab1$_{28\text{-}113}$*) in *N. benthamiana* leaves. At 3dpi, we subjected the samples to 30µM β–Estradiol to induce the expression of the constructs and waited for 6 hours. The samples were collected before and after Dexamethasone infiltration at 0, 15-, 30-, and 60 minutes post-treatment in liquid nitrogen. The total protein was extracted via 1x SDS sample buffer and the expression was checked via GFP and V5 antibodies. In the control sample, GR-mCherry ($P_{35S\text{-}XVE}$::GR-V5-mCherry) was substituted with GR-Cab1 and subjected to the same treatment. The GR-mCherry samples were examined using confocal microscopy to test the functionality of the GR-V5 tag in preventing the proteins from entering the nucleus in the absence of Dexamethasone.

4.26 Hek293T and Hela Transfection:

The cells were grown under the standard conditions at 37^{o}C and 5% CO_2 concentration. The RPMI1640 and DMEM full media were used for Hela and Hek293T cells respectively. the transfection was performed via Lipofectamine 2000 based on manufacturer protocol at 95% confluency. The cells were subjected to microscopy and Co-IP 2 days post-transfection.

5 Results

5.1 Identification of cabbage phenotype caused by overexpression of Umag02193 in *A. thaliana*.

In previous studies, it was shown some of *U. maydis* effectors target conserved host proteins even in non-host plants, using evolutionary conserved mechanisms to manipulate host cellular processes and promote infection (Darino et al., 2021; L. Huang et al., 2023; Khan et al., 2023; Navarrete et al., 2022; Saado et al., 2022). A library of more than 200 *U. maydis* effector lines was generated in the Djamei laboratory before I joined as a technical assistant in the Djamei laboratory. Each *A. thaliana* transgenic line carries an expression construct contains both secreted and non-secreted of an *U. maydis* effector ($P_{35S\text{-}XVE}$::$SP_{\alpha\text{-}Amylases}$-Effector-3xHA-P2A-2xMyc-Effector) under the β−Estradiol inducible promoter. The P2A sequences cause ribosomal “skipping” during translation and effectively separates the two secreted and non-secreted proteins that were transcribed in one mRNA strand (Park et al., 2016). A screening scheme had been established by others and I performed a phenotypic screen of 258 transgenic lines that led among others to the identification of a cabbage-like phenotype upon Umag02193 overexpression. This was the starting point of my thesis to focus on the functional characterization of Cab1, the effector presented the impaired growth and development phenotype.

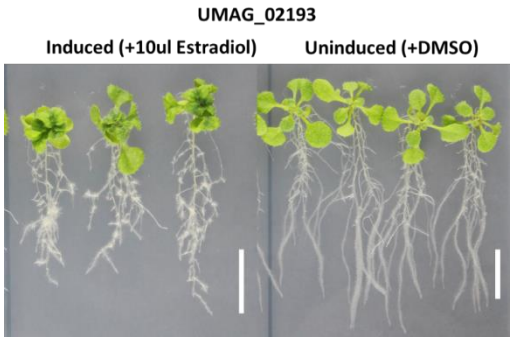

Figure 5-1 Umag_02193 expression causes dwarf cabbage-like leaves in A. thaliana seedlings.

Transgenic *A. thaliana* line expressing both secreted and non-secreted Cab1 ($P_{35S\text{-}XVE}$::$SP_{\alpha\text{-}Amylases}$-$Cab1_{28\text{-}113}$-3xHA-P2A-2xMyc-$Cab1_{28\text{-}113}$), 5 dpg moved to the induction $^1/_2$MS plates containing 10µM β−Estradiol solved in DMSO and phenotyping was done 10 dpi. The control

plates contain the solvent only (DMSO). dpg: days post germination. dpi: days post-induction. Scale bar = 1 cm.

5.2 Characterization of *U. maydis* effector (Cab1) that causes a Cabbage-like phenotype in *A. thaliana* seedlings

5.2.1 Physiological impact of Cab1 on *A. thaliana* growth and development

Cab1 exhibited a strong phenotype in shoots and roots. In the results of Cab1 expression, the expansion of leaves on both the abaxial and adaxial sides became uneven, resulting in a curly appearance. Moreover, the growth of the main axes root was suppressed, while the lateral and hairy roots showed induction, which became more pronounced with long-term induction. At 14dpi, the roots appeared shorter and bunchier compared to the uninduced effector overexpression line and the Col-0 lines. Based on this observation, I named this candidate effector Cabbage 1 (Cab1) (Fig. 6-2 A). Additionally, we examined the expression of the N-terminally epitope-tagged HA-Cab1$_{28\text{-}113}$ by western blot analysis, comparing β–estradiol-induced and uninduced plants (Fig. 6-2 B).

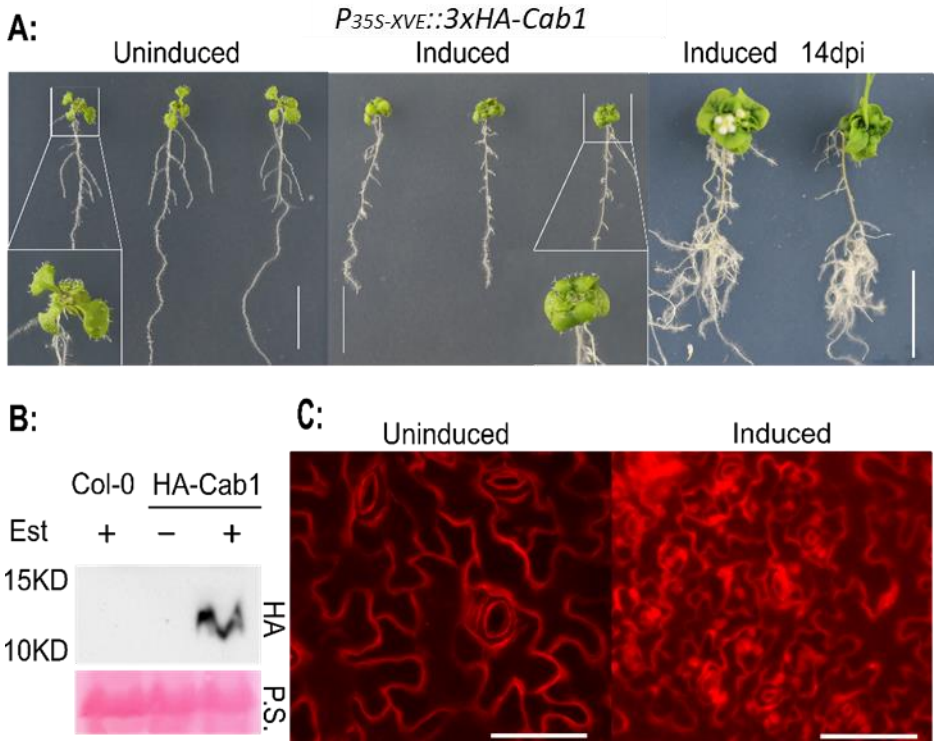

Figure 5-2 Cab1 causes a dwarfed phenotype in A. thaliana by manipulating the cellular development

A. Transgenic *Arabidopsis thaliana* line expressing non-secreted Cab1 ($P_{35S\text{-}XVE}$::3xHA-Cab1$_{28\text{-}113}$), 7 dpg moved to the induction $^1/_2$MS plates containing 10μM β–Estradiol solved

in DMSO and phenotyping was done 5 and 14 dpi. The control plates contain the solvent only (DMSO). dpg: days post germination. dpi: days post-induction. Scale bar = 1 cm.

B. Immunoblotting analysis on Cab1 ($P_{35S\text{-}XVE}$::3xHA-Cab1$_{28\text{-}113}$) protein levels of seedling extracts from *A. thaliana* lines using anti-HA antibody. The expected band size of 14KDa is visible only in β–estradiol-induced seedlings. Ponceau staining was used as an indication of equal protein loading.

C. 14 days post-treatment, Propidium Iodide staining was performed on β–Estradiol-induced and uninduced seedlings, and the stained leaves were subjected to fluorescent microscopy by Pouria Bahrami. Scale bar = 50 µm.

A dwarf phenotype can be either achieved by a reduced number of cells in an organ or a reduction in cell expansion or by a combination of both. Therefore, I examined the number of cells and stomata per square centimeter in 3-week-old HA-Cab1$_{28\text{-}113}$ overexpressing plants (14 days post-β–Estradiol induction) and compared them with uninduced transgenic and Col-0 wild-type plants. After staining the cell walls of the tissue with propidium iodide, I observed that Cab1$_{28\text{-}113}$-expressing plants exhibited a significantly higher number of epidermal cells as well as of guard cells forming stomata per counted area compared to both the uninduced and Col-0 plants (Fig. 6-3). The Cab1 overexpression dwarf phenotype is therefore a result of a reduction in cell expansion whereas a reduction in cell number/reduction in cell divisions was not observable.

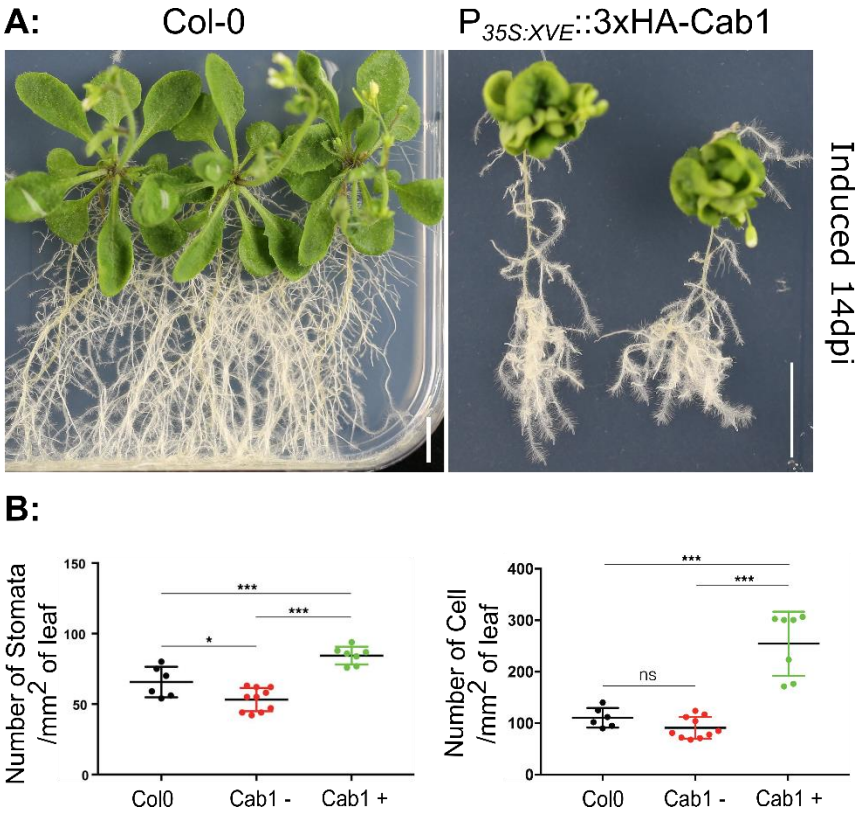

Figure 5-3 The Cab1 expression makes more cells and stomata per 1mm² of leaves.

A. Transgenic *Arabidopsis thaliana* line expressing non-secreted Cab1 ($P_{35S\text{-}XVE}$::3xHA-$Cab1_{28\text{-}113}$), 7 dpg moved to the induction $^1/_2$MS plates containing 10µM β–Estradiol and phenotyping was done 14 dpi. *A. thaliana* ecotype Col-0 was used as control. dpg: days post germination. dpi: days post-induction. Scale bar = 1 cm.
B. The stomata and cells were manually counted per 1cm² of the samples. After 14 days of Cab1 expression, there was an increased number of cells and stomata on the leaves compared to uninduced and Col-0 wild-type plants. Each data point represents the number of cells that were counted per microscopy picture. Statistical analysis was performed using GraphPad, and the significance levels were denoted as * for $p<0.05$ and *** for $p<0.001$, using ANOVA.

5.3 Cab1 is an *U. maydis* secreted protein located in cluster 5A

Cab1 is considered an effector candidate due to the presence of a predicted signal peptide and its position in the previously described potential effector cluster 5A on chromosome 5 of *Ustilago maydis* (Schirawski et al., 2010). Effector cluster 5A consists of five genes that encode predicted secreted proteins (Table 6-1, Fig. 6-4). The NCBI nucleotide and aminoacid blast did not show any similarity between the genes in cluster

5A of *U. maydis* and other fungi. However, synteny analysis reveals a structural similarity between Cluster 5A in *U. maydis* and chromosome 5 in *Sporisorium rellianum*. The nucleotide and amino acid alignments, although low in similarity, show UMAG_02196 aligns with SR10770, UMAG_10070 aligns with SR10769, and UMAG_02192 somehow aligns with SR10766. Consequently, I identified SR10767 as the potential synteny partner for Cab1 and/or Umag_02194. Further amino acid alignment demonstrates that SR10767 has a pairwise identity of 25.6% with UMAG_02194 and a pairwise identity of 21.1% with Cab1. This data, along with MEME and paraline analysis, supports the conclusion that UMAG_02194 should be considered as the potential ortholog of SR10767 in the case of synteny analysis.

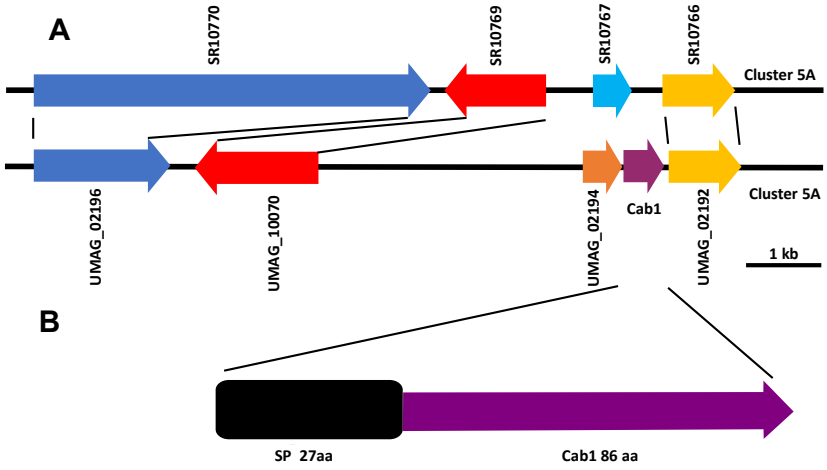

Figure 5-4 Schematic synteny representation of Sporisorium reilianum and U. maydis cluster 5A, Cab1-locus genomic organization.

- **A.** Gene organization of *Sporisorium reilianum* cluster 5 in comparison with *U. maydis* cluster 5a. Arrows indicate the direction of transcription. Color code represents genes with similar synteny in the genome. Based on amino acid and nucleotide alignment, Cab1 has no orthologue.
- **B.** Schematic representation of Cab1 genomic organization. As part of chromosome 5 cluster 5A, Cab1 consists of a 113 amino acid protein in which the first 27 amino acids comprise the N-terminal predicted signal peptide (SP) and the remaining 86 amino acids compose the predicted mature protein.

	Umag	Length	AA Length	phenotype in *A. thaliana*
1	Umag_02192	633 nt	210 aa	No
2	Umag_02193	342 nt	113 aa	Cabbage
3	Umag_02194	330 nt	109 aa	No
4	Umag_10070	1677 nt	558 aa	Not effector gene
5	Umag_02196	2037 nt	2037 aa	No

Table 6-1 cluster 5 A genes nucleotide and amino acid length

To assess Cab1 relative expression during disease progression, a typical feature for an effector would be a transcriptional upregulation. Cab1 expression in *U. maydis* during infection of maize seedlings in comparison to *U. maydis* grown in axenic culture was analyzed using published RNAseq data (Lanver et al., 2018). The Cab1 expression profile during its biotrophic lifecycle of *U. maydis* in maize shows an early transcriptional induction of Cab1 starting 12 hours post-infection, which further increased approximately 10-12-fold, peaking 4 dpi and staying at a similarly high level further till 12 days post-infection (Fig. 6-5).

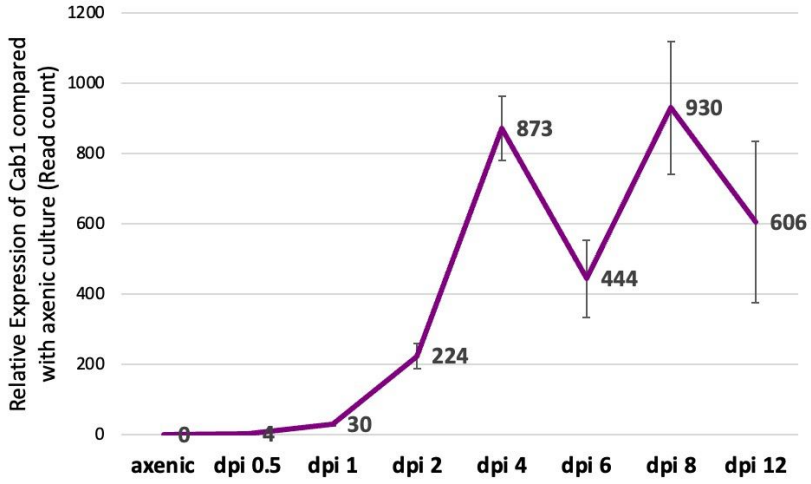

Figure 5-5 Transcriptional levels of Cab1 were calculated from RNAseq data at different time points during the biotrophic growth of U. maydis in maize seedlings.

Transcriptional levels of Cab1 were calculated from RNAseq data at different time points during the biotrophic growth of *U.* maydis in maize seedlings. Data was re-analyzed by previous Postdoc of the lab from the published paper of another group (Lanver et al., 2018).

5.4 mCherry fusion with Cab1 signal peptide localized to the biotrophic interface

Cab1 encodes for a protein of 113 amino acids, with the first 27 residues predicted to function as a signal peptide for secretion. Analysis of Cab1's protein sequence using BLAST revealed no similarities to any other proteins in the NCBI database (Sayers et al., 2022). Additionally, the MEME and AlphaFold online tools did not identify any conserved motifs, domains, or structural similarities in Cab1 (Bailey & Elkan, 1994; Jumper et al., 2021). To determine if the signal peptide of Cab1 is functional, I examined its activity using confocal microscopy during *U. maydis* infection in maize. For this purpose, we generated a construct in which the signal peptide of Cab1$_{1\text{-}27}$ was N-terminally fused to the fluorescent protein mCherry, controlled by the strong biotrophy-induced *Cmu1* promoter (Djamei et al., 2011). The expressing hyphae in the plant epidermis show, that the mCherry fluorescence signal accumulates around the tips and the edges of the hyphae, which is a characteristic location for secreted proteins, as previously demonstrated (Bindics et al., 2022; Darino et al., 2021; Djamei & Kahmann, 2012; Navarrete et al., 2022; Saado et al., 2022; Stirnberg & Djamei, 2016) (Fig. 6-6).

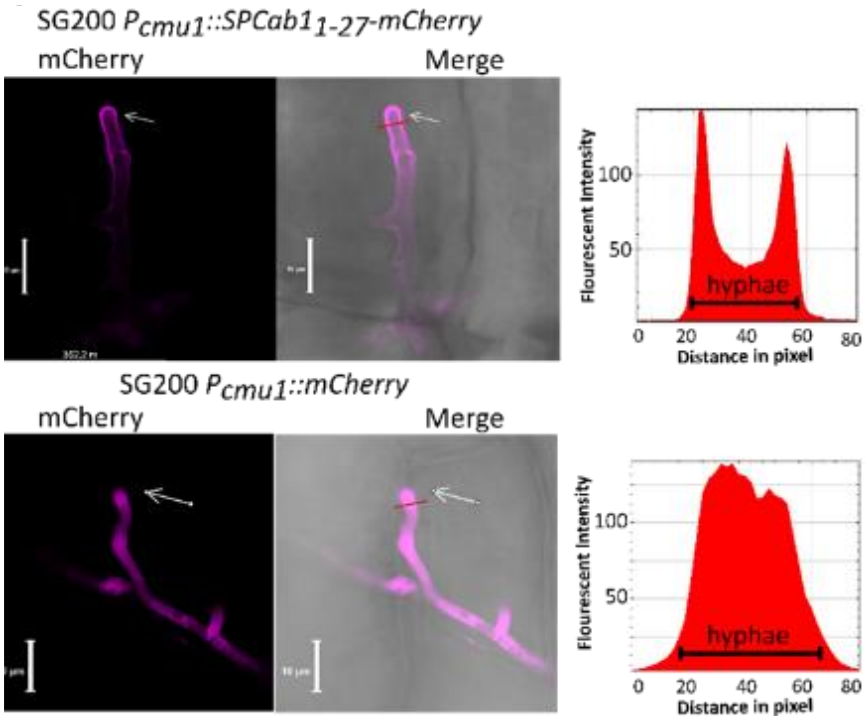

Figure 5-6 U. maydis in planta secretion of Cab1 in the Z. mays tissues.

U. maydis in planta secretion of Cab1 in the native host *Z. mays*. Maize cells infected with *U. maydis* strains expressing mCherry fusions of SP-Cab1 (*P_{cmu1}::SP-Cab1$_{1-27}$-mCherry*) or mCherry without signal peptide (*P_{cmu1}::mCherry*) under the control of *Cmu1* promoter. Confocal microscopy was performed 5 days post-infection. While secreted mCherry strongly accumulates at the cell periphery of the hyphae and hyphal tip (upper panel), localization of mCherry without signal peptide is evenly distributed within the hyphae (lower panel) as indicated with white arrows. Fluorescence intensity profiles the mCherry channel along the transection lines. Scale bar = 10 µm. Microscopy pictures captured by Kishor Ingole.

5.5 Cab1 is localized in the nucleus of the host cell

As the Cab1 overexpression phenotype in *A. thaliana* indicates a conserved plant target in the symplast, the subcellular localization of Cab1 was studied in different plant overexpression systems. Cab1$_{28-113}$ was N-terminally tagged with mCherry under the 35S promoter (P_{35S}::mCherry-Cab1$_{28-113}$). In maize, as the natural host for *U. maydis*, confocal microscopy reveals that mCherry-Cab1$_{28-113}$ localizes specifically in the nucleus of transformed epidermal cells (Fig. 6-7).

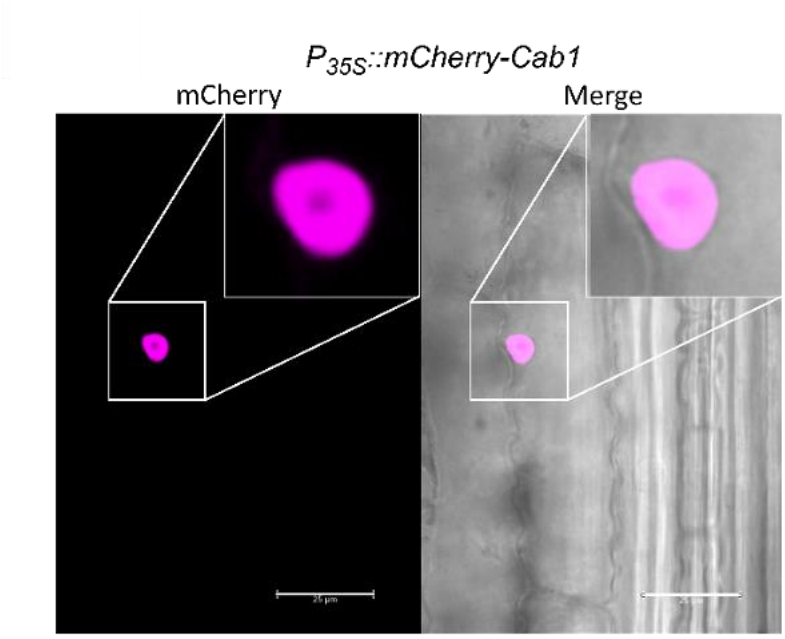

Figure 5-7 Localization of Cab1 (without signal peptide) in Z. mays.

Transient expression of mCherry-Cab1 (P_{35S}::mCherry-Cab1$_{28-113}$) via biolistic transformation in maize leaves was monitored by confocal microscopy. mCherry-Cab1$_{28-113}$ shows only nuclear localization. Scale bar = 25 µm. Microscopy pictures captured by Mamoona Khan-Djamei.

Moreover, Confocal microscopy of Agrobacterium-mediated transformed *N. benthamiana* plants with mCherry-Cab1$_{28\text{-}113}$ confirmed also in this system a solely nuclear localization (Fig. 6-8 A). Both In line with this also stable transgenic *A. thaliana* lines expressing N-terminally mCherry-tagged Cab1$_{28\text{-}113}$ under the β–Estradiol-inducible promoter (P$_{35S\text{-}XVE}$::mCherry-Cab1$_{28\text{-}113}$) show a specific nuclear mCherry signal under the confocal microscope both in roots and shoots (Fig. 6-8 B).

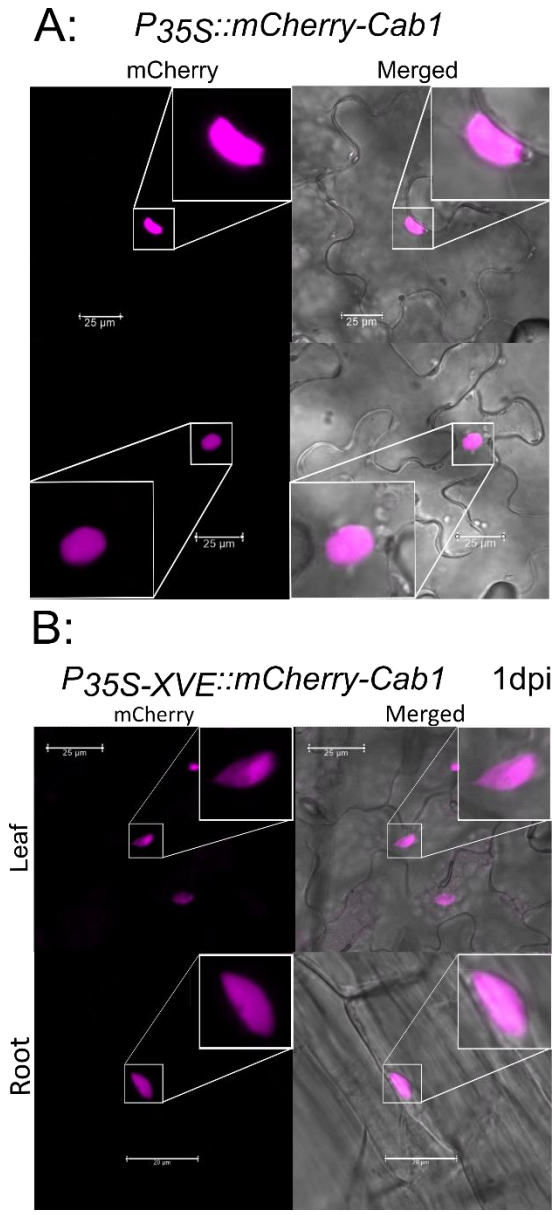

Figure 5-8 Cab1 shows nuclear localization.

A. subcellular localization of Cab1 in *N. benthamiana.* Transient expression of mCherry-Cab1 (*P$_{35S}$::3xHA-mCherry-Cab1$_{28\text{-}113}$*) in plant leaves was observed through confocal

microscopy. Cab1 is localized to the nucleus. Microscopy pictures captured by Kishor Ingole. Scale bar= 25µm.

B. Cab1 shows nuclear localization in *A. thaliana* shoot and root tissue. Expression mCherry-Cab1 (*$P_{35s\text{-}XVE}$::3xHA-mCherry-Cab1$_{28\text{-}113}$*) *A. thaliana* β–Estradiol-inducible transgenic lines were subjected to confocal microscopy 1 day post-induction. Microscopy pictures captured by Kishor Ingole. Scale bar=25µm.

5.6 Cab1 overexpression and cluster 5A deletion had no significant impact on *Ustilago* virulence

To investigate the role of Cab1 in disease establishment and progression, we created over-expression strains of Cab1 (P_{Pit2}::Cab1$_{1\text{-}113}$-3xHA) using the strong biotrophy-induced promoter *pit2*, and the Cab1 and cluster 5A deletion mutants in the solopathogenic strain SG200 background. Neither the cluster 5A (Δ 5A) and Cab1 deletion strains nor the Cab1 overexpression strains exhibited any significant differences in virulence compared to the parental SG200 strain (Fig. 6-9). These findings align with previous studies with the cluster 5A deletion mutant, which also showed no significant impact on virulence (Kämper et al., 2006).

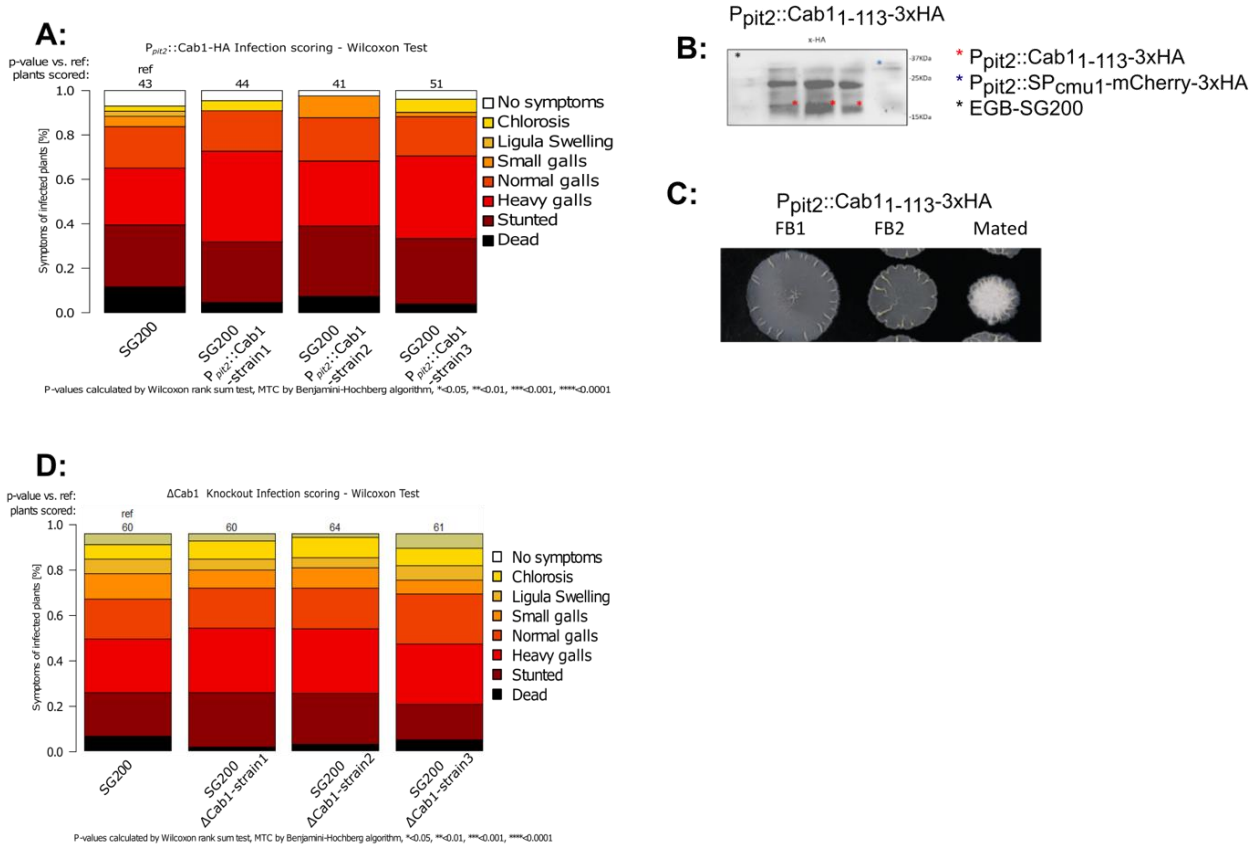

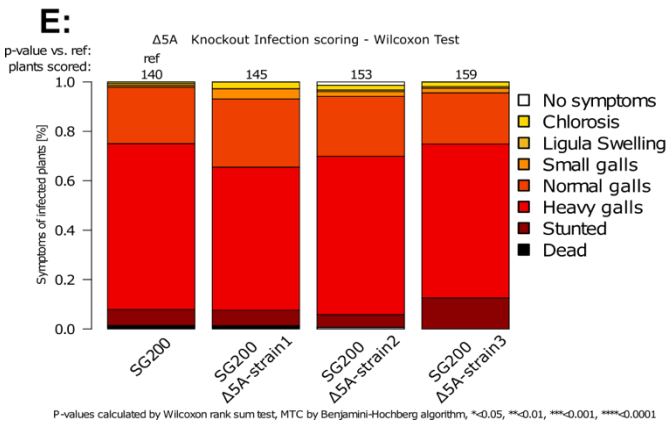

Figure 5-9 Neither Cab1 overexpression in U. maydis nor Cab1 or the cluster5A deletion strains show significant virulence defects in maize seedling infection assays.

A. Cab1 overexpression did not cause significant differences with respect to *U. maydis* virulence in comparison with SG200. Cab1 overexpression strains (P_{pit2}::$Cab1_{1\text{-}113}$-3xHA) were cloned under the strong biotrophy-induced promoter P_{pit2} and introduced into the *ip* locus solopathogenic *U. maydis* strain SG200. Three independent mutant strains were tested on 7-days old seedlings of the EGB maize line and scoring was performed 12 days post-infection (dpi). (* P < 0.05, ** P < 0.01, *** P < 0.001)
B. Immunoblotting analysis on Cab1 (P*pit2*::$Cab1_{1\text{-}113}$-3xHA) protein levels of infected maize leaf extracts using anti-HA antibody. The expected band size of 14KDa is visible in infected samples, mcherry-HA tagged and SG200 were used as negative control.
C. The drop assay revealed no failures in mating and filamentous formation among the Cab1 overexpression strains. The Cab1 (P_{pit2}::$Cab1_{1\text{-}113}$-3xHA) constructs were introduced into *U. may*dis strains FB1/FB2, and drop assays were performed on charcoal plates. These strains were able to mate and form filaments.
D. The deletion of Cab1 did not cause a significant reduction in *U. maydis* virulence in comparison to SG200 during maize seedling infections. The Cab1 mutants were generated in SG200. Three independent deletion strains were tested on 7 days old seedlings with EGB maize line and scoring was performed 12 dpi. (* P < 0.05, ** P < 0.01, *** P < 0.001)
E. The deletion of cluster 5A did not cause a significant reduction in *U. maydis* virulence in comparison to SG200 during maize seedling infections. The cluster 5A deletion mutants (Δ 5A) were generated in SG200. Three independent deletion strains were tested on 7-days old seedlings of the EGB maize line and scoring was performed 12 days post-infection (dpi). (* P < 0.05, ** P < 0.01, *** P < 0.001)

5.7 Mass-spectrometry was performed to find the Cab1 interactor in the host

Due to the dramatic phenotype upon $Cab1_{28\text{-}113}$ overexpression, we assumed that its plant-sided target is likely part of a highly conserved pathway found in dicots as well as monocots. Therefore, we used the transgenic *A. thaliana* lines expressing Myc epitope-

tagged Cab1$_{28\text{-}113}$ under the β−Estradiol-inducible promoter (*P$_{35S\text{-}XVE}$::Myc-Cab1$_{28\text{-}113}$*) for Co-immunoprecipitation followed by mass spectrometry analysis. As a negative control, plants expressing Myc-GFP were used. The results revealed a list of plant proteins associated with Cab1 (Table 6-3).

list of Cab1 potential interactor in Myc-Cab1 Co-IP				
Row	**Gene**	**Protein Name**	**Representative Gene Model**	**Score**
1	BIN2	Shaggy-related protein kinase eta	AT4G18710	2383.5
2	ATOZI1	ARABIDOPSIS THALIANA OZONE-INDUCED PROTEIN 1	AT4G00860	1131
3	SEX4	ATPTPKIS1	At3g52180	390
4	PSBN	PHOTOSYSTEM II REACTION CENTER PROTEIN N	ATCG00700	279
5	FKBP	FKBP-type peptidyl-prolyl cis-trans isomerase	At3g12345	248
6	NEET	CDGSH iron-sulfur domain-containing protein NEET	AT5G51720	232
7	LFNR1	LEAF-TYPE CHLOROPLAST-TARGETED FNR 1	AT5G66190	222
8	CIP1	COP1-interactive protein 1	AT5G41790	232

Table 6-3 list of Cab1 potential interactor in Myc-Cab1 Co-IP

To further investigate these associations, a yeast two-hybrid (Y2H) assay was conducted, and AtBIN2/shaggy-like kinase was identified as a direct interactor of Cab1 (Fig. 6-10).

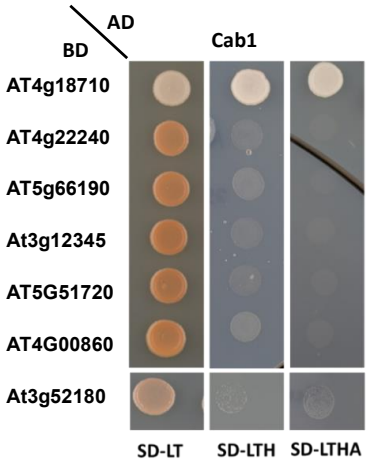

Figure 5-10 Cab1 directly binds to the AtBIN2 as the top potential interactor in MS-IP results

Based on the results from MS-IP (table 6-3), the potential interactors of Cab1 in *A. thaliana* were cloned into pGBKT7 bait vector and transformed into the yeast strain Y187, whereas Cab1 was cloned into pGADT7 activation vector and transformed into the yeast strain AH109. Diploid yeast after mating, containing both plasmids, were dropped on selective synthetic dropout media (SD) and yeast growth was monitored 3 days after spotting. Cab1 only interacted with AtBin2 and the matted cells showed growth on quadruple selection media, the experiment was repeated 3 times independently with comparable results.

5.8 Cab1 directly binds to all GSK3 clades of *Arabidopsis thaliana* and *Zea mays*

The GSK3 family in *A. thaliana* and *Z. mays* consists of 10 members which are divided into 4 clades (Table 5-1). To test the binding specificity of Cab1 to all members of the GSK3 family in *A. thaliana*, I conducted a Y2H assay with members of clade I, II, and IV of At-GSK3. In our experiment, Cab1 demonstrated a strong interaction with all 6 tested At-GSKs (Fig 6-11). This indicates that Cab1 potentially can interact with all clades of At-GSKs. To proceed with further experiments, we focused on Clade II as the primary representative of the GSK3 family in plants and the similarity of the Cab1 phenotype to the Bin2-D reported phenotype.

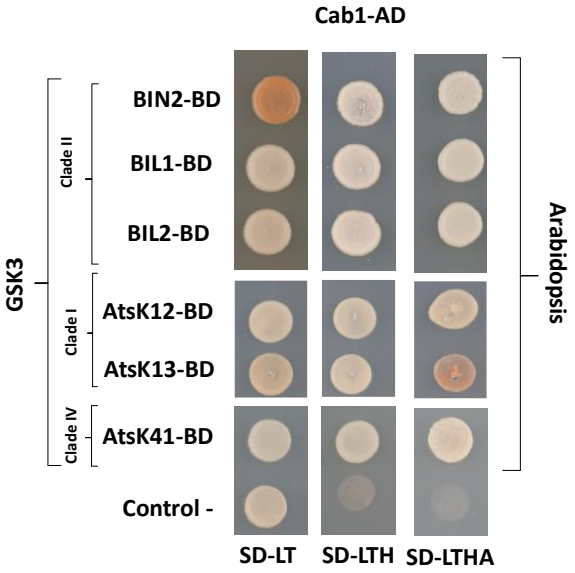

Figure 5-11 Cab1 can interact with 6 At-GSKs of clades I, II and IV

Six out of ten At-GSKs from clades I, II and IV were cloned into pGBKT7 bait vector and transformed into the yeast strain Y187, whereas Cab1 was cloned into pGADT7 activation vector and transformed into the yeast strain AH109. Diploid yeast after mating, containing both plasmids, were dropped on selective synthetic dropout media (SD) and yeast growth was monitored 3 days after spotting. Cab1 interacted with all At-GSK3 and the matted cells showed growth on quadruple selection media, the experiment was repeated 3 times independently with comparable results.

The GSK3 family in *Z. mays* consists of 11 family members, which are grouped into 4 clades, similar to the AtGSKs. To determine if cab1 exhibits comparable binding affinity to all Zm-GSKs, we conducted a primary screen using 4 ZmGSKs from clades I, II, and IV, and performed a Y2H assay (Fig. 6-13). In our experiment, cab1 exhibited strong interaction with all 4 tested Zm-GSKs.

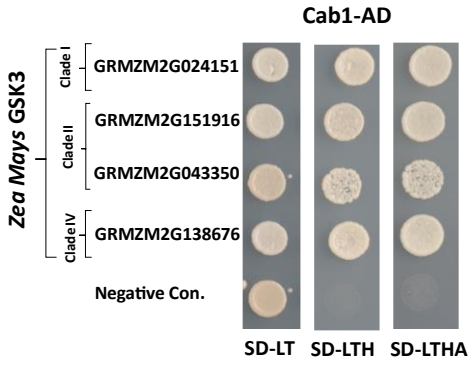

Figure 5-12 Cab1 can interact with 4 Zm-GSKs of clades I, II and IV

four out of eleven Zm-GSKs from clades I, II and IV that represent the most different clades of Zm-GSK3s were cloned into pGBKT7 bait vector and transformed into the yeast strain Y187, whereas Cab1 was cloned into pGADT7 activation vector and transformed into the yeast strain AH109. Diploid yeast after mating, containing both plasmids, were dropped on selective synthetic dropout media (SD) and yeast growth was monitored 3 days after spotting. Cab1 interacted with all tested Zm-GSK3 and the matted cells showed growth on quadruple selection media, the experiment was repeated 3 times independently with comparable results. Afterward, the research focused on At-Bin2 and its three similar Zm-GSK3 orthologues, as they represent the GSK3 family the best.

Consequently, for subsequent experiments, we focused exclusively on three AtBIN2, AtBIL1, and AtBIL2 orthologues in *Z. mays*, namely ZmGSK4, ZmGKS8, ZmGSK1, which serve as the primary representatives of the GSK3 family in plants. Y2H experiments were repeated with these genes, and Cab1 once again showed strong affinity (Fig 6-13).

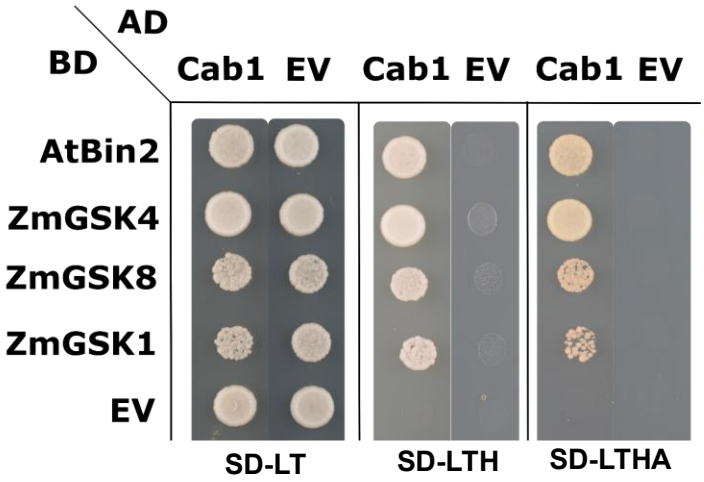

Figure 5-13 Direct interaction of Cab1 and maize BIN2 orthologs in a Yeast-two-Hybrid assay.

AtBIN2 and three close ZmGSK3 orthologues (ZmGSK4, ZmGSK1, ZmGSK8) were cloned into pGBKT7 bait vectors and transformed into the yeast strain Y187, whereas Cab1 was cloned into pGADT7 activation vector and transformed into the yeast strain AH109. Diploid yeast after mating, containing both plasmids, were dropped on selective synthetic dropout media (SD) and yeast growth was monitored 3 days after spotting. The experiment was repeated 3 times independently with comparable results.

Overall, Y2H assay were employed to test Cab1's binding with 6 At-GSKs and 7 Zm-GSKs from clades I, II, and IV. In all cases, Cab1 demonstrated no preference in binding different GSK homologues and orthologues.

5.9 ZmGSK4 has been localized in both the nucleus and cytosol

ZmGSK4's subcellular localization was examined by expressing the eGFP-ZmGSK4 (*P_{35S}::GFP-ZmGSK4*) construct in *N. benthamiana* and *Z. mays* leaves. This was done through Agrobacterium transformation and biolistic bombardment. Respectively confocal microscopy was conducted on the samples 3 days and 1 day after infection, respectively. In both samples, ZmGSK4 displayed a consistent nuclear and cytosolic subcellular localization (Fig. 6-14).

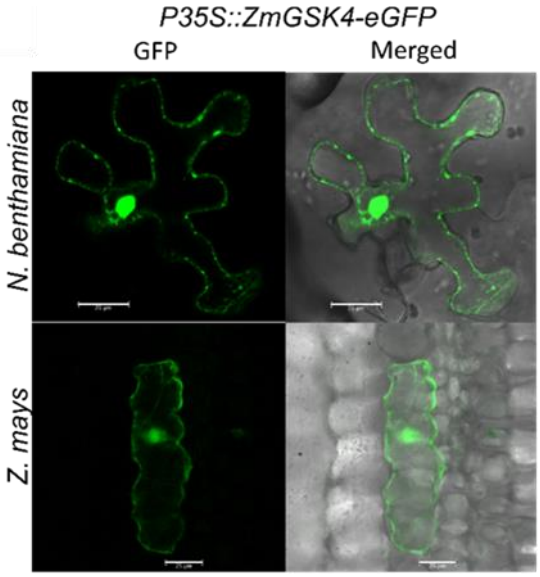

Figure 5-14 localization ZmGSK4 orthologue of AtBIN2 in N. benthamiana and Z. mays.

Localization of ZmGSK4 in *N. benthamiana* and *Z. mays*. Transient expression of GFP-ZmGSK4 (*P_{35S}::GFP-ZmGSK4*) in *N. benthamiana* and *Z. mays* leaves was performed via Agrobacterium GV3101 and biolistic bombardment methods respectively and monitored through confocal microscopy. ZmGSK4 shows Nucleo-cytoplasmic localization. Microscopy pictures captured by Kishor Ingole. Scale bar = 25 µm.

5.10 The BiFC assay revealed that Cab1 specifically interacts with GSKs exclusively within the nucleus.

In order to test if $Cab1_{28\text{-}113}$ and ZmGSK4 co-localize *in planta*, a Bimolecular fluorescence complementation (BiFC) assay was performed in *N. benthamiana* (Gookin & Assmann, 2014). A fluorescent signal was detected in the nucleus when ZmGSK4-C-Venus was co-expressed with $Cab1_{28\text{-}113}$-N-Venus. As negative control, BIN2-C-Venus was co-expressed with NLS-luciferase-N-Venus giving no fluorescent signal. Collectively, these results demonstrate, that $Cab1_{28\text{-}113}$ directly interacts with ZmGSK4 in the nucleus of plant cells (Fig. 6-15). The Cab1-C-Venus BiFC assay was conducted with AtBIN2, AtBIL1, AtBIL2, ZmGSK1, and ZmGSK8 too. In all, we observed similar sub-cellular co-localization.

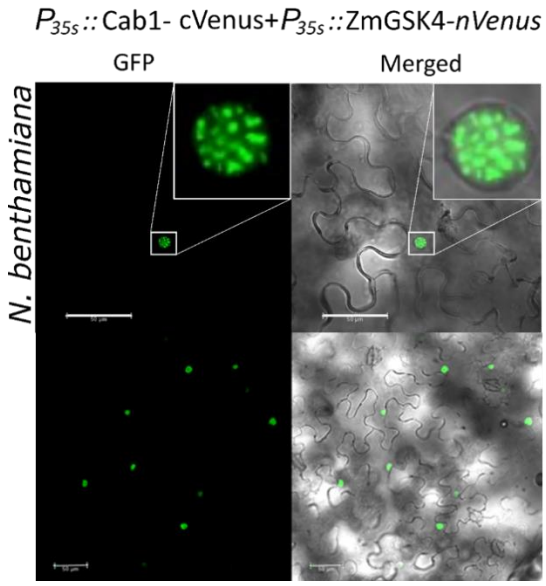

Figure 5-15 In vivo interaction of Cab1 and ZmGSK3 were tested via BiFC in N. benthamiana.

Cab1 C-terminally tagged with cVenus (*P_{35S}::Cab1$_{28-113}$-cVenus*) and ZmGSK4 C-terminally tagged with nVenus (*P_{35S}::ZmGSK4-nVenus*). The constructs were transformed in Agrobacterium strain GV3101 and co-infiltrated in *N. benthamiana* leaves. Confocal microscopy was done 3dpi in the GFP filter. Microscopy pictures captured by Kishor Ingole. Scale bar = 25 µm.

5.11 Cab1$_{28-113}$ overexpressing *A. thaliana* plants resemble phenotypically constitutive active BIN2D mutant plants

Shaggy-like kinases are highly conserved proteins found in all eukaryotes (Groszyk et al., 2018) and BIN2 has been identified as a negative regulator in Brassinosteroid signaling (Yoo et al., 2006). Point mutants in AtBIN2 have been identified which renders the kinase constitutively active. The respective dominant *A. thaliana* mutants (*bin2-1*) are also called Bin2D (D for dominant). *A. thaliana* lines with Bin2D mutation display a pronounced dwarfed phenotype with dark green and curled leaves resembling largely the phenotype observed upon Cab1$_{28-113}$ overexpression (fig. 6-16) (J. Li & Nam, 2002; Montes et al., 2021).

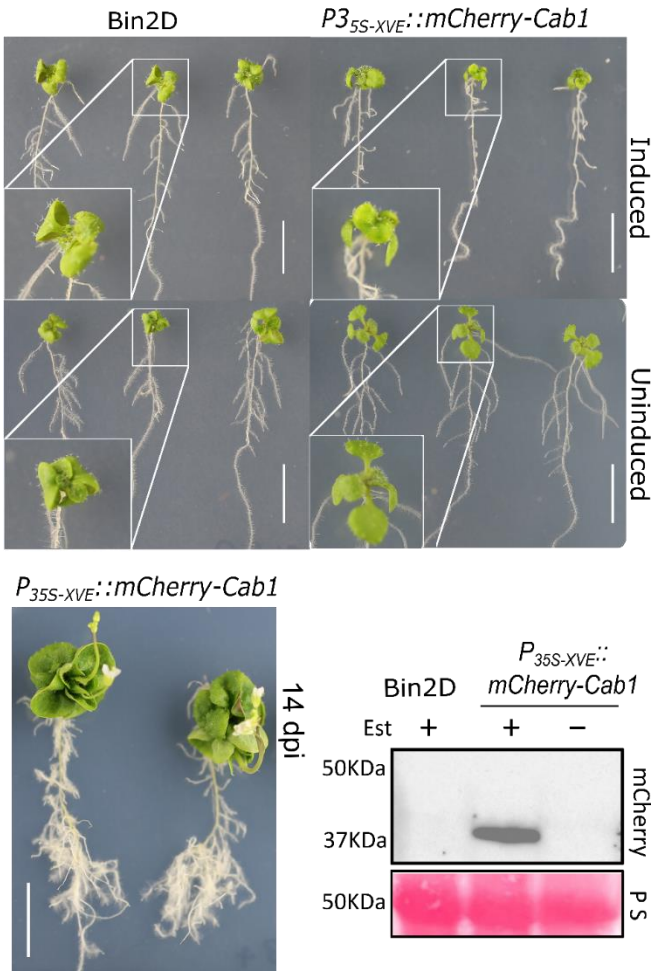

Figure 5-16 Phenotyping of Cab1 and BinD dominant mutant (bin2-1).

Cab1 ($P_{35S\text{-}XVE}$*::mcherry-Cab1*$_{28\text{-}113}$) and Bin2D seedling moved on induction plates containing 10μM β–Estradiol 7 days post germination. Phenotyping was performed at 5 and 14 dpi respectively. Control plates contain DMSO. Western blot was performed with an anti-mCherry antibody. Scale bar= 1cm.

5.12 Nuclear localization of Cab1 plays a crucial role in its effect on BIN2.

The nuclear localization of mCherry-Cab1$_{28\text{-}113}$ signal was observed in *Z. mays*, *N. benthamiana*, and *A. thaliana* through confocal microscopy (Fig. 6-7, 6-8). To investigate the significance of Cab1$_{28\text{-}113}$'s nuclear localization in relation to the observed phenotype, we generated transgenic lines where a Glucocorticoid Receptor (GR) is in fusion with Cab1$_{28\text{-}113}$ (Aoyama & Chua, 1997). The glucocorticoid receptor system enables the posttranslational re-localization of the tagged protein from the cytoplasm to the nucleus upon binding the exogenously added glucocorticoid Dexamethasone (fig 6-17).

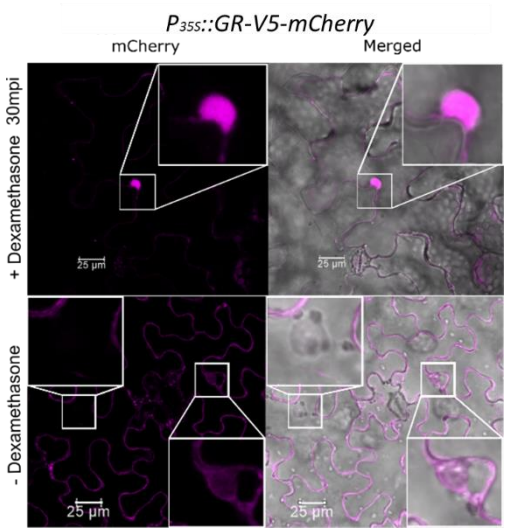

Figure 5-17 Glucocorticoid Receptor tag keeps mCherry proteins out of the nucleus in the absence of Dexamethasone.

GR-V5-mCherry (*P_{35S}::GR-V5-mCherry*) construct transformed into *Agrobacterium tumefaciens*, strain GV3101 and infiltrated in *N. benthamiana* leaves. Confocal microscopy was done 3dpi before and after Dexamethasone treatment. Microscopy pictures captured by Kishor Ingole. Scale bar = 25 µm.

In line with the previous observation of Cab1$_{28\text{-}113}$-BIN2 nuclear co-localization and interaction, the β–Estradiol-induced expression and dexamethasone-induced re-localization of Cab1$_{28\text{-}113}$ to the plant nucleus was found to be directly associated with the cabbage-like phenotype *in planta* (Fig 6-18).

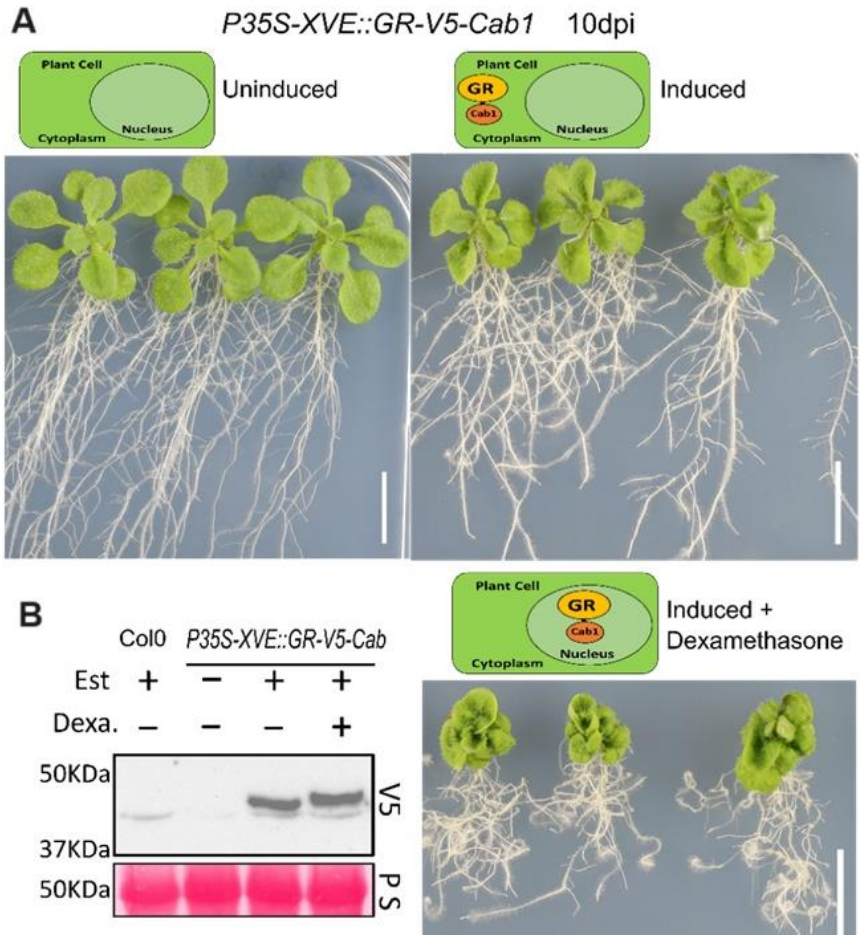

Figure 5-18 the nuclear localization of Cab1 plays a crucial role in its effect on BIN2

A. Mis-localization of Cab1 tagged with glucocorticoid receptor in *A. thaliana*. The Gluco-V5-Cab1 ($P_{35S\text{-}XVE}$*::GR-V5-Cab1*$_{28\text{-}113}$) seedlings grow on selection plates. 9 days old seedlings were shifted either on new control plates with DMSO, or induction plates with 10 μM β–Estradiol only or 10 μM β–Estradiol and 10 μM Dexamethasone respectively (left to right). The strong cabbage phenotype was just observed in the presence of both β–Estradiol and Dexamethasone. Scale bar: 1cm.
B. Immunoblotting analysis on Cab1 ($P_{35S\text{-}XVE}$*::GR-V5-Cab1*$_{28\text{-}113}$) protein levels of seedling extracts from *A. thaliana* lines using anti-V5 antibody. The expected band size of 48KDa (magenta asterisks) is shown only in β–Estradiol-induced seedlings. Ponceau staining was used as an indication of equal protein loading.

5.13 Cab1 binds to the C-terminal part of ZmGSK4 and leads to GSK4-dependent transcriptional activation in yeast

The shaggy-like kinase family consists of conserved proteins, and the activity of them are regulated by various post-translational modifications. AtBSU1 suppresses AtBIN2 activity by dephosphorylating Tyr^{200}, while KIB1 mediates ubiquitination of AtBIN2-Lys^{35}, leading

to its degradation via the proteasome (Y. Song et al., 2023; Zhu et al., 2017). The E263K mutation in the AtBIN2-TREE$^{261-264}$ motif causes dwarf phenotype in *A. thaliana bin2/dwarf12/ucu1* transgenic lines (J. Li et al., 2001; Yan et al., 2009). To identify the target site of Cab1, we focused on ZmGSK4, the closest orthologue to AtBIN2. An alignment was performed using the PRALAINE program to compare the amino acid sequences of AtBIN2 and ZmGSK4, revealing conserved amino acids in ZmGSK4 (fig 6-19 A). Based on the predicted 3D structure and the conserved amino acid sites, ZmGSK4 was divided into four fragments, each fragment fused to the Gal4BD, to assess their interaction with Cab1$_{28-113}$ fused to the GAL4AD. The results showed Cab1$_{28-113}$ binds to the C-terminus of ZmGSK4$_{335-412}$ (fig. 6-19 B). In addition, the MEME program was used to perform an amino acid alignment of the full-length shaggy-like kinase family proteins. This analysis uncovered highly conserved motifs between ZmGSK4 and AtBIN2 (fig. 6-19 C, 6-20), supporting previous research findings (Hou et al., 2022).

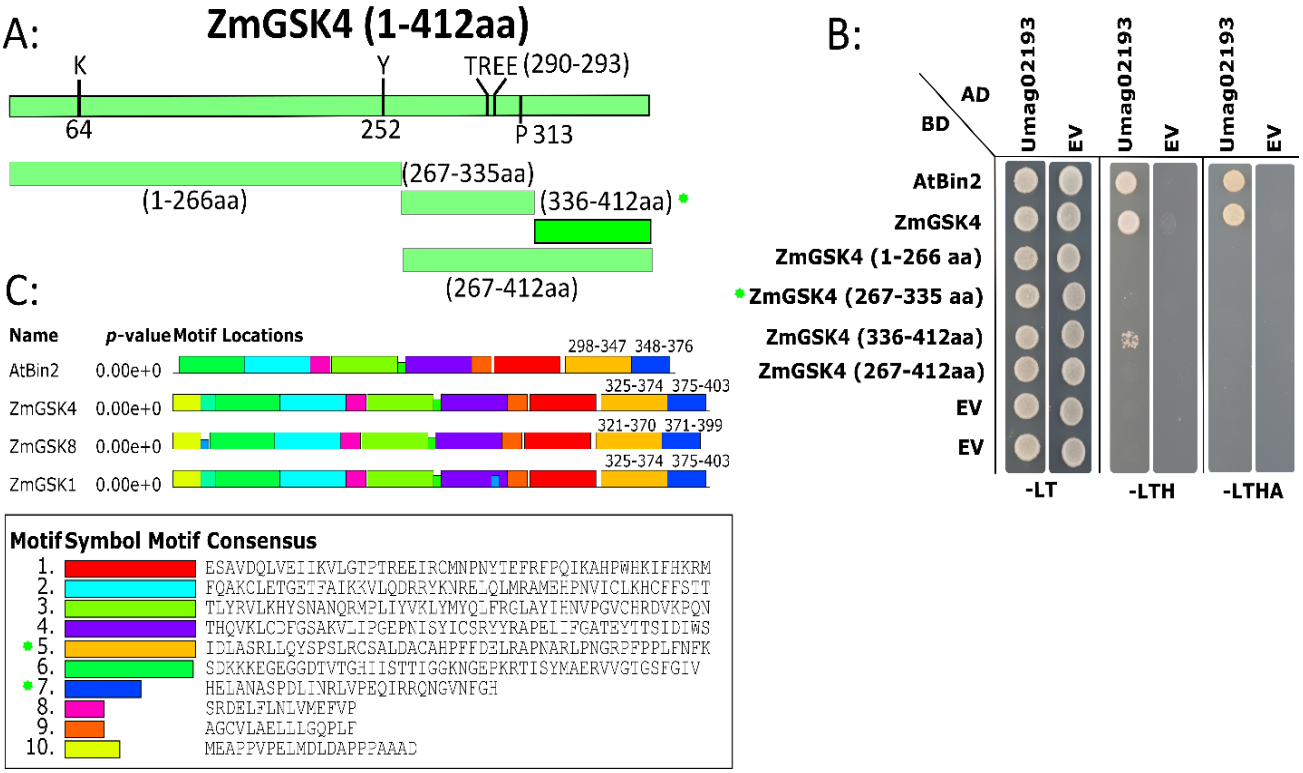

Figure 5-19 Cab1 targets C-terminal of ZmGSK3

A. Schematic representation of truncated ZmGSK4 in a Yeast-two-Hybrid assay. The TREE motif and Pro^{313} are aligned with AtBIN2 TREE$^{261-264}$ motif and Pro^{284}. These motifs are

studied in *A. thaliana bin2/dwarf12/ucu1* mutant lines and presented hyperactive BIN2 phenotype. Phosphorylation of AtBIN2-Tyr^{200} aligned with ZmGSK4-Tyr^{252}, increases BIN2 activity, and AtBIN2-Lys^{35} is aligned with ZmGSK4-lys^{64} which is ubiquitinated with KIB1.

B. Cab1 targets the C-terminus of ZmGSK4. ZmGSK4 has been split into four different pieces, each fragment was cloned into pGBKT7 bait vector and transformed into the yeast strain Y187, whereas Cab1 was cloned into pGADT7 activation vector and transformed into the yeast strain AH109. Diploid yeast after mating, containing both plasmids, were dropped on selective synthetic dropout media (SD) and yeast growth was monitored 3 days after spotting. ZmGSK4 and AtBIN2 were used as positive controls. Cab1 targets the C-terminus of ZmGSK4 (GalBD-ZmGSK4$_{336\text{-}412}$).

C. Cab1 targets two conserved motifs at the C-terminus of AtBIN2 and ZmGSKs. Conserved motif analysis of AtBIN2, ZmGSK1, 4 and 8 amino acids sequence was performed by MEME. Motifs were designated 1–10 and distinguished with different colors. Motifs 5 and 7 (green asterisks) have most overlap with Cab1 binding sites.

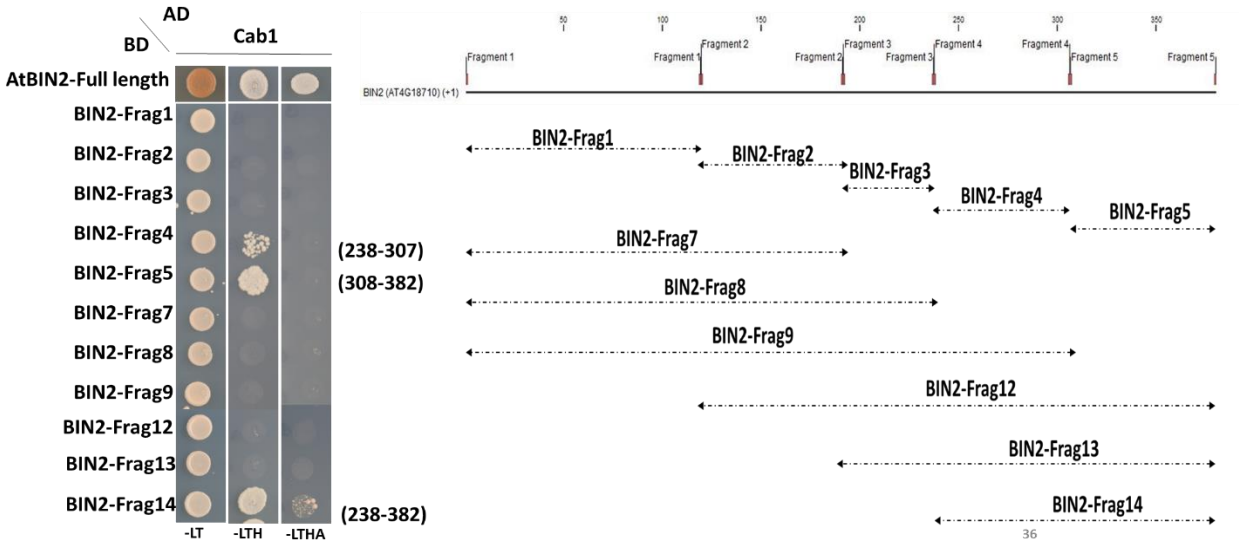

Figure 5-20 Cab1 targets the C-terminus of AtBIN2.

AtBIN2 has been fragmented into 14 different pieces, each fragment was cloned into pGBKT7 bait vectors and transformed into the yeast strain Y187, whereas Cab1 was cloned into pGADT7 activation vector and transformed into the yeast strain AH109. Diploid yeast after mating, containing both plasmids, were dropped on selective synthetic dropout media (SD) and yeast growth was monitored 4 days after spotting. AtBIN2 full length was used as positive controls.

5.14 Cab1 re-localizes BIN2 from the cytosol to the nucleus and increases AtBIN2 stability and activity

From the phenotypic resemblance between Cab1 overexpressing plants and Bin2D constitutively active mutants we hypothesized that Cab1 is leading to an activation of BIN2 in one or the other way. As BIN2 is shuttling between the host cytoplasm and the plant cell nucleus where it inhibits e.g. transcriptional activators of the BR signaling pathway, we wondered if $Cab1_{28\text{-}113}$ expression *in planta* influences the subcellular distribution of ZmGSK4 in the maize cell. Using biolistic co-transformation method in maize leaves we co-expressed mCherry-$Cab1_{28\text{-}113}$ (P_{35S}::mCherry-$Cab1_{28\text{-}113}$) and the AtBIN2 ortholog ZmGSK4-eGFP (P_{35S}::ZmGSK4-eGFP) maize epidermal cells. Confocal microscopy was performed 24h after the transformation. The results indicate, that mCherry-$Cab1_{28\text{-}113}$ caused the re-localization of ZmGSK4-GFP from the cytosol to the cell nucleus (Fig. 6-21 A).

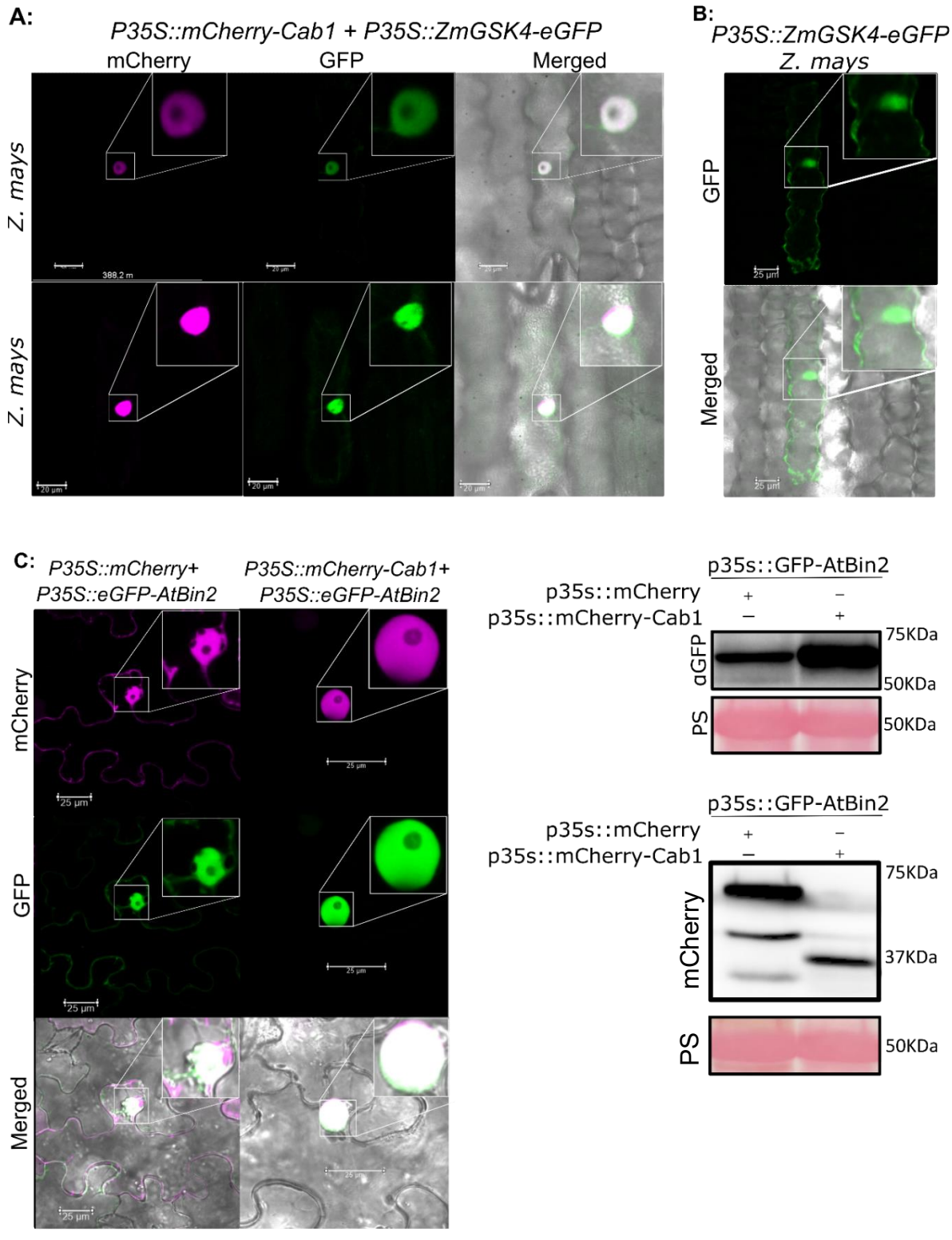

Figure 5-21 BIN2 re-localized into the nucleus by Cab1 co-expression increasing its stability.

A. Cab1 relocalises ZmGSK4 from cytosol to the nucleus. Subcellular co-localization of ZmGSK4 (P_{35S}::ZmGSK4-GFP) co-expressed with Cab1 (P_{35S}::mCherry-cab1$_{28-113}$) via biolistic bombardment in maize plant leaves was observed 1 dpi through confocal microscopy. Left panel: mCherry, Middle panel: GFP, right panel: merged mCherry and GFP. Microscopy pictures captured by Kishor Ingole. Scale bar = 25 µm.
B. ZmGSK4 shows Nucleo-cytoplasmic localization in the absence of Cab1 in *Z. mays*. Transient expression of GFP-ZmGSK4 (*P_{35S}::GFP-ZmGSK4*) in *Z. mays* leaves was performed via biolistic bombardment and monitored through confocal microscopy 1dpi. Microscopy pictures captured by Kishor Ingole. Scale bar = 25 µm.
C. Cab1 re-localizes and stabilizes AtBIN2. AtBIN2 re-localizes into the nucleus in the presence of Cab1 in *N. benthamiana*. Full-length AtBIN2 was fused to GFP (P_{35S}::AtBIN2-GFP) and Cab1 lacking its signal peptide was fused to mCherry (P_{35S}::mCherry-cab1$_{28-113}$) transiently expressed in *N. benthamiana* leaves, transformed via Agrobacterium strain GV3101. Constitutively expressed mCherry (P_{35S}::mCherry-mCherry) were used as controls for the colocalization assay. The samples were subjected to confocal microscopy 3 dpi Upper: mCherry fluorescence, middle panels: GFP fluorescence, Lower panel: merged mCherry and GFP fluorescence, brightfield images. Microscopy pictures captured by Kishor Ingole. Scale bar = 25 µm. The western blot was performed with GFP and mCherry antibodies recognizing the respective fusion proteins.

To test if Cab1$_{28-113}$ expression influences localization and the stability of AtBIN2 in a dicot system, I conducted a transient co-expression experiment using mCherry-Cab1$_{28-113}$ (*P_{35S}::Myc-mCherry-Cab1$_{28-113}$*) and GFP-AtBIN2 (*P_{35S}::GFP-AtBIN2*) in *N. benthamiana* leaves. As a negative control, I used mCherry (*P_{35S}::Myc-mCherry-mCherry*). Confocal microscopy was performed 3 days post-infiltration (Fig 6-21 C). My observations indicate that the presence of Cab1$_{28-113}$ leads to a relocalization of AtBIN2 from the cytosol to the nucleus as already previously shown for the AtBIN2 ortholog in maize. Western blot analysis of leaves either co-expressing AtBIN2-eGFP and mCherry-Cab1$_{28-113}$ or respective mCherry control reveals, that co-expression of mCherry-Cab1$_{28-113}$ leads to stabilization of AtBIN2-GFP *in planta* (Fig 6-21 C).

5.15 Cab1 increases AtBin2-Y^{200} phosphorylation and reduces AtBIN2-K^{35} ubiquitination of AtBin2

Although the *A. thaliana* cabbage phenotype of Cab1$_{28-113}$ overexpression and the Cab1-dependent re-localization and BIN2-stabilization data suggest higher BIN2 activity in the plant nucleus in the presence of Cab1, we conducted a Mass-Spectrometry (MS) to analyze the post-translational modifications (PTMs) on BIN2 in the presence and absence of Cab1. For this purpose, we co-transformed via Agrobacterium-mediated transformation

mCherry-Cab1$_{28\text{-}113}$ (P_{35S}::Myc-mCherry-Cab1$_{28\text{-}113}$) and GFP-AtBIN2 (P_{35S}::GFP-AtBIN2) into *N. benthamiana* leaves. The GFP-AtBIN2 was immunoprecipitated with GFP-antibody and followed by mass spectrometry.

Interestingly, MS results revealed a tenfold increase in AtBIN2 Tyrosine Y^{200} phosphorylation in the presence of Cab1 compared to the control. This finding supports the notion of heightened activity of AtBIN2, providing a potential explanation for the cabbage phenotype (Youn et al., 2013; Zhu et al., 2017). Conversely, AtBIN2-K35 ubiquitination by KIB1 in the cytosol leads to proteasomal degradation of AtBIN2 (Y. Song et al., 2023; Youn et al., 2013). The MS data showed five times less ubiquitination of AtBIN2-Lysine^{35} in the presence of Cab1, which may explain the increased stability of AtBIN2 in the presence of Cab1 (Fig. 6-22).

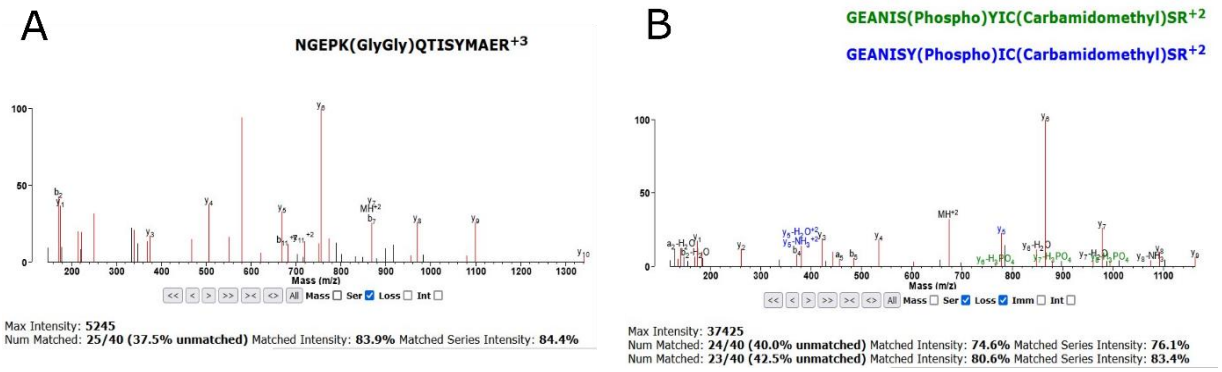

Figure 5-22 Cab1 stabilizes AtBin2 via uLys35 and pTyr^{200}.

Full-length AtBin2 was fused to GFP (P_{35S}::AtBin2-GFP) and Cab1 lacking its signal peptide was fused to mCherry (P_{35S}::mCherry-Cab1$_{28\text{-}113}$) transiently expressed in *N. benthamiana* leaves via Agrobacterium GV3101. Constitutively expressed mCherry (P_{35S}::mCherry-mCherry) were used as controls for the co-localization assay. The samples were subjected to MS 3 days post-induction.

A. uLys^{35} in NGEPK(GlyGly)QTISYMAER peptide was detected 5 times in the control sample with high fidelity (high score and low expectation) while no ms2 was taken in the AtBin2 co-expression with Cab1 sample. Moreover, in the specific retention time window also no precursor appeared in the ms1.
B. pTyr^{200} in GEANIS(Phospho)YIC(Carbamidomethyl)SR^{+2} peptide was detected 10 times in the Cab1 sample in comparison with the control sample.

5.16 Cab1 and Bin2 form nuclear bodies

The formation of nuclear bodies (NB) was a commonly observed characteristic in the Cab1-GSK3 BiFC assay (Fig. 6-16). In order to investigate the other proteins involved in the formation of these NBs, we employed the SplitTurboID assay (Cho et al., 2020) in *N. benthamiana* with certain modifications. The leaf samples were collected and ground in liquid nitrogen (Fig 6-23).

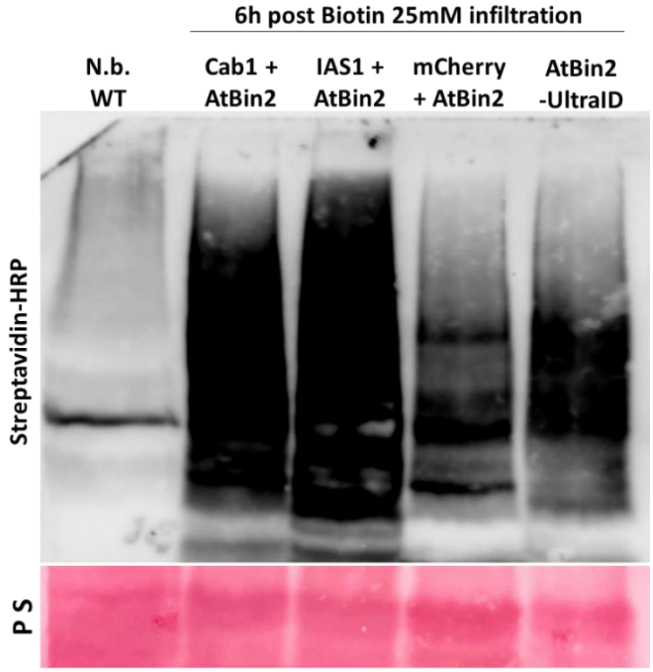

Figure 5-23 SplitTurboID proof of concept.

SplitTurboID fragments biotinylate proteins in proximity when they are forming an active complex. Cab1-V5-N-SplitTurbo (P_{35s}::Cab1$_{28-113}$-V5-N-SplitTurbo$_{1-73}$), and AtBin2-HA-C-SplitTurbo (P_{35s}::AtBin2-HA-N-SplitTurbo$_{74-321}$) transiently expressed in *N.benthamiana* leaves via Agrobacterium GV3101. 6h post-Biotin (25µM) treatment, the samples were harvested in 6M Urea. The western blot developed via Streptavidin-HRP antibody. IAS1-V5-N-SplitTurbo (P_{35s}::IAS1$_{25-175}$-V5-N-SplitTurbo$_{1-73}$) and mCherry-V5-N-SplitTurbo (P_{35s}::mcherry-V5-N-SplitTurbo$_{1-73}$) and AtBin2-UltraID (P_{35s}::AtBin2-UltraID) were used as the control and subjected under same treatments.

The biotinylated proteins were then collected using magnetic beads and subjected to further analysis through mass spectrometry (MS). The most significant biotinylated candidates were chosen and the background proteins were eliminated by subtracting the Cab1-SplitTurboID results from the Bin2-UltraID, IAS1-SplitTurboID, and mCherry-SplitTurboID data sets. Interestingly, we identified Pre-mRNA-splicing factor 38A

(PRP38-At2g40650) as the top hit in our findings, which is associated with the described functions of NBs (table 6-3, 6-4).

Row	Locus	Name	Score
1	At2g40650	"Pre-mRNA-splicing factor 38A"	109
2	AT4G14340	casein kinase I	94.2
3	AT1G53850	Proteasome subunit alpha type-4	74.4
4	AT1G77180	SNW domain-containing protein 1	60
5	AT2G03150	Cell division cycle and apoptosis regulator protein 1	48
6	AT5G11170	ATP-dependent RNA helicase sub2	45
7	AT4G08580	microfibrillar-associated protein-related	34.4
8	AT2G32910	DCD (Development and Cell Death) domain protein	30
9	AT5G14670	ADP-ribosylation factor 1	27

Table 5-3 Top score results of SplitTurboID MASS spectrometry.

GO biological process	Enrichment FDR	nGenes	Pathway Genes	Fold Enrichment	Pathway
	0.030711253	1	7	435.126984	Sodium ion homeostasis
	0.045588221	1	13	234.299145	Response to mannitol
	0.003905075	3	211	43.3064771	RNA splicing
	0.006722174	3	320	28.5552083	mRNA processing
	0.039235121	2	269	22.646014	Response to cadmium ion
	0.006879811	3	408	22.3962418	mRNA metabolic process
	0.012963246	3	582	15.7004582	RNA processing
	0.006879811	4	1049	11.6144476	RNA metabolic process
	0.012963246	4	1403	8.68393126	Nucleic acid metabolic process
	0.023849978	4	1736	7.01817716	Nucleobase-containing compound metabolic process

Table 6-4 Gene Ontology of the biological process enrichment in the Cab1-Bin2 splitTurboID results

To validate SplitTurboID assay was performed based on the presented model. Cab1-V5-N-SplitTurbo (P_{35s}::Cab1$_{28-113}$-V5-N-SplitTurbo$_{1-73}$) and AtBin2-HA-C-SplitTurbo (P_{35s}::AtBin2-HA-N-SplitTurbo$_{74-321}$) transiently expressed in *N. benthamiana* leaves via Agrobacterium GV3101, the samples were harvested in liquid nitrogen and biotinylated proteins. In-gel digestion was performed on the beads and followed up with MASS-spectrometry. The same procedure was used for mCherry-V5-N-SplitTurbo (P_{35s}::mCherry-V5-N-SplitTurbo$_{1-73}$) as the negative control.

The results, Myc-AtPRP38A (P_{35s}::3xMyc-PRP38A) co-expressed with AtBin2-SplitTurboID (P_{35s}::AtBin2-HA-SplitTurboID) and Cab1-SplitTurboID (P_{35s}::Cab1$_{28-113}$-V5-SplitTurboID). mCherry-SplitTurboID (P_{35s}::mCherry-V5-SplitTurboID) was used in the control sample in combination with AtBin2-SplitTurboID (P_{35s}::AtBin2-HA-SplitTurboID) and Myc-AtPRP38A (P_{35s}::3xMyc-PRP38A). The functionality of the SplitTurboID system in biotinylation of the proteins in the proximity of the formed complex, was tested through the utilization of Streptavidin-HRP, and subsequently, Co-IP was conducted using IgG-Myc beads. western blot showed biotinylation of AtPRP38A only happens in the presence of Cab1 (fig 6-24).

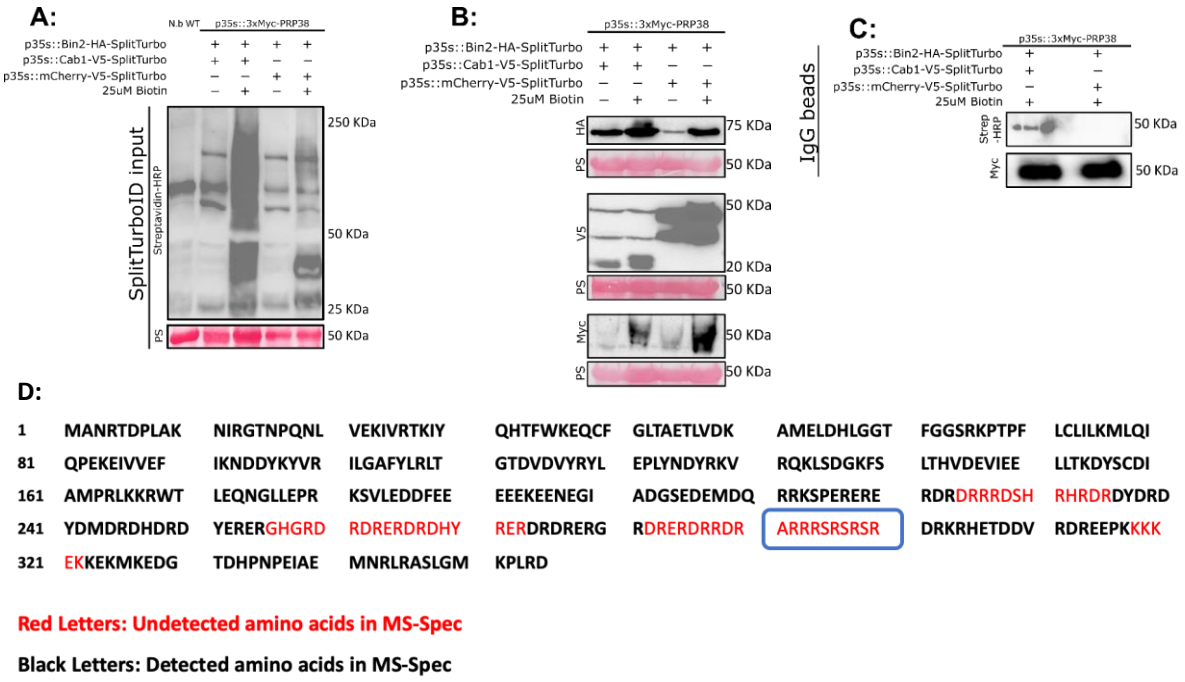

Figure 5-24 AtPRP38 gets biotinylated by AtBin2 only in the presence of Cab1.

A. SplitTurboID assay was repeated in the presence of Myc-AtPRP38 (P_{35s}::Myc-AtPRP38). Myc-AtPRP38 (P_{35s}::Myc-AtPRP38), Cab1-V5-N-SplitTurbo (P_{35s}::Cab1$_{28-113}$-V5-N-SplitTurbo$_{1-73}$), and AtBin2-HA-C-SplitTurbo (P_{35s}::AtBin2-HA-N-SplitTurbo$_{74-321}$) transiently expressed in *N.benthamiana* leaves via Agrobacterium GV3101, after treatment with Biotin (25µM), the samples were harvested in liquid nitrogen. The samples were then prepared in 1xSDS sample buffer.SplitTurboID system's specificity was confirmed using Streptavidin-HRP antibody.
B. expression of all three constructs was verified via HA, V5, and Myc antibodies, respectively.

C. For the Myc-AtPRP38 construct, a pull-down assay was performed using IgG-Myc agarose beads. The biotinylation of AtPRP38 was examined using Streptavidin-HRP antibody.
D. The Mass Spectrometry was performed on the Myc-AtPRP38 construct, and a pull-down assay was conducted using various buffers. The RSRSRS$^{294\text{-}299}$ motif is situated in a highly charged area and it was not detected in the first round of Mass Spectrometry analysis. Phosphorylation of PRP38 at this motif could potentially support the presented model (fig 6-39), as suggested by a previous publication indicating that the activity of PRP38 may be reduced as a consequence of Cab1 expression and negatively impacts on the cell mRNA splicing machinery.

In order to examine the direct interaction between AtPRP38 and AtBin2 in the presence of Cab1, we conducted the BiFC assay. I expressed AtPRP38-C-Venus (*P*$_{35S}$::AtPRP38-C-Venus) and ZmGSK4-N-Venus (*P*$_{35S}$::ZmGSK4-N-Venus) transiently along with Cab1-mCherry (*P*$_{35S}$::Cab1$_{28\text{-}113}$-mCherry) for this purpose. In the negative control, Cab1 was substituted with mCherry (*P*$_{35S}$::mCherry). The samples were subjected to confocal microscopy using GFP and mCherry channels 3 days post-infection (3dpi). Unfortunately, no Venus's signal was detected at 3dpi (Fig. 6-25).

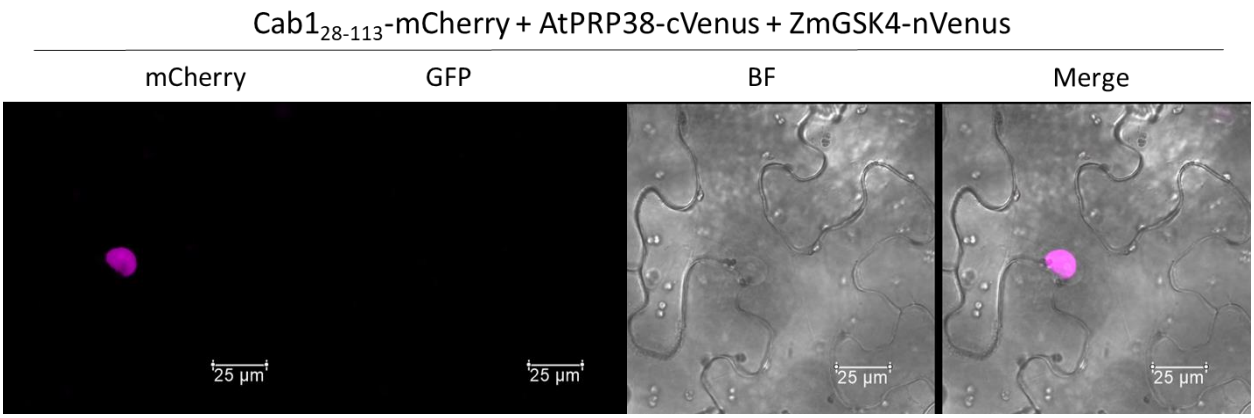

Figure 5-25 The fluorescent Venus signal AtPRP38 and AtBin2 do not observed in the presence of Cab1-mCherry

AtPRP38-C-Venus (*P*$_{35S}$::AtPRP38-C-Venus) and ZmGSK4-N-Venus (*P*$_{35S}$::ZmGSK4-N-Venus) transiently along with Cab1-mCherry (*P*$_{35S}$::Cab1$_{28\text{-}113}$-mCherry). In the negative control, Cab1 was substituted with mCherry (*P*$_{35S}$::mCherry). The samples were subjected to confocal microscopy using GFP and mCherry channels 3 days post-infection (3dpi). Venus's signal was not detected at 3dpi. Microscopy pictures captured by Kishor Ingole. Scale bar = 25 µm.

5.17 Yeast competition assay:

In order to confirm the interaction between AtPRP38 and AtBin2, we conducted the Y3H assay with the presence and absence of Cab1. Gal4BD-AtBin2-GFP-Cab1 (P_{ADH1}::Gal4BD-Myc-AtBin2-P_{TDH3}::GFP-Cab1$_{28\text{-}113}$) and Gal4AD-AtPRP38 (P_{ADH1}::Gal4BD-AtPRP38) constructs were transformed in the yeast strains Y187 and AH109, respectively. the cells were mated and spotted on the selection media. The results showed that the presence of Cab1 causes unknown changes in AtBin2, which in turn enhances the binding affinity to Gal4AD. As a result, yeast growth was observed on SD-LTH plates (Fig. 6-26 A). However, when we spotted the Gal4BD-AtBin2-GFP-Cab1 unmated Y187 cells, there was no growth observed on the proper selection media (Fig. 6-26 B). But when we tried the system on unmated yeast cells, the cells did not show any growth on selection media. To validate these findings, the experiment was repeated using ZmGSK4, which serves as the main AtBin2 orthologue in *Z. mays*. Remarkably, the same results were obtained. In the control samples, GFP-mCherry was substituted with GFP-Cab1 (Fig. 6-26 A).

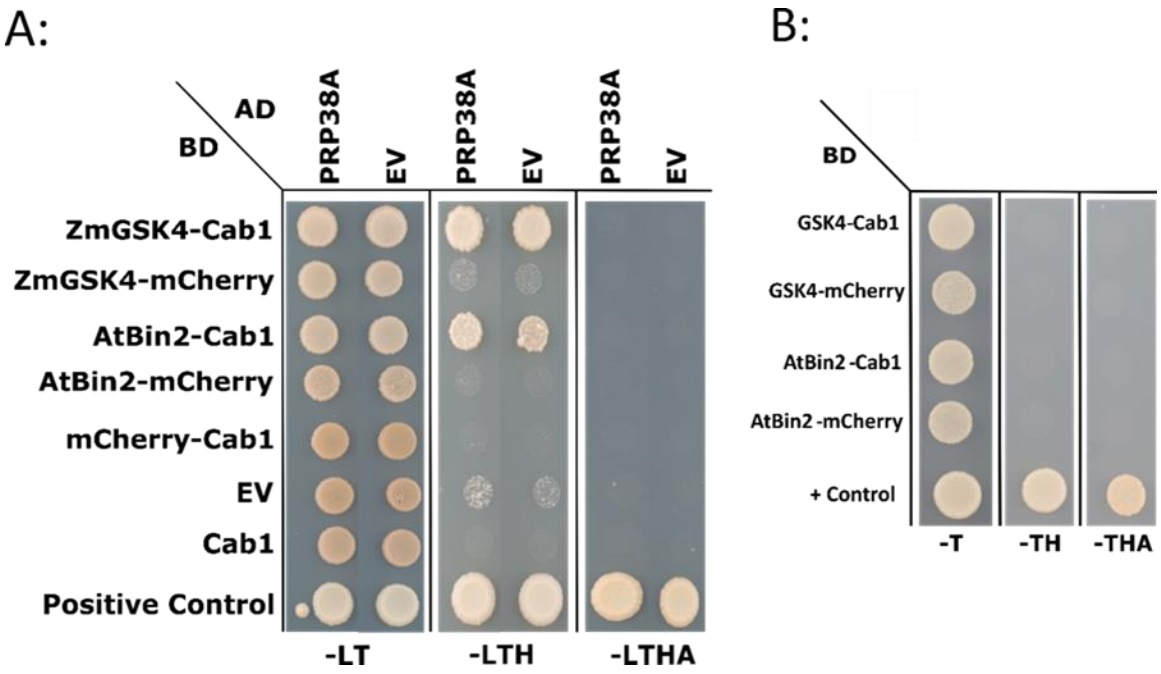

Figure 5-26 study of the potential direct interaction of Gal4BD-AtBin and AtPRP38 in presence of Cab1

A. to investigate the direct interaction of Gal4DB-AtBin2 and Gal4AD-AtPRP38 in presence of Cab1, Gal4BD-AtBin2-GFP-Cab1 (P_{ADH1}::Gal4BD-Myc-AtBin2-P_{TDH3}::GFP-Cab1$_{28\text{-}113}$)

construct was cloned in pGBKT7 bait vector Y187, whereas AtPRP38 was cloned into pGADT7 activation vector and transformed into the yeast strain AH109. Diploid yeast after mating, containing both plasmids, were dropped on selective synthetic dropout media (SD) and yeast growth was monitored 3 days after spotting. The experiment was repeated 3 times independently with comparable results.

B. To investigate the possible auto activity of Gal4DB-ZmGSK4 and Gal4DB-AtBin2 in presence of Cab1, Gal4BD-AtBin2-GFP-Cab1 (P_{ADH1}::Gal4BD-Myc-AtBin2-P_{TDH3}::GFP-Cab1$_{28\text{-}113}$) construct was cloned in pBGKT7 bait vector and transformed into the yeast strain Y187. Non-mated yeast cells, containing the bait plasmid, were dropped on selective synthetic dropout media (SD) contains Leucine and yeast growth was monitored 3 days after spotting. The experiment was repeated 3 times independently with comparable results.

5.18 Total RNA sequencing

Previous studies have demonstrated that the overactivation of AtBIN2 in Bin2D leads to the dwarf phenotype (J. Li & Nam, 2002; Montes et al., 2021). The previous publication demonstrated that BIN2 hyperactivity suppresses SA signaling in plants by phosphorylating TGA3 (Han et al., 2022). To investigate whether the hyperactive BIN2, through Cab1, suppresses SA-induced defense responses or not, Cab1 induced and uninduced transgenic lines were treated by SA. The total RNA of these samples was extracted and subjected for next-generation sequencing. In order to further investigate the impact of Cab1 expression on the gene expression profile of *A. thaliana*, total RNA from 12-days-old seedlings after chemical treatments were extracted and sequenced. The results of total RNA sequencing showed that Cab1 induction suppressed genes involved in cell wall expansion and auxin-responsive genes which is align with macroscopic observations and phenotype (fig. 6.1). Moreover, defense genes were up-regulated when Cab1 was overexpressed (Table 6-6). The findings indicate that Cab1 does not suppress the host's immune responses under SA treatment. Overall, this emphasizes my conclusion about Cab1's role as a development-related effector rather than an immunity suppressor.

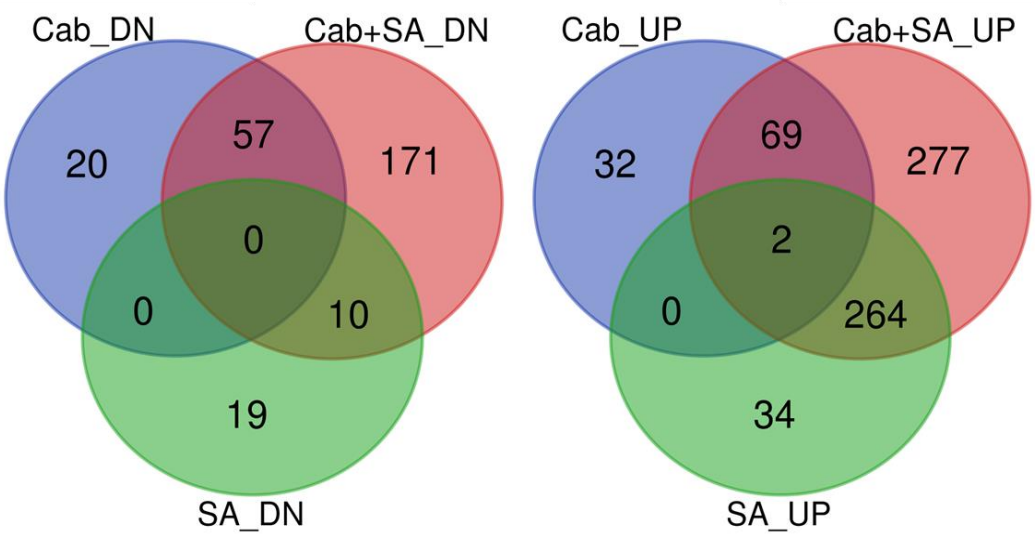

Figure 5-27. Venn diagram of total RNA seq results under different treatments.

Cab_DN/Cab_UP" represents the number of downregulated and upregulated genes resulting from Cab1 overexpression through β–Estradiol treatment, relative to the Mock sample which serves as the control. Similarly, "Cab+SA_DN/Cab+SA_UP" denotes the number of downregulated and upregulated genes resulting from Cab1 overexpression through β–Estradiol treatment and immune responses via SA treatment, again subtracted from the Mock sample used as the control. "SA_DN/SA_UP" signifies the number of genes that are downregulated and upregulated due to SA treatment, subtracted from the Mock sample, which is the control. The experiment was done in three independent replicates. Maxim Prokchorchik did the analysis and made the graph.

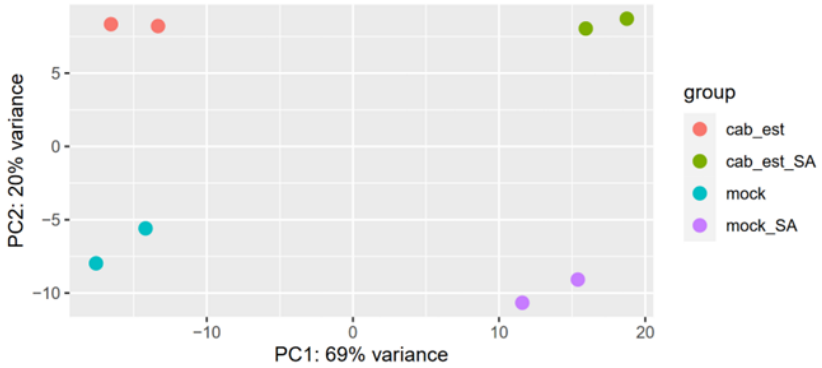

Figure 5-28 PCA diagram of NGS metadata.

The PCA diagram represents the clustering of NGS metadata from independent biological replicates under different treatments. Red dots represent the Cab1 gene expression profile after β–Estradiol treatment, green dots represent the NGS metadata of samples after both β–Estradiol and SA treatments, and purple dots represent the results of the SA treatment on the gene

expression profile. Blue dots correspond to the NGS results of non-treated plants. Maxim Prokchorchik made the PCA graph.

	Enrichment FDR	nGenes	Pathway Genes	Fold Enrichment	Pathway
UP regulated GO biological process	0.048354399	4	88	12.68503214	Plant-type hypersensitive response
	0.048354399	4	89	12.54250369	Programmed cell death induced by symbiont
	0.048354399	4	90	12.40314254	Biological proc. involved in interaction with symbiont
	0.048354399	17	1700	2.790707071	Defense response
Down regulated GO biological process	0.041103161	2	12	64.85446009	Syncytium formation
	0.049491698	2	16	48.64084507	Reg. of asymmetric cell division
	0.049491698	4	153	10.17324864	Plant-type cell wall organization
	4.17E-05	10	415	9.376548447	Response to auxin
	0.000380554	16	1593	3.90836671	Response to hormone

Table 6-6 Effects of Cab1 Induction on A. thaliana's Biological Processes.

The analysis of NGS Metadata by ShinnyGO 0.78 reveals the impact of Cab1 expression on various biological processes. The expression of Cab1 upregulates defense genes, while it downregulates the genes that are involved in cell wall expansion and growth. The analysis was performed by Pouria Bahrami.

5.19 The expression of Cab1 prevents the formation of *H. schachtii* cysts.

H. schachtii, the plant-parasitic nematode, induces structural modifications in host plant roots to create a specialized feeding site called a syncytium. These modifications involve the manipulation of plant cell walls to enable nematode feeding and nutrient uptake (Bohlmann & Sobczak, 2014; Wieczorek & Grundler, 2006). NGS results uncovered the downregulation of EXPs and SAUR upon Cab1 expression. SAUR and EXPs are involved in syncytium formation and asymmetric cell division (M. Huang et al., 2021). We conducted the *H. schachtii* nematode's syncytium formation infection assay to examine the biological impact of Cab1 expression. Counting male and female nematodes separately is important to assess infection severity accurately, understand reproduction dynamics, and analyze the sex survival ratio for insights into nematode biology and ecology. The findings demonstrate a significant reduction in the number of *H. schachtii* syncytia in the presence of Cab1 in comparison with the control (Fig 6-29). Expression of

Cab1 interferes with forming the feeding structure of the nematodes and reduced the cyst number.

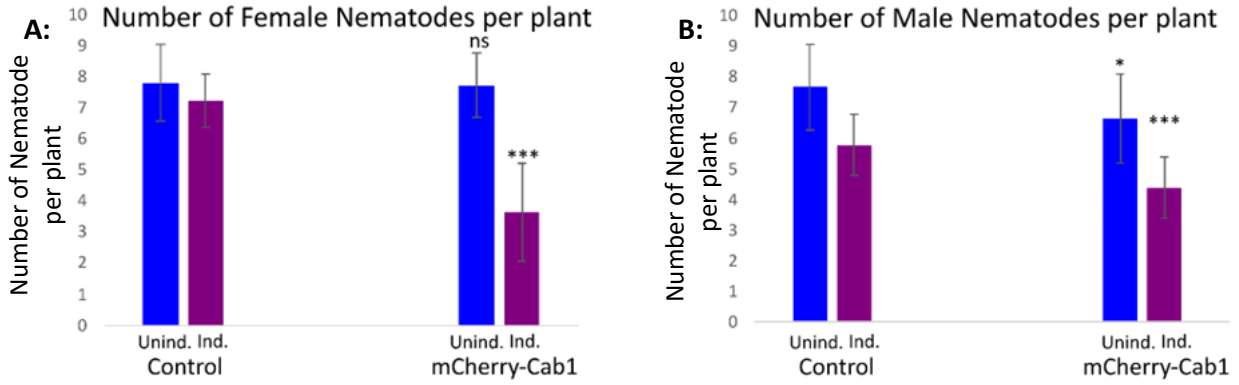

Figure 5-29 The expression of Cab1 prevents the development of H. schachtii female and male nematodes cysts in A. thaliana roots.

A. thaliana transgenic lines expressing mCherry (*$P_{35S\text{-}XVE}$::mCherry*) and Cab1 (*$P_{35S\text{-}XVE}$::mcherry-cab1$_{28\text{-}113}$*) were subjected to *H. schachtii* infection. The number of female nematodes was counted at 14 days post infections (dpi). Statistical analysis was performed using MS-Excel, and the significance levels were denoted as * for $p<0.05$ and *** for $p<0.001$, using T-test. The whole assay and stat were done by Shraddha Dahale. Scale bar = 25 µm.

5.20 BES1 phosphorylation

At the molecular dimension, BIN2 phosphorylates and thereby inactivates BES1 and BZR1 by promoting their cytoplasmic retention via 14-3-3 proteins (Gampala et al., 2007; Ryu et al., 2007), inhibiting their DNA binding activity (Vert & Chory, 2006), and stimulating their degradation (J. X. He et al., 2002; E. J. Kim et al., 2019; Yin et al., 2002). To determine if the impact of Cab1 on BIN2 would cause BES1 dephosphorylation and degradation, BES1-GFP (*P_{35S}::GFP-BES1*) was co-transformed with GR-Cab1$_{28\text{-}113}$ (*$P_{35S\text{-}XVE}$::GR-V5-Cab1$_{28\text{-}113}$*) in *N. benthamiana* leaves. In the control sample, GR-Cab1$_{28\text{-}113}$ (*$P_{35S\text{-}XVE}$::GR-V5-Cab1$_{28\text{-}113}$*) was replaced with GR-mCherry (*$P_{35S\text{-}XVE}$::GR-V5-mCherry*), and the experiment was continued with the same following setup (Fig 6-31). 6h after β–Estradiol infiltration at 3dpi, Dexamethasone was infiltrated and the samples were then examined using confocal microscopy to test the functionality of the GR-V5 tag in preventing the proteins from entering the nucleus in the absence of Dexamethasone.

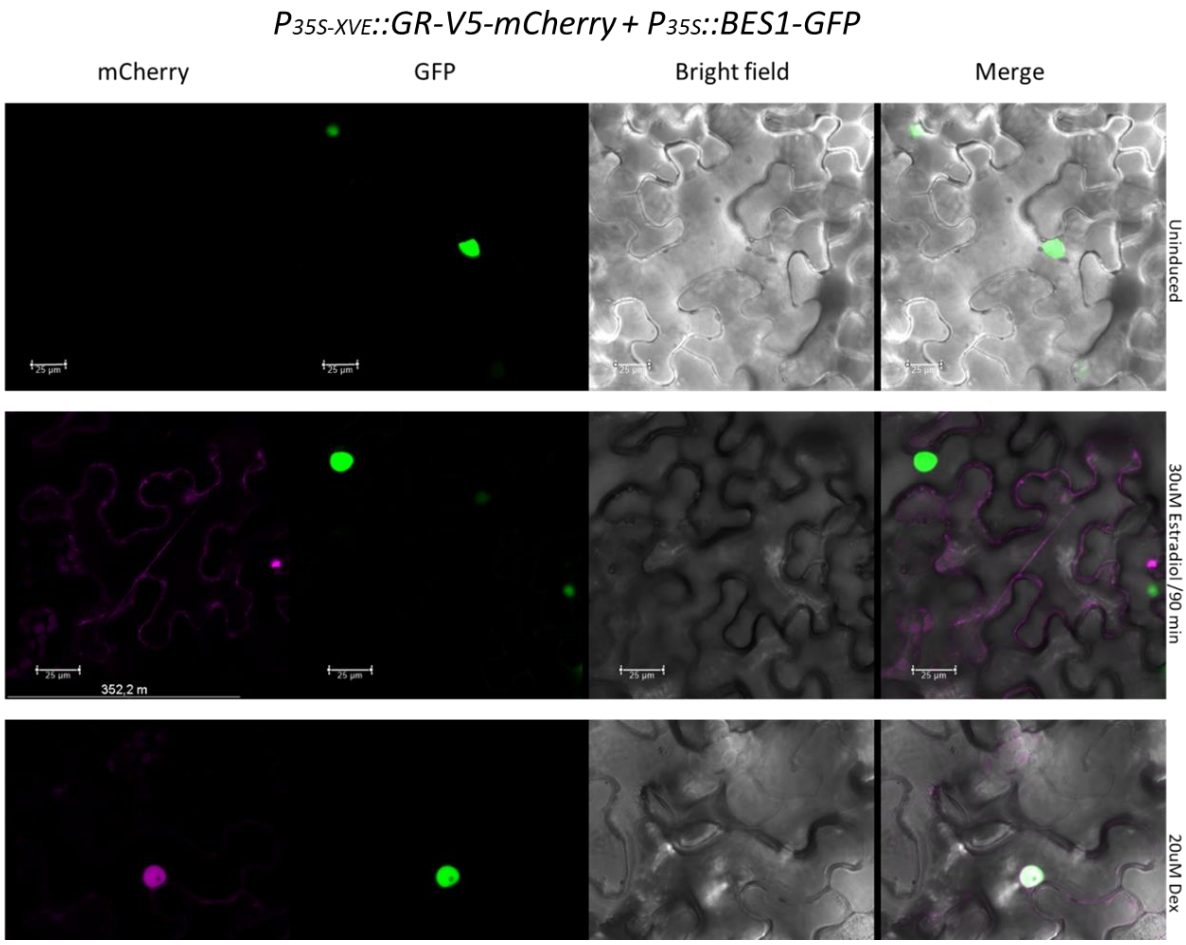

Figure 5-30 expression and translocation of GR-mCherry in N. benthamiana.

BES1-GFP (*P_{35S}::GFP-BES1*) was co-transformed with GR-mCherry (*$P_{35S\text{-}XVE}$::GR-V5-mCherry*) into *N. benthamiana* leaves. The expression of GR-mCherry was observed 6 hours after induction with 30 µM Estradiol. Within 30 minutes of treatment with 20 µM Dexamethasone, GR-mCherry accumulated in the nucleus. Scale bar = 25 µm.

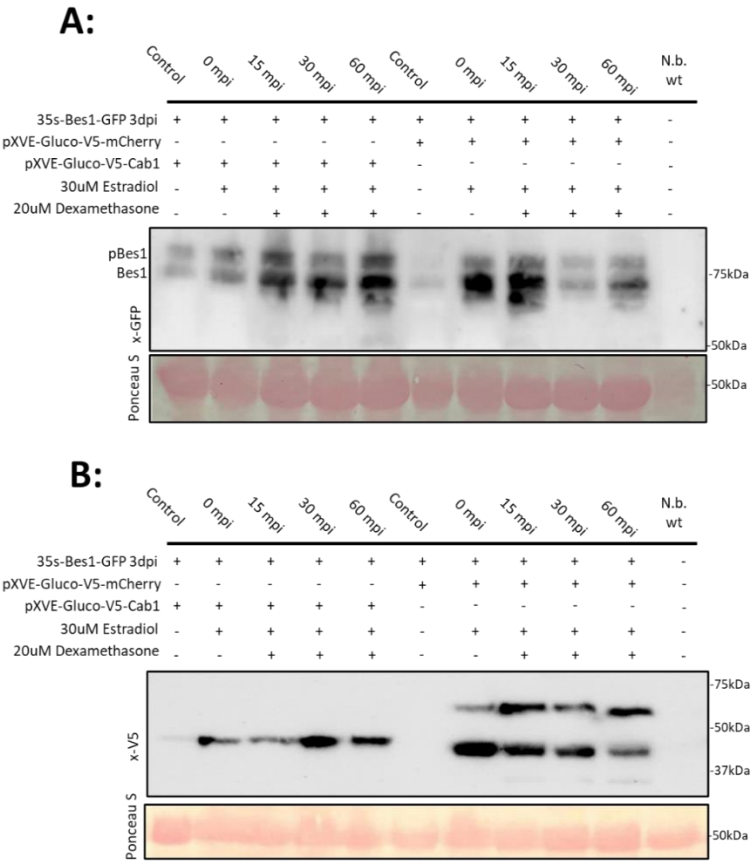

Figure 5-31 BES1-phosphorylation was examined in the presence and absence of Cab1.

- **A.** The phosphorylation status of BES1-GFP was assessed using a GFP antibody.
- **B.** The Expression of GR-mCherry (*$P_{35S\text{-}XVE}$::GR-V5-mCherry*) and GR-Cab1 (*$P_{35S\text{-}XVE}$::GR-V5-Cab1$_{28\text{-}113}$*) was determined using a V5 antibody.

The results showed that the induction of Cab1 did not lead to significant changes in BES1 phosphorylation compared to the mCherry control. However (fig. 6-31), the infiltration of the GSK3-inhibitor, Brassinolide (BL), significantly reduced the phosphorylation of BES1 in the control sample (fig. 6-32). These results demonstrate BES1 is not the downstream target of Cab1-BIN2 complex.

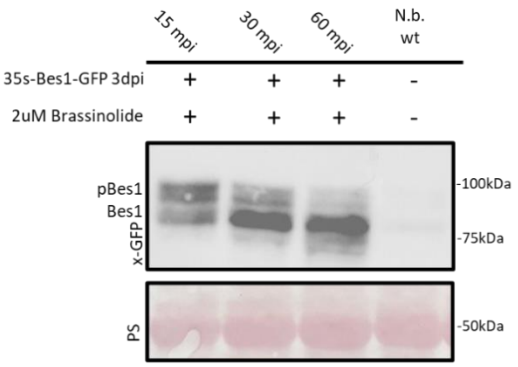

Figure 5-32 Brassinolide (BL) de-phosphorylates BES1.

BES1-GFP (*P35S::GFP-BES1*) was infiltrated into *N. benthamiana* leaves. The phosphorylation status of BES1-GFP was determined at 15-, 30- and 60- min intervals post 2µM Brassinolide induction by GFP antibody.

5.21 Mislocalised lines

To demonstrate the impact of Cab1's subcellular localization on the observed phenotype, Cab1 was tagged with nuclear export signal (NES), nuclear localization signal (NLS), and Myristylation signal peptide (Myr) under β–Estradiol inducible promoter. Phenotyping was conducted on transgenic lines of *A. thaliana*. The phenotype was observed in all three lines. As it was shown before, the GR-Cab1 (*P35S-XVE::GR-V5-Cab128-113*) line exhibited the phenotype only in the presence of Dexamethasone, indicating the necessity of nuclear localization for the observed Cabbage phenotype. We assume that the phenotype in NES-Cab1 (*P35S-XVE::*NES-Myc-Cab128-113) and Myr-Cab1 (*P35S-XVE::*Myr-Myc-Cab128-113) lines arises from the leakage of the signal peptide, causing a small portion of the expressed proteins to reach the nucleus and exhibit the phenotype (fig. 6-33, 6-34).

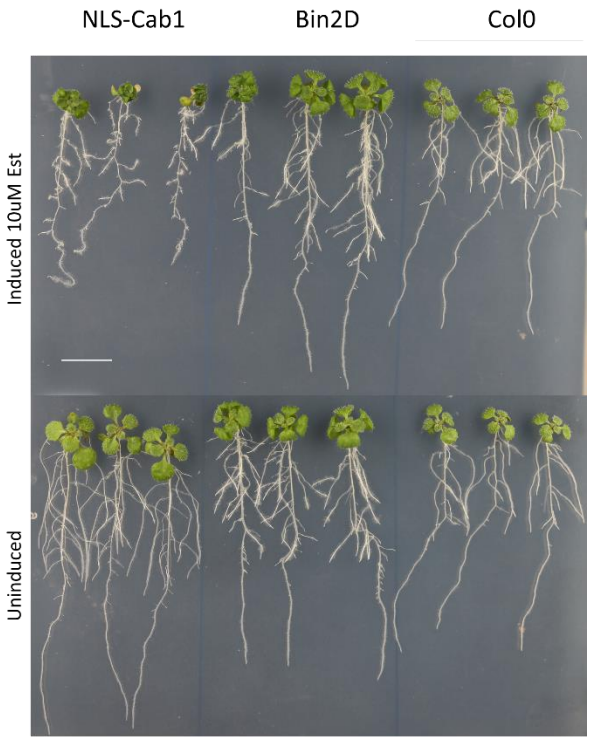

Figure 5-33 NLS-Cab1 expression causes dwarf phenotype in A. thaliana transgenic lines.

The expression of NLS-Cab1 ($P_{35S\text{-}XVE}$*::NLS-Myc-Cab1*$_{28\text{-}113}$) causes dwarf phenotype in *A. thaliana* transgenic lines.

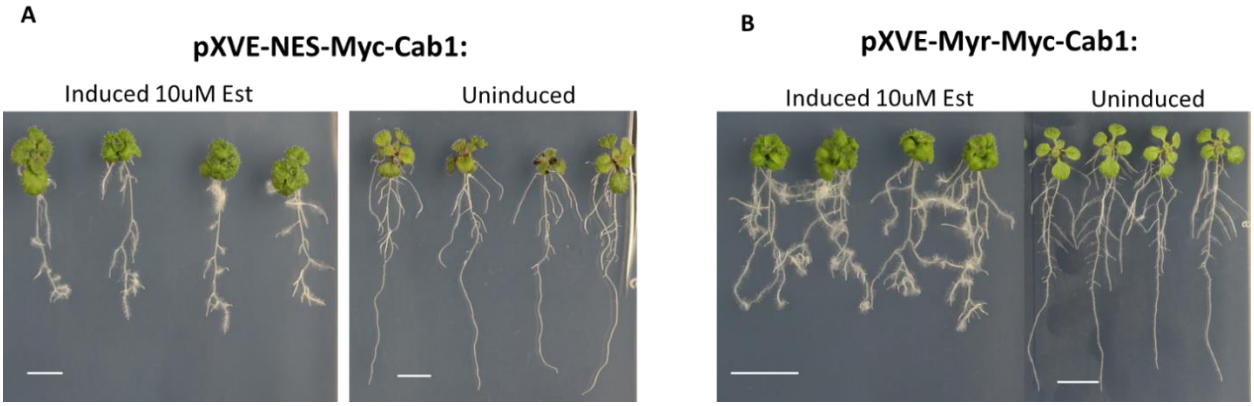

Figure 5-34 NES-Cab1 and Myr-Cab1 expression cause dwarf phenotype in A. thaliana transgenic lines.

(A) The expression of NES-Cab1 ($P_{35S\text{-}XVE}$*::NLS-Myc-Cab1*$_{28\text{-}113}$) causes dwarf phenotype in *A. thaliana* transgenic lines. (B) The expression of Myr-Cab1 ($P_{35S\text{-}XVE}$*::Myr-Myc-Cab1*$_{28\text{-}113}$) causes dwarf phenotype in *A. thaliana* transgenic lines.

5.22 Cab1 can reproduce cabbage like phenotype in absence of AtGSKs-CladeII

The redundancy function of GSKs in *A. thaliana* was demonstrated through genetic, biochemical, and physiological assays. Interestingly, even the *bin2bil1bil2* triple T-DNA insertional mutant (the seeds provided by Prof. Justin W. Walley, IOWA state University, USA (Montes et al., 2021), despite being mutated in all three genes, still responds to BR (Yan et al., 2009). To determine if Cab1, in the absence of the entire AtGSK3-CladeII, can still induce the cabbage phenotype, I conducted a cross between BIN2T and mCherry-Cab1 ($P_{35S\text{-}XVE}$*::mCherry-Cab1*$_{28\text{-}113}$). The resulting homozygous crossed lines (No. 27, 84, 86, 94, 95, 96) were then examined for phenotyping. interestingly, Cab1 was still capable of causing the cabbage phenotype (fig. 6-35). This finding aligns with our previous observation that Cab1 can interact with all GSK3 family clades.

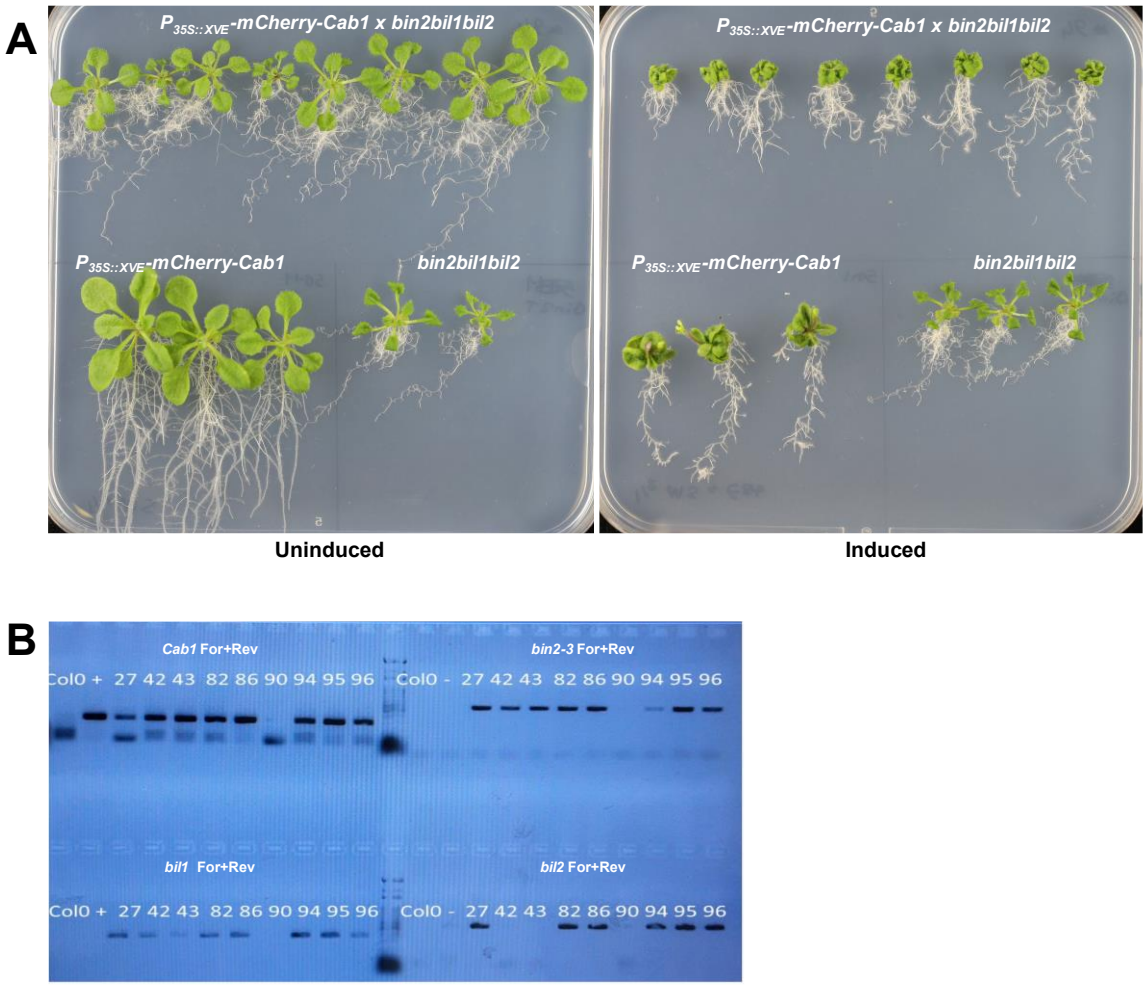

***Figure 5-35 Cab1 caused the dwarf phenotype in bin2bil1bil2* triple T-DNA insertional mutant.**

A. mCherry-Cab1 ($P_{35S\text{-}XVE}$*::mCherry-Cab1*$_{28\text{-}113}$) was crossed with *bin2bil1bil2* triple T-DNA insertional mutant lines was performed. The expression of Cab1 resulted in a dwarf phenotype in the homozygous line No. 95. Similar results were observed in four other crossed lines after genotyping. The genotyping of line No. 27 confirmed the presence of Cab1. However, the line did not exhibit the Cabbage phenotype. Additionally, the expression of Cab1 could not be confirmed through microscopy. Therefore, it is likely that the phenotype disappeared due to the silencing of Cab1.

B. The genotyping of mCherry-Cab1 ($P_{35S\text{-}XVE}$*::mCherry-Cab1*$_{28\text{-}113}$) crossed with *bin2bil1bil2* triple T-DNA insertional mutant lines was performed by published primers (Yan et al., 2009), The presence of Cab1 was subsequently confirmed using Cab1-specific primers. Genomic DNA (gDNA) was extracted from fresh leaf materials using the Che, followed by PCR.

5.23 cluster 5A phenotyping

some effector-genes in *Ustilago* (around 25-30%) are grouped into clusters. Previous studies have shown that genes within each cluster may have similar functions or target the same host protein (Navarrete et al., 2021; Scott et al., 2022). Cab1 is located in cluster 5A along with four other genes. To investigate whether other members of cluster 5A target BIN2 or exhibit a similar phenotype to Cab1, Y2H and phenotyping assays were conducted.

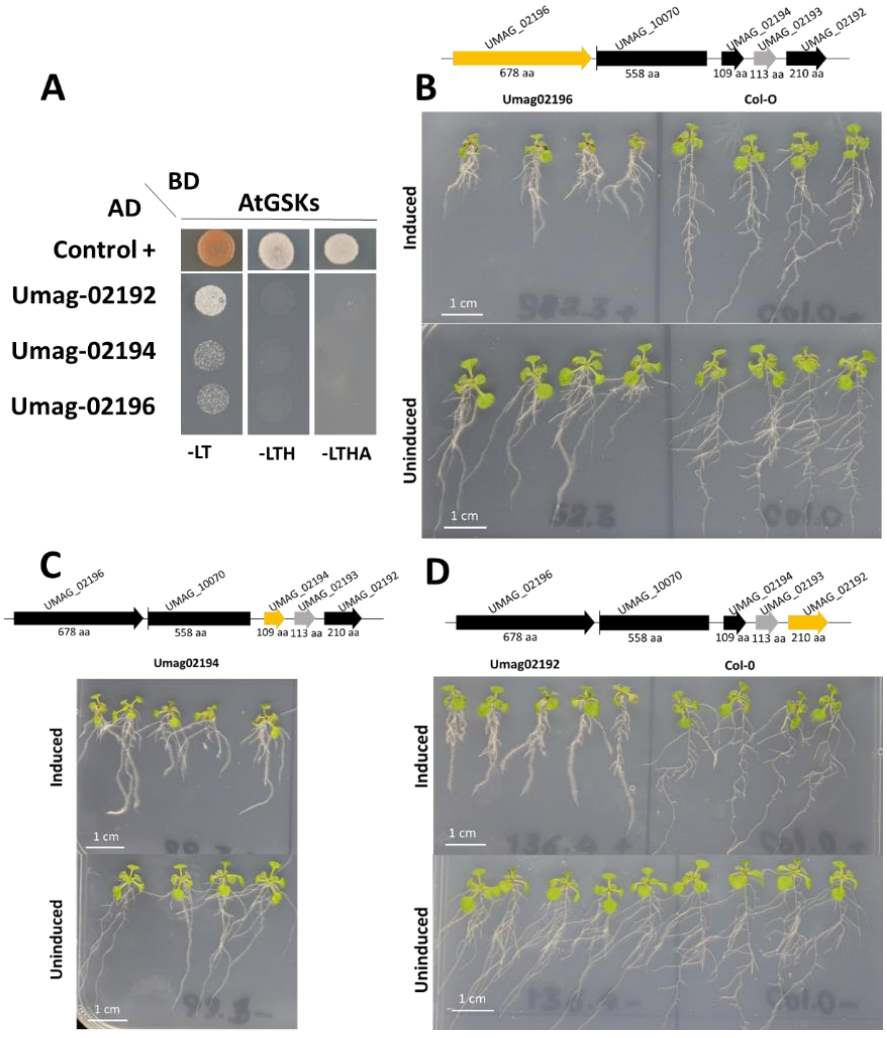

Figure 5-36 Cluster 5A members did not exhibit the Cab1 phenotype.

A Y2H assay was conducted to investigate the interaction between cluster 5A members and AtGSKs. None of the cluster members interacted with AtGSK, and similar results were observed for ZmGSks. (B, C, D) Phenotyping was carried out on the Araffector lines No. 52 (*$P_{35S\text{-}XVE}$::SP-Um02196-HA-P2A-Myc-Um02196*), 99 (*$P_{35S\text{-}XVE}$::SP-Um02194-HA-P2A-Myc-Um02194*), and

136 (*P35S-XVE::SP-Um02192-HA-P2A-Myc-Um02192*), and none of the tested transgenic lines displayed a Cab1-like phenotype.

Three predicted effectors from cluster 5A were tagged with the Gal4AD and used for a targeted Y2H assay. However, none of these genes showed interaction with AtBIN2 (Fig 6-36). To further examine the possibility of a similar phenotype, transgenic *A. thaliana* lines were subjected to phenotyping. No Cab1-like phenotype was observed in any of the other effectors.

5.24 HeLa Data

GSK3-like family kinases that are multifunctional and highly conserved non-receptor Ser/Thr kinases. There are two isoforms in mammalian cells, GSK3α and GSK3β (Beurel et al., 2015). Since Cab1 interacted with various GSK3 isoforms from different clades in *A. thaliana* and *Z. mays*, and affected the activity of AtBIN2 and ZmGSK3, the pharmaceutical potential of Cab1 became a question. Y2H assay demonstrated the direct interaction of Cab1 with HsGSKβ in the nucleus of *S. cerevisiae* (fig. 6-37). Since GSK3α and GSK3β are primarily cytosolic proteins, I further tested this hypothesis in HEK293T and HeLa cell lines.

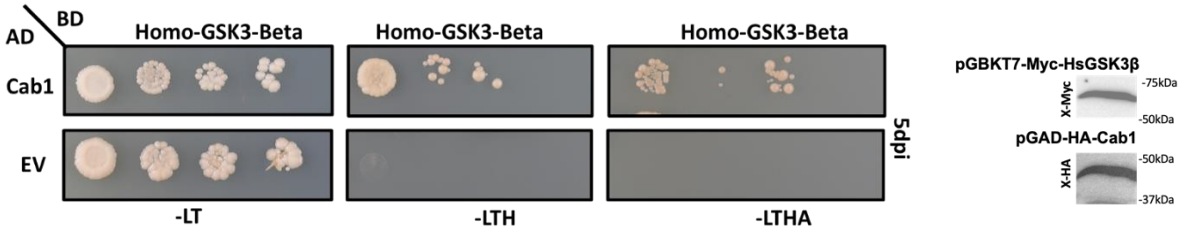

Figure 5-37 Cab1 directly interact with HsGSK3β in Y2H assay

Cab1-mCherry (*PTRE3G::Cab128-113-mCherry*) and GSK3β-GFP (*PTRE3G::GSK3β-GFP*) were transfected into the HEK293T mammalian cell model system. GSK3β-GFP exhibited a strong cytosolic localization, while co-expression of Cab1-mCherry was unable to relocate and accumulate GSK3β-GFP from the cytosol to the nucleus. GSK3β-GFP displayed the same behavior in the presence of mCherry (*PTRE3G::mCherry-mCherry*), which served as the negative control. These results contradict the previous observations regarding the mechanism of action of Cab1 in plants which Cab1 translocated AtBIN2 from cytosol to the nucleus and accumulates BIN2 in the nucleus.

To further investigate the direct interaction between Cab1 and GSK3β, co-transfection samples of Cab1$_{28\text{-}113}$-mCherry+GSK3β-GFP and mCherry+GSK3β-GFP in HEK293T cell lines were subjected to co-immunoprecipitation (CO-IP) using GFP beads. However, the experiment failed due to lysing technical challenges (Fig 6-38). Further troubleshooting experiments were not considered because of time limitations.

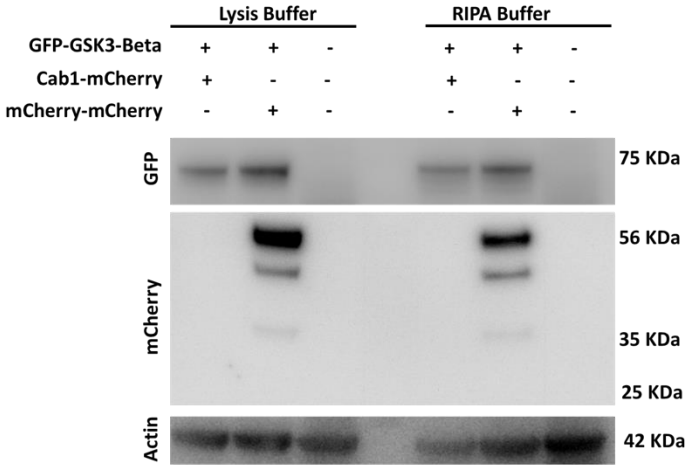

Figure 5-38 Transfected HEK293T total protein extraction by ChromoTek lysis and RIPA buffer.

The total protein was extracted by Lysis and RIPA buffer respectively. The equal amount of total protein was loaded on the gel and subjected to GFP, mCherry, and Actin antibodies. The Cab1-mCherry was not detectable amount.

5.25 Cab1 model of action

Based on the results, I speculate that the action of Cab1 occurs in the following steps. Initially, Cab1 is secreted and translocated from the fungal hyphal tips to the host cell. In the subsequent step, Cab1 relocalizes and accumulates GSK3-BIN2 in the nucleus, enhancing GSK3-BIN2's stability and activity. As a consequence of their interaction, they exert an undefined impact on PRP38 and the RNA processing machinery, leading to the downregulation of the expression of SAURs and EXPs (fig 6-39).

In this model, *U. maydis* employs Cab1 to suppress cell wall expansion and growth, which contradicts the gall-forming nature of *U. maydis*. I hypothesize that Cab1's action could be in response to other gall-forming effectors or specific types of cells, necessitating further investigation. In the support of my presented model, recent publication shows A.

thaliana employs BIN2 hyperactivity and FERONIA to safeguard cell expansion in response to Brassinosteroid-related growth signals (Chaudhary et al., 2023). In this model, BIN2 hyperactivity and FERONIA control the cells from getting overgrowth and raptured. This finding supports my presented model that *U. maydis* expressed Cab1 in response to other gall forming effectors to control the cell wall expansion from getting raptured.

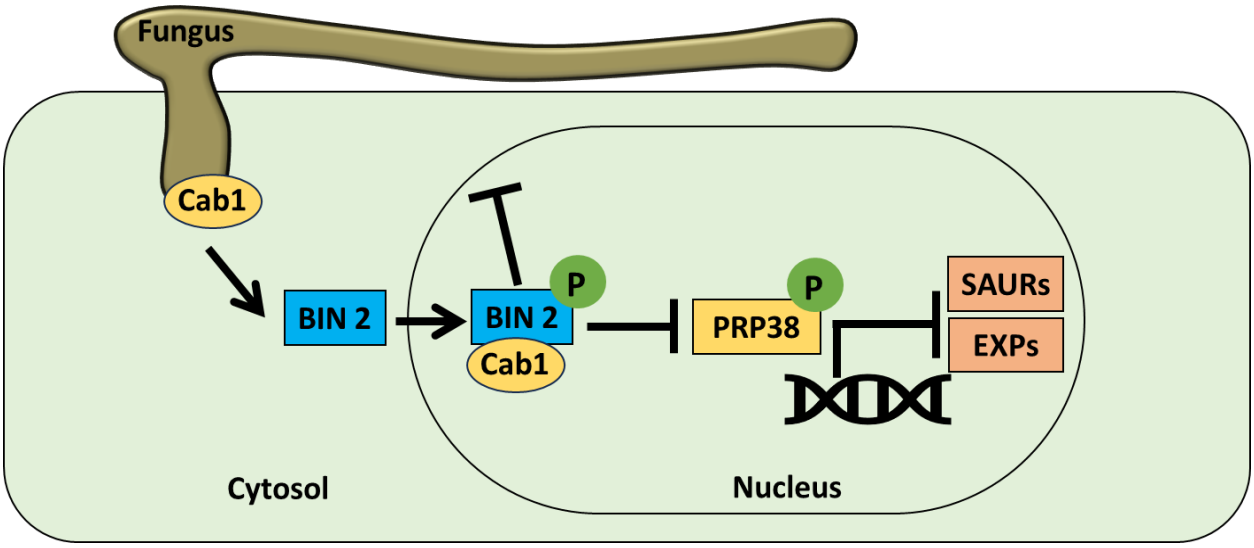

Figure 5-39 The mechanism of Cab1 action

My proposed model of Cab1 action suggests that Cab1 is secreted into the host cell by *U. maydis*. Upon entry, Cab1 re-localizes BIN2 from the cytosol to the host nucleus, effectively preventing BIN2 from returning to the cytosol. Cab1 expression leads to the stabilization of BIN2 via less ubiquitination at Lys^{35}. Simultaneously, Cab1 significantly enhances BIN2 phosphorylation at $Tyrosine^{200}$ compared to the control group, resulting increase BIN2 activity. Based on a literature review, I hypothesized that the Cab1-BIN2 complex phosphorylates and deactivates PRP38 at the RS motif. Consequently, the expression of SAURs and EXPs is downregulated compared to the control group due to the deactivation of PRP38. The downregulation of SAURs and EXPs results in the maintenance of rigidity in the plant cell wall, preventing expansion. This model elucidates Cab1's role in safeguarding cell expansion in response to other gall-forming effectors.

6 Discussion:

The ongoing conflict between plants and pathogens has resulted in complex recognition and suppression mechanisms. Plants have developed various membrane-bound and cytosolic receptors, to detect pathogen effectors and their associated activities (Zhou & Zhang, 2020). *U. maydis*, a plant pathogen, utilizes hundreds of effectors to prevent the immune responses of the host and manipulate its growth and development in its own favor. Knocking out these effectors affects pathogen fitness differently. For instance, Pep1 deletion has a high fitness cost, while cluster 2A deletion enhances *Ustilago* fitness (Scott et al., 2022). While many oomycete genomes show synteny, their effector gene families differ greatly due to rapid evolution driven by host species pressure. Also, species-specific genes encoding effectors were discovered. Several effector genes in the *U. maydis* genome are also present in *S. reilianum*, but their sequences differ and they vary in the number of copies (Schirawski et al., 2010). In our experiments, we observed that overexpression/deletion of Cab1 and deletion of all cluster 5A genes in the *U. maydis* solopathogenic strain SG200 did not result in a significant loss of virulence in seedling infections, consistent with the previous study (Kämper et al., 2006). This could be attributed to redundant functions of effectors or could result from maize-line-specific roles of the effectors, or their specificity towards certain maize organs (Scott et al., 2022).

Hormones play a crucial role in plant development and immunity. Previous studies have demonstrated the importance of manipulating immune-related hormone signaling pathways, such as auxin, salicylic acid (SA), and jasmonic acid (JA) signaling, in the successful infection of *U. maydis* (Darino et al., 2021; Djamei et al., 2011; Navarrete et al., 2022). Recent studies have emphasized BIN2's involvement in plant immunity during biotic stresses. However, the results are contradictory, and the underlying mechanism is not fully known (Han et al., 2022; Y. W. Kim et al., 2022; T. Song et al., 2021). It is important to note that most of the studies on Brassinosteroids (BR) have focused on dicots, revealing their roles in growth, development, sex determination, and responses to abiotic stresses (E. J. Kim & Russinova, 2020; Nolan et al., 2020). Few studies have been conducted on monocots like maize. For instance, the maize BR biosynthetic mutation (*na1)* leads to the feminization of male flowers (Hartwig et al., 2011). Additionally, BR-related transcription factors like ZmBEH1 (BZR1/BES1 homolog gene 1) and ZmBZR1

have been found to regulate leaf angle in maize (X. Wang et al., 2022). Interestingly, ZmSK2 (a homolog of AtBIN2) interacts with ZmIAA28, an Aux/IAA transcription factor known for its negative regulation of auxin signaling (Y. Wang et al., 2022). Overexpression of ZmSK2 leads to pronounced defects in BR signaling and arrests embryonic development at the transition stage. Conversely, knockout lines of *zmsk2* display enlarged embryos (Y. Wang et al., 2022).

BIN2 has been previously identified as a shuttle protein with nucleo-cytoplasmic activities (Vert & Chory, 2006). The regulation of BIN2 in plants involves various mechanisms, including dephosphorylation, post-translational modification, degradation, protein-protein interaction, and re-localization (E. J. Kim & Russinova, 2020; Mao & Li, 2020). Most of the reported post-translational modifications (PTMs) that are crucial for GSK3 activity have been identified in the kinase domains of ZmGSK4$^{30-314}$ and BIN2$^{34-274}$ (Dornelas et al., 1998; Mao et al., 2021). The N-terminal region of GSK family members exhibits variations in amino acid sequences and influencing their sub-cellular localization, while interactions with substrates primarily occur through the amino acid sequences in the C-terminal regions (Rozhon et al., 2022; Yoo et al., 2006; Youn & Kim, 2015). In our study, we observed that Cab1 interacts with the C-terminus of ZmGSK4$^{336-412}$ and facilitates its re-localization from the cytosol to the nucleus. This re-localization of ZmGSK4 in the presence of Cab1 also prevents its proteasomal degradation, which typically occurs through its interaction with the F-box E3 ubiquitin ligase KIB1 in the cytosol (Zhu et al., 2017). Consequently, the autophosphorylation of Tyr200 is also affected by this interaction (J. Li et al., 2020). These results indicate that the nuclear co-localization of Cab1 and BIN2 is crucial for manipulating the downstream targets. Few of GR-Cab1$_{28-113}$ transgenic lines and all Myristylation and NES mis localized Cab1 exhibited the cabbage phenotype after induction. I hypothesize that the phenotype arises due to a high level of Cab1 expression induced by β-Estradiol-inducible promoters, and that some signal peptides exhibit leakiness, failing to entirely prevent Cab1 from entering the nucleus, thus leading to the observed cabbage phenotype.

To date, there have been no reports indicating that plant pathogens specifically target BIN2 and Cab1 is the first reported effector protein that targets BIN2. The intriguing

question is why *Ustilago* targets a crucial negative regulator of the Brassinosteroid (BR) pathway? It was shown that BR and Methyl jasmonate (JA) injections in maize cause localized male sterility with early growth arrest zones within tassels and leading to *Ustilago's* failure to form galls (Ferris & Walbot, 2020; Walbot & Skibbe, 2010). In the context of Ustilago-induced gall development in maize leaves, the expression of Cab1 was found to be higher in "hypertrophic mesophyll tumors" (HTT) compared to hyperplasia tumor (HPT) in bundle sheet cells (Matei et al., 2018). The highest expression of Cab1 was observed in the SG200 Δ*see1* mutant which is unable to produce galls in HPT cells (Matei et al., 2018). recent publication shows *A. thaliana* employs BIN2 hyperactivity and FERONIA to safeguard cell expansion in response to Brassinosteroid-related growth signals. In this model, BIN2 hyperactivity and FERONIA control the plant cells from getting overgrowth and raptured (Chaudhary et al., 2023). These findings support my suggested model that Cab1 acts against the effectors involved in hyperplasia and aligns with my microscopic observations. Due to the inhibition of cell wall expansion, I observed smaller cells and stomata in Arabidopsis-induced plants compared to uninduced plants. This finding suggests that *U. maydis* expressed Cab1 in response to other gall forming effectors to control the cell wall expansion from getting raptured.

The Cab1 dwarf phenotype is caused by impairment in cell wall expansion. The impact of BR signaling on cell wall expansion via SOB3 was described before. SOB3 inhibits the expression and reduces the transcript accumulation of all six members of the SAUR19 subfamily, which are associated with the repression of cell expansion and hypocotyl elongation (Favero et al., 2017). The overexpression of SAUR genes promotes Expansins (EXPs) activity and cell elongation in *A. thaliana* (Pérez-Henríquez & Yang, 2023; van Mourik et al., 2017). EXPs activity leads to increased cell wall plasticity and extensibility, enabling cell growth and development (Mu et al., 2021; Sampedro & Cosgrove, 2005). So, I became interested to look for the interplay of BR with other hormonal pathways in response to the Cab1 expression.

It has been widely studied that both auxin and BR promote cell expansion and hypocotyl elongation. however, the interconnection between auxin and BR involves complex signaling pathways. SAURs genes have been studied due to their role as positive

regulators of cell expansion by modulating auxin polar transport, which is essential for cell elongation and growth (M. Li et al., 2018). I had a closer look at the role of downregulated SAURs in the presence of Cab1. SAUR19 and 20 are known for their involvement in auxin transport modulation (Spartz et al., 2012). While the SAUR26 subfamily is associated with thermo-responsive plant architecture variations (Z. Wang et al., 2019). The BZR1/ARF6/PIF4 (BAP) complex serves as a key interaction point between BR and auxin, activating the SAUR19 subfamily and EXPs (Bouré et al., 2019). Additionally, BZR1 directly interacts with the promoter regions of IAA19 and ARF7, regulating BR-induced differential growth (X. Y. Zhou et al., 2013). Interestingly, in response to the light, plants employ the activation mechanism of Bin2 to suppress BZR1. In this process, HY5 interacts physically with BIN2, leading to increased kinase activity. This interaction enhances the phosphorylation and degradation of BZR1, thereby inhibiting brassinosteroid (BR)-mediated hypocotyl elongation in light conditions (J. Li et al., 2020). These findings present the coordinated regulation of growth and development by the BR and auxin signaling pathways.

Activation of SAURs genes initiates the process of cell wall expansion. EXPs and xyloglucan endotransglucosylases/hydrolases (XTHs) are involved in cell wall loosening and expansion (Ishida & Yokoyama, 2022; Narváez-Barragán et al., 2020). EXPA1 is crucial for hypocotyl elongation (Zhuang et al., 2022) and also affects the expression of various EXPs and XTHs (Samalova et al., 2023). It was shown that EXPA5 and XTH19 are involved in brassinosteroid (BR)-induced hypocotyl elongation (Zhuang et al., 2022) while EXPA19 is associated with the kernel size in rice (Zhao et al., 2023). In summary, the expression of Cab1 leads to the downregulation of SAURs and EXPs and prevents the elongation of the hypocotyl that is induced by auxin polar transport (Sampedro & Cosgrove, 2005; van Mourik et al., 2017; Wieczorek & Grundler, 2006).

The enigmatic involvement of Shaggy-like kinases and AtBin2 in alternative splicing and RNA processing was published (T.-W. Kim et al., 2023; Shinde et al., 2017). The SplitTurboID and MS-IP helped to find proteins involved in nuclear body formation and/or downstream actions of Bin2 in the presence of Cab1. Interestingly, pre-mRNA processing and proteins involved in RNA processing are the most enriched biological process got

recognized by ShinnyGO 0.78 (table 6-3, 6-4). As the highest score candidate, Pre-mRNA-splicing factor 38A (AtPRP38A) is required for the first pre-mRNA cleavage reaction catalyzed by the spliceosome B-complex and is necessary for late spliceosome maturation. Without AtPRP38 activity, the formed spliceosome will get arrested in a catalytic impaired state (Plaschka et al., 2017; Xie et al., 1998). studies showed that shaggy-like kinases phosphorylate the splicing factors at the RSRS motif, and the existence of the RSRSRS motif in AtPRP38A makes it an interesting candidate to follow up on. The phenotype of Cab1 in the suppression of cell wall expansion is done via suppression of Auxin signaling. But still the biological relevance and the possible mechanism behind AtPRP38 and Cab1 was still an important question.

A few studies were performed on AtPRP38, in these studies was shown that AtUBL5 interacts with the C-terminus of AtPRP38 and increases the efficiency of IAA1 mRNA splicing. Knockdown of AtUBL5b resulted in a pattern of insufficient pre-mRNA splicing in several introns of AtCDC2, and in introns of IAA1, IAA4, and IAA5. Defects of pre-mRNA splicing in an AtPRP38 mutant resulted in an insufficient pre-mRNA splicing pattern in the intron of IAA1. Interestingly, knockdown plants of *AtUBL5* showed abnormalities in root elongation, plant development, and auxin response. These results showed that *AtUBL5b* positively regulates plant root elongation and development through pre-mRNA splicing with AtPRP38C in *A. thaliana* (Watanabe et al., 2019).

The lack of introns in most of SAURs makes it difficult to detect alternative splicing of target genes caused by Cab1 expression (G. Li et al., 2022). On the other hand, the existence of several snRNAs in the spliceosome structure needs more coverage of NGS to get detected. Increased NGS coverage can help elucidate the impact of alternative splicing machinery via Cab1 on other downregulated genes related to cell wall expansion, including EXPAs, IAA6, RGF 6, and 9.

The biological similarities between *U. maydis* and human cells was studied before (Juárez-Montiel et al., 2018; Steinberg & Perez-Martin, 2008). Dysfunction of GSK3 in mammalian cells causes different diseases such as cancer, neurodegenerative, Parkinson, Alzheimer, and bipolar disorders (Hur & Zhou, 2010; Kaidanovich-Beilin & Woodgett, 2011; Sutherland, 2011). They phosphorylate multiple proteins on serine (S)

and threonine (T) residues. GSK-3 has important roles as both a tumor suppressor (e.g., inhibition of β-catenin, c-MYC, MCL1) as well as a tumor promoter (e.g., inhibition of the cell cycle inhibitor p27Kip-1) (Duda et al., 2020). Cab1's interaction with GSK3s makes it a potential candidate for studying the effects of its exogenous expression in the mammalian system. Despite the direct interaction of Cab1 and HsGSK3 in the Y2H assay, the relocalization of HsGSK3beta from the cytosol to the nucleus by Cab1 was not observe in Hek293T lines. This contrast may be caused by HsGSK3β cytosolic localization that reduces the chance of Cab1-HsGSK3β interaction in vivo. Due to time and resource limitations, we did not further explore the mammalian system in this study. However, Cab1 has demonstrated the ability to directly bind to the human orthologue of BIN2, this characteristic had not been tested for any *U. maydis* effector previously. This discovery highlights the interdisciplinary potential of *U. maydis* secreted proteins for molecular biology studies with a specific focus on direct therapeutic applications.

Cab1, a unique fungal protein with a novel function, does not possess structural similarity to other proteins according to Alpha fold and in-silico analyses. Extensive in-silico analysis of Cab1's nucleotide and amino acid sequences did not reveal any conserved domain, structure, or motif. My data suggest that Cab1 plays a role in limiting the excessive growth of galls induced by other *Ustilago* growth promoting effectors. Due to the importance of BIN2 in the plant's agricultural traits such as leaf angle and cell size, it is an worthful target for further studies and practical application (Hu et al., 2018; Zhao et al., 2023). My findings regarding Cab1's mechanism of action on BIN2 provide new insights into the field of plant pathology and open up exciting possibilities for further research.

7 Outlook

Studying how *U. maydis* effectors function in non-host systems has revealed a new approach to understanding their role in the context of biotrophic pathogens. This approach led to the discovery of Cab1, which provided the opportunity to further investigations into this novel host target and expanded our understanding of biotrophic pathogens.

In a similar vein, it is advisable to conduct similar studies using comparable methods, while also incorporating newly developed AI tools like Alphafold for studying other *U. maydis* effectors. The findings from SplitTurboID demonstrate its effectiveness as a valuable tool for exploring downstream processes in similar research projects.

Furthermore, the interdisciplinary application of *U. maydis* effectors, case study Cab1, presents an exciting opportunity to be coupled with AI tools, protein engineering, and synthetic biology. This combination holds great potential for further interdisciplinary studies and application.

8 References

Ackerman-Lavert, M., Fridman, Y., Matosevich, R., Khandal, H., Friedlander-Shani, L., Vragović, K., Ben El, R., Horev, G., Tarkowská, D., Efroni, I., & Savaldi-Goldstein, S. (2021). Auxin requirements for a meristematic state in roots depend on a dual brassinosteroid function. *Current Biology : CB*, *31*(20), 4462–4472. https://doi.org/10.1016/j.cub.2021.07.075

Ai, H., Bellstaedt, J., Bartusch, K. S., Eschen-Lippold, L., Babben, S., Balcke, G. U., Tissier, A., Hause, B., Andersen, T. G., Delker, C., & Quint, M. (2023). Auxin-dependent regulation of cell division rates governs root thermomorphogenesis. *The EMBO Journal*, *42*(11), e111926. https://doi.org/10.15252/EMBJ.2022111926

Aoyama, T., & Chua, N. H. (1997). A glucocorticoid-mediated transcriptional induction system in transgenic plants. *The Plant Journal*, *11*(3), 605–612. https://doi.org/10.1046/J.1365-313X.1997.11030605.X

Ardito, F., Giuliani, M., Perrone, D., Troiano, G., & Muzio, L. Lo. (2017). The crucial role of protein phosphorylation in cell signalingand its use as targeted therapy (Review). In *International Journal of Molecular Medicine* (Vol. 40, Issue 2, pp. 271–280). Spandidos Publications. https://doi.org/10.3892/ijmm.2017.3036

Ausubel, F. M., Brent, R., Kingston, R. E., Moore, D. D., Seidman, J. G., & Smith, J. A. (2003). *Current Protocols in Molecular Biology Kevin Struhl (eds.) Current Protocols in Molecular Biology*.

Bailey, T. L., & Elkan, C. (1994). *FITTING A MIXTURE MODEL BY EXPECTATION MAXIMIZATION TO DISCOVER MOTIFS IN BIOPOLYMERS*.

Banuett, F., & Herskowitz, I. (1994). Morphological Transitions in the Life Cycle of Ustilago maydis and Their Genetic Control by the a and Loci. *Exprimental Mycology*, *18*, 247–266.

Bernardo-García, S., de Lucas, M., Martínez, C., Espinosa-Ruiz, A., Davière, J. M., & Prat, S. (2014). BR-dependent phosphorylation modulates PIF4 transcriptional activity and shapes diurnal hypocotyl growth. *Genes & Development*, *28*(15), 1681. https://doi.org/10.1101/GAD.243675.114

Beurel, E., Grieco, S. F., & Jope, R. S. (2015). Glycogen synthase kinase-3 (GSK3): Regulation, actions, and diseases. In *Pharmacology and Therapeutics* (Vol. 148, pp. 114–131). Elsevier Inc. https://doi.org/10.1016/j.pharmthera.2014.11.016

Bindics, J., Khan, M., Uhse, S., Kogelmann, B., Baggely, L., Reumann, D., Ingole, K. D., Stirnberg, A., Rybecky, A., Darino, M., Navarrete, F., Doehlemann, G., & Djamei, A. (2022). Many ways to TOPLESS – manipulation of plant auxin signalling by a cluster of fungal effectors. *New Phytologist*, *236*(4), 1455–1470. https://doi.org/10.1111/nph.18315

Bohlmann, H., & Sobczak, M. (2014). The plant cell wall in the feeding sites of cyst nematodes. In *Frontiers in Plant Science* (Vol. 5, Issue MAR). Frontiers Research Foundation. https://doi.org/10.3389/fpls.2014.00089

Bouré, N., S.Kumar, V., & Arnaud, N. (2019). The BAP Module: A Multisignal Integrator Orchestrating Growth. *Trends in Plant Science*, *24*(7).

Brachmann, A., Weinzierl, G., Kämper, J., & Kahmann, R. (2001). Identification of genes in the bW/bE regulatory cascade in Ustilago maydis. *Molecular Microbiology*, *42*(4), 1047–1063. https://doi.org/10.1046/j.1365-2958.2001.02699.x

Brefort, T., Doehlemann, G., Mendoza-Mendoza, A., Reissmann, S., Djamei, A., & Kallmann, R. (2009). Ustilago maydis as a Pathogen. *Http://Dx.Doi.Org/10.1146/Annurev-Phyto-080508-081923*, *47*, 423–445. https://doi.org/10.1146/ANNUREV-PHYTO-080508-081923

Bruce, S. A., Saville, B. J., & Emery, R. J. N. (2011). Ustilago maydis Produces Cytokinins and Abscisic Acid for Potential Regulation of Tumor Formation in Maize. *Journal of Plant Growth Regulation*, *30*(1), 51–63. https://doi.org/10.1007/s00344-010-9166-8

Callis, J. (2014). The Ubiquitination Machinery of the Ubiquitin System. *The Arabidopsis Book*, *12*, e0174. https://doi.org/10.1199/tab.0174

Caño-Delgado, A., Yin, Y., Yu, C., Vefeados, D., Mora-García, S., Cheng, J. C., Nam, K. H., Li, J., & Chory, J. (2004). BRL1 and BRL3 are novel brassinosteroid receptors that function in vascular differentiation in Arabidopsis. *Development (Cambridge, England)*, *131*(21), 5341–5351. https://doi.org/10.1242/DEV.01403

Čarná, M., Repka, V., Skůpa, P., & Šturdík, E. (2014). Auxins in defense strategies. *Biologia (Poland)*, *69*(10), 1255–1263. https://doi.org/10.2478/S11756-014-0431-3/XML

Carpita, N., Tiemey2, M., & Campbell, M. (2001). Molecular biology of the plant cell wall: searching for the genes that define structure, architecture and dynamics. In *Plant Molecular Biology* (Vol. 47).

Chandler, J. W. (2016). Auxin response factors. In *Plant Cell and Environment* (Vol. 39, Issue 5, pp. 1014–1028). Blackwell Publishing Ltd. https://doi.org/10.1111/pce.12662

Chaudhary, A., Hsiao, Y.-C., Yeh, F.-L. J., Wu, H.-M., Cheung, A. Y., Xu, S.-L., & Wang, Z.-Y. (2023). Brassinosteroid recruits FERONIA to safeguard cell expansion in Arabidopsis. *BioRxiv*, 2023.10.01.560400. https://doi.org/10.1101/2023.10.01.560400

Cheng, Y. T., Zhang, L., & He, S. Y. (2019). Plant-Microbe Interactions Facing Environmental Challenge. In *Cell Host and Microbe* (Vol. 26, Issue 2, pp. 183–192). Cell Press. https://doi.org/10.1016/j.chom.2019.07.009

Cho, K. F., Branon, T. C., Udeshi, N. D., Myers, S. A., Carr, S. A., & Ting, A. Y. (2020). Proximity labeling in mammalian cells with TurboID and split-TurboID. *Nature Protocols*, *15*(12), 3971–3999. https://doi.org/10.1038/s41596-020-0399-0

Christoph, W. B., & Gero, S. (2004). Ustilago maydis , model system for analysis of the molecular basis of fungal pathogenicity. *Molecular Plant Pathology*. https://doi.org/10.1111/J.1364-3703.2004.00210.X

Chung, Y., Maharjan, P. M., Lee, O., Fujioka, S., Jang, S., Kim, B., Takatsuto, S., Tsujimoto, M., Kim, H., Cho, S., Park, T., Cho, H., Hwang, I., & Choe, S. (2011). Auxin stimulates DWARF4 expression and

brassinosteroid biosynthesis in Arabidopsis. *Plant Journal*, *66*(4), 564–578. https://doi.org/10.1111/j.1365-313X.2011.04513.x

Clouse, S. D., Langford, M., & McMorris, T. C. (1996). A brassinosteroid-insensitive mutant in Arabidopsis thaliana exhibits multiple defects in growth and development. *Plant Physiology*, *111*(3), 671. https://doi.org/10.1104/PP.111.3.671

Darino, M., Chia, K. S., Marques, J., Aleksza, D., Soto-Jiménez, L. M., Saado, I., Uhse, S., Borg, M., Betz, R., Bindics, J., Zienkiewicz, K., Feussner, I., Petit-Houdenot, Y., & Djamei, A. (2021). Ustilago maydis effector Jsi1 interacts with Topless corepressor, hijacking plant jasmonate/ethylene signaling. *New Phytologist*, *229*(6), 3393–3407. https://doi.org/10.1111/NPH.17116

Depuydt, S., & Hardtke, C. S. (2011). Hormone signalling crosstalk in plant growth regulation. In *Current Biology* (Vol. 21, Issue 9). https://doi.org/10.1016/j.cub.2011.03.013

Devi, L. L., Pandey, A., Gupta, S., & Singh, A. P. (2022). The interplay of auxin and brassinosteroid signaling tunes root growth under low and different nitrogen forms. *Plant Physiology*, *189*(3), 1757–1773. https://doi.org/10.1093/PLPHYS/KIAC157

Díaz, A., Taberner, A., & Vilaplana, L. (2020). The emergence of a new weed in maize plantations: characterization and genetic structure using microsatellite markers. *Genetic Resources and Crop Evolution*, *67*(1), 225–239. https://doi.org/10.1007/s10722-019-00828-z

Díaz-Troya, S., Pérez-Pérez, M. E., Florencio, F. J., & Crespo, J. L. (2008). The role of TOR in autophagy regulation from yeast to plants and mammals. In *Autophagy* (Vol. 4, Issue 7, pp. 851–865). Taylor and Francis Inc. https://doi.org/10.4161/auto.6555

Djamei, A., & Kahmann, R. (2012). Ustilago maydis: Dissecting the Molecular Interface between Pathogen and Plant. *PLoS Pathogens*, *8*(11). https://doi.org/10.1371/journal.ppat.1002955

Djamei, A., Schipper, K., Rabe, F., Ghosh, A., Vincon, V., Kahnt, J., Osorio, S., Tohge, T., Fernie, A. R., Feussner, I., Feussner, K., Meinicke, P., Stierhof, Y. D., Schwarz, H., MacEk, B., Mann, M., & Kahmann, R. (2011). Metabolic priming by a secreted fungal effector. *Nature*, *478*(7369), 395–398. https://doi.org/10.1038/NATURE10454

Doehlemann, G., Reissmann, S., Aßmann, D., Fleckenstein, M., & Kahmann, R. (2011). Two linked genes encoding a secreted effector and a membrane protein are essential for Ustilago maydis-induced tumour formation. *Molecular Microbiology*, *81*(3), 751–766. https://doi.org/10.1111/j.1365-2958.2011.07728.x

Doehlemann, G., Van Der Linde, K., Aßmann, D., Schwammbach, D., Hof, A., Mohanty, A., Jackson, D., & Kahmann, R. (2009). Pep1, a secreted effector protein of Ustilago maydis, is required for successful invasion of plant cells. *PLoS Pathogens*, *5*(2). https://doi.org/10.1371/journal.ppat.1000290

Dornelas, M. C., Lejeune, B., Dron, M., & Kreis, M. (1998). The Arabidopsis SHAGGY-related protein kinase (ASK) gene family: structure, organization and evolution. *Gene*, *212*(2), 249–257. https://doi.org/10.1016/S0378-1119(98)00147-4

Du, M., Spalding, E. P., & Gray, W. M. (2020). *Rapid Auxin-Mediated Cell Expansion*. https://doi.org/10.1146/annurev-arplant-073019

Duda, P., Akula, S. M., Abrams, S. L., Steelman, L. S., Gizak, A., Rakus, D., & McCubrey, J. A. (2020). GSK-3 and miRs: Master regulators of therapeutic sensitivity of cancer cells. In *Biochimica et Biophysica Acta - Molecular Cell Research* (Vol. 1867, Issue 10). Elsevier B.V. https://doi.org/10.1016/j.bbamcr.2020.118770

Favero, D. S., Le, K. N., & Neff, M. M. (2017). Brassinosteroid signaling converges with SUPPRESSOR OF PHYTOCHROME B4-#3 to influence the expression of SMALL AUXIN UP RNA genes and hypocotyl growth. *Plant Journal*, *89*(6), 1133–1145. https://doi.org/10.1111/tpj.13451

Fei, W., & Liu, Y. (2023). Biotrophic Fungal Pathogens: a Critical Overview. In *Applied Biochemistry and Biotechnology* (Vol. 195, Issue 1, pp. 1–16). Springer. https://doi.org/10.1007/s12010-022-04087-0

Ferris, A. C., & Walbot, V. (2020). *Understanding Ustilago maydis Infection of Multiple Maize Organs*. https://doi.org/10.3390/jof7010008

Friedrichsen, D. M., Joazeiro, C. A. P., Li, J., Hunter, T., & Chory, J. (2000). Brassinosteroid-insensitive-1 is a ubiquitously expressed leucine-rich repeat receptor serine/threonine kinase. *Plant Physiology*, *123*(4), 1247–1255. https://doi.org/10.1104/PP.123.4.1247

Fu, J., & Wang, S. (2011). Insights into auxin signaling in plant-pathogen interactions. *Frontiers in Plant Science*, *2*(NOV). https://doi.org/10.3389/fpls.2011.00074

Gallavotti, A. (2013). The role of auxin in shaping shoot architecture. *Journal of Experimental Botany*, *64*(9), 2593–2608. https://doi.org/10.1093/JXB/ERT141

Gampala, S. S., Kim, T. W., He, J. X., Tang, W., Deng, Z., Bai, M. Y., Guan, S., Lalonde, S., Sun, Y., Gendron, J. M., Chen, H., Shibagaki, N., Ferl, R. J., Ehrhardt, D., Chong, K., Burlingame, A. L., & Wang, Z. Y. (2007). An essential role for 14-3-3 proteins in brassinosteroid signal transduction in Arabidopsis. *Developmental Cell*, *13*(2), 177–189. https://doi.org/10.1016/J.DEVCEL.2007.06.009

Gao, L., Kelliher, T., Nguyen, L., & Walbot, V. (2013). Ustilago maydis reprograms cell proliferation in maize anthers. *Plant Journal*, *75*(6), 903–914. https://doi.org/10.1111/tpj.12270

Gillissen, B., Bergemann, J., Sandmann, C., Schroeer, B., B61ker, M., & Kahmann, R. (1992). A Two-Component Regulatory System for Self/Non-Self Recognition in Ustilago maydis. In *Cell* (Vol. 66).

Gookin, T. E., & Assmann, S. M. (2014). Significant reduction of BiFC non-specific assembly facilitates in planta assessment of heterotrimeric G-protein interactors. *Plant Journal*, *80*(3), 553–567. https://doi.org/10.1111/tpj.12639

Groszyk, J., Yanushevska, Y., Zielezinski, A., Nadolska-Orczyk, A., Karlowski, W. M., & Orczyk, W. (2018). Annotation and profiling of barley GLYCOGEN SYNTHASE3/Shaggy-like genes indicated shift in organ-preferential expression. *PLoS ONE*, *13*(6). https://doi.org/10.1371/journal.pone.0199364

Guo, H., Li, L., Aluru, M., Aluru, S., & Yin, Y. (2013). Mechanisms and networks for brassinosteroid regulated gene expression. *Current Opinion in Plant Biology*, *16*(5), 545–553. https://doi.org/10.1016/J.PBI.2013.08.002

Han, Q., Tan, W., Zhao, Y., Yang, F., Yao, X., Lin, H., & Zhang, D. (2022). Salicylic acid-activated BIN2 phosphorylation of TGA3 promotes Arabidopsis PR gene expression and disease resistance . *The EMBO Journal*, *41*(19). https://doi.org/10.15252/embj.2022110682

Hartwig, T., Chuck, G. S., Fujioka, S., Klempien, A., Weizbauer, R., Potluri, D. P. V., Choe, S., Johal, G. S., & Schulz, B. (2011). Brassinosteroid control of sex determination in maize. *Proceedings of the National Academy of Sciences of the United States of America*, *108*(49), 19814–19819. https://doi.org/10.1073/pnas.1108359108

He, J. X., Gendron, J. M., Yang, Y., Li, J., & Wang, Z. Y. (2002). The GSK3-like kinase BIN2 phosphorylates and destabilizes BZR1, a positive regulator of the brassinosteroid signaling pathway in Arabidopsis. *Proceedings of the National Academy of Sciences of the United States of America*, *99*(15), 10185–10190. https://doi.org/10.1073/PNAS.152342599

He, Z., Wang, Z. Y., Li, J., Zhu, Q., Lamb, C., Ronald, P., & Chory, J. (2000). Perception of brassinosteroids by the extracellular domain of the receptor kinase BRI1. *Science (New York, N.Y.)*, *288*(5475), 2360–2363. https://doi.org/10.1126/SCIENCE.288.5475.2360

Hou, L., Li, Z., Shaheen, A., Zhang, K., Wang, J., Gao, X., & Wu, Q. (2022). Zea mays GSK2 gene is involved in brassinosteroid signaling. *Plant Growth Regulation*. https://doi.org/10.1007/s10725-022-00806-z

Hu, Z., Lu, S. J., Wang, M. J., He, H., Sun, L., Wang, H., Liu, X. H., Jiang, L., Sun, J. L., Xin, X., Kong, W., Chu, C., Xue, H. W., Yang, J., Luo, X., & Liu, J. X. (2018). A Novel QTL qTGW3 Encodes the GSK3/SHAGGY-Like Kinase OsGSK5/OsSK41 that Interacts with OsARF4 to Negatively Regulate Grain Size and Weight in Rice. *Molecular Plant*, *11*(5), 736–749. https://doi.org/10.1016/J.MOLP.2018.03.005

Huang, L., Ökmen, B., Christina Stolze, S., Kastl, M., Khan, M., Hilbig, D., Nakagami, H., Djamei, A., & Doehlemann, G. (2023). The fungal pathogen Ustilago maydis targets the maize corepressor TPL2 to modulate host transcription for tumorigenesis. *Bioarchive*. https://doi.org/10.1101/2023.06.12.544564

Huang, M., Bulut, A., Shrestha, B., Matera, C., Grundler, F. M. W., & Schleker, A. S. S. (2021). Bacillus firmus I-1582 promotes plant growth and impairs infection and development of the cyst nematode Heterodera schachtii over two generations. *Scientific Reports*, *11*(1). https://doi.org/10.1038/s41598-021-93567-0

Hughes, P. W. (2020). OsGSK2 Integrates Jasmonic Acid and Brassinosteroid Signaling in Rice. *The Plant Cell*, *32*(9), 2669–2670. https://doi.org/10.1105/TPC.20.00531

Hur, E. M., & Zhou, F. Q. (2010). GSK3 signalling in neural development. In *Nature Reviews Neuroscience* (Vol. 11, Issue 8, pp. 539–551). https://doi.org/10.1038/nrn2870

Ishida, K., & Yokoyama, R. (2022). Reconsidering the function of the xyloglucan endotransglucosylase/hydrolase family. *Journal of Plant Research*, *135*(2), 145–156. https://doi.org/10.1007/s10265-021-01361-w

J. Cosgrove, D. (2000). Loosening of plant cell walls by expansins. *Nature*.

Jing, H., & Strader, L. C. (2019). Interplay of Auxin and Cytokinin in Lateral Root Development. *International Journal of Molecular Sciences*, *20*(3). https://doi.org/10.3390/IJMS20030486

Johnson, K., & Lenhard, M. (2011). Genetic control of plant organ growth. In *New Phytologist* (Vol. 191, Issue 2, pp. 319–333). https://doi.org/10.1111/j.1469-8137.2011.03737.x

Jones, J. D. G., & Dangl, J. L. (2006). *The Plant immune system*. https://doi.org/10.1038

Juárez-Montiel, M., Tesillo-Moreno, P., Cruz-Angeles, A., Soberanes-Gutiérrez, V., Chávez-Camarillo, G., Ibarra, J. A., Hernández-Rodríguez, C., & Villa-Tanaca, L. (2018). Heterologous expression and characterization of the aspartic endoprotease Pep4um from Ustilago maydis, a homolog of the human Chatepsin D, an important breast cancer therapeutic target. *Molecular Biology Reports*, *45*(5), 1155–1163. https://doi.org/10.1007/s11033-018-4267-8

Jumper, J., Evans, R., Pritzel, A., Green, T., Figurnov, M., Ronneberger, O., Tunyasuvunakool, K., Bates, R., Žídek, A., Potapenko, A., Bridgland, A., Meyer, C., Kohl, S. A. A., Ballard, A. J., Cowie, A., Romera-Paredes, B., Nikolov, S., Jain, R., Adler, J., … Hassabis, D. (2021). Highly accurate protein structure prediction with AlphaFold. *Nature*, *596*(7873), 583–589. https://doi.org/10.1038/s41586-021-03819-2

Kaidanovich-Beilin, O., & Woodgett, J. R. (2011). GSK-3: Functional Insights from Cell Biology and Animal Models. *Frontiers in Molecular Neuroscience*, *4*. https://doi.org/10.3389/fnmol.2011.00040

Kämper, J. (2004). A PCR-based system for highly efficient generation of gene replacement mutants in Ustilago maydis. *Molecular Genetics and Genomics*, *271*(1), 103–110. https://doi.org/10.1007/s00438-003-0962-8

Kämper, J., Kahmann, R., Bölker, M., Ma, L. J., Brefort, T., Saville, B. J., Banuett, F., Kronstad, J. W., Gold, S. E., Müller, O., Perlin, M. H., Wösten, H. A. B., De Vries, R., Ruiz-Herrera, J., Reynaga-Peña, C. G., Snetselaar, K., McCann, M., Pérez-Martín, J., Feldbrügge, M., … Birren, B. W. (2006). Insights from the genome of the biotrophic fungal plant pathogen Ustilago maydis. *Nature*, *444*(7115), 97–101. https://doi.org/10.1038/NATURE05248

Katzen, F. (2007). Gateway(®) recombinational cloning: a biological operating system. *Expert Opinion on Drug Discovery*, *2*(4), 571–589. https://doi.org/10.1517/17460441.2.4.571

Kaur, S., Samota, M. K., Choudhary, M., Choudhary, M., Pandey, A. K., Sharma, A., & Thakur, J. (2022). How do plants defend themselves against pathogens-Biochemical mechanisms and genetic interventions. In *Physiology and Molecular Biology of Plants* (Vol. 28, Issue 2, pp. 485–504). Springer. https://doi.org/10.1007/s12298-022-01146-y

Khan, M., Uhse, S., Bindics, J., Kogelmann, B., Nagarajan, N., Ingole, K. D., & Djamei, A. (2023). Tip of the iceberg? Three novel TOPLESS interacting effectors of the gall-inducing fungus Ustilago maydis. *Bioarchive*. https://doi.org/10.1101/2023.06.12.544640

Kim, E. J., Lee, S. H., Park, C. H., Kim, S. H., Hsu, C. C., Xu, S., Wang, Z. Y., Kim, S. K., & Kim, T. W. (2019). Plant U-Box40 Mediates Degradation of the Brassinosteroid-Responsive Transcription Factor BZR1 in Arabidopsis Roots. *The Plant Cell*, *31*(4), 791–808. https://doi.org/10.1105/TPC.18.00941

Kim, E. J., & Russinova, E. (2020). Brassinosteroid signalling. In *Current Biology* (Vol. 30, Issue 7, pp. R294–R298). Cell Press. https://doi.org/10.1016/j.cub.2020.02.011

Kim, H., Park, P. J., Hwang, H. J., Lee, S. Y., Oh, M. H., & Kim, S. G. (2006). Brassinosteroid signals control expression of the AXR3/IAA17 gene in the cross-talk point with auxin in root development. *Bioscience, Biotechnology and Biochemistry*, *70*(4), 768–773. https://doi.org/10.1271/bbb.70.768

Kim, T. W., Guan, S., Burlingame, A. L., & Wang, Z. Y. (2011). The CDG1 Kinase Mediates Brassinosteroid Signal Transduction from BRI1 Receptor Kinase to BSU1 Phosphatase and GSK3-like Kinase BIN2. *Molecular Cell*, *43*(4), 561–571. https://doi.org/10.1016/j.molcel.2011.05.037

Kim, T.-W., Guan, S., Sun, Y., Deng, Z., Tang, W., Shang, J.-X., Sun, Y., Burlingame, A. L., & Wang, Z.-Y. (2009). Brassinosteroid signal transduction from cell-surface receptor kinases to nuclear transcription factors. *Nature Cell Biology*. https://doi.org/10.1038/ncb1970

Kim, T.-W., Park, C. H., Hsu, C.-C., Kim, Y.-W., Ko, Y.-W., Zhang, Z., Zhu, J.-Y., Hsiao, Y.-C., Branon, T., Kaasik, K., Saldivar, E., Li, K., Pasha, A., Provart, N. J., Burlingame, A. L., Xu, S.-L., Ting, A. Y., & Wang, Z.-Y. (2023). Mapping the signaling network of BIN2 kinase using TurboID-mediated biotin labeling and phosphoproteomics. *The Plant Cell*, *35*(3), 975–993. https://doi.org/10.1093/PLCELL/KOAD013

Kim, Y. W., Youn, J. H., Roh, J., Kim, J. M., Kim, S. K., & Kim, T. W. (2022). Brassinosteroids enhance salicylic acid-mediated immune responses by inhibiting BIN2 phosphorylation of clade I TGA transcription factors in Arabidopsis. *Molecular Plant*, *15*(6), 991–1007. https://doi.org/10.1016/j.molp.2022.05.002

Kinoshita, T., Caño-Delgado, A., Seto, H., Hiranuma, S., Fujioka, S., Yoshida, S., & Chory, J. (2005). Binding of brassinosteroids to the extracellular domain of plant receptor kinase BRI1. *Nature*, *433*(7022), 167–171. https://doi.org/10.1038/NATURE03227

Krogh, A., Larsson, B., Von Heijne, G., & Sonnhammer, E. L. L. (2001). Predicting transmembrane protein topology with a hidden Markov model: Application to complete genomes. *Journal of Molecular Biology*, *305*(3), 567–580. https://doi.org/10.1006/jmbi.2000.4315

Kuhn, A., Harborough, S. R., McLaughlin, H. M., Natarajan, B., Verstraeten, I., Friml, J., Kepinski, S., & Østergaard, L. (2020). Direct ETTIN-auxin interaction controls chromatin states in gynoecium development. *ELife*, *9*. https://doi.org/10.7554/eLife.51787

Lampropoulos, A., Sutikovic, Z., Wenzl, C., Maegele, I., Lohmann, J. U., & Forner, J. (2013). GreenGate - A Novel, Versatile, and Efficient Cloning System for Plant Transgenesis. *PLOS ONE*, *8*(12), e83043. https://doi.org/10.1371/JOURNAL.PONE.0083043

Lanver, D., Berndt, P., Tollot, M., Naik, V., Vranes, M., Warmann, T., Münch, K., Rössel, N., & Kahmann, R. (2014). Plant Surface Cues Prime Ustilago maydis for Biotrophic Development. *PLoS Pathogens*, *10*(7). https://doi.org/10.1371/journal.ppat.1004272

Lanver, D., Müller, A. N., Happel, P., Schweizer, G., Haas, F. B., Franitza, M., Pellegrin, C., Reissmann, S., Altmüller, J., Rensing, S. A., & Kahmann, R. (2018). The biotrophic development of ustilago maydis studied by RNA-seq analysis. *Plant Cell*, *30*(2), 300–323. https://doi.org/10.1105/tpc.17.00764

Lanver, D., Tollot, M., Schweizer, G., Lo Presti, L., Reissmann, S., Ma, L. S., Schuster, M., Tanaka, S., Liang, L., Ludwig, N., & Kahmann, R. (2017). Ustilago maydis effectors and their impact on virulence. In *Nature Reviews Microbiology* (Vol. 15, Issue 7, pp. 409–421). Nature Publishing Group. https://doi.org/10.1038/nrmicro.2017.33

Li, G., Wang, Q., Lu, L., Wang, S., Chen, X., Khan, M. H. U., Zhang, Y., & Yang, S. (2022). Identification of the soybean small auxin upregulated RNA (SAUR) gene family and specific haplotype for drought tolerance. *Biologia*, *77*(4), 1197–1217. https://doi.org/10.1007/s11756-022-01010-0

Li, H., Luo, L., Wang, Y., Zhang, J., & Huang, Y. (2022). Genome-Wide Characterization and Phylogenetic Analysis of GSK Genes in Maize and Elucidation of Their General Role in Interaction with BZR1. *International Journal of Molecular Sciences*, *23*(15). https://doi.org/10.3390/ijms23158056

Li, J., & Chory, J. (1997). A putative leucine-rich repeat receptor kinase involved in brassinosteroid signal transduction. *Cell*, *90*(5), 929–938. https://doi.org/10.1016/S0092-8674(00)80357-8

Li, J., & Nam, K. H. (2002). Regulation of Brassinosteroid Signaling by a GSK3/SHAGGY-Like Kinase. *Science*, *295*(5558), 1299–1301. https://doi.org/10.1126/SCIENCE.1065769

Li, J., Nam, K. H., Vafeados, D., & Chory, J. (2001). BIN2, a new brassinosteroid-insensitive locus in Arabidopsis. *Plant Physiology*, *127*(1), 14–22. https://doi.org/10.1104/PP.127.1.14

Li, J., Terzaghi, W., Gong, Y., Li, C., Ling, J. J., Fan, Y., Qin, N., Gong, X., Zhu, D., & Deng, X. W. (2020). Modulation of BIN2 kinase activity by HY5 controls hypocotyl elongation in the light. *Nature Communications*, *11*(1). https://doi.org/10.1038/s41467-020-15394-7

Li, M., Sun, P., Kang, T., Xing, H., Yang, D., Zhang, J., & Paré, P. W. (2018). Mapping podophyllotoxin biosynthesis and growth-related transcripts with high elevation in Sinopodophyllum hexandrum. *Industrial Crops and Products*, *124*, 510–518. https://doi.org/10.1016/j.indcrop.2018.08.007

Li, T., Lei, W., He, R., Tang, X., Han, J., Zou, L., Yin, Y., Lin, H., & Zhang, D. (2020). Brassinosteroids regulate root meristem development by mediating BIN2-UPB1 module in Arabidopsis. *PLOS Genetics*, *16*(7), e1008883. https://doi.org/10.1371/JOURNAL.PGEN.1008883

Li, Z., & He, Y. (2020). Roles of Brassinosteroids in Plant Reproduction. *International Journal of Molecular Sciences*, *21*(3). https://doi.org/10.3390/IJMS21030872

Ma, L. S., Wang, L., Trippel, C., Mendoza-Mendoza, A., Ullmann, S., Moretti, M., Carsten, A., Kahnt, J., Reissmann, S., Zechmann, B., Bange, G., & Kahmann, R. (2018). The Ustilago maydis repetitive effector Rsp3 blocks the antifungal activity of mannose-binding maize proteins. *Nature Communications*, *9*(1). https://doi.org/10.1038/s41467-018-04149-0

Machyna, M., Kehr, S., Straube, K., Kappei, D., Buchholz, F., Butter, F., Ule, J., Hertel, J., Stadler, P. F., & Neugebauer, K. M. (2014). The coilin interactome identifies hundreds of small noncoding RNAs that traffic through cajal bodies. *Molecular Cell*, *56*(3), 389–399. https://doi.org/10.1016/j.molcel.2014.10.004

Machyna, M., Neugebauer, K. M., & Staněk, D. (2015). Coilin: The first 25 years. *RNA Biology*, *12*(6), 590–596. https://doi.org/10.1080/15476286.2015.1034923

Majda, M., & Robert, S. (2018). The Role of Auxin in Cell Wall Expansion. *International Journal of Molecular Sciences*, *19*(4). https://doi.org/10.3390/IJMS19040951

Mao, J., & Li, J. (2020). Regulation of three key kinases of brassinosteroid signaling pathway. In *International Journal of Molecular Sciences* (Vol. 21, Issue 12, pp. 1–32). MDPI AG. https://doi.org/10.3390/ijms21124340

Mao, J., Li, W., Liu, J., & Li, J. (2021). Versatile Physiological Functions of Plant GSK3-Like Kinases. *Genes*, *12*(5), 697. https://doi.org/10.3390/genes12050697

Mapuranga, J., Zhang, N., Zhang, L., Chang, J., & Yang, W. (2022). Infection Strategies and Pathogenicity of Biotrophic Plant Fungal Pathogens. In *Frontiers in Microbiology* (Vol. 13). Frontiers Media S.A. https://doi.org/10.3389/fmicb.2022.799396

Marowa, P., Ding, A., & Kong, Y. (2016). Expansins: roles in plant growth and potential applications in crop improvement. In *Plant Cell Reports* (Vol. 35, Issue 5, pp. 949–965). Springer Verlag. https://doi.org/10.1007/s00299-016-1948-4

Matei, A., Ernst, C., Günl, M., Thiele, B., Altmüller, J., Walbot, V., Usadel, B., & Doehlemann, G. (2018). How to make a tumour: cell type specific dissection of Ustilago maydis-induced tumour development in maize leaves. *New Phytologist*, *217*(4), 1681–1695. https://doi.org/10.1111/nph.14960

Meyer, H. M. (2020). In search of function: nuclear bodies and their possible roles as plant environmental sensors. In *Current Opinion in Plant Biology* (Vol. 58, pp. 33–40). Elsevier Ltd. https://doi.org/10.1016/j.pbi.2020.10.002

Misas-Villamil, J. C., van der Hoorn, R. A. L., & Doehlemann, G. (2016). Papain-like cysteine proteases as hubs in plant immunity. In *New Phytologist* (Vol. 212, Issue 4, pp. 902–907). Blackwell Publishing Ltd. https://doi.org/10.1111/nph.14117

Montes, C., Liao, C.-Y., Nolan, T. M., Song, G., Clark, N. M., Guo, H., Bassham, D. C., Yin, Y., & Walley, J. W. (2021). *Interplay between brassinosteroids and TORC signaling in Arabidopsis revealed by integrated multi-dimensional analysis*. https://doi.org/10.1101/2021.02.12.431003

Mu, Q., Li, X., Luo, J., Pan, Q., Li, Y., & Gu, T. (2021). Characterization of expansin genes and their transcriptional regulation by histone modifications in strawberry. In *Planta* (Vol. 254, Issue 2). Springer Science and Business Media Deutschland GmbH. https://doi.org/10.1007/s00425-021-03665-6

Mueller, A. N., Ziemann, S., Treitschke, S., Aßmann, D., & Doehlemann, G. (2013). Compatibility in the Ustilago maydis-Maize Interaction Requires Inhibition of Host Cysteine Proteases by the Fungal Effector Pit2. *PLoS Pathogens*, *9*(2). https://doi.org/10.1371/journal.ppat.1003177

Nagarajan, N., Khan, M., & Djamei, A. (2023). Manipulation of Auxin Signaling by Smut Fungi during Plant Colonization. *Journal of Fungi*, *9*(12), 1184. https://doi.org/10.3390/jof9121184

Nakamura, A., Higuchi, K., Goda, H., Fujiwara, M. T., Sawa, S., Koshiba, T., Shimada, Y., & Yoshida, S. (2003). Brassinolide Induces IAA5, IAA19, and DR5, a Synthetic Auxin Response Element in Arabidopsis, Implying a Cross Talk Point of Brassinosteroid and Auxin Signaling. *Plant Physiology*, *133*(4), 1843–1853. https://doi.org/10.1104/pp.103.030031

Narváez-Barragán, D. A., Tovar-Herrera, O. E., Segovia, L., Serrano, M., & Martinez-Anaya, C. (2020). Expansin-related proteins: Biology, microbe–plant interactions and associated plant-defense responses. *Microbiology (United Kingdom)*, *166*(11), 1007–1018. https://doi.org/10.1099/mic.0.000984

Navarrete, F., Gallei, M., Kornienko, A. E., Saado, I., Darino, M. A., Khan, M., Bindics, J., & Djamei, A. (2022). TOPLESS promotes plant immunity by repressing auxin signaling and is targeted by the fungal effector Naked1. *Plant Communications*. https://doi.org/10.1101/2021.05.04.442566

Navarrete, F., Grujic, N., Stirnberg, A., Saado, I., Aleksza, D., Gallei, M., Adi, H., Alcântara, A., Khan, M., Bindics, J., Trujillo, M., & Djamei, A. (2021). The Pleiades are a cluster of fungal effectors that inhibit host defenses. *PLOS Pathogens*, *17*(6), e1009641. https://doi.org/10.1371/JOURNAL.PPAT.1009641

Navarrete, F., Grujic, N., Stirnberg, A., Saadoid, I., Alekszaid, D., Gallei, M., Adi, H., Alcâ Ntaraid, A., Khanid, M., Bindicsid, J., Trujilloid, M., & Djameiid, A. (2021). *The Pleiades are a cluster of fungal effectors that inhibit host defenses*. https://doi.org/10.1371/journal.ppat.1009641

Nolan, T. M., Brennan, B., Yang, M., Chen, J., Zhang, M., Li, Z., Wang, X., Bassham, D. C., Walley, J., & Yin, Y. (2017). Selective Autophagy of BES1 Mediated by DSK2 Balances Plant Growth and Survival. *Developmental Cell*, *41*(1), 33-46.e7. https://doi.org/10.1016/J.DEVCEL.2017.03.013

Nolan, T. M., Vukašinoví, N., Hsu, C.-W., Zhang, J., Vanhoutte, I., Shahan, R., Taylor, I. W., Greenstreet, L., Heitz, M., Wang, P., Szekely, P., Brosnan, A., Yin, Y., Schiebinger, G., Ohler, U., Russinova, E., & Benfey, P. N. (2022). *Brassinosteroid gene regulatory networks at cellular resolution*. https://doi.org/10.1101/2022.09.16.508001

Nolan, T. M., Vukasinović, N., Liu, D., Russinova, E., & Yin, Y. (2020). Brassinosteroids: Multidimensional regulators of plant growth, development, and stress responses. *Plant Cell*, *32*(2), 298–318. https://doi.org/10.1105/tpc.19.00335

Novaković, L., Guo, T., Bacic, A., Sampathkumar, A., & Johnson, K. L. (2018). Hitting the wall—sensing and signaling pathways involved in plant cell wall remodeling in response to abiotic stress. In *Plants* (Vol. 7, Issue 4). MDPI AG. https://doi.org/10.3390/plants7040089

Ökmen, B., Kemmerich, B., Hilbig, D., Wemhöner, R., Aschenbroich, J., Perrar, A., Huesgen, P. F., Schipper, K., & Doehlemann, G. (2018). Dual function of a secreted fungalysin metalloprotease in Ustilago maydis. *New Phytologist*, *220*(1), 249–261. https://doi.org/10.1111/nph.15265

Ortíz-Castro, R., Contreras-Cornejo, H. A., Macías-Rodríguez, L., & López-Bucio, J. (2009). The role of microbial signals in plant growth and development. In *Plant Signaling and Behavior* (Vol. 4, Issue 8, pp. 701–712). Landes Bioscience. https://doi.org/10.4161/psb.4.8.9047

Park, A., Yun, T., Hill, T. E., Ikegami, T., Juelich, T. L., Smith, J. K., Zhang, L., Freiberg, A. N., & Lee, B. (2016). Optimized P2A for reporter gene insertion into Nipah virus results in efficient ribosomal skipping and wild-type lethality. *Journal of General Virology*, *97*, 839–843. https://doi.org/10.1099/jgv.0.000405

Penninckx, I. A. M. A., Thomma, B. P. H. J., Buchala, A., Métraux, J.-P., & Broekaert, W. F. (1998). Concomitant Activation of Jasmonate and Ethylene Response Pathways Is Required for Induction of a Plant Defensin Gene in Arabidopsis. In *The Plant Cell* (Vol. 10). https://academic.oup.com/plcell/article/10/12/2103/5999444

Pérez-Henríquez, P., & Yang, Z. (2023). Extranuclear auxin signaling: a new insight into auxin's versatility. *New Phytologist*, *237*(4), 1115–1121. https://doi.org/10.1111/nph.18602

Plaschka, C., Lin, P. C., & Nagai, K. (2017). Structure of a pre-catalytic spliceosome. *Nature*, *546*(7660), 617–621. https://doi.org/10.1038/nature22799

Presti, L. Lo, & Kahmann, R. (2017). How filamentous plant pathogen effectors are translocated to host cells. *Current Opinion in Plant Biology* , *38*, 19–24.

R. Green, M., & Sambrook, J. (2012). *Molecular Cloning This is a free sample of content from Molecular Cloning: A Laboratory Manual, 4th edition. Click here for more information or to buy the book*. www.cshlpress.org

Redkar, A., Hoser, R., Schilling, L., Zechmann, B., Krzymowska, M., Walbot, V., & Doehlemann, G. (2015). A Secreted Effector Protein of Ustilago maydis Guides Maize Leaf Cells to Form Tumors. *The Plant Cell*, *27*(4), 1332. https://doi.org/10.1105/TPC.114.131086

Reineke, G., Heinze, B., Schirawski, J., Buettner, H., Kahmann, R., & Basse, C. W. (2008). Indole-3-acetic acid (IAA) biosynthesis in the smut fungus Ustilago maydis and its relevance for increased IAA levels in infected tissue and host tumour formation. *Molecular Plant Pathology*, *9*(3), 339–355. https://doi.org/10.1111/j.1364-3703.2008.00470.x

Ren, H., Park, M. Y., Spartz, A. K., Wong, J. H., & Gray, W. M. (2018). A subset of plasma membrane-localized PP2C.D phosphatases negatively regulate SAUR-mediated cell expansion in Arabidopsis. *PLoS Genetics*, *14*(6). https://doi.org/10.1371/journal.pgen.1007455

Rozhon, W., Sharma, A., Unterholzner, S. J., Gruszka, D., & Zolkiewicz, K. (2022). *OPEN ACCESS EDITED BY Glycogen synthase kinases in model and crop plants-From negative regulators of brassinosteroid signaling to multifaceted hubs of various signaling pathways and modulators of plant reproduction and yield*. https://doi.org/10.3389/fpls.2022.939487

Ryu, H., Kim, K., Cho, H., Park, J., Choe, S., & Hwang, I. (2007). Nucleocytoplasmic Shuttling of BZR1 Mediated by Phosphorylation Is Essential in Arabidopsis Brassinosteroid Signaling. *The Plant Cell*, *19*(9), 2749–2762. https://doi.org/10.1105/TPC.107.053728

Saado, I., Chia, K.-S., Betz, R., Alcântara, A., Pettkó-Szandtner, A., Navarrete, F., D'Auria, J. C., Kolomiets, M. V, Melzer, M., Feussner, I., & Djamei, A. (2022). Effector-mediated relocalization of a maize lipoxygenase protein triggers susceptibility to Ustilago maydis . *The Plant Cell*, *34*(7), 2785–2805. https://doi.org/10.1093/plcell/koac105

Saidi, Y., Hearn, T. J., & Coates, J. C. (2012). Function and evolution of 'green' GSK3/Shaggy-like kinases. *Trends in Plant Science*, *17*(1), 39–46. https://doi.org/10.1016/J.TPLANTS.2011.10.002

Sakamoto, T., & Fujioka, S. (2013). Auxins increase expression of the brassinosteroid receptor and brassinosteroid-responsive genes in arabidopsis. *Plant Signaling and Behavior*, *8*(4). https://doi.org/10.4161/psb.23509

Samalova, M., Melnikava, A., Elsayad, K., Peaucelle, A., Gahurova, E., Gumulec, J., Spyroglou, I., Zemlyanskaya, E. V, Ubogoeva, E. V, Balkova, D., Demko, M., Blavet, N., Alexiou, P., Benes, V., Mouille, G., & Hejatko, J. (2023). Hormone-regulated expansins: Expression, localization, and cell wall biomechanics in Arabidopsis root growth. *Plant Physiology*. https://doi.org/10.1093/plphys/kiad228

Sampedro, J., & Cosgrove, D. J. (2005). The expansin superfamily. In *Genome Biology* (Vol. 6, Issue 12). https://doi.org/10.1186/gb-2005-6-12-242

Sandhu, K. S., Singh, N., & Malhi, N. S. (2007). Some properties of corn grains and their flours I: Physicochemical, functional and chapati-making properties of flours. *Food Chemistry*, *101*(3), 938–946. https://doi.org/10.1016/j.foodchem.2006.02.040

Sayers, E. W., Bolton, E. E., Brister, J. R., Canese, K., Chan, J., Comeau, D. C., Connor, R., Funk, K., Kelly, C., Kim, S., Madej, T., Marchler-Bauer, A., Lanczycki, C., Lathrop, S., Lu, Z., Thibaud-Nissen, F., Murphy, T., Phan, L., Skripchenko, Y., … Sherry, S. T. (2022). Database resources of the national center for biotechnology information. *Nucleic Acids Research*, *50*(D1), D20–D26. https://doi.org/10.1093/nar/gkab1112

Schirawski, J., Mannhaupt, G., Münch, K., Brefort, T., Schipper, K., Doehlemann, G., Di Stasio, M., Rössel, N., Mendoza-Mendoza, A., Pester, D., Müller, O., Winterberg, B., Meyer, E., Ghareeb, H., Wollenberg, T., Münsterkötter, M., Wong, P., Walter, M., Stukenbrock, E., … Kahmann, R. (2010). Pathogenicity determinants in smut fungi revealed by genome comparison. *Science (New York, N.Y.)*, *330*(6010), 1546–1548. https://doi.org/10.1126/SCIENCE.1195330

Schulz, B., Banuett, F., Dahl, M., Schlesinger, R., Schafer, W., Martin, T., Herskowitqt, I., & Kahmann', R. (1990). The b Alleles of U. maydis, Whose Combinations Program Pathogenic Development, Code for Polypeptides Containing a Homeodomain-Related Motif. In *Cell* (Vol. 60).

Scott, B., Mesarich, C., Carter, D., Chowdhary, A., Heitman, J., & Kück, U. (2022). *Plant Relationships THE MYCOTA 5 A Comprehensive Treatise on Fungi as Experimental Systems for Basic and Applied Research Series Editors*.

Shinde, M. Y., Sidoli, S., Kulej, K., Mallory, M. J., Radens, C. M., Reicherter, A. L., Myers, R. L., Barash, Y., Lynch, K. W., Garcia, B. A., & Klein, P. S. (2017). Phosphoproteomics reveals that glycogen synthase kinase-3 phosphorylates multiple splicing factors and is associated with alternative splicing. *Journal of Biological Chemistry*, *292*(44), 18240–18255. https://doi.org/10.1074/jbc.M117.813527

Singh, B. K., Delgado-Baquerizo, M., Egidi, E., Guirado, E., Leach, J. E., Liu, H., & Trivedi, P. (2023). Climate change impacts on plant pathogens, food security and paths forward. In *Nature Reviews Microbiology*. Nature Research. https://doi.org/10.1038/s41579-023-00900-7

Song, T., Zhang, Y., Zhang, Q., Zhang, X., Shen, D., Yu, J., Yu, M., Pan, X., Cao, H., Yong, M., Qi, Z., Du, Y., Zhang, R., Yin, X., Qiao, J., Liu, Y., Liu, W., Sun, W., Zhang, Z., … Liu, Y. (2021). The N-terminus of an Ustilaginoidea virens Ser-Thr-rich glycosylphosphatidylinositol-anchored protein elicits plant immunity as a MAMP. *Nature Communications*, *12*(1). https://doi.org/10.1038/s41467-021-22660-9

Song, W., Hu, L., & Ma, Z. (2022). *Importance of Tyrosine Phosphorylation in Hormone-Regulated Plant Growth and Development*. https://doi.org/10.3390/ijms23126603

Song, Y., Wang, Y., Yu, Q., Sun, Y., Zhang, J., Zhan, J., & Ren, M. (2023). Regulatory network of GSK3-like kinases and their role in plant stress response. *Frontiers in Plant Science*, *14*, 732. https://doi.org/10.3389/FPLS.2023.1123436/BIBTEX

Song, Y., Zhai, Y., Li, L., Yang, Z., Ge, X., Yang, Z., Zhang, C., Li, F., & Ren, M. (2021). BIN2 negatively regulates plant defence against Verticillium dahliae in Arabidopsis and cotton. *Plant Biotechnology Journal*, *19*(10), 2097. https://doi.org/10.1111/PBI.13640

Spartz, A. K., Lee, S. H., Wenger, J. P., Gonzalez, N., Itoh, H., Inzé, D., Peer, W. A., Murphy, A. S., Overvoorde, P. J., & Gray, W. M. (2012). The SAUR19 subfamily of SMALL AUXIN UP RNA genes promote cell expansion. *Plant Journal*, *70*(6), 978–990. https://doi.org/10.1111/j.1365-313X.2012.04946.x

Staněk, D., & Fox, A. (2017). Nuclear bodies: news insights into structure and function. In *Current Opinion in Cell Biology* (Vol. 46, pp. 94–101). Elsevier Ltd. https://doi.org/10.1016/j.ceb.2017.05.001

Steinberg, G., & Perez-Martin, J. (2008). Ustilago maydis, a new fungal model system for cell biology. In *Trends in Cell Biology* (Vol. 18, Issue 2, pp. 61–67). https://doi.org/10.1016/j.tcb.2007.11.008

Stirnberg, A., & Djamei, A. (2016). Characterization of ApB73, a virulence factor important for colonization of Zea mays by the smut Ustilago maydis. *Molecular Plant Pathology*, *17*(9), 1467–1479. https://doi.org/10.1111/mpp.12442

Stortenbeker, N., & Bemer, M. (2019). The SAUR gene family: The plant's toolbox for adaptation of growth and development. In *Journal of Experimental Botany* (Vol. 70, Issue 1, pp. 17–27). Oxford University Press. https://doi.org/10.1093/jxb/ery332

Stotz, H. U., Mitrousia, G. K., de Wit, P. J. G. M., & Fitt, B. D. L. (2014). Effector-triggered defence against apoplastic fungal pathogens. In *Trends in Plant Science* (Vol. 19, Issue 8, pp. 491–500). Elsevier Ltd. https://doi.org/10.1016/j.tplants.2014.04.009

Sun, P., Tian, Q. Y., Chen, J., & Zhang, W. H. (2010). Aluminium-induced inhibition of root elongation in Arabidopsis is mediated by ethylene and auxin. *Journal of Experimental Botany*, *61*(2), 347–356. https://doi.org/10.1093/jxb/erp306

Sutherland, C. (2011). What are the bona fide GSK3 substrates? In *International Journal of Alzheimer's Disease*. https://doi.org/10.4061/2011/505607

Tanaka, S., Brefort, T., Neidig, N., Djamei, A., Kahnt, J., Vermerris, W., Koenig, S., Feussner, K., Feussner, I., & Kahmann, R. (2014). A secreted Ustilago maydis effector promotes virulence by targeting anthocyanin biosynthesis in maize. *ELife*, *3*. https://doi.org/10.7554/elife.01355

Tanaka, S., & Kahmann, R. (2021). Cell wall–associated effectors of plant-colonizing fungi. *Mycologia*, *113*(2), 247–260. https://doi.org/10.1080/00275514.2020.1831293

Tang, W., Kim, T. W., Oses-Prieto, J. A., Sun, Y., Deng, Z., Zhu, S., Wang, R., Burlingame, A. L., & Wang, Z. Y. (2008). BSKs mediate signal transduction from the receptor kinase BRI1 in Arabidopsis. *Science*, *321*(5888), 557–560. https://doi.org/10.1126/SCIENCE.1156973/SUPPL_FILE/TANG.SOM.PDF

Tang, W., Yuan, M., Wang, R., Yang, Y., Wang, C., Oses-Prieto, J. A., Kim, T. W., Zhou, H. W., Deng, Z., Gampala, S. S., Gendron, J. M., Jonassen, E. M., Lillo, C., DeLong, A., Burlingame, A. L., Sun, Y., & Wang, Z. Y. (2011). PP2A activates brassinosteroid-responsive gene expression and plant growth by

dephosphorylating BZR1. *Nature Cell Biology 2011 13:2*, *13*(2), 124–131. https://doi.org/10.1038/ncb2151

Tian, H., Lv, B., Ding, T., Bai, M., & Ding, Z. (2017). Auxin-BR Interaction Regulates Plant Growth and Development. *Frontiers in Plant Science*, *8*. https://doi.org/10.3389/FPLS.2017.02256

Uhse, S., & Djamei, A. (2018). Effectors of plant-colonizing fungi and beyond. *PLOS Pathogens*, *14*(6), e1006992. https://doi.org/10.1371/JOURNAL.PPAT.1006992

van Mourik, H., van Dijk, A. D. J., Stortenbeker, N., Angenent, G. C., & Bemer, M. (2017). Divergent regulation of Arabidopsis SAUR genes: A focus on the SAUR10-clade. *BMC Plant Biology*, *17*(1). https://doi.org/10.1186/s12870-017-1210-4

Vernoux, T., Brunoud, G., Farcot, E., Morin, V., Van Den Daele, H., Legrand, J., Oliva, M., Das, P., Larrieu, A., Wells, D., Guédon, Y., Armitage, L., Picard, F., Guyomarc'H, S., Cellier, C., Parry, G., Koumproglou, R., Doonan, J. H., Estelle, M., … Traas, J. (2011). The auxin signalling network translates dynamic input into robust patterning at the shoot apex. *Molecular Systems Biology*, *7*. https://doi.org/10.1038/msb.2011.39

Vert, G., & Chory, J. (2006). Downstream nuclear events in brassinosteroid signalling. *Nature 2006 441:7089*, *441*(7089), 96–100. https://doi.org/10.1038/nature04681

Walbot, V., & Skibbe, D. S. (2010). Maize host requirements for Ustilago maydis tumor induction. *Sexual Plant Reproduction*, *23*(1), 1–13. https://doi.org/10.1007/s00497-009-0109-0

Walcher, C. L., Chory, J., Nemhauser, J. L., Biochimie, ¶ †, & Molé, P. (2008). *Integration of auxin and brassinosteroid pathways by Auxin Response Factor 2 Gré gory Vert*. www.pnas.org/cgi/content/full/

Walcher, C. L., & Nemhauser, J. L. (2012). Bipartite promoter element required for auxin response. *Plant Physiology*, *158*(1), 273–282. https://doi.org/10.1104/pp.111.187559

Wan, R., Bai, R., & Shi, Y. (2019). Molecular choreography of pre-mRNA splicing by the spliceosome. In *Current Opinion in Structural Biology* (Vol. 59, pp. 124–133). Elsevier Ltd. https://doi.org/10.1016/j.sbi.2019.07.010

Wang, L., Li, J., & Di, L. jun. (2022). Glycogen synthesis and beyond, a comprehensive review of GSK3 as a key regulator of metabolic pathways and a therapeutic target for treating metabolic diseases. In *Medicinal Research Reviews* (Vol. 42, Issue 2, pp. 946–982). John Wiley and Sons Inc. https://doi.org/10.1002/med.21867

Wang, L., & Ruan, Y. L. (2013). Regulation of cell division and expansion by sugar and auxin signaling. *Frontiers in Plant Science*, *4*(MAY), 163. https://doi.org/10.3389/FPLS.2013.00163/BIBTEX

Wang, Q., Sawyer, I. A., Sung, M. H., Sturgill, D., Shevtsov, S. P., Pegoraro, G., Hakim, O., Baek, S., Hager, G. L., & Dundr, M. (2016). Cajal bodies are linked to genome conformation. *Nature Communications*, *7*. https://doi.org/10.1038/ncomms10966

Wang, X., Chen, J., Xie, Z., Liu, S., Nolan, T., Ye, H., Zhang, M., Guo, H., Schnable, P. S., Li, Z., & Yin, Y. (2014). Histone lysine methyltransferase SDG8 is involved in brassinosteroid-regulated gene

expression in Arabidopsis thaliana. *Molecular Plant*, *7*(8), 1303–1315. https://doi.org/10.1093/MP/SSU056

Wang, X., Wang, X., Sun, S., Tu, X., Lin, K., Qin, L., Wang, X., Li, G., Zhong, S., & Li, P. (2022). Characterization of regulatory modules controlling leaf angle in maize. *Plant Physiology*, *190*(1), 500–515. https://doi.org/10.1093/PLPHYS/KIAC308

Wang, Y., Xu, J., Yu, J., Zhu, D., & Zhao, Q. (2022). Maize GSK3-like kinase ZmSK2 is involved in embryonic development. *Plant Science*, *318*, 111221. https://doi.org/10.1016/J.PLANTSCI.2022.111221

Wang, Z., Yang, L., Liu, Z., Lu, M., Wang, M., Sun, Q., Lan, Y., Shi, T., Wu, D., & Hua, J. (2019). Natural variations of growth thermo-responsiveness determined by SAUR26/27/28 proteins in Arabidopsis thaliana. *New Phytologist*, *224*(1), 291–305. https://doi.org/10.1111/nph.15956

Watanabe, E., Mano, S., Nishimura, M., & Yamada, K. (2019). AtUBL5 regulates growth and development through pre-mRNA splicing in Arabidopsis thaliana. *PLoS ONE*, *14*(11). https://doi.org/10.1371/journal.pone.0224795

Wei, Z., & Li, J. (2016). Brassinosteroids Regulate Root Growth, Development, and Symbiosis. *Molecular Plant*, *9*(1), 86–100. https://doi.org/10.1016/J.MOLP.2015.12.003

Wieczorek, K., & Grundler, F. M. W. (2006). Expanding nematode-induced Syncytia: The role of expansins. *Plant Signaling and Behavior*, *1*(5), 223–224. https://doi.org/10.4161/psb.1.5.3426

Xie, J., Beickman, K., Otte, E., & Rymond, B. C. (1998). Progression through the spliceosome cycle requires Prp38p function for U4/U6 snRNA dissociation. In *The EMBO Journal* (Vol. 17, Issue 10).

Yan, Z., Zhao, J., Peng, P., Chihara, R. K., & Li, J. (2009). BIN2 Functions Redundantly with Other Arabidopsis GSK3-Like Kinases to Regulate Brassinosteroid Signaling. *Plant Physiology*, *150*(2), 710–721. https://doi.org/10.1104/PP.109.138099

Yang, F., Fan, Y., Wu, X., Cheng, Y., Liu, Q., Feng, L., Chen, J., Wang, Z., Wang, X., Yong, T., Liu, W., Liu, J., Du, J., Shu, K., & Yang, W. (2018). Auxin-to-gibberellin ratio as a signal for light intensity and quality in regulating soybean growth and matter partitioning. *Frontiers in Plant Science*, *9*, 56. https://doi.org/10.3389/FPLS.2018.00056/BIBTEX

Yin, Y., Wang, Z. Y., Mora-Garcia, S., Li, J., Yoshida, S., Asami, T., & Chory, J. (2002). BES1 accumulates in the nucleus in response to brassinosteroids to regulate gene expression and promote stem elongation. *Cell*, *109*(2), 181–191. https://doi.org/10.1016/S0092-8674(02)00721-3

Yoo, M. J., Albert, V. A., Soltis, P. S., & Soltis, D. E. (2006). Phylogenetic diversification of glycogen synthase kinase 3/SHAGGY-like kinase genes in plants. *BMC Plant Biology*, *6*(1), 1–14. https://doi.org/10.1186/1471-2229-6-3/FIGURES/7

Yoshimitsu, Y., Tanaka, K., Fukuda, W., Asami, T., Yoshida, S., Hayashi, K. ichiro, Kamiya, Y., Jikumaru, Y., Shigeta, T., Nakamura, Y., Matsuo, T., & Okamoto, S. (2011). Transcription of DWARF4 plays a crucial role in auxin-regulated root elongation in addition to brassinosteroid homeostasis in arabidopsis thaliana. *PLoS ONE*, *6*(8). https://doi.org/10.1371/journal.pone.0023851

Youn, J. H., & Kim, T. W. (2015). Functional insights of plant GSK3-like kinases: multi-taskers in diverse cellular signal transduction pathways. *Molecular Plant*, *8*(4), 552–565. https://doi.org/10.1016/J.MOLP.2014.12.006

Youn, J. H., Kim, T. W., Kim, E. J., Bu, S., Kim, S. K., Wang, Z. Y., & Kim, T. W. (2013). Structural and functional characterization of arabidopsis GSK3-like kinase AtSK12. *Molecules and Cells*, *36*(6), 564–570. https://doi.org/10.1007/s10059-013-0266-8

Yu, X., Li, L., Zola, J., Aluru, M., Ye, H., Foudree, A., Guo, H., Anderson, S., Aluru, S., Liu, P., Rodermel, S., & Yin, Y. (2011). A brassinosteroid transcriptional network revealed by genome-wide identification of BESI target genes in Arabidopsis thaliana. *The Plant Journal : For Cell and Molecular Biology*, *65*(4), 634–646. https://doi.org/10.1111/J.1365-313X.2010.04449.X

Yu, Z., Zhang, F., Friml, J., & Ding, Z. (2022). Auxin signaling: Research advances over the past 30 years. *Journal of Integrative Plant Biology*, *64*(2), 371–392. https://doi.org/10.1111/jipb.13225

Zhang, B., Gao, Y., Zhang, L., & Zhou, Y. (2021). The plant cell wall: Biosynthesis, construction, and functions. In *Journal of Integrative Plant Biology* (Vol. 63, Issue 1, pp. 251–272). Blackwell Publishing Ltd. https://doi.org/10.1111/jipb.13055

Zhang, S., Li, C., Si, J., Han, Z., & Chen, D. (2022). Action Mechanisms of Effectors in Plant-Pathogen Interaction. In *International Journal of Molecular Sciences* (Vol. 23, Issue 12). MDPI. https://doi.org/10.3390/ijms23126758

Zhao, H., Fu, Y., Zhang, G., Luo, Y., Yang, W., Liang, X., Yin, L., Zheng, Z., Wang, Y., Li, Z., Zhu, H., Huang, J., Tan, Q., Bu, S., Liu, G., Wang, S., & Liu, Z. (2023). *GS6.1 controls kernel size and plant architecture in rice*. https://doi.org/10.21203/rs.3.rs-2616757/v1

Zhou, J. M., & Zhang, Y. (2020). Plant Immunity: Danger Perception and Signaling. *Cell*, *181*(5), 978–989. https://doi.org/10.1016/J.CELL.2020.04.028

Zhou, X. Y., Song, L., & Xue, H. W. (2013). Brassinosteroids regulate the differential growth of arabidopsis hypocotyls through auxin signaling components IAA19 and ARF7. *Molecular Plant*, *6*(3), 887–904. https://doi.org/10.1093/mp/sss123

Zhu, J. Y., Li, Y., Cao, D. M., Yang, H., Oh, E., Bi, Y., Zhu, S., & Wang, Z. Y. (2017). The F-box protein KIB1 mediates brassinosteroid-induced inactivation and degradation of GSK3-like kinases in Arabidopsis. *Molecular Cell*, *66*(5), 648. https://doi.org/10.1016/J.MOLCEL.2017.05.012

Zhuang, Y., Lian, W., Tang, X., Qi, G., Wang, Di., Chai, G., & Zhou, G. (2022). MYB42 inhibits hypocotyl cell elongation by coordinating brassinosteroid homeostasis and signalling in Arabidopsis thaliana. *Annals of Botany*, *129*(4), 403–413. https://doi.org/10.1093/aob/mcab152

9 List of figures

10 List of tables

11 Appendix I:

The contribution of Pouria Bahrami on the other unpublished project during PhD is written here.

1- Making *A. thaliana* transgenic line ($P_{35S\text{-}XVE}$*::mCherry-Umag05824*$_{23\text{-}176}$) under supervision of Mamoona Khan-Djamei.
2- Cloning following GSK3s of *Z. mays* and *A. thaliana*, making constructs. Needs to clarify that GSK3s constructs and clones were made with the main focus on Cab1 project and used or will be used for Umag_05824 project. The other constructs were made specifically to study Umag_05824 that is mentioned in the table. DNA number refers to the general plasmid list of Djamei lab and maps are stored under the same number in Djamei lab server (table 12-1).
3- Performing Y2H with full length AtBin2, 5 ZmGSK3s, HsGSKBeta orthologues (Fig. 12-1)
4- Performing Y2H with truncated ZmGSK11 (Zm00001d012869) to define the target site (fig. 12-2)
5- Performing SplitTurboID to find potential downstream targets (table 12-2)

Table 11-1 the list shared and/or specific constructs for Cab1 and E2 projects.

DNA. No.	Description	Date	Res.	made by
6513	pGG-35S-At2g18980-V5-hyg			Mamoona/Pouria
6514	pGG-35S-At2g18980-mcherry-Myc-Hyg			Mamoona/Pouria
6515	pGG-35S-At2g18980-mcherryNLS-Myc-hyg			Mamoona/Pouria
6516	pGG-35S-At2g18980-mcherryNES-Myc-V5-hyg			Mamoona/Pouria
6517	pGG-XVE-At2g18980-V5-hyg			Mamoona/Pouria
6518	pGG-35S-GFP-At18980-V5-Hyg			Mamoona/Pouria
6519	pGG-pAP3-GUS-hyg			Mamoona/Pouria
6689	pXVE-Ha-mcherry-UMAG-05824, stopdummy,Term-BASTA resistance			Pouria
6690	p35s-Ha-mcherry-UMAG-05824, stopdummy,Term-BASTA resistance			Pouria
6691	pXVE-SP-UMAG-05824, mCherry-HA-stop,Term-BASTA resistance			Pouria
6692	p35s-SP-UMAG-05824, mCherry-HA-stop,Term-BASTA resistance			Pouria
6697	Umag-05824-pXVE-3xHA-Ntag-Basta_Oleosin:GFP			Pouria
6698	Umag-05824-pXVE-Sec. Effector-3xHA-P2A-mCherry-myc-Basta_Oleosin:GFP			Pouria
6699	Umag-05824-35s-3xHA-Ntag-Basta_Oleosin:GFP			Pouria
6700	Umag-05824-35s-Sec. Effector-3xHA-P2A-mCherry-myc-Basta_Oleosin:GFP			Pouria
6847	p123-proUmag-05824-GUS			pouria
6858	P123-Pit2-Umag-05824 w/o SP-mCherry-3HA			pouria
6859	P123-Pit2-Umag-05824 native SP -mCherry-3HA			pouria
6876	pJet-LOC100273692 (GRMZM2G075992; GRMZM6G733144) M8 BspHI-Not			pouria
6877	pJet-LOC100283734 (GRMZM5G835235) M9 BspHI-Not			pouria
6878	pJet-LOC100283610 (GRMZM2G151916) M3 Nco-Not			pouria

6879	pGBKT7-LOC100283610 (GRMZM2G151916) M3 Nco-Not			pouria
6880	pJet-LOC542518 (GRMZM2G138676) Fragment 5 CD			pouria
6937	Pv101-p19-p2A-UMAG_05824 -p2A-mCherry			pouria
7397	pv101-p19-P2A-glucocorticoid receptor_UMAG_05824_V5			pouria
7679	Pjet-At4g22240-CD-At4g22240	22.02.21	Amp	Pouria
7680	Pjet-BIL1-AT2G30980-BspHI-NotI	22.02.21	Amp	Pouria
7681	Pjet-BIL2-AT1G06390-NcoI-NotI	22.02.21	Amp	Pouria
7811	pGBKT7-GSK3-BIL1 (At2g30980)	14.06.21	Kan	Pouria
7812	pGBKT7-GSK3-BIL2-AT1G06390	14.06.21	Kan	Pouria
7813	pGBKT7-At3g52180 (Sex4)	14.06.21	Kan	Pouria
7814	pGBKT7-FBKP-At3g12345	14.06.21	Kan	Pouria
7815	pGBKT7-NEET-At5g51720	14.06.21	Kan	Pouria
7816	pGBKT7-At4g22240	14.06.21	Kan	Pouria
7817	pGBKT7-Q9FKW6-At5g66190	14.06.21	Kan	Pouria
7818	pGBKT7-ATCG00700	14.06.21	Kan	Pouria
7819	pGBKT7-AT4G00860 (AT0ZI1)	14.06.21	Kan	Pouria
7820	pGBKT7-AT3G05840.2 (AtSK12)	14.06.21	Kan	Pouria
7821	pGBKT7-At5g14640 (SK13)	14.06.21	Kan	Pouria
7822	pGBKT7-AT1G09840 (AtsK41)	14.06.21	Kan	Pouria
7823	pGBKT7-GSK3-LOC100282499 (GRMZM2G024151)-M1	14.06.21	Kan	Pouria
7824	pGBKT7-GSK3-LOC100283610 (GRMZM2G151916) M3	14.06.21	Kan	Pouria
7825	pGBKT7-GSK3-LOC100192496 (GRMZM2G043350) M4	14.06.21	Kan	Pouria
7826	pGBKT7-GSK3-LOC542518 (GRMZM2G138676) M7	14.06.21	Kan	Pouria
7827	pGBKT7-GSK3-LOC100273692 (GRMZM2G075992; GRMZM6G733144) M8	14.06.21	Kan	Pouria
7828	pGBKT7-GSK3-LOC100283734 (GRMZM5G835235) M9	14.06.21	Kan	Pouria
7829	pGBKT7-GSK3-BIN2 (AT4G18710) Fargment 1	14.06.21	Kan	Pouria
7830	pGBKT7-GSK3-BIN2 (AT4G18710) Fargment 2	14.06.21	Kan	Pouria

7831	pGBKT7-GSK3-BIN2 (AT4G18710) Fragment 3	14.06.21	Kan	Pouria
7832	pGBKT7-GSK3-BIN2 (AT4G18710) Fragment 4	14.06.21	Kan	Pouria
7833	pGBKT7-GSK3-BIN2 (AT4G18710) Fargment 5	14.06.21	Kan	Pouria
7834	pGBKT7-GSK3-BIN2 (AT4G18710) Fargment 7	14.06.21	Kan	Pouria
7835	pGBKT7-GSK3-BIN2 (AT4G18710) Fragment 8	14.06.21	Kan	Pouria
7836	pGBKT7-GSK3-BIN2 (AT4G18710) Fragment 9	14.06.21	Kan	Pouria
7837	pGBKT7-GSK3-BIN2 (AT4G18710) Fargment 12	14.06.21	Kan	Pouria
7838	pGBKT7-GSK3-BIN2 (AT4G18710) Fragment 13	14.06.21	Kan	Pouria
7839	pGBKT7-GSK3-BIN2 (AT4G18710) Fargment 14	14.06.21	Kan	Pouria
7840	pJet1-GSK3-BIN2 (AT4G18710) Fargment 1	14.06.21	Amp	Pouria
7841	pJet1-GSK3-BIN2 (AT4G18710) Fargment 2	14.06.21	Amp	Pouria
7842	pJet1-GSK3-BIN2 (AT4G18710) Fragment 3	14.06.21	Amp	Pouria
7843	pJet1-GSK3-BIN2 (AT4G18710) Fragment 4	14.06.21	Amp	Pouria
7844	pJet1-GSK3-BIN2 (AT4G18710) Fragment 5	14.06.21	Amp	Pouria
7845	pJet1-GSK3-BIN2 (AT4G18710) Fargment 7	14.06.21	Amp	Pouria
7846	pJet1-GSK3-BIN2 (AT4G18710) Fragment 8	14.06.21	Amp	Pouria
7847	pJet1-GSK3-BIN2 (AT4G18710) Fragment 9	14.06.21	Amp	Pouria
7848	pJet1-GSK3-BIN2 (AT4G18710) Fargment 12	14.06.21	Amp	Pouria
7849	pJet1-GSK3-BIN2 (AT4G18710) Fragment 13	14.06.21	Amp	Pouria
7850	pJet1-GSK3-BIN2 (AT4G18710) Fargment 14	14.06.21	Amp	Pouria
7851	pJet1-GSK3-LOC542518 (GRMZM2G138676) Fragment 1	14.06.21	Amp	Pouria
7852	pJet1-GSK3-LOC542518 (GRMZM2G138676) Fargment 2	14.06.21	Amp	Pouria
7853	pJet1-GSK3-LOC542518 (GRMZM2G138676) Fragment 3	14.06.21	Amp	Pouria
7854	pGBKT7-GSK3-LOC542518 (GRMZM2G138676) Fragment 1	14.06.21	Kan	Pouria
7855	pGBKT7-GSK3-LOC542518 (GRMZM2G138676) Fargment 2	14.06.21	Kan	Pouria
7856	pGBKT7-GSK3-LOC542518 (GRMZM2G138676) Fragment 3	14.06.21	Kan	Pouria
7906	pJet-CD-GSK3-LOC100282499 (GRMZM2G024151)-M1	19,07,21	Amp	Pouria

7907	pJet-CD-GSK3-LOC100283610 (GRMZM2G151916) M3 (Zm00001eb238820, orthologue of BIL2)	19,07,21	Amp	Pouria
7908	pJet-CD-GSK3-LOC100192496 (GRMZM2G043350) M4	19,07,21	Amp	Pouria
7909	pJet-CD-GSK3-LOC542518 (GRMZM2G138676) M7	19,07,21	Amp	Pouria
7910	pJet-CD-GSK3-LOC100283734 (GRMZM5G835235) M9	19,07,21	Amp	Pouria
7911	103_35S_dummy_LOC100282499 (GRMZM2G024151) M1 CD_linker-GFP-UBQ10_pMAS_Bas	19,07,21	Spect	Pouria
7912	103_35S_dummy_LOC100283610 (GRMZM2G151916) M3 CD-linker-GFP-UBQ10_pMAS_Bas	19,07,21	Spect	Pouria
7913	103_35S_dummy_LOC100192496 (GRMZM2G043350) M4 CD-linker-GFP-UBQ10_pMAS_Bas	19,07,21	Spect	Pouria
7914	103_35S_dummy_LOC542518 (GRMZM2G138676) M7 CD_linker-GFP_UBQ10_pMAS_Bas	19,07,21	Spect	Pouria
7915	103_35S_dummy_LOC100283734 (GRMZM5G835235) M9-linker-GFP_UBQ10_pMAS_Bas	19,07,21	Spect	Pouria
7916	103_35S_dummy_LOC100282499 (GRMZM2G024151) M1 CD_eGFP-UBQ10_pMAS_Bas	23,05,21	Spect	Pouria
7917	103_35S_dummy_LOC100283610 (GRMZM2G151916) M3 CD_eGFP-UBQ10_pMAS_Bas	23,05,21	Spect	Pouria
7918	103_35S_dummy_LOC100192496 (GRMZM2G043350) M4 CD_eGFP-UBQ10_pMAS_Bas	23,05,21	Spect	Pouria
7919	103_35S_dummy-LOC542518 (GRMZM2G138676) M7 CD_eGFP--UBQ10__pMAS_Bas	23,05,21	Spect	Pouria
7920	103_35S_dummy_NM_001365756 M8 new seq CD_eGFP-UBQ10_pMAS_Bas	23,05,21	Spect	Pouria
7921	103 _35S_dummy_LOC100283734 (GRMZM5G835235) M9_eGFP-UBQ10_pMAS_Bas	23,05,21	Spect	Pouria
7923	pGBKT7-LOC542518 (GRMZM2G138676) Fargment 4	23,05,21	Kan	Pouria
7924	pGBKT7-LOC542518 (GRMZM2G138676) Fragment 5	23,05,21	Kan	Pouria
7925	pGBKT7-LOC542518 (GRMZM2G138676) Fragment 6	23,05,21	Kan	Pouria

7926	pGBKT7-LOC542518 (GRMZM2G138676) Fargment 7	23,05,21	Kan	Pouria
7927	pJet-LOC542518 (GRMZM2G138676) Fargment 4 Nco-Not	23,05,21	Amp	Pouria
7928	pJet-LOC542518 (GRMZM2G138676) Fragment 5 Nco-Not	23,05,21	Amp	Pouria
7929	pJet-LOC542518 (GRMZM2G138676) Fragment 6 Nco-Not	23,05,21	Amp	Pouria
8072	103-35S-dummy-LOC100283610 (GRMZM2G151916) M3-MYC-N-terminal Venus part-UBQ10-Bas	22,10,21	Spec	Pouria
8073	103-35S-dummy-LOC100273692 (GRMZM2G075992; GRMZM6G733144) M8 new seq-MYC-linker-N-terminal Venus-UBQ10-Bas	22,10,21	Spec	Pouria
8074	103-35S-dummy-UMAG_02193-linker-HA_c-term Split Venus-UBQ10-Bas	22,10,21	Spec	Pouria
8075	103-35S-N-terminal Venus part_MYC-LOC100283610 (GRMZM2G151916) M3-dummy-UBQ10-Bas	22,10,21	Spec	Pouria
8076	103-35S-N-terminal Venus part_MYC-LOC100273692 (GRMZM2G075992; GRMZM6G733144) M8 new seq-dummy-UBQ10-Bas	22,10,21	Spec	Pouria
8077	103-35S-c-term Split Venus linker HA-UMAG_02193-dummy-UBQ10-Bas	22,10,21	Spec	Pouria
8084	pJet- GSK3-LOC100273692 (GRMZM2G075992; GRMZM6G733144) M8-CD	28.10.21	amp	Pouria
8085	pJet-LOC542518 (GRMZM2G138676) Fargment 7	28.10.21	Amp	Pouria
8105	103-35S-glucocorticoid-GRMZM2G151916) M3 CD-dummy-UBQ10-Bas	28.10.21	Amp	Pouria
8126	pJet-AT1G19350.3-BES1-CD	07,12,2021	Amp	Pouria
8195	pGG-35S-omega-AT1G19350-BES1-eGFP-UBQ10-Bas	27,01,2022	spec	Pouria
8516	103-pEF2-gluco_UMAG_05824_dummy-UBQ10-HygR	28.03.22	Spec	Pouria
8517	103-pEF2-gluco_mCherry_dummy-UBQ10-HygR	28.03.22	Spec	Pouria
8519	103-pEF2-gluco-V5_UMAG_05824_dummy-UBQ10-HygR	28.03.22	Spec	Pouria
8520	103-pEF2-gluco-V5_mCherry_dummy-UBQ10-HygR	28.03.22	Spec	Pouria
8525	pJet-glycogen synthase kinase 3 Beta Nco-Not	28.03.2022	Amp	Pouria

8526	pGBKT7-Homo sapiens glycogen synthase kinase 3 Beta	28.03.2022	Kan	Pouria
8621	pJet-At5g14640 (AtSK13) CD	10.05.2022	Amp	Pouria
8622	pJet-At2g30980 (BIL1) CD	10.05.2022	Amp	Pouria
8624	103-35S-dummy-At5g14640 (AtSK13)-MYC-NtVenus-UBQ10_Bas	10.05.2022	Spec	Pouria
8625	103-35s-dummy-At2g30980 (BIL1)_MYC--NtVenus-UBQ10-Bas	10.05.2022	Spec	Pouria
8627	pJet-AT1G09840 (AtsK41) CD	10.05.2022	Amp	Pouria
8683	103-35S-omega-GFP-HA-sTurboID low affinity C terminal-UBQ10_Bas	15.06.2022	spect	Pouria
8685	103-35S-omega-UMAG_05824-V5-sTurboID low affinity N terminal-UBQ10-pMAS_Bas	15.06.2022	spect	Pouria
8686	103-35S-omega-mCherry-V5-sTurboID low affinity N terminal-UBQ10-Bas	15.06.2022	spect	Pouria
8693	103-35s-dummy-AT1G09840 (AtsK41)-MYC-NtVenus-UBQ10-pMAS_Bas	15.06.2022	spect	Pouria
8887	PB-T3G-ERP2 backbone BE Amp Res.	18.07.2022	Amp	Pouria
8910	Pjet-BIN2-CD-At4g18710	19.07.2022	Amp	Pouria
8911	103-35S-omega-BIN2-At4g18710-HA-linker-sTurboID low affinity C-UBQ10-Bas	19.07.2022	spect	Pouria
8912	103-35S-omega-BIN2-At4g18710-V5-linker-sTurboID low affinity N terminal-UBQ10-Bas	19.07.2022	spect	Pouria
8913	103-35S-Myc-ultraID-linker-BIN2-At4g18710-dummy-UBQ10-Bas	19.07.2022	spect	Pouria
8914	103-35s-omega-BIN2-At4g18710-linker-Myc-UltraID-UBQ10-Bas	19.07.2022	spect	Pouria
8955	103-pEF2-HA-mCh-UMAG_05824-dummy-UBQ10-HygR	15.08.2022	Spect/Hyg	Pouria
9171	pJet-CD-GRMZM2G151916 (LOC100283610) M3	25.11.2022	amp	Pouria
9172	pJet-CD-GRMZM2G045330 (gsk1 - glycogen synthase kinase1)Zm00001d039407 (old M5)	25.11.2022	amp	Pouria
9173	pJet-CD- GRMZM2G472625 (gsk2 - glycogen synthase kinase2)Zm00001d008893(M6)	25.11.2022	amp	Pouria
9174	pGBKT7-GRMZM2G151916-Frag1-1~798bp-266aa-BspHI-Not (M3)	25.11.2022	Kan	Pouria
9175	pGBKT7-GRMZM2G151916-Frag4-799~1005bp-69aa-BspHI-Not (M3)	25.11.2022	Kan	Pouria
9176	pGBKT7-GRMZM2G151916-Frag5-1005~1228bp-74aa-Nco-Not (M3)	25.11.2022	Kan	Pouria
9177	pGBKT7-GRMZM2G151916-Frag4+5-798~1228bp-143aa-BspHI-Not (M3)	25.11.2022	Kan	Pouria

9178	168-6XHis-SUMO--GFP-dummy	25.11.2022	Spect	Pouria
9179	168-6XHis-SUMO--mCherry-dummy	25.11.2022	Spect	Pouria
9180	168-His6TrxPP-GFP-dummy	25.11.2022	Spect	Pouria
9181	168--His6TrxPP-mCherry-dummy	25.11.2022	Spect	Pouria
9182	168-His6TrxPP-UMAG_05824-dummy	25.11.2022	Spect	Pouria
9184	168-6XHis-SUMO-UMAG_05824-dummy	25.11.2022	Spect	Pouria
9188	pJet-ADH1-Gal4BD-Myc-GRMZM2G151916 (M3)-yADH-Terminator	25.11.2022	Amp	Pouria
9190	pJet-TDH3 (GAPDH) pro_eGFP-mCherry-dummy-CYC1_term	25.11.2022	Amp	Pouria
9191	pYG dest (Spec -Leu)-pADH1-Gal4 AD-HA-A.t BSU1-CYC1	25.11.2022	spect	Pouria
9193	187_YeastGateVector_A-F_part1:ADH1-Gal4BD-Myc-GRMZM2G151916 M3__dummy_yADH-Terminator_Part2:TDH3 (GAPDH) pro_eGFP-mCherry-dummy-CYC1_term	25.11.2022	spect	Pouria
9279	103-35S-GAL4BD-AtBIN2(At4g18710)-StopCODON-3xMyc-UBQ10-Basta	24.01.2023	Spec	Pouria
9280	103-35S-Gal4BD-GRMZM2G151916 M3-3xMyc-UBQ10-Bas	24.01.2023	Spec	Pouria
9400	pJET_BIN2_nostop	28.02.2023	Amp	Pouria
9500	187-ADH1-Promoter-Gal4BD-Myc-AtBIN2-CD-At4g18710-dummy-ADH-Terminator_pJet-TDH3 (GAPDH) pro_eGFP-mCherry-dummy-CYC1_term	25.03.23	Spect	Pouria
9656	187-pADH1-Gal4BD-UMAG_02193-dummy-yADH-Terminator	29.03.23	Spect	Pouria
9660	PB-T3G-ERP2 -Myc-Mcherry-UMAG_02193-dummy-1	29.03.23	Amp	Pouria
9661	PB-T3G-ERP2-dummy-UMAG_02193-linker_mCherry_DE	29.03.23	Amp	Pouria
9662	PB-T3G-ERP2- Myc-Mcherry-mCherry-dummy-1	29.03.23	Amp	Pouria
9663	PB-T3G-ERP2-dummy-mCherry-linker_mCherry_DE	29.03.23	Amp	Pouria
9664	PB-T3G-ERP2-eGFP-Homo sapiens glycogen synthase kinase 3 beta-(GSK3B) CD-dummy-1	29.03.23	Amp	Pouria
9665	PB-T3G-ERP2-dummy-Homo sapiens glycogen synthase kinase 3 beta-eGFP	29.03.23	Amp	Pouria

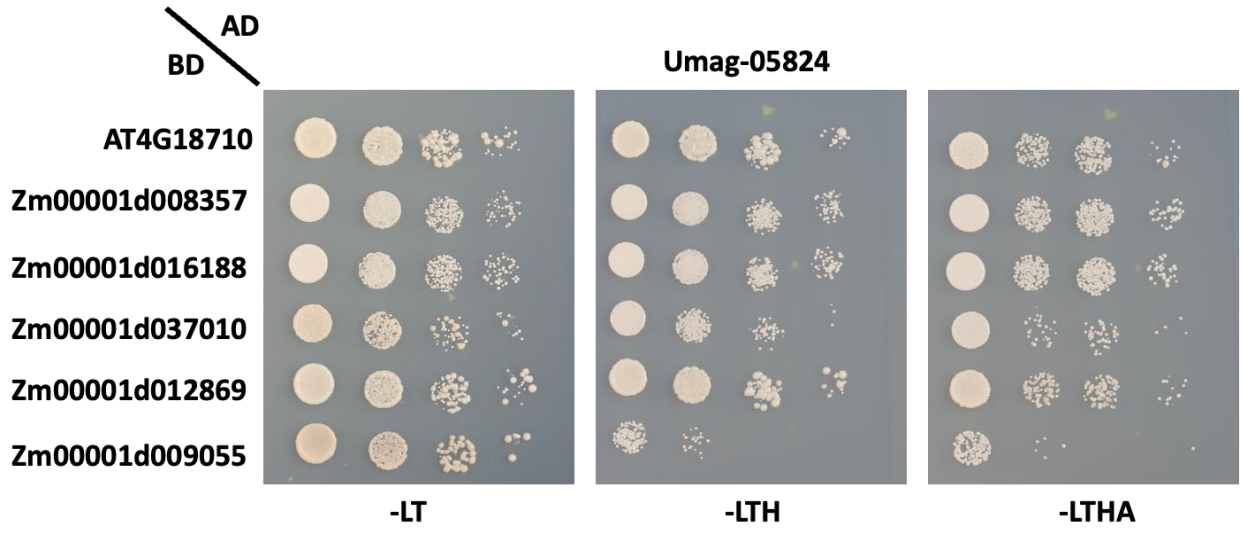

Figure 11-1 Y2H assay AtBin2 and 5 ZmGSK3s with Umag05824

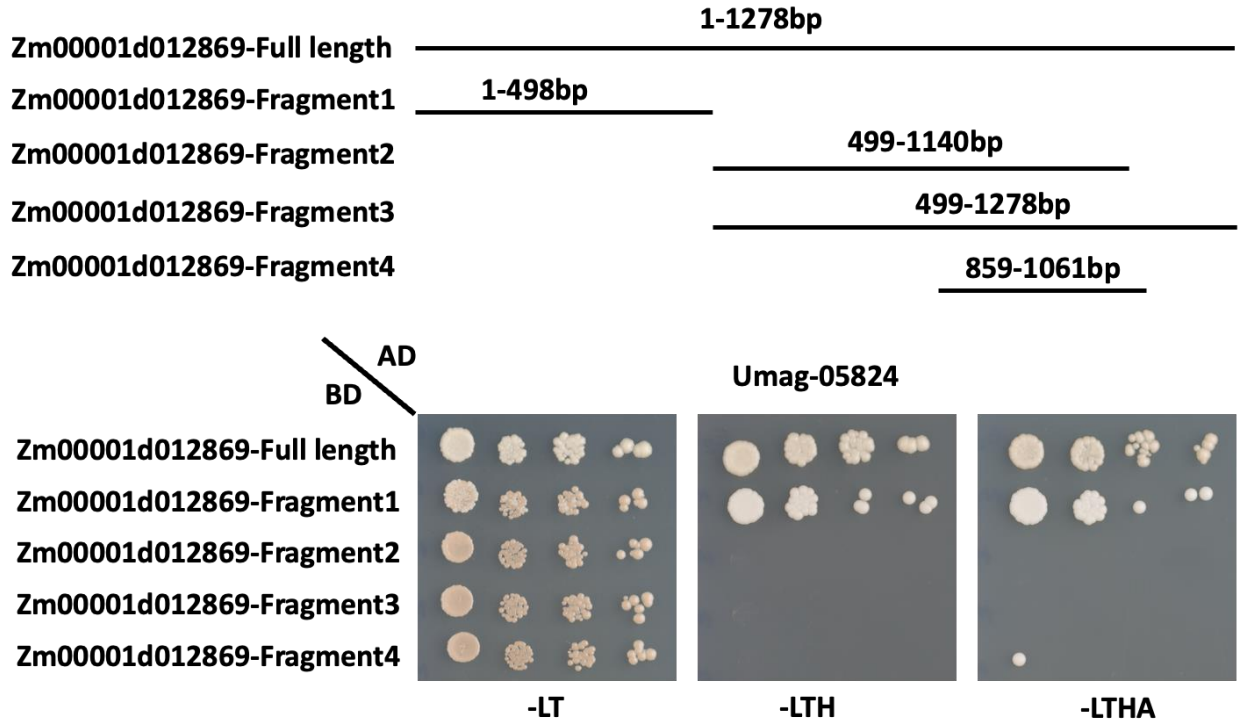

Figure 11-2 Y2H of truncated ZmGSK11 (Zm00001d012869) with Umag05824

Table 11-2 SplitTurboID results of Umag05824 and AtBin2 co-expression in N. benthamian

row	*N. bentamiana*	Destription	A.t ortholgue	Description
1	E2_Niben101Scf01434g03006.1	Linoleate 9S-lipoxygenase 6	AT1G55020	lipoxygenase 1 [Arabidopsis thaliana]
2	E2_Niben101Scf02296g00016.1	glucose-6-phosphate dehydrogenase 6	AT5G40760	glucose-6-phosphate dehydrogenase 6
3	E2_Niben101Scf03628g14021.1	phosphoenolpyruvate carboxylase 1	AT1G53310	phosphoenolpyruvate carboxylase 1
4	E2_Niben101Scf02637g00012.1	Vacuolar protein sorting-associated protein 27	AT1G21380	Target of Myb protein 1
5	E2_Niben101Scf01485g00002.1	Poly(U)-specific endoribonuclease-B	AT4G17100	poly(U)-specific endoribonuclease-B protein
6	E2_Niben101Scf11383g03008.1	Protein kinase superfamily protein	AT5G58140	phototropin 2
7	E2_Niben101Scf01063g04003.1	Class E vacuolar protein-sorting machinery protein HSE1	AT5G16880	Target of Myb protein 1
8	E2_Niben101Scf05078g04001.1	GYF domain-containing protein	AT1G27430	GYF domain-containing protein
9	E2_Niben101Scf01382g01004.1	Eukaryotic translation initiation factor 4G	At5g57870	eukaryotic initiation factor 4, eIF4-like protein
10	E2_Niben101Scf07463g01012.1	Ubiquitin carboxyl-terminal hydrolase 34	AT5G06190	UBP12 [Arabidopsis thaliana]
11	E2_Niben101Scf09203g00003.1	Protein kinase superfamily protein	AT3G22750	Protein kinase superfamily protein
12	E2_Niben101Scf11232g01012.1	beta-glucan-binding protein 4 [Medicago truncatula]	AT5G15870	glycosyl hydrolase family 81 protein
13	E2_Niben101Scf15153g02001.1	Phosphoenolpyruvate carboxykinase [ATP]	AT4G43150	PEPCK
14	E2_Niben101Scf02581g04013.1	Respiratory burst oxidase homolog protein C	AT5G46420	RBOHD
15	E2_Niben101Scf03580g01006.1	Fructose-bisphosphate aldolase	AT2G36460	Aldolase superfamily protein
16	E2_Niben101Scf06009g00025.1	soluble N-ethylmaleimide-sensitive factor adaptor protein 33	AT5G61210	soluble N-ethylmaleimide-sensitive factor adaptor protein 33
17	E2_Niben101Scf13098g00013.1	Cyclin-dependent kinase G-2	AT4G28980	CDK-activating kinase 1AT
18	E2_Niben101Scf00254g05005.1	General vesicular transport factor p115	At3g27530	putative p115-like protein
19	E2_Niben101Scf00712g10025.1	Calcium-binding EF hand family protein	AT1G20760	Calcium-binding EF hand family protein
20	E2_Niben101Scf02268g06007.1	Calmodulin-binding transcription activator protein with CG-1 and Ankyrin domains	At2g22300	Calmodulin-binding transcription activator 3

12 Appendix II: Cab1 paper draft

The Limits to Growth, *Ustilago maydis* effector Cab1 suppresses cell wall expansion by triggering Bin2 kinase activity

Pouria Bahrami[1,2], Kishor Ingole[1], Mamoona Khan[1,2], Aladár Pettkó-Szandtner[3], Maxim Prokchorchik[1], Shraddha Dahale[1], Natália Sousa Teixeira-Silva[1], Armin Djamei[1,2*]

[1] Department of Plant Pathology, Institute of Crop Science and Resource Conservation (INRES), University of Bonn, Bonn, Germany

[2]Leibniz Institute of Plant Genetics and Crop Plant Research (IPK), OT Gatersleben, Corrensstr. 3, D-06466 Stadt Seeland, Germany.

[3]Institute of Biochemistry, Biological Research Centre, Szeged, 6726, Hungary.

*Corresponding author: Djamei@uni-bonn.de

Summary

- Plant biotrophic pathogens employ secreted molecules, so-called effectors to suppress the host immune system and to redirect the metabolism and development in their own favor.
- Putative effectors of the gall-inducing maize pathogenic fungus *Ustilago maydis* were screened for their capability to target conserved Brassinosteroid (BR) signaling in plants.
- Here we present a fungal effector, Cab1, genetically located in cluster 5A. Cab1 targets BIN2 (Shaggy-like kinase 3) at the C-terminal domain and promotes its active state *in planta.*
- Cab1-mediated relocalization of BIN2 (Glycogen synthase kinase 3) suppresses SAURs and Expansins-mediated cell wall expansion.

Keywords: Expansins, Brassinosteroids, Auxin, plant pathogen, Glycogen synthase kinase 3, BIN2, *Ustilago maydis*

Introduction

The biotrophic fungus *Ustilago maydis* causes smut disease in maize (*Zea mays*) and teosinte *(Zea mays ssp. parviglumis)*. *U. maydis* is able to cause galls in all aerial parts of its host plants, a distinctive characteristic compared to other smut fungi such as *Ustilago hordei, Tilletia caries, Tilletia laevis* (Christoph & Gero, 2004). Upon the biotrophy phase, *U. maydis* secretes manipulative molecules, so-called effectors, to shape the interaction with its host. After secretion of effectors, they act either as so-called apoplastic effectors in biotrophic interphase, an interface formed between the fungal infective intracellular hyphae and the plant plasma membrane, or are further translocated into the host cytosol (symplastic effectors) (Lanver et al., 2018; Uhse & Djamei, 2018). Effectors play essential roles in promoting pathogen establishment and progression, suppressing host immunity, and modifying the host's metabolism to facilitate the completion of the pathogen's life cycle (Scott et al., 2022; Y. Song et al., 2021). It has been shown that *U. maydis* secretes also small molecule effectors with phytohormone activities e.g., auxins, cytokinins, and abscisic acid during plant colonization (Bruce et al., 2011; Reineke et al., 2008). Besides small molecules, secretion signal prediction of all open reading frames suggest that *U. maydis* possesses around 550 secreted proteins of which many potentially functioning as effectors (Redkar et al., 2015).

So far only a limited number of effectors of *U. maydis* have been functionally characterized. Among the apoplastic effectors functionally characterized, Pep1 suppresses ROS accumulation around growing hyphae (Doehlemann et al., 2009), while Pit2 inhibits the maize apoplastic papain-like cysteine proteases (PLCPs) (Misas-Villamil et al., 2016). Fly1 interacts with and modifies the plant chitinase-A enzyme and reducing its ability to break down the fungus's cell wall (Ökmen et al., 2018). Additionally, Sta1 seems to change the structure of the fungal cell wall, allowing it to grow in specific plant tissues (Tanaka & Kahmann, 2021). On the other hand, a greater number of cytoplasmic effectors have been more extensively studied. For instance, See1 is involved in reactivating DNA synthesis in infected tissues (Matei et al., 2018). Another effector, Tin2, stabilizes the maize protein kinase ZmTKK1, thereby activating the anthocyanin biosynthesis pathway during the disease cycle (Tanaka et al., 2014). Additionally, *U. maydis* Cluster 10A contains 10 effectors, most of which suppress ROS accumulation. For example, Tay1 inhibits

cytoplasmic ROS production, while Mer1 targets the host nucleus to promote the degradation of RFI2s, which are negative regulators of ROS production (Navarrete et al., 2021).

Plant hormone biosynthesis and signaling pathways are another important effector hub. For instance, CMU1 has been observed to interfere with the biosynthesis of Salicylic acid (SA), while Jsi1 interferes with the c-terminal WD40 domain of the central transcriptional Co-repressor TOPLESS (TPL), thereby inducing Jasmonic acid (JA) and Ethylene signaling pathways (Djamei et al., 2011; Scott et al., 2022). With a whole suit of effectors *U. maydis* targets also the N-terminal TPD domain of the TPL and TOPLESS-related (TPR) family, thereby de-repressing mainly auxin signaling (Bindics et al., 2022; L. Huang et al., 2023; Khan et al., 2023; Navarrete et al., 2022). The induction of growth hormone auxin signaling by effectors exploits growth-defense antagonisms as TPL/TPR acts as a positive regulator of PAMP-triggered immunity responses (Navarrete et al., 2022) and is consistent considering *U. maydis* as a gall-inducing fungus. The feature to exploit growth signaling pathways is frequently found also in other plant biotrophic pathogens (Mapuranga et al., 2022). Previous studies have demonstrated that the auxin signaling pathway increase plant susceptibility to biotrophic pathogens (Čarná et al., 2014; Fu & Wang, 2011). Considering the importance of auxin in plant immunity, it is not surprising that *U. maydis* secretes multiple effectors to modulate auxin signaling within the host. For example, the effectors Nkd1, Tips 1-5 have been identified to interact with transcriptional co-repressors TOPLESS/TOPLESS-related (TPL/TPRs), resulting in the de-repression of auxin signaling in plants. These interactions ultimately promote the susceptibility of the host to *U. maydis* (Navarrete et al., 2022; Navarrete, Grujic, Stirnberg, Saadoid, et al., 2021). Recently, additional TPL interactors of *U. maydis* including Tips 6-8 have been reported. These findings indicate that the TPL class of corepressors and auxin signaling serves as a significant hub for *U. maydis* effector proteins (L. Huang et al., 2023; Khan et al., 2023).

U. maydis induces hypertrophy and hyperplasia, resulting in the formation of galls in various aerial parts of maize (Matei et al., 2018). Auxin is a key phytohormone, the molecular mechanism of auxin signaling involves auxin binding to Transport Inhibitor Response 1 (TIR1) and Auxin Signaling F-Box (AFB) proteins, triggering the degradation of auxin/Indole-3-Acetic Acid (Aux/IAA) proteins, de-repression of auxin response factors (ARFs), binding to auxin response elements

(AuxREs) in target gene promoters, and subsequent modulation of gene expression (Du et al., 2020; Z. Yu et al., 2022). Noteworthy, ARFs are divided into two main groups: in Arabidopsis, activator ARFs, including ARF5, ARF6, ARF7, ARF8, and ARF19 are rich in glutamine, while repressor ARFs are abundant in serine, threonine, and proline. Certain repressor ARFs, such as ARF2, ARF3, ARF9, and ARF18, inhibit auxin-responsive gene expression by enlisting TPL/TPRs in Arabidopsis. The Aux/IAA-ARF module is better suited for activator ARFs than repressor ARFs. Although there is little evidence supporting the activation of repressor ARFs by Aux/IAA degradation, they remain significant members of the Arabidopsis ARF family (Chandler, 2016; Kuhn et al., 2020; Vernoux et al., 2011). Through its influence on various cellular processes, auxin controls cell elongation, division, and differentiation, ultimately impacting overall plant growth and development (Ai et al., 2023; Gallavotti, 2013).

The plant cell wall (CW) consists of polysaccharides like hemicellulose, cellulose, and pectin, along with lignin and glycoproteins. It envelops plant cells, providing diverse shapes, sizes, and physicochemical properties for various roles during development (Carpita et al., 2001). CW plays vital roles in morphogenesis, mechanical support, water and nutrient conduction, and defense against stresses (B. Zhang et al., 2021). One of the primary effects of auxin is its ability to promote cell elongation by regulating the expression of cell wall-related genes and the activity of cell wall-loosening enzymes. These lead to the relaxation of the cell wall, enabling cell expansion and subsequent changes in the cell shape and architecture (Ai et al., 2023; Gallavotti, 2013; Majda & Robert, 2018). Additionally, auxin impacts cell division and differentiation, further influencing plant cell shape and architecture (L. Wang & Ruan, 2013). Small Auxin Up-regulated RNAs (SAURs), show rapid induction in response to auxin treatment, and both transcripts and protein have a high turnover upon induction (Stortenbeker & Bemer, 2019). SAURs interact with the PM-localized PP2C.D family and inhibit their function (Du et al., 2020). The inhibition of PP2C.D keeps the PM localized H+-ATPases pumps phosphorylated and activate. This increase in PM H+-ATPase activity, acidifies the apoplast, and promotes expansins (EXPs) activity and cell wall loosening enzymes in *A. thaliana* (van Mourik et al., 2017). Transgenic lines of *A. thaliana* with overexpressed SAUR19 and the triple mutant of PP2C.D (*d2d5d6*) displayed a similar phenotype, including elongated cells in seedlings, leaves, stems, and floral organs (Ren et al., 2018). EXPs are

small and non-enzymatic proteins found in all plants and enable the local sliding of wall polymers by reducing adhesion between wall polysaccharides in the apoplast (Marowa et al., 2016). EXPs promote the spillage between microfibrils by cutting non-covalent bonds between cellulose and Hemicellulose and increase cell wall plasticity and extensibility, enabling cell growth and development (J. Cosgrove, 2000; Mu et al., 2021; Sampedro & Cosgrove, 2005). In summary, according to the auxin-mediated acidic growth model, the downregulation of SAURs and EXPs hinders the plant cell wall loosening and consequently suppresses cell growth and development (Du et al., 2020; Sampedro & Cosgrove, 2005; van Mourik et al., 2017; Wieczorek & Grundler, 2006).

Hormone signaling pathways frequently crosstalk and act either synergistically or antagonistically to each other as part of the systemic decision-making processes that shape plant responses to internal and external cues. Auxin signaling modulates plant immunity as it crosstalks with well-established defense hormone signalings pathways, including the Salicylic acid (SA) and Jasmonic acid (JA) pathways (C. Han et al., 2023; Ruan et al., 2019). In growth and developmental processes, auxin signaling frequently interacts with other growth hormone signaling pathways including those regulated by Cytokinins, Gibberellins, and Brassinosteroids (BRs) (Jing & Strader, 2019; Yang et al., 2018).

The interconnection between the auxin and BR pathways in plants is a complex and dynamic network that plays a crucial role in coordinating growth and development. Both auxin and BR are essential hormones involved in regulating various aspects of plant physiology, including cell elongation, division, and differentiation (Ai et al., 2023; Devi et al., 2022; Tian et al., 2017).

BRs are steroid phytohormones playing a key role in different aspects of plant growth and development, such as cell division and elongation, photomorphogenesis, and reproduction (Z. Li & He, 2020; Nolan et al., 2020). Besides, BRs are also important for fine-tuning the responses to both biotic and abiotic stressors (W. Song et al., 2022). To give an impression, in *A. thaliana* between 5000 to 8000 genes are on the transcriptional level modulated by Brassinosteroids (BRs) (Guo et al., 2013; Nolan et al., 2017a; X. Wang et al., 2014).

At the core of the BR signaling pathway is the perception of BRs by the membrane-localized receptor kinase, BRASSINOSTEROID-INSENSITIVE 1 (BRI1), and its homologs (Friedrichsen et al.,

2000; Z. He et al., 2000), BRI1-LIKE1 (BRL1) and BRI1-LIKE3 (BRL3) (Caño-Delgado et al., 2004; Kinoshita et al., 2005; Nolan et al., 2020). BRI1 was identified through molecular studies of *A. thaliana* BR mutants (Clouse et al., 1996; J. Li & Chory, 1997; Nolan et al., 2020). Upon binding to BRs, BRI1 forms a complex with its co-receptor BRI1-Associated Kinase 1 (BAK1) and undergoes autophosphorylation, and initiates a phosphorylation cascade of its downstream signaling components (T. W. Kim et al., 2011; J. Li & Chory, 1997; W. Song et al., 2022; Tang et al., 2008). One of the major mechanisms of BR action is the phosphorylation and activation of the serine-threonine phosphatase BRI1 SUPPRESSOR 1 (BSU1) via receptor-like cytoplasmic kinases, the BR-Signaling Kinases (BSKs), leading to dephosphorylation and inhibition of glycogen synthase kinase3 (GSK3)-like kinase BRASSINOSTEROID INSENSITIVE2 (BIN2). BIN2 acts as a negative regulator in BR signaling by phosphorylating and thereby inhibiting BR-regulated transcription factors BRASSINOSTEROID INSENSITIVE 1-EMS-SUPPRESSOR 1 (BES1) and BRASSINAZOLE RESISTANT 1 (BZR1) (J. X. He et al., 2002; J. Li et al., 2001; J. Li & Nam, 2002; Youn & Kim, 2015). BIN2-induced phosphorylation inactivates BES1 and BZR1 by promoting their cytoplasmic retention via 14-3-3 proteins (Gampala et al., 2007; J. X. He et al., 2002; J. Li et al., 2001; J. Li & Nam, 2002; Ryu et al., 2007; Youn & Kim, 2015), inhibiting their DNA binding activity (Vert & Chory, 2006), and stimulating their degradation (J. X. He et al., 2002; E. J. Kim et al., 2019; Yin et al., 2002). The presence of BRs triggers a feedback mechanism that inhibits BIN2 activity. The inactivation of BIN2 by BRs along with the dephosphorylation of the atypical basic helix–loop–helix (bHLH) transcription factors BES1 and BZR1 by PROTEIN PHOSPHATASE 2A (PP2A) (Tang et al., 2011) allows these transcription factors to become active in the nucleus to control BR-responsive gene expression again (J. X. He et al., 2002; Nolan et al., 2017; Tang et al., 2008; Yin et al., 2002; X. Yu et al., 2011).

GSK3s are multifunctional and highly conserved non-receptor Ser/Thr kinases. They are involved in various developmental and stress-responsive pathways as light stress signaling networks or are required for growth and development (Hou et al., 2022; T. Li et al., 2020; Saidi et al., 2012; Wei & Li, 2016). Plants' GSK3-family kinases are encoded by multiple genes and have been grouped into four clades; clade II members, BIN2, BIN2-Like1 (BIL1), and BIN2-like2 (BIL2) mainly function in the BR signaling pathway (Nolan et al., 2022; Youn & Kim, 2015). While, mammalian cells have only two isoforms GSK3α and GSK3β (Beurel et al., 2015).

BIN2 as the most studied GSK3s in *A. thaliana*, The *bin2-1* (E263K) mutation is a semi-dominant mutation leading to hyperactive kinase activity (J. Li et al., 2001). In terms of phenotype, *bin2-1* mutants are similar to BR biosynthesis mutants and display pleiotropic phenotypes including severe dwarfism, a dark-green color, and a de-etiolation phenotype when grown in darkness. In the case of BR-deficient mutants, these phenotypes could be rescued by the external application of BRs (Clouse et al., 1996; J. Li & Chory, 1997; Nolan et al., 2020). BIN2 can also phosphorylate and inhibits the activity of several other transcription factors, including PIF4 (PHYTOCHROME-INTERACTING FACTOR 4) and JAZ proteins (JASMONATE ZIM-DOMAIN), which are involved in regulating various aspects of plant growth and development (Bernardo-García et al., 2014; Hughes, 2020). SOB3 (SUPPRESSOR OF PHYA-105 3) mainly functions as a negative regulator of BR signaling in light response. SOB3 inhibits the expression and reduces the transcript accumulation of all six members of the SAUR19 subfamily, which are associated with the repression of cell expansion and hypocotyl elongation (Favero et al., 2017).

The hypertrophy and hyperplasia in the infected tissue form galls, which are prominent symptoms linked to *U. maydis* infection. At 2 days post-infection (dpi), the host cells undergo metabolic and transcriptional reprogramming, resulting in hyperplasia (cell division) in leaf bundle sheet cells and hypertrophy (cell enlargement) in leaf mesophyll cells (Matei et al., 2018). In anthers, *U. maydis* induces ectopic periclinal and anticlinal divisions and cell expansion, depending on the developmental stage of the anther or the affected cell type(Gao et al., 2013).

In this study, we present evidence that the *U. maydis* effector Cab1 enhances the activity and stability of BIN2, inhibiting thereby BR signaling and consequently cell expansion. As a result of Cab1 expression, BIN2 accumulates in the nucleus and suppresses the expression of SAURs and EXPs. The function of Cab1 appears to control cell wall overgrowth, and its expression may be in response to other unknown gall-forming effectors of *U. maydis*.

Materials and methods:

Organisms used in this study and their growth conditions

The maize varieties EGB (Early Golden Bantam) and B73 were used in this study. The sequenced maize line B73 was chosen for making cDNA and cloning, while maize Early Golden Bantam (EGB) line plants were used for the secretion assay, bombardment, and virulence assays with *U. maydis* knockout (KO) strains followed by disease scoring (Kämper et al., 2006). The plants were grown under controlled glasshouse conditions with a photoperiod of 16 hours of light at 28 °C and 8 hours of darkness at 22 °C and watered every 5 days. Specific methods will be further described below.

A. thaliana (ecotype Columbia-0), all *A. thaliana* transgenic lines, and *Nicotiana benthamiana* was grown in a growth chamber under 8 h: 16 h, light: dark cycle at 21 °C and 60% humidity. *A. thaliana* and *N. benthamiana* plants were watered by flooding every 3 days.

The solopathogenic *U. maydis* strain SG200 (Kämper et al., 2006) was the progenitor strain used to generate all the mutants and knockout strains by homologous recombination. All the strains were grown in YPD plates or broth supplemented with 100 µg/mL Ampicillin and appropriate selective agent at 28 °C, liquid cultures were shaken at 180 rpm.

Molecular cloning

All gene models and the corresponding accession number employed in this study are documented in supplementary Table 1 (Tabel S. 1). All the plant and yeast expressi on plasmids constructs were generated via standard molecular procedures (R. Green & Sambrook, 2012) by using either Greengate (Lampropoulos et al., 2013) or Gateway cloning (Katzen, 2007). All the employed plasmids were cloned in Mach1 (Thermo Fisher Scientific, Waltham, MS, USA) cells and grown in dYT liquid medium or on YT agar plates supplemented with the appropriate antibiotic.

U. maydis knockout strains and mutants

To create cluster 5A knockout strains (Kämper, 2004). The flanking regions of the cluster, encompassing approximately 1 kb upstream of UMAG_02192 and 1 kb downstream of

UMAG_02196, were cloned into the plasmid pGAM1311. In a similar manner, a knockout mutant of Cab1 was produced. This involved cloning regions approximately 600 pb before and 600 bp after Cab1 into the plasmid pGAM1311. This strategy allowed us to create the desired genetic modifications. For the Cab1 overexpression strain, full-length Cab1 was cloned under the *Pit2* strong biotrophic promoter (Doehlemann et al., 2011) and the Cab1 (P_{Pit2}::Cab1-3xHA) fusion construct was integrated into the *ip* locus *U. maydis* solopathogenic strain SG200 (Kämper et al., 2006).

Maize infection assay and scoring

Three independent biological replicates were performed for each transgenic strain. *U. maydis* strains were grown in YEPSL (0.4% yeast extract, 0.4% peptone, 2% sucrose). Cell suspensions in H_2O were adjusted to OD600=1.0. These suspensions were then injected into the stems of 7-day-old EGB maize seedlings using a syringe, as described by Kämper et al. (2006). The scoring was performed at 12 dpi. The infection symptoms were classified based on the disease rating proposed by Kämper et al. (2006) with slight modifications in the different gall categories. Additionally, the categories of "no symptoms," "stunted," and "dead" were included along with the five previous categories of "chlorosis," "small galls," "normal galls," "big galls," and "heavy galls" (Kämper et al., 2006). The disease index was calculated using Wilcoxon test analysis in R, with the *U. maydis* strain SG200 applied as the reference (Navarrete et al., 2022; Navarrete, Grujic, Stirnberg, Saado, et al., 2021; Saado et al., 2022; Stirnberg & Djamei, 2016) .

Cab1 secretion assay

To visualize Cab1 secretion *in planta,* the signal peptide the first 27 amino acids (Krogh et al., 2001) was fused with the C-terminal mCherry. Expression was driven by a strong biotrophy-induced *cmu1* promoter (Djamei et al., 2011) and transgene was integrated into the *ip* locus of the solopathogenic *U. maydis* strain SG200 (Kämper et al., 2006). Three independent transgenic SG200 strains carrying the secretion construct (P_{cmu1}::$Cab1_{1-27}$-mCherry) were implemented for infection of 7-day-old *Z. mays* EGB plants and were grown under controlled conditions. At 4 dpi, plant leaf slices were collected and confocal microscopy was used to visualize the secretion. The mCherry any signal peptide attached (P_{cmu1}::mCherry) was used as a negative control.

Biolistic transformation of maize

Leaves of 12-d-old maize were transiently transformed using 1.0 µm gold particles coated with 7 µg of each plasmid DNA delivered with the biolistic particle system (BioRad) and the details were described previously in (Djamei et al., 2011). Fluorescence emission was captured 1 day after transformation by confocal microscopye.

Phenotyping of *A. thaliana*

Transgenic *A. thaliana* lines were generated by overexpressing candidate effectors coding sequences under an β–Estradiol-inducible promoter. The effector genes were cloned without the signal peptide coding part and were genetically fused with Myc-epitope coding sequences at the N-terminus ($P_{35S\text{-}XVE}$::Myc-Effector). *A. thaliana* plants were transformed using *Agrobacterium* strain GV3101 (pSoup) via floral dipping. T2 plants were grown under selection and 7 days old transgenic plants were transferred to induction $^1/_2$ MS plates containing either 10µM β–Estradiol dissolved in DMSO or on control plates containing only the respective amount of DMSO. Plants were screened for root and shoot phenotypes 5-, 10-, and 15-days post-induction (dpi), respectively. Myc-Cab1 ($P_{35S\text{-}XVE}$::Myc-$Cab1_{28\text{-}113}$) was subjected to Co-immunoprecipitation followed by Mass Spectrometry (CoIP-MASS) to identify corresponding Cab1-associated plant proteins.

The GR-$Cab1_{28\text{-}113}$ ($P_{35S\text{-}XVE}$::Glucocorticoid-receptor-V5-$Cab1_{28\text{-}113}$) construct was generated, following the previously described methodology (Aoyama & Chua, 1997). This construct is a fusion of the N-terminal glucocorticoid receptor, a V5 epitope tag, and $Cab1_{28\text{-}113}$ expressed under the β–Estradiol-inducible expression system. The resulting GR-$Cab1_{28\text{-}113}$ transgenic plants were initially grown on selection plates and subsequently transferred to induction plates 7 days after germination to initiate the expression. In the induction plates, the absence of Dexamethasone causes the accumulation of expressed GR-$Cab1_{28\text{-}113}$ in the cytosol. while, in the induction plates with Dexamethasone, the expressed proteins relocate to the nucleus, resulting in the appearance of the phenotype.

Total RNA extraction and RNA-sequnecing

Total RNA was extracted from 14-days-old *A. thaliana* mCherry-Cab1$_{28\text{-}113}$ (P$_{35S\text{-}XVE}$::mCherry-Cab1$_{28\text{-}113}$) seedlings, treated with 10uM β–Estradiol. The extraction was performed using a plant total RNA extraction kit (Macherey-Nagel Bioanalysis Dueren, Germany Cat:740949) according to the manufacturer's instructions. The RNA-seq was performed at Novagen, UK and raw fastq files were analysed in-house. The Illumina reads were trimmed and quality filtered using trimmomatic-0.39 (Bolger, A. M., Lohse, M., & Usadel, B. (2014). Trimmomatic: A flexible trimmer for Illumina Sequence Data. Bioinformatics, btu170) with standard settings (LEADING:3 TRAILING:3 SLIDINGWINDOW:4:15 MINLEN:36). Quality trimmed and filtered reads were aligned to *A. thaliana* reference transcripts using Hisat2 (https://www.nature.com/articles/s41587-019-0201-4) and quantified with Stringtie (ref 10.1186/s13059-019-1910-1) or directly analyzed with Salmon (Patro, R., Duggal, G., Love, M. I., Irizarry, R. A., & Kingsford, C. (2017). Salmon provides fast and bias-aware quantification of transcript expression. Nature Methods.) The read counts were further analyzed with DESeq2 (10.1186/s13059-014-0550-8.) and the differentially expressed genes were assigned with at least 10 read coverage, more than 1.5-fold change, and with adjusted p-value <0.05. GO enrichment was analyzed by shinyGO 0.80 (10.1093/bioinformatics/btz931).

Co-immunoprecipitation assay in *Nicotiana benthamiana*

Agroinfiltration of GFP-Bin2 (P$_{35S}$::GFP-AtBin2) and mCherry-Cab1 (P$_{35S}$::mCherry-Cab1$_{28\text{-}113}$) constructs under the control of strong 35S cauliflower mosaic virus (CaMV) promoter was performed for co-immunoprecipitation experiments. The constructs were infiltrated into *N. benthamina* leaves. The leaves were harvested 3 days post-infiltration (dpi) and frozen directly in liquid nitrogen prior further processing. Co-IP was conducted using µMACS™ Micro Beads system from Miltenyi Biotech (Bergisch Gladbach, Germany) following the manufacturer's protocol. The immunoprecipitated proteins were detected with anti-GFP and mCherry rabbit antibodies according to the manufacturer's protocol. The experiments were repeated independently at least two times.

Bimolecular fluorescence complementation assay

AtBin2 or ZmGSK4, and $Cab_{28\text{-}113}$, were fused either the C-terminal half of Venus (cVenus) or the N-terminal half of Venus (nVenus) fluorescent proteins, respectively, as previously described (Gookin & Assmann, 2014; Navarrete et al., 2022). Protein expression was driven by the constitutive 35S promoter and co-infiltration of these constructs was performed in the epidermal cells of *N. benthamiana*. Confocal microscopy was carried out three days post-infiltration. As negative control, NLS-luciferase-nVenus was co-expressed with ZmGSK4-cVenus, and microscopy was performed under the same experimental conditions.

Yeast transformation and two-hybrid assays

All yeast work has been conducted following the yeast protocols handbook (Clontech, 196 Mountainview, CA) and the previously described protocol (Navarrete, Grujic, Stirnberg, Saado, et al., 2021). Briefly, the Y187 strain (MAT α) was transformed with bait vectors (pGBKT7), while the AH109 strain (MAT a) was transformed with prey vectors (pGAD, pADGG – a modified version of pGADT7), using the LiAc/PEG method. For the yeast two-hybrid (Y2H) assay, the GAL4 activation domain from the prey vector pADGG was fused to the open reading frame of *U. maydis* Cab1 effector without the signal peptide ($Cab1_{28\text{-}113}$), and the GAL4 binding domain from the bait vector pGBKT7 was fused to the genes AtBin2, ZmGSK1, ZmGSK4, and ZmGSK8. The presence of the respective plasmids in the transformants was confirmed by PCR analysis. Positive interactions were determined by the growth of mated yeasts on intermediate or high stringency media five days after inoculation in spotting assays. All experiments were repeated three times to ensure the reliability and reproducibility of the results.

***Heterodera schachtii*, syncytium forming nematode infection assay**

The cyst-forming assay was conducted following a standard protocol (M. Huang et al., 2021). Briefly, surface-sterilized mCherry-$Cab1_{28\text{-}113}$ ($P_{35S\text{-}XVE}$::mCherry-$Cab1_{28\text{-}113}$) *A. thaliana* seeds were subjected to vernalization on KNOP-medium at 4 °C. The plates were then transferred to the climate chamber under a red/blue light source, maintaining the 16-h/8-h light/dark photoperiod at 24 °C. After 12 days of growth, mCherry-$Cab1_{28\text{-}113}$ were transferred on induction plates containing 10 µM β–Estradiol, 12 days post germination. For nematode propagation, *Sinapis alba* was used, and each plant was subjected to 60 active freshly hatched second-stage juveniles (J2s)

nematodes. The infection rate was measured by the number of syncytia formed 14 day-post infection.

Results:

An *U. maydis* effector candidate causes drastic phenotypic developmental impairment in *Arabidopsis*

Ustilago maydis infecting maize causes dramatic morphological, developmental and numerous metabolic changes in its host, likely due to the direct or indirect activity of its effectors(Brefort et al., 2009; Djamei & Kahmann, 2012; Navarrete, Grujic, Stirnberg, Saado, et al., 2021; Scott et al., 2022; Uhse & Djamei, 2018). Whereas many effectors might target monocot or even maize-specific host proteins, others might act on highly conserved pathways and might be therefore also showing their manipulative activity in heterologous plant systems. To identify *U. maydis* effectors that target conserved plant developmental pathways,we generated transgenic *A. thaliana* lines expressing putative *U. maydis* effector candidates lacking their predicted endogenous signal peptide under the β–estradiol-inducible promoter. These lines were then screened upon effector candidate expression for any alterations in plant growth and development. The transgenic plants were initially grown on selection plates and subsequently transferred onto induced (+ β–estradiol) or uninduced (- β–estradiol) $^{1}/_{2}$MS plates after 7 days. Phenotyping was conducted at 5-, 10-, and 15-days post-induction (dpi). Among the candidates, plants expressing Umag-02193 exhibited the strongest phenotype in shoots and roots. In the results of Umag-02193 expression, the expansion of leaves on both the abaxial and adaxial sides became uneven, resulting in a curly appearance. Moreover, the growth of the main axes root was suppressed, while the lateral and hairy roots showed induction, which became more pronounced with long-term induction. At 14dpi, the roots appeared shorter and bunchier compared to the uninduced and col-0 lines. Based on this observation, we named this candidate effector Cabbage 1 (Cab1) (Fig. 1A). Additionally, we examined the expression of the N-terminally epitope-tagged HA-Cab1$_{28\text{-}113}$ by western blot analysis, comparing β–estradiol-induced and uninduced plants (Fig. 1B).

A dwarf phenotype can be either achieved by a reduced number of cells in an organ or a reduction in cell expansion or by a combination of both. Therefore, we examined the number of cells and stomata per square centimeter in 3-week-old HA-Cab1$_{28\text{-}113}$ overexpressing plants (14 days post-

β–estradiol induction) and compared them with uninduced transgenic and Col-0 wild-type plants. After staining the cell walls of the tissue with propidium iodide, we observed that Cab1$_{28-113}$-expressing plants exhibited a significantly higher number of epidermal cells as well as of guard cells forming stomata per counted area compared to both the uninduced and Col-0 plants (Fig. 1C, D; Fig. S1A, B). The Cab1 overexpression dwarf phenotype is therefore a result of a reduction in cell expansion whereas a reduction in cell number / reduction in cell divisions was not observable.

Cab1 is a secreted effector, targeting and acting in the plant cell nucleus

Cab1 is considered an effector candidate due to the presence of a predicted signal peptide and its position in the previously described potential effector cluster 5A on chromosome 5 of *Ustilago maydis* (Schirawski et al., 2010). Effector cluster 5A consists of five genes that encode predicted secreted proteins (Fig. 2A). To assess Cab1 relative expression during disease progression, a typical feature for an effector would be a transcriptional upregulation, Cab1 expression of in *U. maydis*-infected maize seedlings in comparison to *U. maydis* axenic culture were analyzed using published RNAseq data (Lanver et al., 2018). The Cab1 expression profile during its biotrophic lifecycle of *U. maydis* in maize shows an early transcriptional induction of Cab1 starting 12 hours post-infection, which further increased approximately 10-12-fold, peaking 4 dpi and staying at a similarly high level further till 12 days post-infection (Fig. 2B).

To investigate the role of Cab1 in disease establishment and progression, we created over-expression strains of Cab1 (P_{Pit2}::Cab1$_{1-113}$-3xHA) using the strong biotrophy-induced promoter *Pit2*, and the cluster 5A deletion mutant in the solopathogenic strain SG200 background. Neither the cluster 5A deletion strains nor the Cab1 overexpression strains exhibited any significant differences in virulence compared to the parental SG200 strain (Fig. S2 A, B). These findings align with previous studies with the cluster 5A deletion mutant, which also showed no significant impact on virulence (Kämper et al., 2006).

Cab1 encodes for a protein of 113 amino acids, with the first 27 residues predicted to function as a signal peptide for secretion. Analysis of Cab1's protein sequence using BLAST revealed no similarities to any other proteins in the NCBI database (Sayers et al., 2022). Additionally, the MEME and AlphaFold online tools did not identify any conserved motifs, domains, or structural

similarities in Cab1 (Bailey & Elkan, 1994; Jumper et al., 2021). To determine if the signal peptide of Cab1 is functional, we examined its activity using confocal microscopy during *U. maydis* infection in maize. For this purpose, we generated a construct in which the signal peptide of $Cab1_{1-27}$ was N-terminally fused to the fluorescent protein mCherry, controlled by the strong biotrophy-induced *Cmu1* promoter (Djamei et al., 2011). The expressing hyphae in the plant epidermis show, that the mCherry fluorescence signal accumulates around the tips and the edges of the hyphae, which is a characteristic location for secreted proteins, as previously demonstrated (Bindics et al., 2022; Darino et al., 2021; Djamei & Kahmann, 2012; Doehlemann et al., 2009; Mueller et al., 2013; Navarrete et al., 2022; Navarrete, Grujic, Stirnberg, Saado, et al., 2021; Saado et al., 2022; Stirnberg & Djamei, 2016) (Fig. 2 C).

As the Cab1 overexpression phenotype in *A. thaliana* indicates a conserved plant target in the symplast, the subcellular localization of Cab1 was studied in different plant overexpression systems. $Cab1_{28-113}$ was N-terminally tagged with mCherry under the 35S promoter (P_{35S}::mCherry-$Cab1_{28-113}$). In maize, as the natural host for *U. maydis*, confocal microscopy reveals that mCherry-$Cab1_{28-113}$ localizes specifically in the nucleus of transformed epidermal cells (Fig. 2 D). Confocal microscopy of Agrobacterium-mediated transformed *N. benthamiana* plants with mCherry-$Cab1_{28-113}$ confirmed also in this system a solely nuclear localization (Fig. S2. C). In line with this also stable transgenic *A. thaliana* lines expressing N-terminally mCherry-tagged $Cab1_{28-113}$ under the estradiol-inducible promoter ($P_{35S-XVE}$::mCherry-$Cab1_{28-113}$) show a specific nuclear mCherry signal in the confocal microscope both in root and shoots (Fig. S2. D).

Cab1 directly binds Bin2 and its paralogs from both *Arabidopsis thaliana* and *Zea mays*

Due to the dramatic phenotype upon $Cab1_{28-113}$ overexpression we assumed that its plant-sided target is likely part of a highly conserved pathway found in dicots as well as monocots. Therefore, we used the transgenic *A. thaliana* lines expressing Myc epitope-tagged $Cab1_{28-113}$ under the estradiol-inducible promoter ($P_{35S-XVE}$::Myc-$Cab1_{28-113}$) for Co-immunoprecipitation followed by mass spectrometry analysis. As a negative control, plants expressing Myc-GFP were used. The results revealed a list of plant proteins associated with Cab1 (Table S. 2). To further investigate these associations, a yeast two-hybrid (Y2H) assay was conducted, and AtBIN2/shaggy-like kinase

was identified as a direct interactor of Cab1 (Fig. 3 A). BIN2/Glycogen synthase kinase 3 belongs to a family of 10 kinases that are grouped into 4 different subgroups in *A. thaliana* (Yoo et al., 2006). Nucleotide alignment of 10 *A. thaliana* and 11 *Z. mays* GSK3 revealed three close AtBIN2, AtBil1 and AtBil2 orthologues in *Z. maize* (ZmGSK4, ZmGSK1, and ZmGSK8)as previously identified by (H. Li et al., 2022) (Fig 3. A, Table S. 2). To assess their interaction with $Cab1_{28\text{-}113}$, the three maize BIN2 orthologs were tested by Y2H $Cab1_{28\text{-}113}$ exhibited strong interactions also under high stringency conditions, with all three AtBIN2 maize orthologs (Fig. 3 B). As $Cab1_{28\text{-}113}$ seems to interact in Y2H with all AtBIN2 orthologs of maize, we focused on the closest ortholog to verify its interaction *in planta*.

ZmGSK4, like most proteins in the GSK3 family, exhibits nuclear and cytosolic localization (Fig. 3 C). In order to test if $Cab1_{28\text{-}113}$ and ZmGSK4 co-localize *in planta*, a Bimolecular fluorescence complementation (BiFC) assay was performed in *N. benthamiana*(Gookin & Assmann, 2014). A fluorescent signal was detected in the nucleus when ZmGSK4-C-Venus was co-expressed with $Cab1_{28\text{-}113}$-N-Venus. As negative control, BIN2-C-Venus was co-expressed with NLS-luciferase-N-Venus giving no fluorescent signal. Collectively, these results demonstrate, that $Cab1_{28\text{-}113}$ directly interacts with ZmGSK4 in the nucleus of plant cells (Fig. 3 D).

$Cab1_{28\text{-}113}$ overexpressing *A. thaliana* plants resemble phenotypically constitutive active Bin2D mutant plants

Shaggy-like kinases are highly conserved proteins found in all eukaryotes (Groszyk et al., 2018) and BIN2 has been identified as a negative regulator in Brassinosteroid signaling (Yoo et al., 2006). Point mutants in AtBIN2 have been identified which renders the kinase constitutively active. The respective dominant *A. thaliana* mutants (*bin2-1*) are also called Bin2D (D for dominant). *A. thaliana* lines with Bin2D mutation display a pronounced dwarfed phenotype with dark green and curled leaves resembling largely the phenotype observed upon $Cab1_{28\text{-}113}$ overexpression (fig. 4 A) (J. Li & Nam, 2002; Montes et al., 2021).

The nuclear localization of mCherry-$Cab1_{28\text{-}113}$ signal was observed in *Z. mays*, *N. benthamiana*, and *A. thaliana* through confocal microscopy (Fig. 2 D, Fig S. 3 A, B). To investigate the significance of $Cab1_{28\text{-}113}$'s nuclear localization in relation to the observed phenotype, we generated

transgenic lines where a glucocorticoid receptor (GR) is in fusion with Cab1$_{28\text{-}113}$(Aoyama & Chua, 1997). The glucocorticoid receptor system enables the posttranslational re-localization of the tagged protein from the cytoplasm to the nucleus under the external control of the glucocorticoid Dexamethasone (fig 4. D, Fig S. 4). In line with the previous observation of Cab1$_{28\text{-}113}$-BIN2 nuclear co-localization and interaction, the estradiol-induced expression and dexamethasone-induced re-localization of Cab1$_{28\text{-}113}$ to the plant nucleus was found to be directly associated with the cabbage-like phenotype *in planta* (Fig 4B and 4C).

Cab1 re-localizes BIN2 from the cytosol to the nucleus and increases AtBIN2 stability and activity

From the phenotypic resemblance between Cab1 overexpressing plants and Bin2D constitutively active mutants we hypothesized that Cab1 is leading to an activation of BIN2 in one or the other way. As BIN2 is shuttling between the host cytoplasm and the plant cell nucleus where it inhibits e.g. transcriptional activators of the BR signaling pathway we wondered if Cab1$_{28\text{-}113}$ expression *in planta* influences the subcellular distribution of ZmGSK4 in the maize cell. Using biolistic co-transformation method in maize leaves we coexpressedmCherry-Cab1$_{28\text{-}113}$ (P$_{35S}$::mCherry-Cab1$_{28\text{-}113}$) and the AtBIN2 ortholog ZmGSK4-eGFP (P$_{35S}$::ZmGSK4-eGFP)into maize epidermal cells. Confocal microscopy was performed 24h after the transformation. The results indicate, that mCherry-Cab1$_{28\text{-}113}$ caused the re-localization of ZmGSK4-GFP from the cytosol to the cell nucleus (Fig.6 A).

To test if Cab1$_{28\text{-}113}$ expression influences also localization and the stability of AtBIN2 in a dicot system we conducted a transient co-expression experiment using mCherry-Cab1$_{28\text{-}113}$ (*P$_{35S}$::Myc-mCherry-Cab1$_{28\text{-}113}$*) and GFP-AtBIN2 (*P$_{35S}$::GFP-AtBIN2*) in *N. benthamiana* leaves. As negative control, we used mCherry (*P$_{35S}$::Myc-mCherry-mCherry*). Confocal microscopy was performed 3 days post-infiltration (Fig 6. B). Our observations indicate that the presence of Cab1$_{28\text{-}113}$ leads to a relocalization of AtBIN2 from the cytosol to the nucleus as already previously shown for the AtBIN2 ortholog in maize. Western blot analysis of leaves either co-expressing AtBIN2-eGFP and mCherry-Cab1$_{28\text{-}113}$ or respective mCherry control reveals, that co-expression of mCherry-Cab1$_{28\text{-}113}$ leads to stabilization of AtBIN2-GFP *in planta* (Fig 6. B, Fig S. 5).

Cab1 increases AtBIN2-Y^{200} phosphorylation and the kinase activity of AtBIN2

Although the *A. thaliana* cabbage phenotype of $Cab1_{28\text{-}113}$ overexpression and the Cab1-dependent re-localization and BIN2-stabilization data suggest higher BIN2 activity in the plant nucleus in the presence of Cab1, we conducted a Kinase assay as well as Mass-Spectrometry (MS) to analyze directly BIN2 kinase activity and to analyze potential changes of post-translational modifications (PTMs) on BIN2 in the presence and absence of Cab1. For this purpose, we co-transformed via Agrobacterium-mediated transformation mCherry-$Cab1_{28\text{-}113}$ (P_{35S}::Myc-mCherry-$Cab1_{28\text{-}113}$) and GFP-AtBIN2 (P_{35S}::GFP-AtBIN2) into *N. benthamiana* leaves, performed from the harvested leaf material an Immunoprecipitation with GFP-antibody to isolate GFP-AtBIN2 and performed on one hand mass spectrometry as well as kinase assays using myeline basic protein (MBP) as a kinase substrate .

Interestingly, MS results revealed ten times increase in AtBIN2 Tyrosin Y^{200} phosphorylation in the presence of Cab1 compared to the control. This finding supports the notion of heightened activity of AtBIN2, providing a potential explanation for the cabbage phenotype. Conversely, AtBIN2-K35 ubiquitination by KIB1 in the cytosol leads to proteasomal degradation of AtBIN2. The MS data showed five times less ubiquitination of AtBIN2-$Lysine^{35}$ in the presence of Cab1, which may explain the increased stability of AtBIN2 in the presence of Cab1 (Fig. S. 6 A, B).

Using the same sample adjustment, we conducted a Kinase assay to further investigate the activity of AtBIN2. Immunoprecipitation (IP) was performed on GFP-AtBIN2 samples using IgG beads. Interestingly, in the presence of Cab1, AtBIN2 exhibited significantly higher kinase activity compared to the control (fig 6. C). These findings provide additional support for our previous results indicating increased stability and activity of AtBIN2 in the presence of Cab1.

Total RNA sequencing

Previous studies have demonstrated that the overactivation of AtBIN2 in Bin2D leads to the dwarf phenotype (J. Li & Nam, 2002; Montes et al., 2021). In order to further investigate the impact of Cab1 expression on the gene expression profile of *A. thaliana*, we utilized the *A. thaliana* inducible transgenic line ($P_{35S\text{-}XVE}$*::mCherry-*$Cab1_{28\text{-}113}$). Total RNA was extracted and sequenced from 12-day-old seedlings after 24 hours of 10uM Estradiol induction. The results from the total

RNA sequencing revealed that the induction of Cab1 led to the suppression of genes involved in cell wall expansion and auxin-responsive genes, while defense genes were up-regulated.

Discussion:

The ongoing conflict between plants and pathogens has resulted in complex recognition and suppression mechanisms. Plants have developed various membrane-bound and cytosolic receptors, to detect pathogen effectors and their associated activities (Zhou & Zhang, 2020). *U. maydis*, a plant pathogen, utilizes hundreds of effectors to prevent the immune responses of the host and manipulate its growth and development in its own favor. Knocking out these effectors affects pathogen fitness differently. For instance, Pep1 deletion has a high fitness cost, while cluster 2A deletion enhances *Ustilago* fitness (Scott et al., 2022). While many oomycete genomes show synteny, their effector gene families differ greatly due to rapid evolution driven by host species pressure. Also, species-specific genes encoding effectors were discovered. Several effector genes in the *U. maydis* genome are also present in *S. reilianum*, but their sequences differ and they vary in the number of copies (Schirawski et al., 2010). In our experiments, we observed that overexpression/deleteion of Cab1 and deletion of all cluster 5A genes in the *U. maydis* solopathogenic strain SG200 did not result in a significant loss of virulence, consistent with the previous study (Kämper et al., 2006). This could be attributed to redundant functions of effectors or could result from maize-line-specific roles of the effectors, or their specificity towards certain maize organs (Scott et al., 2022).

Hormones play a crucial role in plant development and immunity. Previous studies have demonstrated the importance of manipulating immune-related hormone signaling pathways, such as auxin, salicylic acid (SA), and jasmonic acid (JA) signaling, in the successful infection of *U. maydis* (Darino et al., 2021; Djamei et al., 2011; Navarrete et al., 2022). Recent studies have emphasized BIN2's involvement in plant immunity during biotic stresses. However, the results are contradictory, and the underlying mechanism is not fully known (Han et al., 2022; Y. W. Kim et al., 2022; T. Song et al., 2021). It is important to note that most of the studies on Brassinosteroids (BR) have focused on dicots, revealing their roles in growth, development, sex determination, and responses to abiotic stresses (E. J. Kim & Russinova, 2020; Nolan et al., 2020). Few studies have been conducted on monocots like maize. For instance, the maize BR biosynthetic mutation (*na1)* leads to the feminization of male flowers (Hartwig et al., 2011).

Additionally, BR-related transcription factors like ZmBEH1 (BZR1/BES1 homolog gene 1) and ZmBZR1 have been found to regulate leaf angle in maize (X. Wang et al., 2022). Interestingly, ZmSK2 (a homolog of AtBIN2) interacts with ZmIAA28, an Aux/IAA transcription factor known for its negative regulation of auxin signaling (Y. Wang et al., 2022). Overexpression of ZmSK2 leads to pronounced defects in BR signaling and arrests embryonic development at the transition stage. Conversely, knockout lines of *zmsk2* display enlarged embryos (Y. Wang et al., 2022).

BIN2 has been previously identified as a shuttle protein with nucleo-cytoplasmic activities (Vert & Chory, 2006). The regulation of BIN2 in plants involves various mechanisms, including dephosphorylation, post-translational modification, degradation, protein-protein interaction, and re-localization (E. J. Kim & Russinova, 2020; Mao & Li, 2020). Most of the reported post-translational modifications (PTMs) that are crucial for GSK3 activity have been identified in the kinase domains of ZmGSK4$^{30\text{-}314}$ and BIN2$^{34\text{-}274}$ (Dornelas et al., 1998; Mao et al., 2021). The N-terminal region of GSK family members exhibits variations in amino acid sequences and influencing their sub-cellular localization, while interactions with substrates primarily occur through the amino acid sequences in the C-terminal regions (Rozhon et al., 2022; Yoo et al., 2006; Youn & Kim, 2015). In our study, we observed that Cab1 interacts with the C-terminal of ZmGSK4$^{336\text{-}412}$ and facilitates its re-localization from the cytosol to the nucleus. This re-localization of ZmGSK4 in the presence of Cab1 also prevents its proteasomal degradation, which typically occurs through its interaction with the F-box E3 ubiquitin ligase KIB1 in the cytosol(Zhu et al., 2017). Consequently, the autophosphorylation of Tyr200 is also affected by this interaction (J. Li et al., 2020). These results indicate that the nuclear co-localization of cab1 and BIN2 is crucial for manipulating the downstream targets.

To date, there have been no reports indicating that plant pathogens specifically target BIN2 and Cab1 is the first reported effector protein that targets BIN2. The intriguing question is why *Ustilago* targets a crucial negative regulator of the Brassinosteroid (BR) pathway. while It was shown that BR and Methyl jasmonate (JA) injections in maize cause localized male sterility with early growth arrest zones within tassels and leading to *Ustilago's* failure to form galls (Ferris & Walbot, 2020; Walbot & Skibbe, 2010). In the context of Ustilago-induced tumor development in maize leaves, the expression of Cab1 was found to be higher in hypertrophic mesophyll tumors

(HTT) compared to hyperplasia bundle sheet cells (HPT) (Matei et al., 2018). The highest expression of Cab1 was observed in the SG200 *Δsee1* mutant which is unable to produce galls in HPT cells (Matei et al., 2018). These findings suggest that Cab1 may act against the effectors involved in hyperplasia and aligns with our microscopic observations. They show that due to the inhibition of cell wall expansion, we observed smaller cells and stomata in Arabidopsis-induced plants compared to uninduced plants.

The Cab1 strong dwarf phenotype is caused by impairment in cell wall expansion and development. The impact of BR signaling on cell wall expansion via SOB3 was described before. SOB3 inhibits the expression and reduces the transcript accumulation of all six members of the SAUR19 subfamily, which are associated with the repression of cell expansion and hypocotyl elongation (Favero et al., 2017). The overexpression of SAUR genes promotes Expansins (EXPs) activity and cell elongation in *A. thaliana* (Pérez-Henríquez & Yang, 2023; van Mourik et al., 2017). EXPs activity leads to increased cell wall plasticity and extensibility, enabling cell growth and development (Mu et al., 2021; Sampedro & Cosgrove, 2005). So, we became interested to look for the interplay of BR with other hormonal pathways in response to the Cab1 expression.

It has been widely studied that both auxin and BR promote cell expansion and hypocotyl elongation. however, the interconnection between auxin and BR involves complex signaling pathways. SAURs genes have been studied due to their role as positive regulators of cell expansion by modulating auxin polar transport, which is essential for cell elongation and growth (M. Li et al., 2018). We had a closer look at the role of downregulated SAURs in the presence of Cab1. SAUR19 and 20 are known for their involvement in auxin transport modulation (Spartz et al., 2012). While the SAUR26 subfamily is associated with thermo-responsive architecture variations (Z. Wang et al., 2019). The BZR1/ARF6/PIF4 (BAP) complex serves as a key interaction point between BR and auxin, activating the SAUR19 subfamily and EXPs (Bouré et al., 2019). Additionally, BZR1 directly interacts with the promoter regions of IAA19 and ARF7, regulating BR-induced differential growth (X. Y. Zhou et al., 2013). Interestingly, in response to the light, plants employ the activation mechanism of BIN2 to suppress BZR1. In this process, HY5 interacts physically with BIN2, leading to increased kinase activity. This interaction enhances the phosphorylation and degradation of BZR1, thereby inhibiting brassinosteroid (BR)-mediated

hypocotyl elongation in light conditions (J. Li et al., 2020). These findings present the coordinated regulation of growth and development by the BR and auxin signaling pathways.

Activation of SAURs genes initiates the process of cell wall expansion. EXPs and xyloglucan endotransglucosylases/hydrolases (XTHs) are involved in cell wall loosening and expansion (Ishida & Yokoyama, 2022; Narváez-Barragán et al., 2020). EXPA1 is crucial for hypocotyl elongation (Zhuang et al., 2022) and also affects the expression of various EXPs and XTHs (Samalova et al., 2023). It was shown that EXPA5 and XTH19 are involved in brassinosteroid (BR)-induced hypocotyl elongation (Zhuang et al., 2022) while EXPA19 is associated with the kernel size in rice (Zhao et al., 2023). In summary, the expression of Cab1 leads to the downregulation of SAURs and EXPs and prevents the elongation of the hypocotyl that is induced by auxin polar transport (Sampedro & Cosgrove, 2005; van Mourik et al., 2017; Wieczorek & Grundler, 2006).

Cab1, a unique fungus protein with a novel function, does not possess structural similarity to other proteins according to Alpha fold and in-silico analyses. Extensive in-silico analysis of Cab1's nucleotide and amino acid sequences did not identify any conserved domain, structure, or motif. Our data suggest that Cab1 plays a role in limiting the excessive growth of galls induced by other *Ustilago* growth promoting effectors. Despite the importance of BIN2 in the plant's agricultural traits such as leaf angle and gain size (Hu et al., 2018; Zhao et al., 2023). Our findings regarding Cab1's mechanism of action on BIN2 provide new insights into the field of plant pathology and open up exciting possibilities for further research.

References:

Ackerman-Lavert, M., Fridman, Y., Matosevich, R., Khandal, H., Friedlander-Shani, L., Vragović, K., Ben El, R., Horev, G., Tarkowská, D., Efroni, I., & Savaldi-Goldstein, S. (2021). Auxin requirements for a meristematic state in roots depend on a dual brassinosteroid function. *Current Biology : CB*, *31*(20), 4462–4472. https://doi.org/10.1016/j.cub.2021.07.075

Ai, H., Bellstaedt, J., Bartusch, K. S., Eschen-Lippold, L., Babben, S., Balcke, G. U., Tissier, A., Hause, B., Andersen, T. G., Delker, C., & Quint, M. (2023). Auxin-dependent regulation of cell division rates governs root thermomorphogenesis. *The EMBO Journal*, *42*(11), e111926. https://doi.org/10.15252/EMBJ.2022111926

Aoyama, T., & Chua, N. H. (1997). A glucocorticoid-mediated transcriptional induction system in transgenic plants. *The Plant Journal*, *11*(3), 605–612. https://doi.org/10.1046/J.1365-313X.1997.11030605.X

Ardito, F., Giuliani, M., Perrone, D., Troiano, G., & Muzio, L. Lo. (2017). The crucial role of protein phosphorylation in cell signalingand its use as targeted therapy (Review). In *International Journal of Molecular Medicine* (Vol. 40, Issue 2, pp. 271–280). Spandidos Publications. https://doi.org/10.3892/ijmm.2017.3036

Ausubel, F. M., Brent, R., Kingston, R. E., Moore, D. D., Seidman, J. G., & Smith, J. A. (2003). *Current Protocols in Molecular Biology Kevin Struhl (eds.) Current Protocols in Molecular Biology*.

Bailey, T. L., & Elkan, C. (1994). *FITTING A MIXTURE MODEL BY EXPECTATION MAXIMIZATION TO DISCOVER MOTIFS IN BIOPOLYMERS*.

Banuett, F., & Herskowitz, I. (1994). Morphological Transitions in the Life Cycle of Ustilago maydis and Their Genetic Control by the a and Loci. *Exprimental Mycology*, *18*, 247–266.

Bernardo-García, S., de Lucas, M., Martínez, C., Espinosa-Ruiz, A., Davière, J. M., & Prat, S. (2014). BR-dependent phosphorylation modulates PIF4 transcriptional activity and shapes diurnal hypocotyl growth. *Genes & Development*, *28*(15), 1681. https://doi.org/10.1101/GAD.243675.114

Beurel, E., Grieco, S. F., & Jope, R. S. (2015). Glycogen synthase kinase-3 (GSK3): Regulation, actions, and diseases. In *Pharmacology and Therapeutics* (Vol. 148, pp. 114–131). Elsevier Inc. https://doi.org/10.1016/j.pharmthera.2014.11.016

Bindics, J., Khan, M., Uhse, S., Kogelmann, B., Baggely, L., Reumann, D., Ingole, K. D., Stirnberg, A., Rybecky, A., Darino, M., Navarrete, F., Doehlemann, G., & Djamei, A. (2022). Many ways to TOPLESS – manipulation of plant auxin signalling by a cluster of fungal effectors. *New Phytologist*, *236*(4), 1455–1470. https://doi.org/10.1111/nph.18315

Bohlmann, H., & Sobczak, M. (2014). The plant cell wall in the feeding sites of cyst nematodes. In *Frontiers in Plant Science* (Vol. 5, Issue MAR). Frontiers Research Foundation. https://doi.org/10.3389/fpls.2014.00089

Bouré, N., S.Kumar, V., & Arnaud, N. (2019). The BAP Module: A Multisignal Integrator Orchestrating Growth. *Trends in Plant Science*, *24*(7).

Brachmann, A., Weinzierl, G., Kämper, J., & Kahmann, R. (2001). Identification of genes in the bW/bE regulatory cascade in Ustilago maydis. *Molecular Microbiology*, *42*(4), 1047–1063. https://doi.org/10.1046/j.1365-2958.2001.02699.x

Brefort, T., Doehlemann, G., Mendoza-Mendoza, A., Reissmann, S., Djamei, A., & Kallmann, R. (2009). Ustilago maydis as a Pathogen. *Http://Dx.Doi.Org/10.1146/Annurev-Phyto-080508-081923*, *47*, 423–445. https://doi.org/10.1146/ANNUREV-PHYTO-080508-081923

Bruce, S. A., Saville, B. J., & Emery, R. J. N. (2011). Ustilago maydis Produces Cytokinins and Abscisic Acid for Potential Regulation of Tumor Formation in Maize. *Journal of Plant Growth Regulation*, *30*(1), 51–63. https://doi.org/10.1007/s00344-010-9166-8

Callis, J. (2014). The Ubiquitination Machinery of the Ubiquitin System. *The Arabidopsis Book*, *12*, e0174. https://doi.org/10.1199/tab.0174

Caño-Delgado, A., Yin, Y., Yu, C., Vefeados, D., Mora-García, S., Cheng, J. C., Nam, K. H., Li, J., & Chory, J. (2004). BRL1 and BRL3 are novel brassinosteroid receptors that function in vascular differentiation in Arabidopsis. *Development (Cambridge, England)*, *131*(21), 5341–5351. https://doi.org/10.1242/DEV.01403

Čarná, M., Repka, V., Skůpa, P., & Šturdík, E. (2014). Auxins in defense strategies. *Biologia (Poland)*, *69*(10), 1255–1263. https://doi.org/10.2478/S11756-014-0431-3/XML

Carpita, N., Tiemey2, M., & Campbell, M. (2001). Molecular biology of the plant cell wall: searching for the genes that define structure, architecture and dynamics. In *Plant Molecular Biology* (Vol. 47).

Chandler, J. W. (2016). Auxin response factors. In *Plant Cell and Environment* (Vol. 39, Issue 5, pp. 1014–1028). Blackwell Publishing Ltd. https://doi.org/10.1111/pce.12662

Chaudhary, A., Hsiao, Y.-C., Yeh, F.-L. J., Wu, H.-M., Cheung, A. Y., Xu, S.-L., & Wang, Z.-Y. (2023). Brassinosteroid recruits FERONIA to safeguard cell expansion in Arabidopsis. *BioRxiv*, 2023.10.01.560400. https://doi.org/10.1101/2023.10.01.560400

Cheng, Y. T., Zhang, L., & He, S. Y. (2019). Plant-Microbe Interactions Facing Environmental Challenge. In *Cell Host and Microbe* (Vol. 26, Issue 2, pp. 183–192). Cell Press. https://doi.org/10.1016/j.chom.2019.07.009

Cho, K. F., Branon, T. C., Udeshi, N. D., Myers, S. A., Carr, S. A., & Ting, A. Y. (2020). Proximity labeling in mammalian cells with TurboID and split-TurboID. *Nature Protocols*, *15*(12), 3971–3999. https://doi.org/10.1038/s41596-020-0399-0

Christoph, W. B., & Gero, S. (2004). Ustilago maydis , model system for analysis of the molecular basis of fungal pathogenicity. *Molecular Plant Pathology*. https://doi.org/10.1111/J.1364-3703.2004.00210.X

Chung, Y., Maharjan, P. M., Lee, O., Fujioka, S., Jang, S., Kim, B., Takatsuto, S., Tsujimoto, M., Kim, H., Cho, S., Park, T., Cho, H., Hwang, I., & Choe, S. (2011). Auxin stimulates DWARF4 expression and brassinosteroid biosynthesis in Arabidopsis. *Plant Journal*, *66*(4), 564–578. https://doi.org/10.1111/j.1365-313X.2011.04513.x

Clouse, S. D., Langford, M., & McMorris, T. C. (1996). A brassinosteroid-insensitive mutant in Arabidopsis thaliana exhibits multiple defects in growth and development. *Plant Physiology*, *111*(3), 671. https://doi.org/10.1104/PP.111.3.671

Darino, M., Chia, K. S., Marques, J., Aleksza, D., Soto-Jiménez, L. M., Saado, I., Uhse, S., Borg, M., Betz, R., Bindics, J., Zienkiewicz, K., Feussner, I., Petit-Houdenot, Y., & Djamei, A. (2021). Ustilago maydis effector Jsi1 interacts with Topless corepressor, hijacking plant jasmonate/ethylene signaling. *New Phytologist*, *229*(6), 3393–3407. https://doi.org/10.1111/NPH.17116

Depuydt, S., & Hardtke, C. S. (2011). Hormone signalling crosstalk in plant growth regulation. In *Current Biology* (Vol. 21, Issue 9). https://doi.org/10.1016/j.cub.2011.03.013

Devi, L. L., Pandey, A., Gupta, S., & Singh, A. P. (2022). The interplay of auxin and brassinosteroid signaling tunes root growth under low and different nitrogen forms. *Plant Physiology*, *189*(3), 1757–1773. https://doi.org/10.1093/PLPHYS/KIAC157

Díaz, A., Taberner, A., & Vilaplana, L. (2020). The emergence of a new weed in maize plantations: characterization and genetic structure using microsatellite markers. *Genetic Resources and Crop Evolution*, *67*(1), 225–239. https://doi.org/10.1007/s10722-019-00828-z

Díaz-Troya, S., Pérez-Pérez, M. E., Florencio, F. J., & Crespo, J. L. (2008). The role of TOR in autophagy regulation from yeast to plants and mammals. In *Autophagy* (Vol. 4, Issue 7, pp. 851–865). Taylor and Francis Inc. https://doi.org/10.4161/auto.6555

Djamei, A., & Kahmann, R. (2012). Ustilago maydis: Dissecting the Molecular Interface between Pathogen and Plant. *PLoS Pathogens*, *8*(11). https://doi.org/10.1371/journal.ppat.1002955

Djamei, A., Schipper, K., Rabe, F., Ghosh, A., Vincon, V., Kahnt, J., Osorio, S., Tohge, T., Fernie, A. R., Feussner, I., Feussner, K., Meinicke, P., Stierhof, Y. D., Schwarz, H., MacEk, B., Mann, M., & Kahmann, R. (2011). Metabolic priming by a secreted fungal effector. *Nature*, *478*(7369), 395–398. https://doi.org/10.1038/NATURE10454

Doehlemann, G., Reissmann, S., Aßmann, D., Fleckenstein, M., & Kahmann, R. (2011). Two linked genes encoding a secreted effector and a membrane protein are essential for Ustilago maydis-induced tumour formation. *Molecular Microbiology*, *81*(3), 751–766. https://doi.org/10.1111/j.1365-2958.2011.07728.x

Doehlemann, G., Van Der Linde, K., Aßmann, D., Schwammbach, D., Hof, A., Mohanty, A., Jackson, D., & Kahmann, R. (2009). Pep1, a secreted effector protein of Ustilago maydis, is required for successful invasion of plant cells. *PLoS Pathogens*, *5*(2). https://doi.org/10.1371/journal.ppat.1000290

Dornelas, M. C., Lejeune, B., Dron, M., & Kreis, M. (1998). The Arabidopsis SHAGGY-related protein kinase (ASK) gene family: structure, organization and evolution. *Gene*, *212*(2), 249–257. https://doi.org/10.1016/S0378-1119(98)00147-4

Du, M., Spalding, E. P., & Gray, W. M. (2020). *Rapid Auxin-Mediated Cell Expansion*. https://doi.org/10.1146/annurev-arplant-073019

Duda, P., Akula, S. M., Abrams, S. L., Steelman, L. S., Gizak, A., Rakus, D., & McCubrey, J. A. (2020). GSK-3 and miRs: Master regulators of therapeutic sensitivity of cancer cells. In *Biochimica et Biophysica*

Acta - Molecular Cell Research (Vol. 1867, Issue 10). Elsevier B.V. https://doi.org/10.1016/j.bbamcr.2020.118770

Favero, D. S., Le, K. N., & Neff, M. M. (2017). Brassinosteroid signaling converges with SUPPRESSOR OF PHYTOCHROME B4-#3 to influence the expression of SMALL AUXIN UP RNA genes and hypocotyl growth. *Plant Journal*, *89*(6), 1133–1145. https://doi.org/10.1111/tpj.13451

Fei, W., & Liu, Y. (2023). Biotrophic Fungal Pathogens: a Critical Overview. In *Applied Biochemistry and Biotechnology* (Vol. 195, Issue 1, pp. 1–16). Springer. https://doi.org/10.1007/s12010-022-04087-0

Ferris, A. C., & Walbot, V. (2020). *Understanding Ustilago maydis Infection of Multiple Maize Organs*. https://doi.org/10.3390/jof7010008

Friedrichsen, D. M., Joazeiro, C. A. P., Li, J., Hunter, T., & Chory, J. (2000). Brassinosteroid-insensitive-1 is a ubiquitously expressed leucine-rich repeat receptor serine/threonine kinase. *Plant Physiology*, *123*(4), 1247–1255. https://doi.org/10.1104/PP.123.4.1247

Fu, J., & Wang, S. (2011). Insights into auxin signaling in plant-pathogen interactions. *Frontiers in Plant Science*, *2*(NOV). https://doi.org/10.3389/fpls.2011.00074

Gallavotti, A. (2013). The role of auxin in shaping shoot architecture. *Journal of Experimental Botany*, *64*(9), 2593–2608. https://doi.org/10.1093/JXB/ERT141

Gampala, S. S., Kim, T. W., He, J. X., Tang, W., Deng, Z., Bai, M. Y., Guan, S., Lalonde, S., Sun, Y., Gendron, J. M., Chen, H., Shibagaki, N., Ferl, R. J., Ehrhardt, D., Chong, K., Burlingame, A. L., & Wang, Z. Y. (2007). An essential role for 14-3-3 proteins in brassinosteroid signal transduction in Arabidopsis. *Developmental Cell*, *13*(2), 177–189. https://doi.org/10.1016/J.DEVCEL.2007.06.009

Gao, L., Kelliher, T., Nguyen, L., & Walbot, V. (2013). Ustilago maydis reprograms cell proliferation in maize anthers. *Plant Journal*, *75*(6), 903–914. https://doi.org/10.1111/tpj.12270

Gillissen, B., Bergemann, J., Sandmann, C., Schroeer, B., B61ker, M., & Kahmann, R. (1992). A Two-Component Regulatory System for Self/Non-Self Recognition in Ustilago maydis. In *Cell* (Vol. 66).

Gookin, T. E., & Assmann, S. M. (2014). Significant reduction of BiFC non-specific assembly facilitates in planta assessment of heterotrimeric G-protein interactors. *Plant Journal*, *80*(3), 553–567. https://doi.org/10.1111/tpj.12639

Groszyk, J., Yanushevska, Y., Zielezinski, A., Nadolska-Orczyk, A., Karlowski, W. M., & Orczyk, W. (2018). Annotation and profiling of barley GLYCOGEN SYNTHASE3/Shaggy-like genes indicated shift in organ-preferential expression. *PLoS ONE*, *13*(6). https://doi.org/10.1371/journal.pone.0199364

Guo, H., Li, L., Aluru, M., Aluru, S., & Yin, Y. (2013). Mechanisms and networks for brassinosteroid regulated gene expression. *Current Opinion in Plant Biology*, *16*(5), 545–553. https://doi.org/10.1016/J.PBI.2013.08.002

Han, Q., Tan, W., Zhao, Y., Yang, F., Yao, X., Lin, H., & Zhang, D. (2022). Salicylic acid-activated BIN2 phosphorylation of TGA3 promotes Arabidopsis PR gene expression and disease resistance . *The EMBO Journal*, *41*(19). https://doi.org/10.15252/embj.2022110682

Hartwig, T., Chuck, G. S., Fujioka, S., Klempien, A., Weizbauer, R., Potluri, D. P. V., Choe, S., Johal, G. S., & Schulz, B. (2011). Brassinosteroid control of sex determination in maize. *Proceedings of the National Academy of Sciences of the United States of America*, *108*(49), 19814–19819. https://doi.org/10.1073/pnas.1108359108

He, J. X., Gendron, J. M., Yang, Y., Li, J., & Wang, Z. Y. (2002). The GSK3-like kinase BIN2 phosphorylates and destabilizes BZR1, a positive regulator of the brassinosteroid signaling pathway in Arabidopsis. *Proceedings of the National Academy of Sciences of the United States of America*, *99*(15), 10185–10190. https://doi.org/10.1073/PNAS.152342599

He, Z., Wang, Z. Y., Li, J., Zhu, Q., Lamb, C., Ronald, P., & Chory, J. (2000). Perception of brassinosteroids by the extracellular domain of the receptor kinase BRI1. *Science (New York, N.Y.)*, *288*(5475), 2360–2363. https://doi.org/10.1126/SCIENCE.288.5475.2360

Hou, L., Li, Z., Shaheen, A., Zhang, K., Wang, J., Gao, X., & Wu, Q. (2022). Zea mays GSK2 gene is involved in brassinosteroid signaling. *Plant Growth Regulation*. https://doi.org/10.1007/s10725-022-00806-z

Hu, Z., Lu, S. J., Wang, M. J., He, H., Sun, L., Wang, H., Liu, X. H., Jiang, L., Sun, J. L., Xin, X., Kong, W., Chu, C., Xue, H. W., Yang, J., Luo, X., & Liu, J. X. (2018). A Novel QTL qTGW3 Encodes the GSK3/SHAGGY-Like Kinase OsGSK5/OsSK41 that Interacts with OsARF4 to Negatively Regulate Grain Size and Weight in Rice. *Molecular Plant*, *11*(5), 736–749. https://doi.org/10.1016/J.MOLP.2018.03.005

Huang, L., Ökmen, B., Christina Stolze, S., Kastl, M., Khan, M., Hilbig, D., Nakagami, H., Djamei, A., & Doehlemann, G. (2023). The fungal pathogen Ustilago maydis targets the maize corepressor TPL2 to modulate host transcription for tumorigenesis. *Bioarchive*. https://doi.org/10.1101/2023.06.12.544564

Huang, M., Bulut, A., Shrestha, B., Matera, C., Grundler, F. M. W., & Schleker, A. S. S. (2021). Bacillus firmus I-1582 promotes plant growth and impairs infection and development of the cyst nematode Heterodera schachtii over two generations. *Scientific Reports*, *11*(1). https://doi.org/10.1038/s41598-021-93567-0

Hughes, P. W. (2020). OsGSK2 Integrates Jasmonic Acid and Brassinosteroid Signaling in Rice. *The Plant Cell*, *32*(9), 2669–2670. https://doi.org/10.1105/TPC.20.00531

Hur, E. M., & Zhou, F. Q. (2010). GSK3 signalling in neural development. In *Nature Reviews Neuroscience* (Vol. 11, Issue 8, pp. 539–551). https://doi.org/10.1038/nrn2870

Ishida, K., & Yokoyama, R. (2022). Reconsidering the function of the xyloglucan endotransglucosylase/hydrolase family. *Journal of Plant Research*, *135*(2), 145–156. https://doi.org/10.1007/s10265-021-01361-w

J. Cosgrove, D. (2000). Loosening of plant cell walls by expansins. *Nature*.

Jing, H., & Strader, L. C. (2019). Interplay of Auxin and Cytokinin in Lateral Root Development. *International Journal of Molecular Sciences*, *20*(3). https://doi.org/10.3390/IJMS20030486

Johnson, K., & Lenhard, M. (2011). Genetic control of plant organ growth. In *New Phytologist* (Vol. 191, Issue 2, pp. 319–333). https://doi.org/10.1111/j.1469-8137.2011.03737.x

Jones, J. D. G., & Dangl, J. L. (2006). *The Plant immune system*. https://doi.org/10.1038

Juárez-Montiel, M., Tesillo-Moreno, P., Cruz-Angeles, A., Soberanes-Gutiérrez, V., Chávez-Camarillo, G., Ibarra, J. A., Hernández-Rodríguez, C., & Villa-Tanaca, L. (2018). Heterologous expression and characterization of the aspartic endoprotease Pep4um from Ustilago maydis, a homolog of the human Chatepsin D, an important breast cancer therapeutic target. *Molecular Biology Reports*, *45*(5), 1155–1163. https://doi.org/10.1007/s11033-018-4267-8

Jumper, J., Evans, R., Pritzel, A., Green, T., Figurnov, M., Ronneberger, O., Tunyasuvunakool, K., Bates, R., Žídek, A., Potapenko, A., Bridgland, A., Meyer, C., Kohl, S. A. A., Ballard, A. J., Cowie, A., Romera-Paredes, B., Nikolov, S., Jain, R., Adler, J., … Hassabis, D. (2021). Highly accurate protein structure prediction with AlphaFold. *Nature*, *596*(7873), 583–589. https://doi.org/10.1038/s41586-021-03819-2

Kaidanovich-Beilin, O., & Woodgett, J. R. (2011). GSK-3: Functional Insights from Cell Biology and Animal Models. *Frontiers in Molecular Neuroscience*, *4*. https://doi.org/10.3389/fnmol.2011.00040

Kämper, J. (2004). A PCR-based system for highly efficient generation of gene replacement mutants in Ustilago maydis. *Molecular Genetics and Genomics*, *271*(1), 103–110. https://doi.org/10.1007/s00438-003-0962-8

Kämper, J., Kahmann, R., Bölker, M., Ma, L. J., Brefort, T., Saville, B. J., Banuett, F., Kronstad, J. W., Gold, S. E., Müller, O., Perlin, M. H., Wösten, H. A. B., De Vries, R., Ruiz-Herrera, J., Reynaga-Peña, C. G., Snetselaar, K., McCann, M., Pérez-Martín, J., Feldbrügge, M., … Birren, B. W. (2006). Insights from the genome of the biotrophic fungal plant pathogen Ustilago maydis. *Nature*, *444*(7115), 97–101. https://doi.org/10.1038/NATURE05248

Katzen, F. (2007). Gateway(®) recombinational cloning: a biological operating system. *Expert Opinion on Drug Discovery*, *2*(4), 571–589. https://doi.org/10.1517/17460441.2.4.571

Kaur, S., Samota, M. K., Choudhary, M., Choudhary, M., Pandey, A. K., Sharma, A., & Thakur, J. (2022). How do plants defend themselves against pathogens-Biochemical mechanisms and genetic interventions. In *Physiology and Molecular Biology of Plants* (Vol. 28, Issue 2, pp. 485–504). Springer. https://doi.org/10.1007/s12298-022-01146-y

Khan, M., Uhse, S., Bindics, J., Kogelmann, B., Nagarajan, N., Ingole, K. D., & Djamei, A. (2023). Tip of the iceberg? Three novel TOPLESS interacting effectors of the gall-inducing fungus Ustilago maydis. *Bioarchive*. https://doi.org/10.1101/2023.06.12.544640

Kim, E. J., Lee, S. H., Park, C. H., Kim, S. H., Hsu, C. C., Xu, S., Wang, Z. Y., Kim, S. K., & Kim, T. W. (2019). Plant U-Box40 Mediates Degradation of the Brassinosteroid-Responsive Transcription Factor BZR1 in Arabidopsis Roots. *The Plant Cell*, *31*(4), 791–808. https://doi.org/10.1105/TPC.18.00941

Kim, E. J., & Russinova, E. (2020). Brassinosteroid signalling. In *Current Biology* (Vol. 30, Issue 7, pp. R294–R298). Cell Press. https://doi.org/10.1016/j.cub.2020.02.011

Kim, H., Park, P. J., Hwang, H. J., Lee, S. Y., Oh, M. H., & Kim, S. G. (2006). Brassinosteroid signals control expression of the AXR3/IAA17 gene in the cross-talk point with auxin in root development. *Bioscience, Biotechnology and Biochemistry*, *70*(4), 768–773. https://doi.org/10.1271/bbb.70.768

Kim, T. W., Guan, S., Burlingame, A. L., & Wang, Z. Y. (2011). The CDG1 Kinase Mediates Brassinosteroid Signal Transduction from BRI1 Receptor Kinase to BSU1 Phosphatase and GSK3-like Kinase BIN2. *Molecular Cell*, *43*(4), 561–571. https://doi.org/10.1016/j.molcel.2011.05.037

Kim, T.-W., Guan, S., Sun, Y., Deng, Z., Tang, W., Shang, J.-X., Sun, Y., Burlingame, A. L., & Wang, Z.-Y. (2009). Brassinosteroid signal transduction from cell-surface receptor kinases to nuclear transcription factors. *Nature Cell Biology*. https://doi.org/10.1038/ncb1970

Kim, T.-W., Park, C. H., Hsu, C.-C., Kim, Y.-W., Ko, Y.-W., Zhang, Z., Zhu, J.-Y., Hsiao, Y.-C., Branon, T., Kaasik, K., Saldivar, E., Li, K., Pasha, A., Provart, N. J., Burlingame, A. L., Xu, S.-L., Ting, A. Y., & Wang, Z.-Y. (2023). Mapping the signaling network of BIN2 kinase using TurboID-mediated biotin labeling and phosphoproteomics. *The Plant Cell*, *35*(3), 975–993. https://doi.org/10.1093/PLCELL/KOAD013

Kim, Y. W., Youn, J. H., Roh, J., Kim, J. M., Kim, S. K., & Kim, T. W. (2022). Brassinosteroids enhance salicylic acid-mediated immune responses by inhibiting BIN2 phosphorylation of clade I TGA transcription factors in Arabidopsis. *Molecular Plant*, *15*(6), 991–1007. https://doi.org/10.1016/j.molp.2022.05.002

Kinoshita, T., Caño-Delgado, A., Seto, H., Hiranuma, S., Fujioka, S., Yoshida, S., & Chory, J. (2005). Binding of brassinosteroids to the extracellular domain of plant receptor kinase BRI1. *Nature*, *433*(7022), 167–171. https://doi.org/10.1038/NATURE03227

Krogh, A., Larsson, B., Von Heijne, G., & Sonnhammer, E. L. L. (2001). Predicting transmembrane protein topology with a hidden Markov model: Application to complete genomes. *Journal of Molecular Biology*, *305*(3), 567–580. https://doi.org/10.1006/jmbi.2000.4315

Kuhn, A., Harborough, S. R., McLaughlin, H. M., Natarajan, B., Verstraeten, I., Friml, J., Kepinski, S., & Østergaard, L. (2020). Direct ETTIN-auxin interaction controls chromatin states in gynoecium development. *ELife*, *9*. https://doi.org/10.7554/eLife.51787

Lampropoulos, A., Sutikovic, Z., Wenzl, C., Maegele, I., Lohmann, J. U., & Forner, J. (2013). GreenGate - A Novel, Versatile, and Efficient Cloning System for Plant Transgenesis. *PLOS ONE*, *8*(12), e83043. https://doi.org/10.1371/JOURNAL.PONE.0083043

Lanver, D., Berndt, P., Tollot, M., Naik, V., Vranes, M., Warmann, T., Münch, K., Rössel, N., & Kahmann, R. (2014). Plant Surface Cues Prime Ustilago maydis for Biotrophic Development. *PLoS Pathogens*, *10*(7). https://doi.org/10.1371/journal.ppat.1004272

Lanver, D., Müller, A. N., Happel, P., Schweizer, G., Haas, F. B., Franitza, M., Pellegrin, C., Reissmann, S., Altmüller, J., Rensing, S. A., & Kahmann, R. (2018). The biotrophic development of ustilago maydis studied by RNA-seq analysis. *Plant Cell*, *30*(2), 300–323. https://doi.org/10.1105/tpc.17.00764

Lanver, D., Tollot, M., Schweizer, G., Lo Presti, L., Reissmann, S., Ma, L. S., Schuster, M., Tanaka, S., Liang, L., Ludwig, N., & Kahmann, R. (2017). Ustilago maydis effectors and their impact on virulence. In *Nature Reviews Microbiology* (Vol. 15, Issue 7, pp. 409–421). Nature Publishing Group. https://doi.org/10.1038/nrmicro.2017.33

Li, G., Wang, Q., Lu, L., Wang, S., Chen, X., Khan, M. H. U., Zhang, Y., & Yang, S. (2022). Identification of the soybean small auxin upregulated RNA (SAUR) gene family and specific haplotype for drought tolerance. *Biologia*, *77*(4), 1197–1217. https://doi.org/10.1007/s11756-022-01010-0

Li, H., Luo, L., Wang, Y., Zhang, J., & Huang, Y. (2022). Genome-Wide Characterization and Phylogenetic Analysis of GSK Genes in Maize and Elucidation of Their General Role in Interaction with BZR1. *International Journal of Molecular Sciences*, *23*(15). https://doi.org/10.3390/ijms23158056

Li, J., & Chory, J. (1997). A putative leucine-rich repeat receptor kinase involved in brassinosteroid signal transduction. *Cell*, *90*(5), 929–938. https://doi.org/10.1016/S0092-8674(00)80357-8

Li, J., & Nam, K. H. (2002). Regulation of Brassinosteroid Signaling by a GSK3/SHAGGY-Like Kinase. *Science*, *295*(5558), 1299–1301. https://doi.org/10.1126/SCIENCE.1065769

Li, J., Nam, K. H., Vafeados, D., & Chory, J. (2001). BIN2, a new brassinosteroid-insensitive locus in Arabidopsis. *Plant Physiology*, *127*(1), 14–22. https://doi.org/10.1104/PP.127.1.14

Li, J., Terzaghi, W., Gong, Y., Li, C., Ling, J. J., Fan, Y., Qin, N., Gong, X., Zhu, D., & Deng, X. W. (2020). Modulation of BIN2 kinase activity by HY5 controls hypocotyl elongation in the light. *Nature Communications*, *11*(1). https://doi.org/10.1038/s41467-020-15394-7

Li, M., Sun, P., Kang, T., Xing, H., Yang, D., Zhang, J., & Paré, P. W. (2018). Mapping podophyllotoxin biosynthesis and growth-related transcripts with high elevation in Sinopodophyllum hexandrum. *Industrial Crops and Products*, *124*, 510–518. https://doi.org/10.1016/j.indcrop.2018.08.007

Li, T., Lei, W., He, R., Tang, X., Han, J., Zou, L., Yin, Y., Lin, H., & Zhang, D. (2020). Brassinosteroids regulate root meristem development by mediating BIN2-UPB1 module in Arabidopsis. *PLOS Genetics*, *16*(7), e1008883. https://doi.org/10.1371/JOURNAL.PGEN.1008883

Li, Z., & He, Y. (2020). Roles of Brassinosteroids in Plant Reproduction. *International Journal of Molecular Sciences*, *21*(3). https://doi.org/10.3390/IJMS21030872

Ma, L. S., Wang, L., Trippel, C., Mendoza-Mendoza, A., Ullmann, S., Moretti, M., Carsten, A., Kahnt, J., Reissmann, S., Zechmann, B., Bange, G., & Kahmann, R. (2018). The Ustilago maydis repetitive effector Rsp3 blocks the antifungal activity of mannose-binding maize proteins. *Nature Communications*, *9*(1). https://doi.org/10.1038/s41467-018-04149-0

Machyna, M., Kehr, S., Straube, K., Kappei, D., Buchholz, F., Butter, F., Ule, J., Hertel, J., Stadler, P. F., & Neugebauer, K. M. (2014). The coilin interactome identifies hundreds of small noncoding RNAs that traffic through cajal bodies. *Molecular Cell*, *56*(3), 389–399. https://doi.org/10.1016/j.molcel.2014.10.004

Machyna, M., Neugebauer, K. M., & Staněk, D. (2015). Coilin: The first 25 years. *RNA Biology*, *12*(6), 590–596. https://doi.org/10.1080/15476286.2015.1034923

Majda, M., & Robert, S. (2018). The Role of Auxin in Cell Wall Expansion. *International Journal of Molecular Sciences*, *19*(4). https://doi.org/10.3390/IJMS19040951

Mao, J., & Li, J. (2020). Regulation of three key kinases of brassinosteroid signaling pathway. In *International Journal of Molecular Sciences* (Vol. 21, Issue 12, pp. 1–32). MDPI AG. https://doi.org/10.3390/ijms21124340

Mao, J., Li, W., Liu, J., & Li, J. (2021). Versatile Physiological Functions of Plant GSK3-Like Kinases. *Genes*, *12*(5), 697. https://doi.org/10.3390/genes12050697

Mapuranga, J., Zhang, N., Zhang, L., Chang, J., & Yang, W. (2022). Infection Strategies and Pathogenicity of Biotrophic Plant Fungal Pathogens. In *Frontiers in Microbiology* (Vol. 13). Frontiers Media S.A. https://doi.org/10.3389/fmicb.2022.799396

Marowa, P., Ding, A., & Kong, Y. (2016). Expansins: roles in plant growth and potential applications in crop improvement. In *Plant Cell Reports* (Vol. 35, Issue 5, pp. 949–965). Springer Verlag. https://doi.org/10.1007/s00299-016-1948-4

Matei, A., Ernst, C., Günl, M., Thiele, B., Altmüller, J., Walbot, V., Usadel, B., & Doehlemann, G. (2018). How to make a tumour: cell type specific dissection of Ustilago maydis-induced tumour development in maize leaves. *New Phytologist*, *217*(4), 1681–1695. https://doi.org/10.1111/nph.14960

Meyer, H. M. (2020). In search of function: nuclear bodies and their possible roles as plant environmental sensors. In *Current Opinion in Plant Biology* (Vol. 58, pp. 33–40). Elsevier Ltd. https://doi.org/10.1016/j.pbi.2020.10.002

Misas-Villamil, J. C., van der Hoorn, R. A. L., & Doehlemann, G. (2016). Papain-like cysteine proteases as hubs in plant immunity. In *New Phytologist* (Vol. 212, Issue 4, pp. 902–907). Blackwell Publishing Ltd. https://doi.org/10.1111/nph.14117

Montes, C., Liao, C.-Y., Nolan, T. M., Song, G., Clark, N. M., Guo, H., Bassham, D. C., Yin, Y., & Walley, J. W. (2021). *Interplay between brassinosteroids and TORC signaling in Arabidopsis revealed by integrated multi-dimensional analysis*. https://doi.org/10.1101/2021.02.12.431003

Mu, Q., Li, X., Luo, J., Pan, Q., Li, Y., & Gu, T. (2021). Characterization of expansin genes and their transcriptional regulation by histone modifications in strawberry. In *Planta* (Vol. 254, Issue 2). Springer Science and Business Media Deutschland GmbH. https://doi.org/10.1007/s00425-021-03665-6

Mueller, A. N., Ziemann, S., Treitschke, S., Aßmann, D., & Doehlemann, G. (2013). Compatibility in the Ustilago maydis-Maize Interaction Requires Inhibition of Host Cysteine Proteases by the Fungal Effector Pit2. *PLoS Pathogens*, *9*(2). https://doi.org/10.1371/journal.ppat.1003177

Nagarajan, N., Khan, M., & Djamei, A. (2023). Manipulation of Auxin Signaling by Smut Fungi during Plant Colonization. *Journal of Fungi*, *9*(12), 1184. https://doi.org/10.3390/jof9121184

Nakamura, A., Higuchi, K., Goda, H., Fujiwara, M. T., Sawa, S., Koshiba, T., Shimada, Y., & Yoshida, S. (2003). Brassinolide Induces IAA5, IAA19, and DR5, a Synthetic Auxin Response Element in Arabidopsis, Implying a Cross Talk Point of Brassinosteroid and Auxin Signaling. *Plant Physiology*, *133*(4), 1843–1853. https://doi.org/10.1104/pp.103.030031

Narváez-Barragán, D. A., Tovar-Herrera, O. E., Segovia, L., Serrano, M., & Martinez-Anaya, C. (2020). Expansin-related proteins: Biology, microbe–plant interactions and associated plant-defense responses. *Microbiology (United Kingdom)*, *166*(11), 1007–1018. https://doi.org/10.1099/mic.0.000984

Navarrete, F., Gallei, M., Kornienko, A. E., Saado, I., Darino, M. A., Khan, M., Bindics, J., & Djamei, A. (2022). TOPLESS promotes plant immunity by repressing auxin signaling and is targeted by the fungal effector Naked1. *Plant Communications*. https://doi.org/10.1101/2021.05.04.442566

Navarrete, F., Grujic, N., Stirnberg, A., Saado, I., Aleksza, D., Gallei, M., Adi, H., Alcântara, A., Khan, M., Bindics, J., Trujillo, M., & Djamei, A. (2021). The Pleiades are a cluster of fungal effectors that inhibit host defenses. *PLOS Pathogens*, *17*(6), e1009641. https://doi.org/10.1371/JOURNAL.PPAT.1009641

Navarrete, F., Grujic, N., Stirnberg, A., Saadoid, I., Alekszaid, D., Gallei, M., Adi, H., Alcâ Ntaraid, A., Khanid, M., Bindicsid, J., Trujilloid, M., & Djameiid, A. (2021). *The Pleiades are a cluster of fungal effectors that inhibit host defenses*. https://doi.org/10.1371/journal.ppat.1009641

Nolan, T. M., Brennan, B., Yang, M., Chen, J., Zhang, M., Li, Z., Wang, X., Bassham, D. C., Walley, J., & Yin, Y. (2017). Selective Autophagy of BES1 Mediated by DSK2 Balances Plant Growth and Survival. *Developmental Cell*, *41*(1), 33-46.e7. https://doi.org/10.1016/J.DEVCEL.2017.03.013

Nolan, T. M., Vukašinoví, N., Hsu, C.-W., Zhang, J., Vanhoutte, I., Shahan, R., Taylor, I. W., Greenstreet, L., Heitz, M., Wang, P., Szekely, P., Brosnan, A., Yin, Y., Schiebinger, G., Ohler, U., Russinova, E., & Benfey, P. N. (2022). *Brassinosteroid gene regulatory networks at cellular resolution*. https://doi.org/10.1101/2022.09.16.508001

Nolan, T. M., Vukasinović, N., Liu, D., Russinova, E., & Yin, Y. (2020). Brassinosteroids: Multidimensional regulators of plant growth, development, and stress responses. *Plant Cell*, *32*(2), 298–318. https://doi.org/10.1105/tpc.19.00335

Novaković, L., Guo, T., Bacic, A., Sampathkumar, A., & Johnson, K. L. (2018). Hitting the wall—sensing and signaling pathways involved in plant cell wall remodeling in response to abiotic stress. In *Plants* (Vol. 7, Issue 4). MDPI AG. https://doi.org/10.3390/plants7040089

Ökmen, B., Kemmerich, B., Hilbig, D., Wemhöner, R., Aschenbroich, J., Perrar, A., Huesgen, P. F., Schipper, K., & Doehlemann, G. (2018). Dual function of a secreted fungalysin metalloprotease in Ustilago maydis. *New Phytologist*, *220*(1), 249–261. https://doi.org/10.1111/nph.15265

Ortíz-Castro, R., Contreras-Cornejo, H. A., Macías-Rodríguez, L., & López-Bucio, J. (2009). The role of microbial signals in plant growth and development. In *Plant Signaling and Behavior* (Vol. 4, Issue 8, pp. 701–712). Landes Bioscience. https://doi.org/10.4161/psb.4.8.9047

Park, A., Yun, T., Hill, T. E., Ikegami, T., Juelich, T. L., Smith, J. K., Zhang, L., Freiberg, A. N., & Lee, B. (2016). Optimized P2A for reporter gene insertion into Nipah virus results in efficient ribosomal skipping and wild-type lethality. *Journal of General Virology*, *97*, 839–843. https://doi.org/10.1099/jgv.0.000405

Penninckx, I. A. M. A., Thomma, B. P. H. J., Buchala, A., Métraux, J.-P., & Broekaert, W. F. (1998). Concomitant Activation of Jasmonate and Ethylene Response Pathways Is Required for Induction of a Plant Defensin Gene in Arabidopsis. In *The Plant Cell* (Vol. 10). https://academic.oup.com/plcell/article/10/12/2103/5999444

Pérez-Henríquez, P., & Yang, Z. (2023). Extranuclear auxin signaling: a new insight into auxin's versatility. *New Phytologist*, *237*(4), 1115–1121. https://doi.org/10.1111/nph.18602

Plaschka, C., Lin, P. C., & Nagai, K. (2017). Structure of a pre-catalytic spliceosome. *Nature*, *546*(7660), 617–621. https://doi.org/10.1038/nature22799

Presti, L. Lo, & Kahmann, R. (2017). How filamentous plant pathogen effectors are translocated to host cells. *Current Opinion in Plant Biology* , *38*, 19–24.

R. Green, M., & Sambrook, J. (2012). *Molecular Cloning This is a free sample of content from Molecular Cloning: A Laboratory Manual, 4th edition. Click here for more information or to buy the book*. www.cshlpress.org

Redkar, A., Hoser, R., Schilling, L., Zechmann, B., Krzymowska, M., Walbot, V., & Doehlemann, G. (2015). A Secreted Effector Protein of Ustilago maydis Guides Maize Leaf Cells to Form Tumors. *The Plant Cell*, *27*(4), 1332. https://doi.org/10.1105/TPC.114.131086

Reineke, G., Heinze, B., Schirawski, J., Buettner, H., Kahmann, R., & Basse, C. W. (2008). Indole-3-acetic acid (IAA) biosynthesis in the smut fungus Ustilago maydis and its relevance for increased IAA levels in infected tissue and host tumour formation. *Molecular Plant Pathology*, *9*(3), 339–355. https://doi.org/10.1111/j.1364-3703.2008.00470.x

Ren, H., Park, M. Y., Spartz, A. K., Wong, J. H., & Gray, W. M. (2018). A subset of plasma membrane-localized PP2C.D phosphatases negatively regulate SAUR-mediated cell expansion in Arabidopsis. *PLoS Genetics*, *14*(6). https://doi.org/10.1371/journal.pgen.1007455

Rozhon, W., Sharma, A., Unterholzner, S. J., Gruszka, D., & Zolkiewicz, K. (2022). *OPEN ACCESS EDITED BY Glycogen synthase kinases in model and crop plants-From negative regulators of brassinosteroid signaling to multifaceted hubs of various signaling pathways and modulators of plant reproduction and yield*. https://doi.org/10.3389/fpls.2022.939487

Ryu, H., Kim, K., Cho, H., Park, J., Choe, S., & Hwang, I. (2007). Nucleocytoplasmic Shuttling of BZR1 Mediated by Phosphorylation Is Essential in Arabidopsis Brassinosteroid Signaling. *The Plant Cell*, *19*(9), 2749–2762. https://doi.org/10.1105/TPC.107.053728

Saado, I., Chia, K.-S., Betz, R., Alcântara, A., Pettkó-Szandtner, A., Navarrete, F., D'Auria, J. C., Kolomiets, M. V, Melzer, M., Feussner, I., & Djamei, A. (2022). Effector-mediated relocalization of a maize lipoxygenase protein triggers susceptibility to Ustilago maydis . *The Plant Cell*, *34*(7), 2785–2805. https://doi.org/10.1093/plcell/koac105

Saidi, Y., Hearn, T. J., & Coates, J. C. (2012). Function and evolution of 'green' GSK3/Shaggy-like kinases. *Trends in Plant Science*, *17*(1), 39–46. https://doi.org/10.1016/J.TPLANTS.2011.10.002

Sakamoto, T., & Fujioka, S. (2013). Auxins increase expression of the brassinosteroid receptor and brassinosteroid-responsive genes in arabidopsis. *Plant Signaling and Behavior*, *8*(4). https://doi.org/10.4161/psb.23509

Samalova, M., Melnikava, A., Elsayad, K., Peaucelle, A., Gahurova, E., Gumulec, J., Spyroglou, I., Zemlyanskaya, E. V, Ubogoeva, E. V, Balkova, D., Demko, M., Blavet, N., Alexiou, P., Benes, V., Mouille, G., & Hejatko, J. (2023). Hormone-regulated expansins: Expression, localization, and cell wall biomechanics in Arabidopsis root growth. *Plant Physiology*. https://doi.org/10.1093/plphys/kiad228

Sampedro, J., & Cosgrove, D. J. (2005). The expansin superfamily. In *Genome Biology* (Vol. 6, Issue 12). https://doi.org/10.1186/gb-2005-6-12-242

Sandhu, K. S., Singh, N., & Malhi, N. S. (2007). Some properties of corn grains and their flours I: Physicochemical, functional and chapati-making properties of flours. *Food Chemistry*, *101*(3), 938–946. https://doi.org/10.1016/j.foodchem.2006.02.040

Sayers, E. W., Bolton, E. E., Brister, J. R., Canese, K., Chan, J., Comeau, D. C., Connor, R., Funk, K., Kelly, C., Kim, S., Madej, T., Marchler-Bauer, A., Lanczycki, C., Lathrop, S., Lu, Z., Thibaud-Nissen, F., Murphy, T., Phan, L., Skripchenko, Y., … Sherry, S. T. (2022). Database resources of the national center for biotechnology information. *Nucleic Acids Research*, *50*(D1), D20–D26. https://doi.org/10.1093/nar/gkab1112

Schirawski, J., Mannhaupt, G., Münch, K., Brefort, T., Schipper, K., Doehlemann, G., Di Stasio, M., Rössel, N., Mendoza-Mendoza, A., Pester, D., Müller, O., Winterberg, B., Meyer, E., Ghareeb, H., Wollenberg, T., Münsterkötter, M., Wong, P., Walter, M., Stukenbrock, E., … Kahmann, R. (2010). Pathogenicity determinants in smut fungi revealed by genome comparison. *Science (New York, N.Y.)*, *330*(6010), 1546–1548. https://doi.org/10.1126/SCIENCE.1195330

Schulz, B., Banuett, F., Dahl, M., Schlesinger, R., Schafer, W., Martin, T., Herskowitqt, I., & Kahmann', R. (1990). The b Alleles of U. maydis, Whose Combinations Program Pathogenic Development, Code for Polypeptides Containing a Homeodomain-Related Motif. In *Cell* (Vol. 60).

Scott, B., Mesarich, C., Carter, D., Chowdhary, A., Heitman, J., & Kück, U. (2022). *Plant Relationships THE MYCOTA 5 A Comprehensive Treatise on Fungi as Experimental Systems for Basic and Applied Research Series Editors*.

Shinde, M. Y., Sidoli, S., Kulej, K., Mallory, M. J., Radens, C. M., Reicherter, A. L., Myers, R. L., Barash, Y., Lynch, K. W., Garcia, B. A., & Klein, P. S. (2017). Phosphoproteomics reveals that glycogen synthase kinase-3 phosphorylates multiple splicing factors and is associated with alternative splicing. *Journal of Biological Chemistry*, *292*(44), 18240–18255. https://doi.org/10.1074/jbc.M117.813527

Singh, B. K., Delgado-Baquerizo, M., Egidi, E., Guirado, E., Leach, J. E., Liu, H., & Trivedi, P. (2023). Climate change impacts on plant pathogens, food security and paths forward. In *Nature Reviews Microbiology*. Nature Research. https://doi.org/10.1038/s41579-023-00900-7

Song, T., Zhang, Y., Zhang, Q., Zhang, X., Shen, D., Yu, J., Yu, M., Pan, X., Cao, H., Yong, M., Qi, Z., Du, Y., Zhang, R., Yin, X., Qiao, J., Liu, Y., Liu, W., Sun, W., Zhang, Z., … Liu, Y. (2021). The N-terminus of an Ustilaginoidea virens Ser-Thr-rich glycosylphosphatidylinositol-anchored protein elicits plant immunity as a MAMP. *Nature Communications*, *12*(1). https://doi.org/10.1038/s41467-021-22660-9

Song, W., Hu, L., & Ma, Z. (2022). *Importance of Tyrosine Phosphorylation in Hormone-Regulated Plant Growth and Development*. https://doi.org/10.3390/ijms23126603

Song, Y., Wang, Y., Yu, Q., Sun, Y., Zhang, J., Zhan, J., & Ren, M. (2023). Regulatory network of GSK3-like kinases and their role in plant stress response. *Frontiers in Plant Science*, *14*, 732. https://doi.org/10.3389/FPLS.2023.1123436/BIBTEX

Song, Y., Zhai, Y., Li, L., Yang, Z., Ge, X., Yang, Z., Zhang, C., Li, F., & Ren, M. (2021). BIN2 negatively regulates plant defence against Verticillium dahliae in Arabidopsis and cotton. *Plant Biotechnology Journal*, *19*(10), 2097. https://doi.org/10.1111/PBI.13640

Spartz, A. K., Lee, S. H., Wenger, J. P., Gonzalez, N., Itoh, H., Inzé, D., Peer, W. A., Murphy, A. S., Overvoorde, P. J., & Gray, W. M. (2012). The SAUR19 subfamily of SMALL AUXIN UP RNA genes promote cell expansion. *Plant Journal*, *70*(6), 978–990. https://doi.org/10.1111/j.1365-313X.2012.04946.x

Staněk, D., & Fox, A. (2017). Nuclear bodies: news insights into structure and function. In *Current Opinion in Cell Biology* (Vol. 46, pp. 94–101). Elsevier Ltd. https://doi.org/10.1016/j.ceb.2017.05.001

Steinberg, G., & Perez-Martin, J. (2008). Ustilago maydis, a new fungal model system for cell biology. In *Trends in Cell Biology* (Vol. 18, Issue 2, pp. 61–67). https://doi.org/10.1016/j.tcb.2007.11.008

Stirnberg, A., & Djamei, A. (2016). Characterization of ApB73, a virulence factor important for colonization of Zea mays by the smut Ustilago maydis. *Molecular Plant Pathology*, *17*(9), 1467–1479. https://doi.org/10.1111/mpp.12442

Stortenbeker, N., & Bemer, M. (2019). The SAUR gene family: The plant's toolbox for adaptation of growth and development. In *Journal of Experimental Botany* (Vol. 70, Issue 1, pp. 17–27). Oxford University Press. https://doi.org/10.1093/jxb/ery332

Stotz, H. U., Mitrousia, G. K., de Wit, P. J. G. M., & Fitt, B. D. L. (2014). Effector-triggered defence against apoplastic fungal pathogens. In *Trends in Plant Science* (Vol. 19, Issue 8, pp. 491–500). Elsevier Ltd. https://doi.org/10.1016/j.tplants.2014.04.009

Sun, P., Tian, Q. Y., Chen, J., & Zhang, W. H. (2010). Aluminium-induced inhibition of root elongation in Arabidopsis is mediated by ethylene and auxin. *Journal of Experimental Botany*, *61*(2), 347–356. https://doi.org/10.1093/jxb/erp306

Sutherland, C. (2011). What are the bona fide GSK3 substrates? In *International Journal of Alzheimer's Disease*. https://doi.org/10.4061/2011/505607

Tanaka, S., Brefort, T., Neidig, N., Djamei, A., Kahnt, J., Vermerris, W., Koenig, S., Feussner, K., Feussner, I., & Kahmann, R. (2014). A secreted Ustilago maydis effector promotes virulence by targeting anthocyanin biosynthesis in maize. *ELife*, *3*. https://doi.org/10.7554/elife.01355

Tanaka, S., & Kahmann, R. (2021). Cell wall–associated effectors of plant-colonizing fungi. *Mycologia*, *113*(2), 247–260. https://doi.org/10.1080/00275514.2020.1831293

Tang, W., Kim, T. W., Oses-Prieto, J. A., Sun, Y., Deng, Z., Zhu, S., Wang, R., Burlingame, A. L., & Wang, Z. Y. (2008). BSKs mediate signal transduction from the receptor kinase BRI1 in Arabidopsis. *Science*, *321*(5888), 557–560. https://doi.org/10.1126/SCIENCE.1156973/SUPPL_FILE/TANG.SOM.PDF

Tang, W., Yuan, M., Wang, R., Yang, Y., Wang, C., Oses-Prieto, J. A., Kim, T. W., Zhou, H. W., Deng, Z., Gampala, S. S., Gendron, J. M., Jonassen, E. M., Lillo, C., DeLong, A., Burlingame, A. L., Sun, Y., & Wang, Z. Y. (2011). PP2A activates brassinosteroid-responsive gene expression and plant growth by

dephosphorylating BZR1. *Nature Cell Biology 2011 13:2*, *13*(2), 124–131. https://doi.org/10.1038/ncb2151

Tian, H., Lv, B., Ding, T., Bai, M., & Ding, Z. (2017). Auxin-BR Interaction Regulates Plant Growth and Development. *Frontiers in Plant Science*, *8*. https://doi.org/10.3389/FPLS.2017.02256

Uhse, S., & Djamei, A. (2018). Effectors of plant-colonizing fungi and beyond. *PLOS Pathogens*, *14*(6), e1006992. https://doi.org/10.1371/JOURNAL.PPAT.1006992

van Mourik, H., van Dijk, A. D. J., Stortenbeker, N., Angenent, G. C., & Bemer, M. (2017). Divergent regulation of Arabidopsis SAUR genes: A focus on the SAUR10-clade. *BMC Plant Biology*, *17*(1). https://doi.org/10.1186/s12870-017-1210-4

Vernoux, T., Brunoud, G., Farcot, E., Morin, V., Van Den Daele, H., Legrand, J., Oliva, M., Das, P., Larrieu, A., Wells, D., Guédon, Y., Armitage, L., Picard, F., Guyomarc'H, S., Cellier, C., Parry, G., Koumproglou, R., Doonan, J. H., Estelle, M., … Traas, J. (2011). The auxin signalling network translates dynamic input into robust patterning at the shoot apex. *Molecular Systems Biology*, *7*. https://doi.org/10.1038/msb.2011.39

Vert, G., & Chory, J. (2006). Downstream nuclear events in brassinosteroid signalling. *Nature 2006 441:7089*, *441*(7089), 96–100. https://doi.org/10.1038/nature04681

Walbot, V., & Skibbe, D. S. (2010). Maize host requirements for Ustilago maydis tumor induction. *Sexual Plant Reproduction*, *23*(1), 1–13. https://doi.org/10.1007/s00497-009-0109-0

Walcher, C. L., Chory, J., Nemhauser, J. L., Biochimie, ¶ †, & Molé, P. (2008). *Integration of auxin and brassinosteroid pathways by Auxin Response Factor 2 Gré gory Vert*. www.pnas.org/cgi/content/full/

Walcher, C. L., & Nemhauser, J. L. (2012). Bipartite promoter element required for auxin response. *Plant Physiology*, *158*(1), 273–282. https://doi.org/10.1104/pp.111.187559

Wan, R., Bai, R., & Shi, Y. (2019). Molecular choreography of pre-mRNA splicing by the spliceosome. In *Current Opinion in Structural Biology* (Vol. 59, pp. 124–133). Elsevier Ltd. https://doi.org/10.1016/j.sbi.2019.07.010

Wang, L., Li, J., & Di, L. jun. (2022). Glycogen synthesis and beyond, a comprehensive review of GSK3 as a key regulator of metabolic pathways and a therapeutic target for treating metabolic diseases. In *Medicinal Research Reviews* (Vol. 42, Issue 2, pp. 946–982). John Wiley and Sons Inc. https://doi.org/10.1002/med.21867

Wang, L., & Ruan, Y. L. (2013). Regulation of cell division and expansion by sugar and auxin signaling. *Frontiers in Plant Science*, *4*(MAY), 163. https://doi.org/10.3389/FPLS.2013.00163/BIBTEX

Wang, Q., Sawyer, I. A., Sung, M. H., Sturgill, D., Shevtsov, S. P., Pegoraro, G., Hakim, O., Baek, S., Hager, G. L., & Dundr, M. (2016). Cajal bodies are linked to genome conformation. *Nature Communications*, *7*. https://doi.org/10.1038/ncomms10966

Wang, X., Chen, J., Xie, Z., Liu, S., Nolan, T., Ye, H., Zhang, M., Guo, H., Schnable, P. S., Li, Z., & Yin, Y. (2014). Histone lysine methyltransferase SDG8 is involved in brassinosteroid-regulated gene

expression in Arabidopsis thaliana. *Molecular Plant*, *7*(8), 1303–1315. https://doi.org/10.1093/MP/SSU056

Wang, X., Wang, X., Sun, S., Tu, X., Lin, K., Qin, L., Wang, X., Li, G., Zhong, S., & Li, P. (2022). Characterization of regulatory modules controlling leaf angle in maize. *Plant Physiology*, *190*(1), 500–515. https://doi.org/10.1093/PLPHYS/KIAC308

Wang, Y., Xu, J., Yu, J., Zhu, D., & Zhao, Q. (2022). Maize GSK3-like kinase ZmSK2 is involved in embryonic development. *Plant Science*, *318*, 111221. https://doi.org/10.1016/J.PLANTSCI.2022.111221

Wang, Z., Yang, L., Liu, Z., Lu, M., Wang, M., Sun, Q., Lan, Y., Shi, T., Wu, D., & Hua, J. (2019). Natural variations of growth thermo-responsiveness determined by SAUR26/27/28 proteins in Arabidopsis thaliana. *New Phytologist*, *224*(1), 291–305. https://doi.org/10.1111/nph.15956

Watanabe, E., Mano, S., Nishimura, M., & Yamada, K. (2019). AtUBL5 regulates growth and development through pre-mRNA splicing in Arabidopsis thaliana. *PLoS ONE*, *14*(11). https://doi.org/10.1371/journal.pone.0224795

Wei, Z., & Li, J. (2016). Brassinosteroids Regulate Root Growth, Development, and Symbiosis. *Molecular Plant*, *9*(1), 86–100. https://doi.org/10.1016/J.MOLP.2015.12.003

Wieczorek, K., & Grundler, F. M. W. (2006). Expanding nematode-induced Syncytia: The role of expansins. *Plant Signaling and Behavior*, *1*(5), 223–224. https://doi.org/10.4161/psb.1.5.3426

Xie, J., Beickman, K., Otte, E., & Rymond, B. C. (1998). Progression through the spliceosome cycle requires Prp38p function for U4/U6 snRNA dissociation. In *The EMBO Journal* (Vol. 17, Issue 10).

Yan, Z., Zhao, J., Peng, P., Chihara, R. K., & Li, J. (2009). BIN2 Functions Redundantly with Other Arabidopsis GSK3-Like Kinases to Regulate Brassinosteroid Signaling. *Plant Physiology*, *150*(2), 710–721. https://doi.org/10.1104/PP.109.138099

Yang, F., Fan, Y., Wu, X., Cheng, Y., Liu, Q., Feng, L., Chen, J., Wang, Z., Wang, X., Yong, T., Liu, W., Liu, J., Du, J., Shu, K., & Yang, W. (2018). Auxin-to-gibberellin ratio as a signal for light intensity and quality in regulating soybean growth and matter partitioning. *Frontiers in Plant Science*, *9*, 56. https://doi.org/10.3389/FPLS.2018.00056/BIBTEX

Yin, Y., Wang, Z. Y., Mora-Garcia, S., Li, J., Yoshida, S., Asami, T., & Chory, J. (2002). BES1 accumulates in the nucleus in response to brassinosteroids to regulate gene expression and promote stem elongation. *Cell*, *109*(2), 181–191. https://doi.org/10.1016/S0092-8674(02)00721-3

Yoo, M. J., Albert, V. A., Soltis, P. S., & Soltis, D. E. (2006). Phylogenetic diversification of glycogen synthase kinase 3/SHAGGY-like kinase genes in plants. *BMC Plant Biology*, *6*(1), 1–14. https://doi.org/10.1186/1471-2229-6-3/FIGURES/7

Yoshimitsu, Y., Tanaka, K., Fukuda, W., Asami, T., Yoshida, S., Hayashi, K. ichiro, Kamiya, Y., Jikumaru, Y., Shigeta, T., Nakamura, Y., Matsuo, T., & Okamoto, S. (2011). Transcription of DWARF4 plays a crucial role in auxin-regulated root elongation in addition to brassinosteroid homeostasis in arabidopsis thaliana. *PLoS ONE*, *6*(8). https://doi.org/10.1371/journal.pone.0023851

Youn, J. H., & Kim, T. W. (2015). Functional insights of plant GSK3-like kinases: multi-taskers in diverse cellular signal transduction pathways. *Molecular Plant*, *8*(4), 552–565. https://doi.org/10.1016/J.MOLP.2014.12.006

Youn, J. H., Kim, T. W., Kim, E. J., Bu, S., Kim, S. K., Wang, Z. Y., & Kim, T. W. (2013). Structural and functional characterization of arabidopsis GSK3-like kinase AtSK12. *Molecules and Cells*, *36*(6), 564–570. https://doi.org/10.1007/s10059-013-0266-8

Yu, X., Li, L., Zola, J., Aluru, M., Ye, H., Foudree, A., Guo, H., Anderson, S., Aluru, S., Liu, P., Rodermel, S., & Yin, Y. (2011). A brassinosteroid transcriptional network revealed by genome-wide identification of BESI target genes in Arabidopsis thaliana. *The Plant Journal : For Cell and Molecular Biology*, *65*(4), 634–646. https://doi.org/10.1111/J.1365-313X.2010.04449.X

Yu, Z., Zhang, F., Friml, J., & Ding, Z. (2022). Auxin signaling: Research advances over the past 30 years. *Journal of Integrative Plant Biology*, *64*(2), 371–392. https://doi.org/10.1111/jipb.13225

Zhang, B., Gao, Y., Zhang, L., & Zhou, Y. (2021). The plant cell wall: Biosynthesis, construction, and functions. In *Journal of Integrative Plant Biology* (Vol. 63, Issue 1, pp. 251–272). Blackwell Publishing Ltd. https://doi.org/10.1111/jipb.13055

Zhang, S., Li, C., Si, J., Han, Z., & Chen, D. (2022). Action Mechanisms of Effectors in Plant-Pathogen Interaction. In *International Journal of Molecular Sciences* (Vol. 23, Issue 12). MDPI. https://doi.org/10.3390/ijms23126758

Zhao, H., Fu, Y., Zhang, G., Luo, Y., Yang, W., Liang, X., Yin, L., Zheng, Z., Wang, Y., Li, Z., Zhu, H., Huang, J., Tan, Q., Bu, S., Liu, G., Wang, S., & Liu, Z. (2023). *GS6.1 controls kernel size and plant architecture in rice*. https://doi.org/10.21203/rs.3.rs-2616757/v1

Zhou, J. M., & Zhang, Y. (2020). Plant Immunity: Danger Perception and Signaling. *Cell*, *181*(5), 978–989. https://doi.org/10.1016/J.CELL.2020.04.028

Zhou, X. Y., Song, L., & Xue, H. W. (2013). Brassinosteroids regulate the differential growth of arabidopsis hypocotyls through auxin signaling components IAA19 and ARF7. *Molecular Plant*, *6*(3), 887–904. https://doi.org/10.1093/mp/sss123

Zhu, J. Y., Li, Y., Cao, D. M., Yang, H., Oh, E., Bi, Y., Zhu, S., & Wang, Z. Y. (2017). The F-box protein KIB1 mediates brassinosteroid-induced inactivation and degradation of GSK3-like kinases in Arabidopsis. *Molecular Cell*, *66*(5), 648. https://doi.org/10.1016/J.MOLCEL.2017.05.012

Zhuang, Y., Lian, W., Tang, X., Qi, G., Wang, Di., Chai, G., & Zhou, G. (2022). MYB42 inhibits hypocotyl cell elongation by coordinating brassinosteroid homeostasis and signalling in Arabidopsis thaliana. *Annals of Botany*, *129*(4), 403–413. https://doi.org/10.1093/aob/mcab152

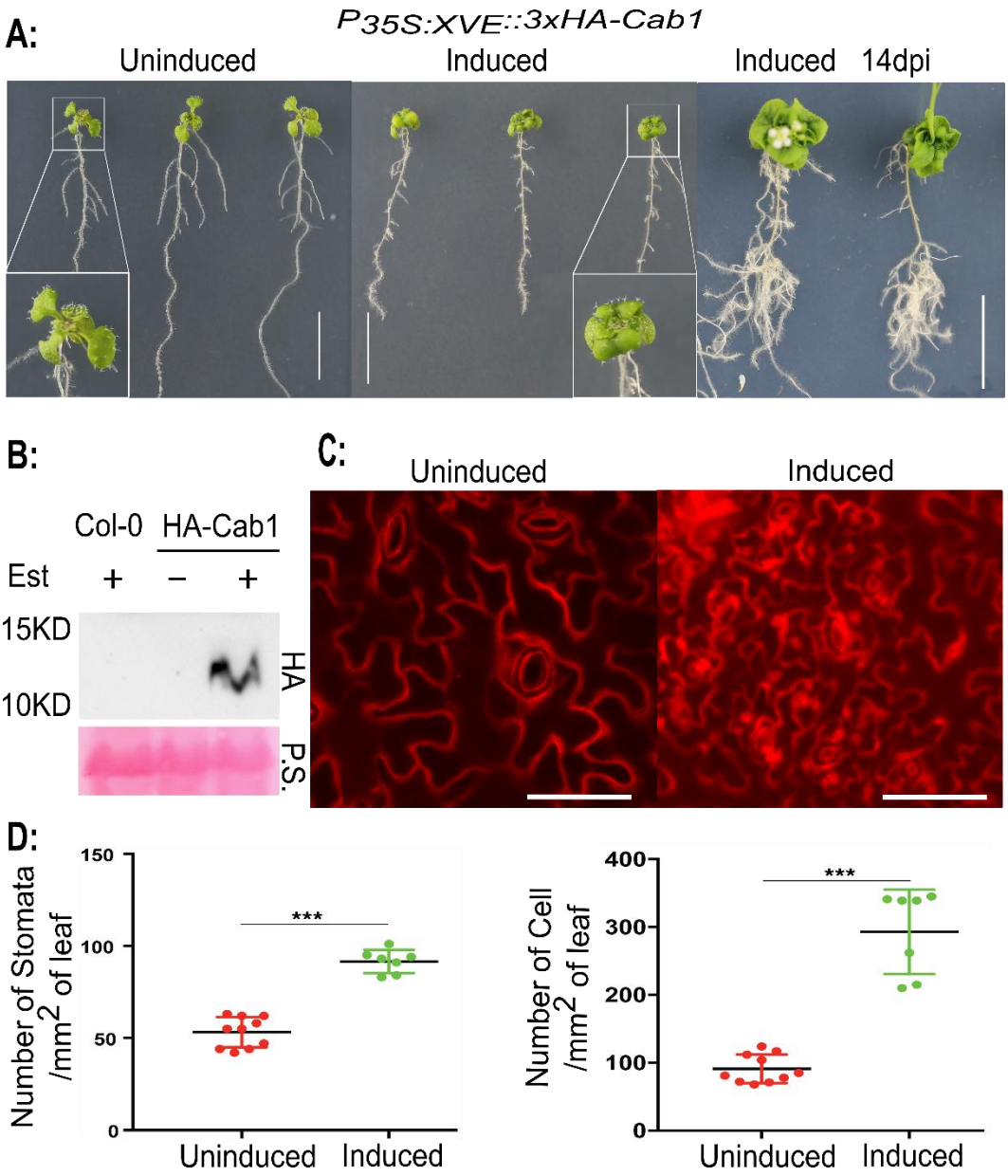

Figure 1: Cab1 expression causes a dwarf phenotype in *A. thaliana* by repressing cell-expansion

- **a.** Transgenic *Arabidopsis thaliana* line expressing non-secreted Cab1 ($P_{35S\text{-}XVE}$::3xHA-$Cab1_{28\text{-}113}$), 7 dpg moved to the induction $^1/_2$MS plates containing 10µM β–Estradiol solved in DMSO and phenotyping was done 5 and 14 dpi. The control plates contain the solvent only (DMSO). dpg: days post germination. dpi: days post-induction. Scale bar = 1 cm.
- **b.** Immunoblotting analysis on Cab1 ($P_{35S\text{-}XVE}$::3xHA-$Cab1_{28\text{-}113}$) protein levels of seedling extracts from *A. thaliana* lines using anti-HA antibody. The expected band size of 14KDa is visible only in estradiol-induced seedlings. Ponceau staining was used as an indication of equal protein loading.
- **c.** 14 days post-treatment, Propidium Iodide staining was performed on β–Estradiol-induced and uninduced seedlings, and the stained leaves were subjected to fluorescent microscopy. Scale bar = 50 µm.

d. The number of stomata and epidermal cells was counted manually per $1mm^2$ of samples. 14 days of Cab1 expression leads to higher number of cells and stomata per area of leaf in comparison with uninduced plants. Statistical analysis was done by GraphPad. * $p<0.05$,*** $p<0.001$, ANOVA.

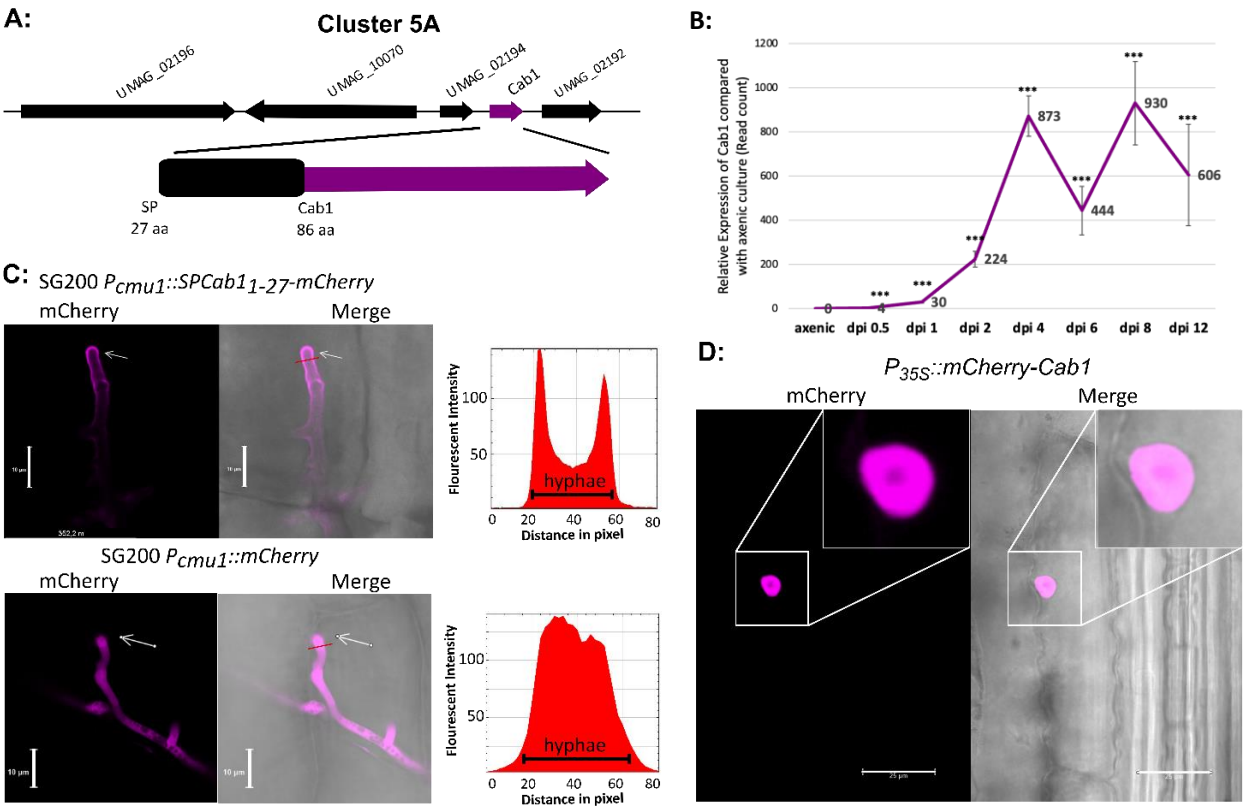

Figure 2: Cab1 is a secreted effector, targeting and acting in the plant cell nucleus

- **a.** Schematic representation of Cab1 genomic organization. As part of chromosome 5 cluster 5A, Cab1 consists of a 113 amino acid protein in which the first 27 amino acids comprise the N-terminal predicted signal peptide (SP) and the remaining 86 amino acids compose the predicted mature protein.
- **b.** Transcriptional levels of Cab1 were calculated from RNAseq data at different time points during the biotrophic growth of *U.* maydis in maize seedlings. Data was generated based on Lanver et al., 2018.
- **c.** *U. maydis in planta* secretion of Cab1 in the native host *Z. mays*. Maize cells infected with *U. maydis* strains expressing mCherry fusions of SP-Cab1 (*P_{cmu1}::SP-Cab1$_{1-27}$-mCherry*) or mCherry without signal peptide (*PCmu1::mCherry*) under the control of *Cmu1* promoter. Confocal microscopy was performed 5 days post-infection. While secreted mCherry strongly accumulates at the cell periphery of the hyphae and hyphal tip (upper panel), localization of mCherry without signal peptide is evenly distributed within the hyphae (lower panel) as indicated with white arrows. Fluorescence intensity profiles the mCherry channel along the transection lines. Scale bar = 10 µm.
- **d.** Localization of Cab1 (without signal peptide) in *Z. mays*. Transient expression of mCherry-Cab1 (P_{35S}::mCherry-Cab1$_{28-113}$) via biolistic transformation in maize leaves was monitored by confocal microscopy. mCherry-Cab1$_{28-113}$ shows only nuclear localization. Scale bar = 25 µm.

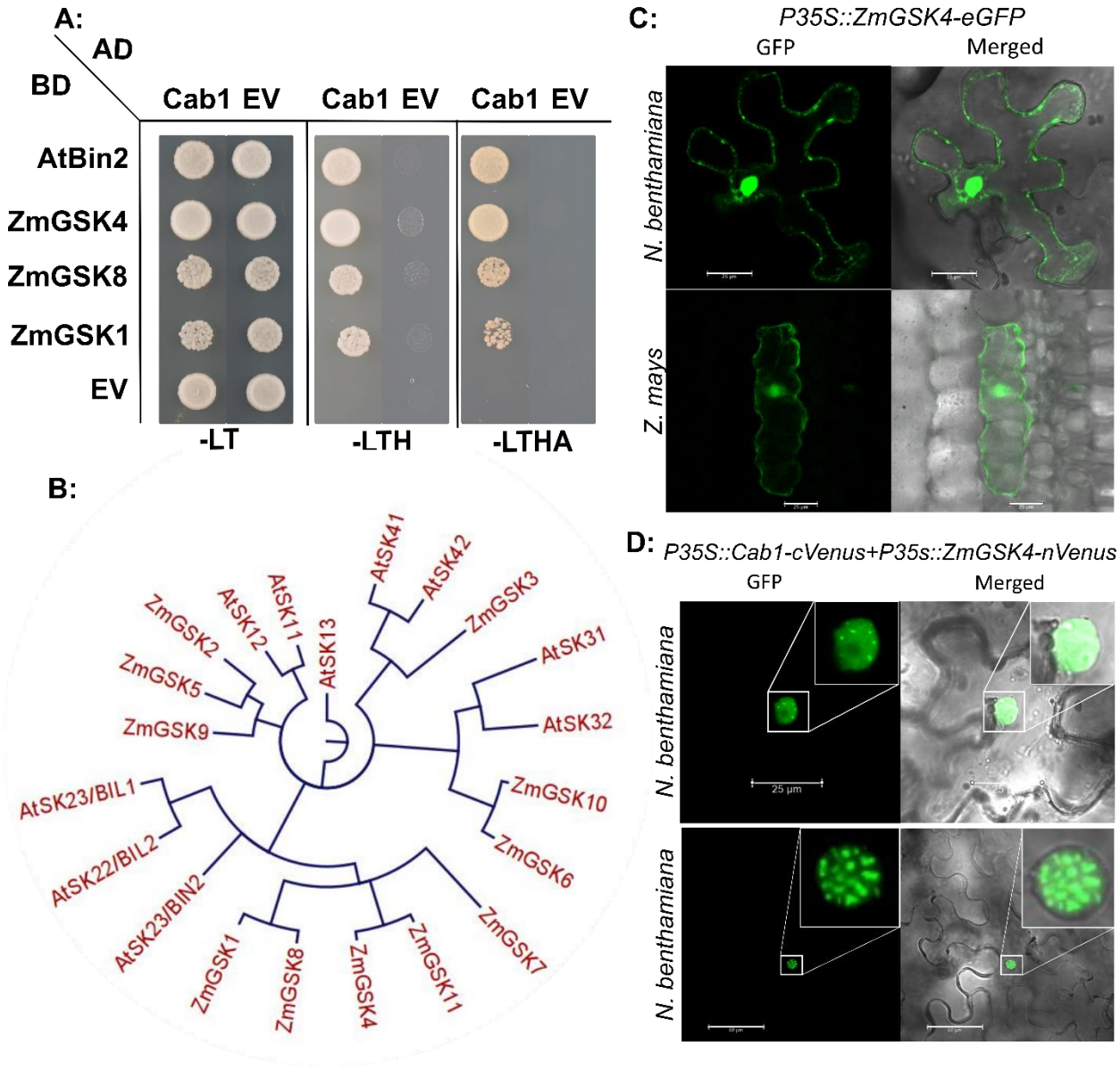

Fig 3:Cab1 interacts with shaggy-like kinases proteins in the nucleus.

a. Direct interaction of Cab1 and BIN2 in a Yeast-two-Hybrid assay. AtBIN2 and three close ZmGSK3 orthologues (ZmGSK4, ZmGSK1, ZmGSK8) were cloned into pGBKT7 bait vectors and transformed into the yeast strain Ah187, whereas Cab1 was cloned into pGADT7 activation vector and transformed into the yeast strain AH109. Diploid yeast after mating, containing both plasmids, were dropped on selective synthetic dropout media (SD) and yeast growth was monitored 3 days after spotting. The experiment was repeated 3 times independently with comparable results.
b. phylogenetic-analysis results of GSK-3 proteins from *A. thaliana* and *Zea mays*. The phylogenetic tree was constructed using CLC workbench and the maximum likelihood method with 1000 bootstraps. Different clades of the GSK family are marked with different colors.
c. Localization of ZmGSK4 in *N. benthamiana* and *Z. mays*. Transient expression of GFP-ZmGSK4 (*P_{35S}::GFP-ZmGSK4*) in *N. benthamiana* and *Z. mays* leaves was performed via agrotransformation

and biolistic bombardment methods respectively and monitored through confocal microscopy. ZmGSK4 shows Nucleo-cytoplasmic localization. Scale bar = 25 µm.

d. *In vivo* interaction of Cab1 and ZmGSK3 were tested via BiFC in *N. benthamiana*. Cab1 C-terminally tagged with cVenus (*P_{35S}::Cab1$_{28-113}$-cVenus*) and ZmGSK4 C-terminally tagged with nVenus (*P_{35S}::ZmGSK4-nVenus*). The constructs transformed in Agrobacterium strain GV3101 and co-infiltrated in *N. benthamiana* leaves. Confocal microscopy was done 3dpi in the GFP filter. Scale bar = 25 µm.

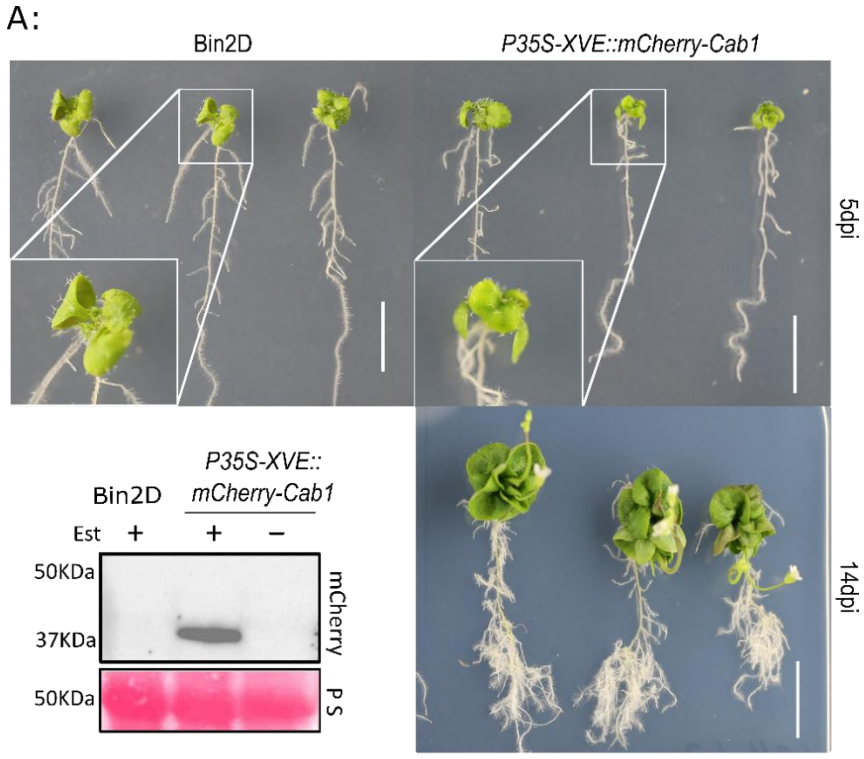
A:
Bin2D
P35S-XVE::mCherry-Cab1
5dpi
14dpi
P35S-XVE::
Bin2D
mCherry-Cab1
Est + + −
50KDa
37KDa
mCherry
50KDa
P S

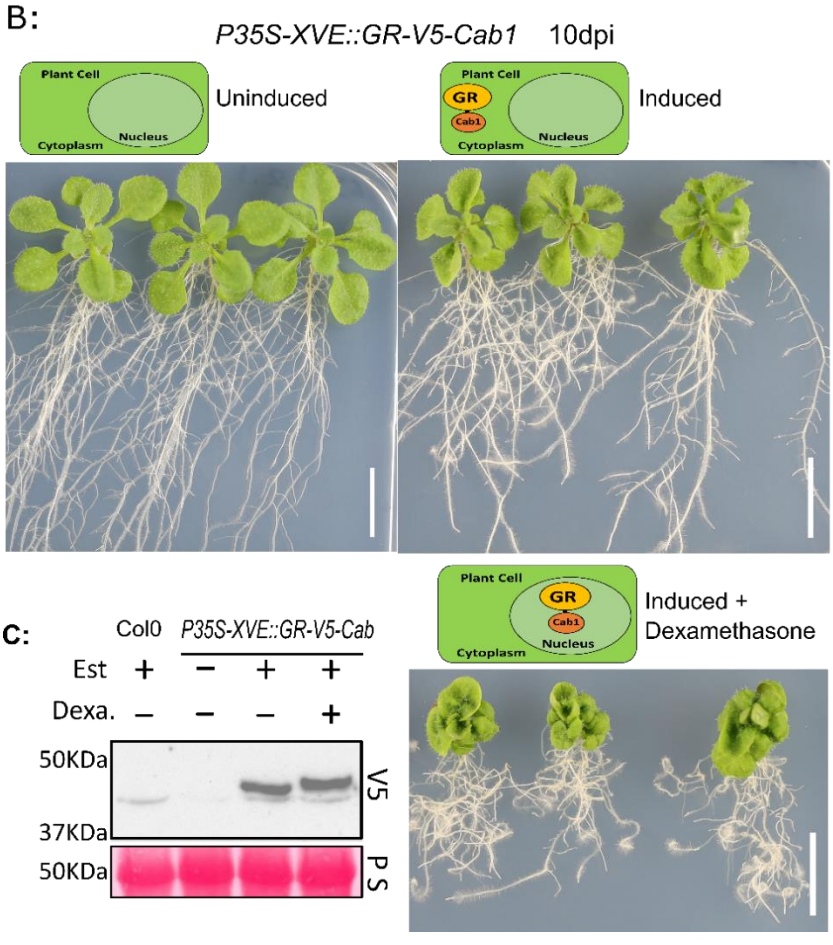
B:
P35S-XVE::GR-V5-Cab1 10dpi
Plant Cell
Cytoplasm
Nucleus
Uninduced
GR
Cab1
Induced
Induced +
Dexamethasone
C:
Col0
P35S-XVE::GR-V5-Cab
Est + − + +
Dexa. − − − +
50KDa
37KDa
V5
50KDa
P S

Fig 4: Cab1 nuclear localization in A. thaliana leads similar phenotype of BIN2 dominant mutant

a. Resemblance in the shoot phenotype between Cab1 overexpression and Bin2D dominant mutant (*bin2-1*) plants. 9 days old Cab1 ($P_{35S\text{-}XVE}$*::mcherry- cab1*$_{28\text{-}113}$) and Bin2D seedling moved on induction plates containing 10µM Estradiol. Phenotyping was performed at 5 and 14 dpi respectively. Control plates contain DMSO. Western blot was performed with an anti-mCherry antibody. Scale bar= 1cm.
b. Mis-localization of Cab1 tagged with glucocorticoid receptor in *A. thaliana*. The Gluco-V5-Cab1 ($P_{35S\text{-}XVE}$*::GR-V5-Cab1*$_{28\text{-}113}$) seedlings grow on selection plates. 9 days old seedlings were shifted either on new control plates with DMSO, or induction plates with 10 µM Estradiol only or 10 µM Estradiol and 10 µM Dexamethasone respectively (left to right). The strong cabbage phenotype was just observed in the presence of both Estradiol and Dexamethasone. Scale bar: 1cm.
c. Immunoblotting analysis on Cab1 ($P_{35S\text{-}XVE}$*::GR-V5-Cab1*$_{28\text{-}113}$) protein levels of seedling extracts from *A. thaliana* lines using anti-V5 antibody. The expected band size of 48KDa (magenta asterisks) is shown only in estradiol-induced seedlings. Ponceau staining was used as an indication of equal protein loading.

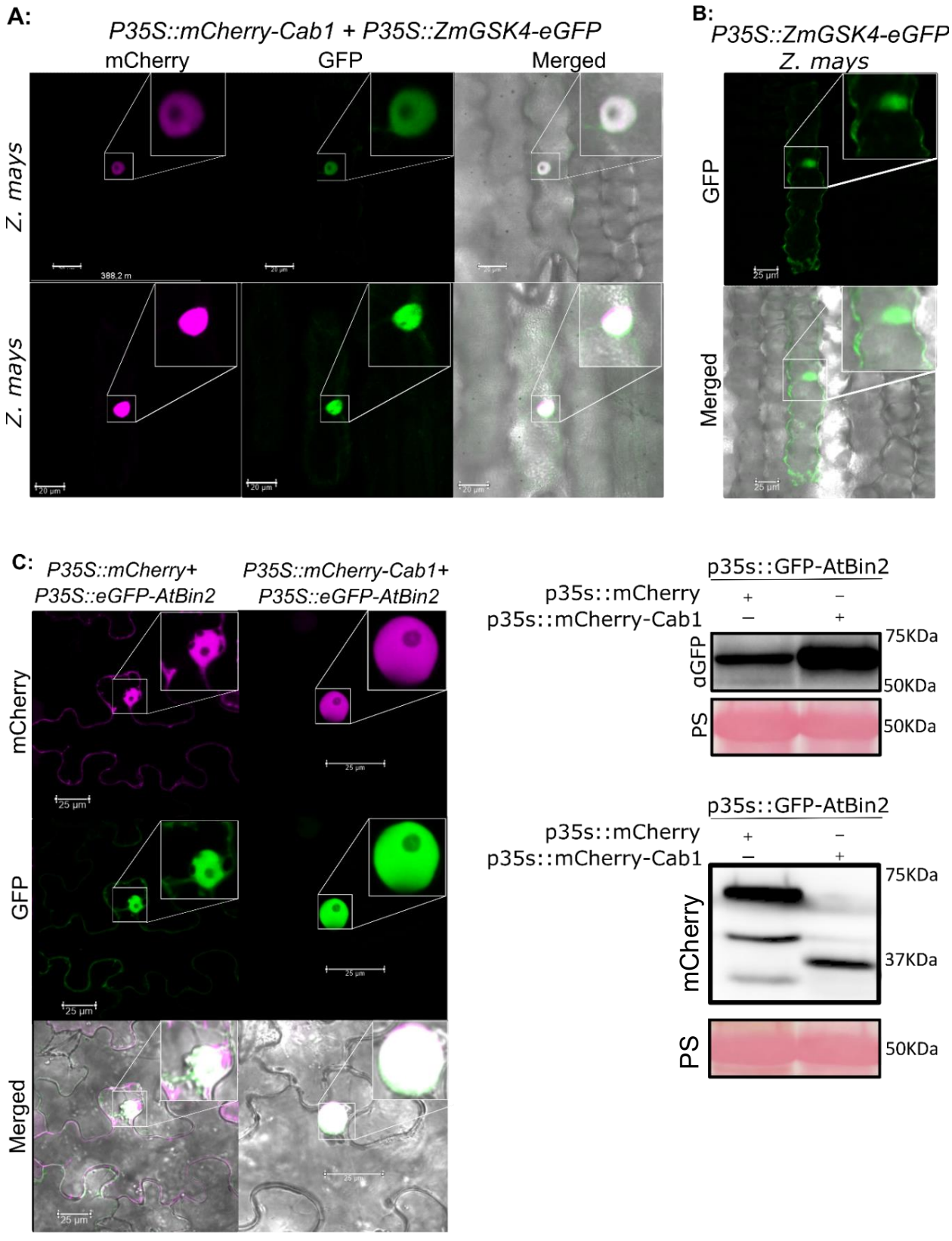
A:
P35S::mCherry-Cab1 + P35S::ZmGSK4-eGFP
mCherry
GFP
Merged
Z. mays
Z. mays
B:
P35S::ZmGSK4-eGFP
Z. mays
GFP
Merged
C:
P35S::mCherry+
P35S::eGFP-AtBin2
P35S::mCherry-Cab1+
P35S::eGFP-AtBin2
mCherry
GFP
Merged
p35s::GFP-AtBin2
p35s::mCherry
p35s::mCherry-Cab1
75KDa
αGFP
50KDa
PS
50KDa
p35s::GFP-AtBin2
p35s::mCherry
p35s::mCherry-Cab1
75KDa
mCherry
37KDa
PS
50KDa

Fig5: BIN2 re-localized into the nucleus by Cab1 co-expression to increase its stability and kinase activity.

a. Cab1 relocalises ZmSGK4 from cytosol to the nucleus. Subcellular co-localization of ZmGSK4 (P_{35S}::ZmGSK4-GFP) co-expressed with Cab1 (P_{35S}::mCherry-cab1$_{28-113}$) via biolistic bombardment in maize plant leaves was observed 1 dpi through confocal microscopy. Left panel: mCherry, Middle panel: GFP, right panel: merged mCherry and GFP. Scale bar = 25 µm.
b. ZmGSK4 shows Nucleo-cytoplasmic localization in the absence of Cab1 in *Z. mays*. Transient expression of GFP-ZmGSK4 (*P_{35S}::GFP-ZmGSK4*) in *Z. mays* leaves was performed via biolistic bombardment and monitored through confocal microscopy 1dpi. Scale bar = 25 µm.
c. Cab1 re-localizes and stabilizes AtBIN2. AtBIN2 re-localizes into the nucleus in the presence of Cab1 in *N. benthamiana*. Full-length AtBIN2 was fused to GFP (P_{35S}::AtBIN2-GFP) and Cab1 lacking its signal peptide was fused to mCherry (P_{35S}::mCherry-cab1$_{28-113}$) transiently expressed in *N. benthamiana* leaves, transformedvia Agrobacterium strain GV3101. Constitutively expressed mCherry (P_{35S}::mCherry-mCherry) were used as controls for the colocalization assay. The samples were subjected to confocal microscopy 3 dpi Upper: mCherry fluorescence, middle panels: GFP fluorescence, Lower panel: merged mCherry and GFP fluorescence, brightfield images. Scale bar = 25 µm. The western blot was performed with GFP and mCherry antibodies recognizing the respective fusion proteins.

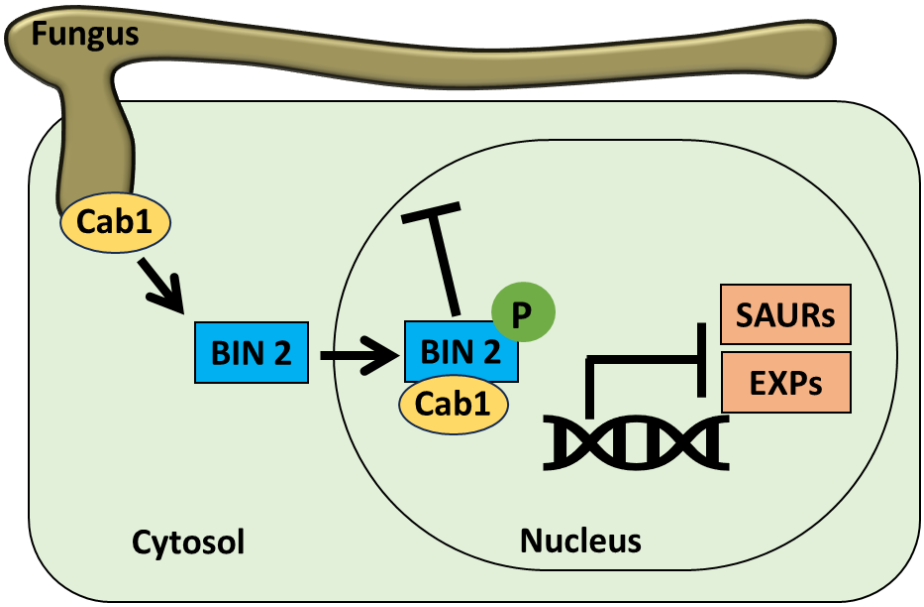

Fig6: Model: Cab1 targets plant Shaggy-like kinases to manipulate the plant cell expansion. Cab1 re-localizes BIN2 from the cytosol to the host nucleus, effectively preventing BIN2 from returning to the cytosol. Cab1 expression leads to the stabilization of BIN2 via less ubiquitination at Lys^{35}. Simultaneously, Cab1 significantly enhances BIN2 phosphorylation at $Tyrosine^{200}$ compared to the control group, resulting increase BIN2 activity. Consequently, the expression of SAURs and EXPs is downregulated compared to the control. The downregulation of SAURs and EXPs results in the maintenance of rigidity in the plant cell wall, preventing expansion. This model elucidates Cab1's role in safeguarding cell wall rapturing.

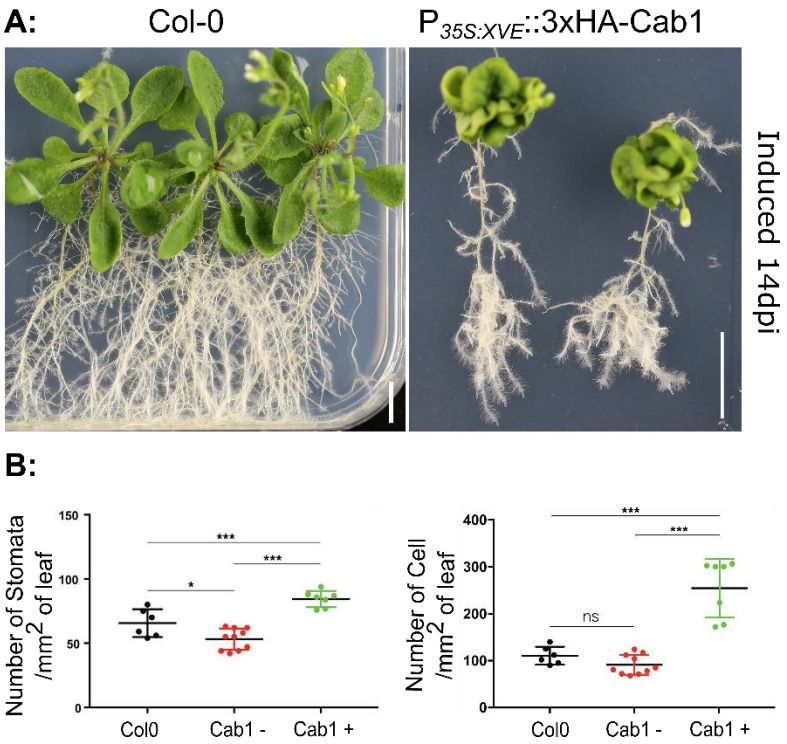

Fig S. 1. Cab1 expression causes a dwarf phenotype in *A. thaliana* by repressing cell-expansion

a. Transgenic *Arabidopsis thaliana* line expressing non-secreted Cab1 ($P_{35S\text{-}XVE}$::3xHA-$Cab1_{28\text{-}113}$), 7 dpg moved to the induction $^1/_2$MS plates containing 10µM β–Estradiol and phenotyping was done 14 dpi. *A. thaliana* ecotype Col-0 was used as control. dpg: days post germination. dpi: days post-induction. Scale bar = 1 cm.
b. The stomata and cells were manually counted per 1mm^2 of the samples. After 14 days of Cab1 expression, there was an increased number of cells and stomata on the leaves compared to uninduced and Col-0 wild-type plants. Each data point represents the number of cells/stomata that were counted per microscopy picture. Statistical analysis was performed using GraphPad, and the significance levels were denoted as * for $p<0.05$ and *** for $p<0.001$, using ANOVA.

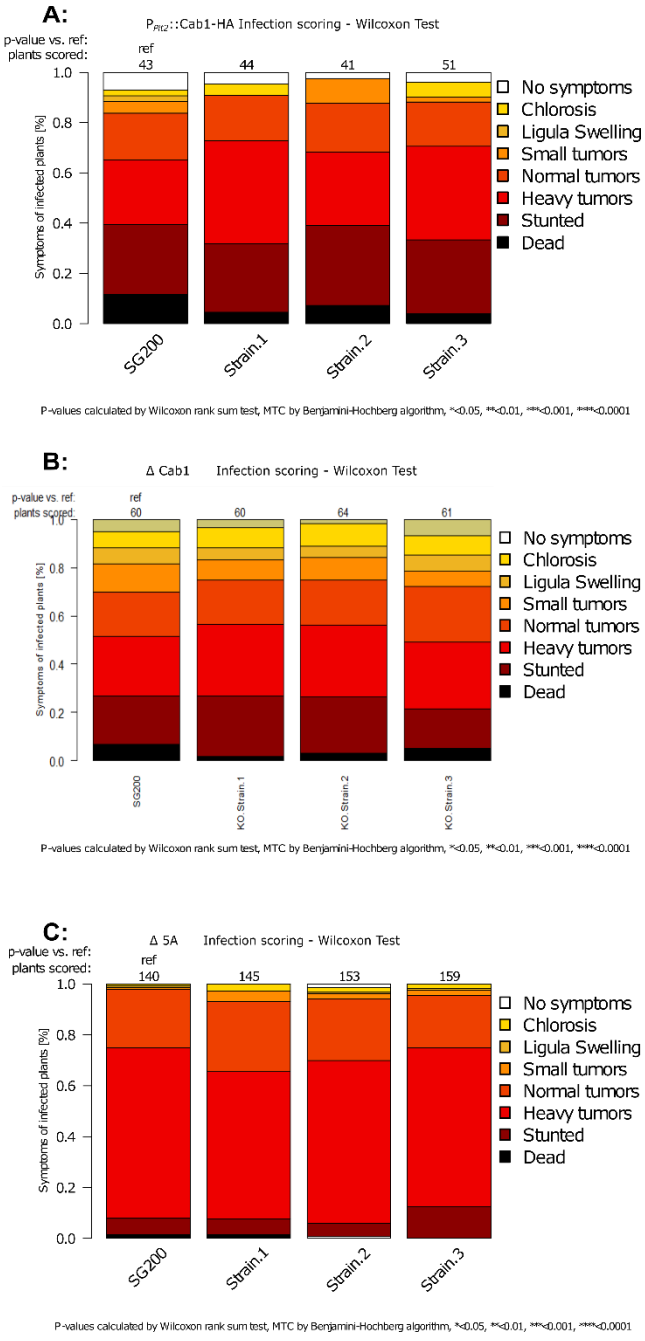

Fig S. 2. Neither Cab1 overexpression in *U. maydis* nor Cab1 or the cluster5A deletion strains show significant virulence defects in maize seedling infection assays.

a. Cab1 overexpression did not cause significant differences in respect to *U. maydis* virulence in comparison with SG200. Cab1 overexpression strains (P_{Pit2}::Cab1$_{1\text{-}113}$-3xHA) were cloned under the strong biotrophy-induced promoter P_{pit2} and introduced

into the *ip* locus solopathogenic *U. maydis* strain SG200. Three independent mutant strains were tested on 7-days old seedlings of the EGB maize line and scoring was performed 12 days post-infection (dpi). (* $P < 0.05$, ** $P < 0.01$, *** $P < 0.001$)

b. The deletion of Cab1 did not cause a significant reduction in *U. maydis* virulence in comparison to SG200 during maize seedling infections. The Cab1 mutants were generated in SG200. Three independent deletion strains were tested on 7 days old seedlings with EGB maize line and scoring was performed 12 dpi. (* $P < 0.05$, ** $P < 0.01$, *** $P < 0.001$)

c. The deletion of cluster 5A did not cause a significant reduction in *U. maydis* virulence in comparison to SG200 during maize seedling infections. The cluster 5A deletion mutants (Δ 5A) were generated in SG200. Three independent deletion strains were tested on 7-days old seedlings of the EGB maize line and scoring was performed 12 days post-infection (dpi). (* $P < 0.05$, ** $P < 0.01$, *** $P < 0.001$)

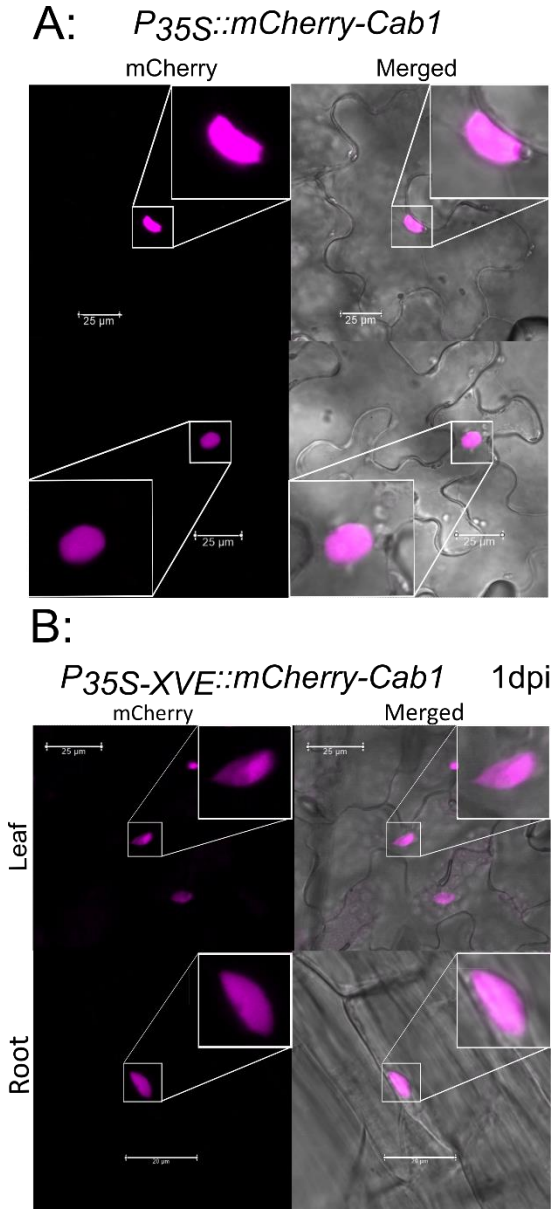

Fig S. 3. Cab1 shows nuclear localization.

A: subcellular localization of Cab1 in *N. benthamiana.* Transient expression of mCherry-Cab1 (*P_{35S}::3xHA-mCherry-Cab1$_{28-113}$*) in plant leaves was observed through confocal microscopy. Cab1 is localized in the nucleus. Scale bar= 25uM

B: Cab1 shows nuclear localization in *A. thaliana* shoot and root tissue. Expression mCherry-Cab1 (*$P_{35s-XVE}$::3xHA-mCherry-Cab1$_{28-113}$*) *A. thaliana* estradiol-inducible transgenic lines were subjected to confocal microscopy 1 day post-induction. Scale bar=25uM

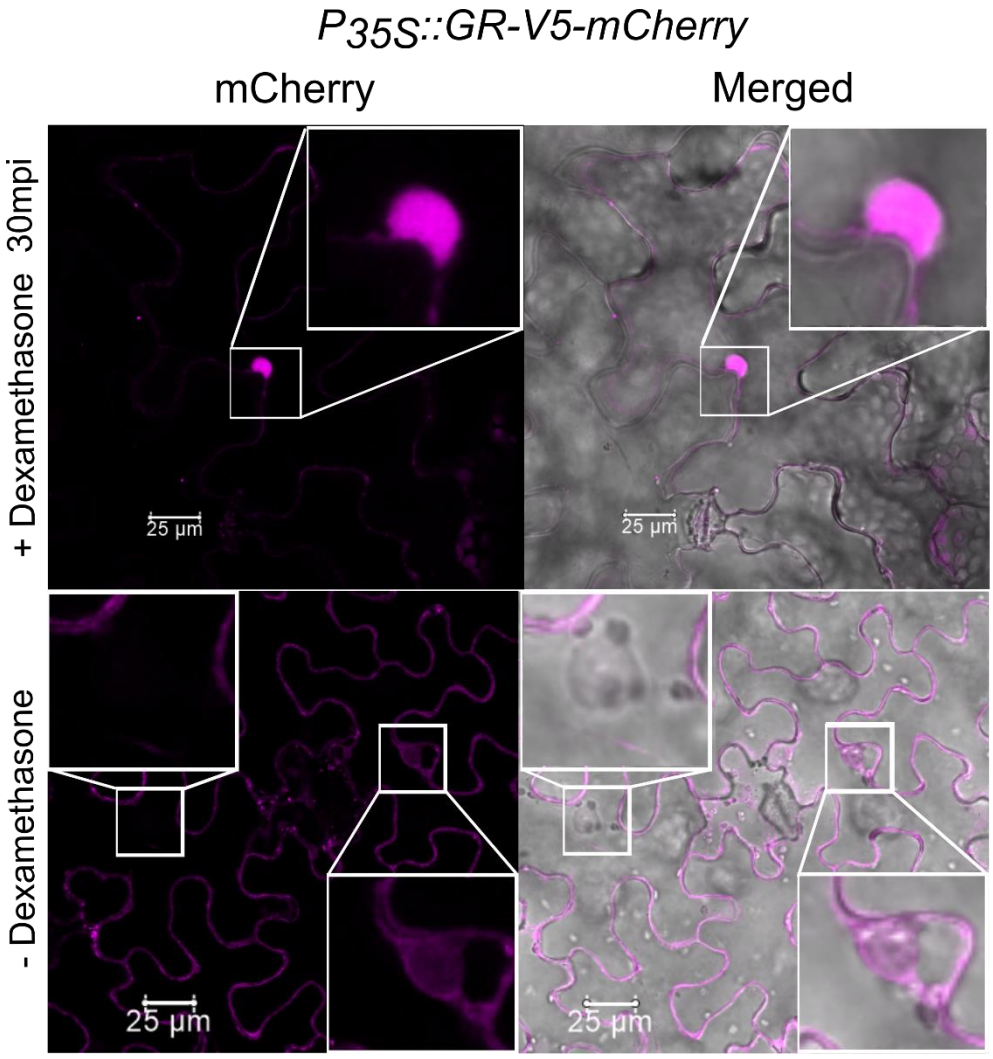

Fig. S. 4. . GR-V5-mCherry (*$P_{35S\text{-}XVE}$::GR-V5-mCherry*) construct transformed into *Agrobacterium tumefaciens*, strain GV3101 and infiltrated in *N. benthamiana* leaves. Confocal microscopy was done 3dpi before and after Dexamethasone treatment. Scale bar = 25 µm.

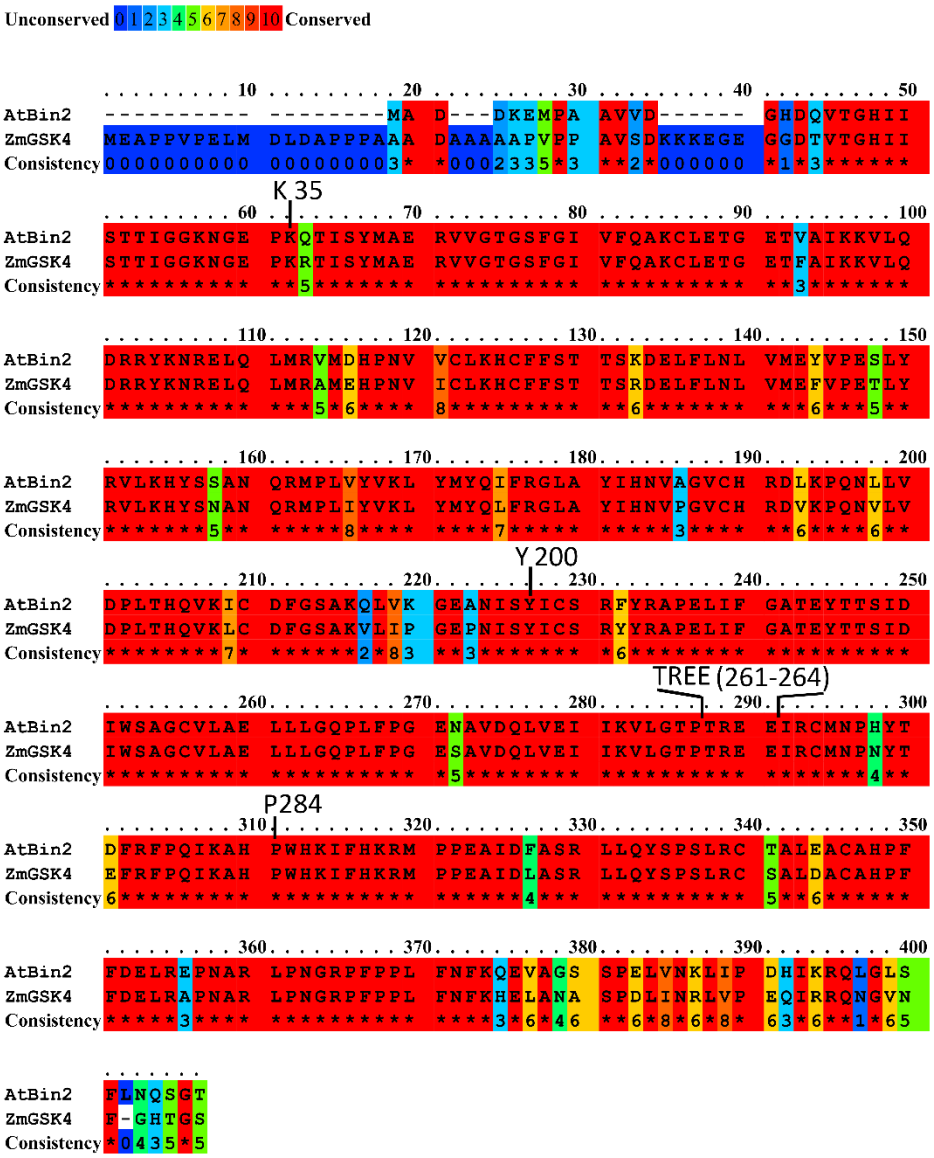

Fig S. 5: **The amino acid alignment of AtBIN2 and ZmGSK4.** ZmGSK4 is the closest orthologue of AtBIN2 in *Z. mays*. The important amino acids and motifs were marked. Tyr^{200} is the autophosphorylation site that plays an important role in Bin2 activity (J. Li et al., 2020). E263K mutation at TREE$^{261\text{-}264}$ motif causes the gain of function BIN2 (*bin2-1)* with strong dwarf phenotype and dark green leaves.

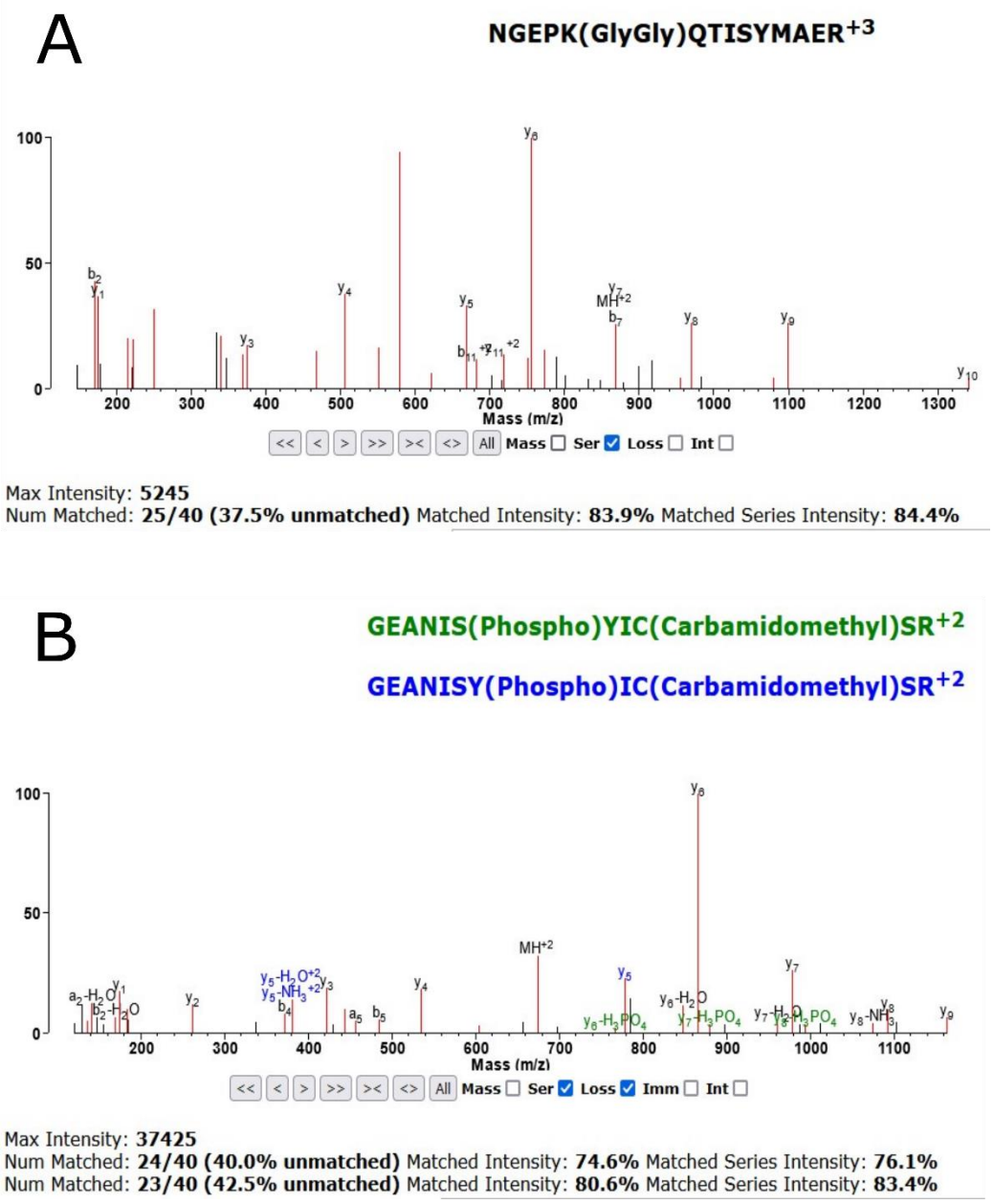

GEANIS(Phospho)YIC(Carbamidomethyl)SR^{+2}

Fig S. 6. Cab1 stabilizes and activates AtBin2 via uLys^{35} and pTyr^{200} respectively. Full-length AtBin2 was fused to GFP (*P$_{35S}$::AtBin2-GFP*) and Cab1 lacking its signal peptide was fused to mCherry (*P$_{35S}$::mCherry-cab1$_{28-113}$*) transiently expressed in *N. benthamiana* leaves via *A. tumefaciens* strain GV3101. Constitutively expressed mCherry (*P$_{35S}$::mCherry-mCherry*) was used as the control for the colocalization assay. The samples were subjected to Mass spectrometry 3 days post-induction.

A: uLys^{35} in NGEPK(GlyGly)QTISYMAER peptide was detected 5 times in the control sample with high fidelity (high score and low expectation) while no ms2 was taken in the AtBin2 co-expression with Cab1 sample. Moreover, in the specific retention time window also no precursor appeared in the ms1.

B: pTyr^{200} in GEANIS(Phospho)YIC(Carbamidomethyl)SR^{+2} peptide was detected 10 times in the Cab1 sample in comparison with the control sample.

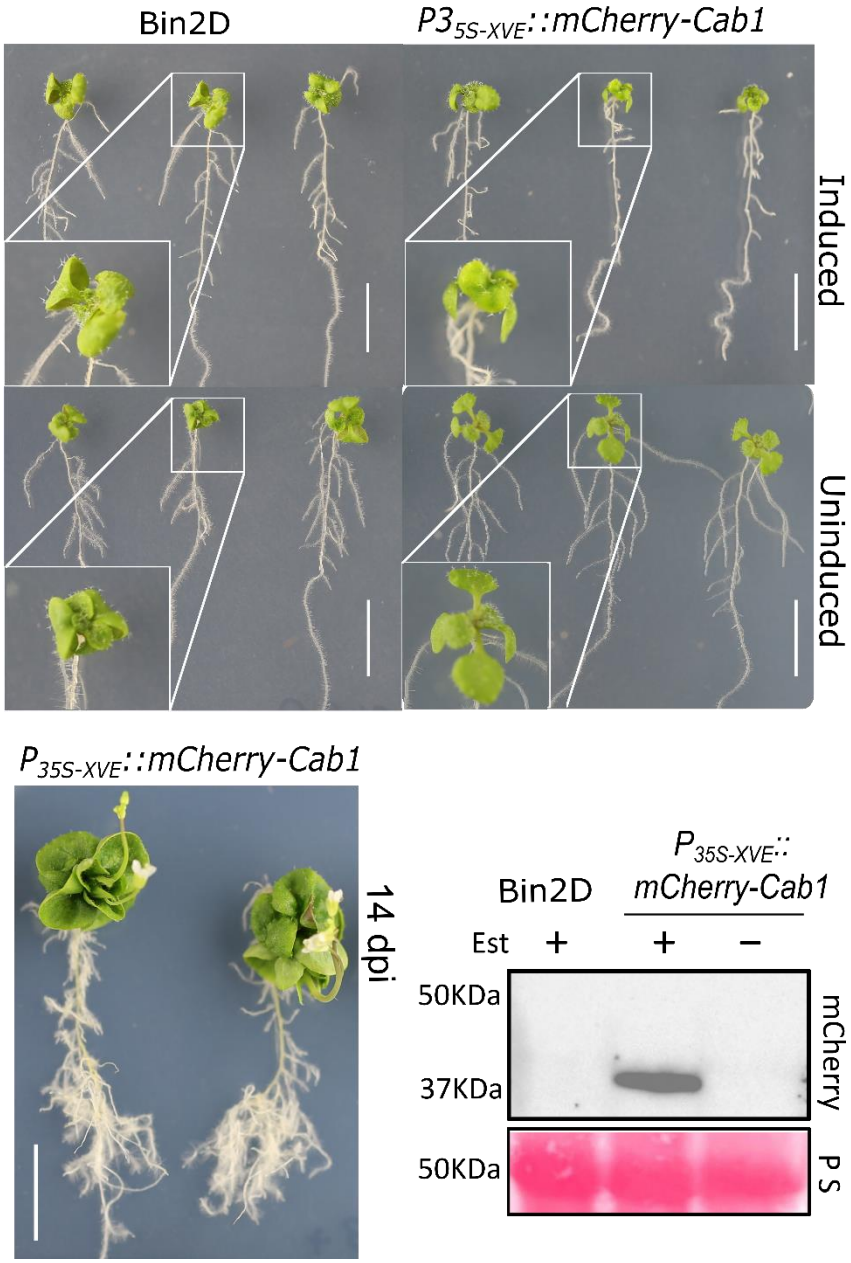

Fig S. 7.

Resemblance in the shoot phenotype between Cab1 overexpression and Bin2D dominant mutant (*bin2-1*) plants. 9 days old Cab1 ($P_{35S\text{-}XVE}$*::mcherry-Cab1*$_{28\text{-}113}$) and Bin2D seedling moved on induction plates containing 10µM Estradiol. Phenotyping was performed at 5 and 14 dpi respectively. Control plates contain DMSO as the solvent. The Bin2D phenotype is observed in both the induction and control plates, whereas the Cab1 phenotype only manifests in the induction plate. Western blot was performed with an anti-mCherry antibody. Scale bar= 1cm.

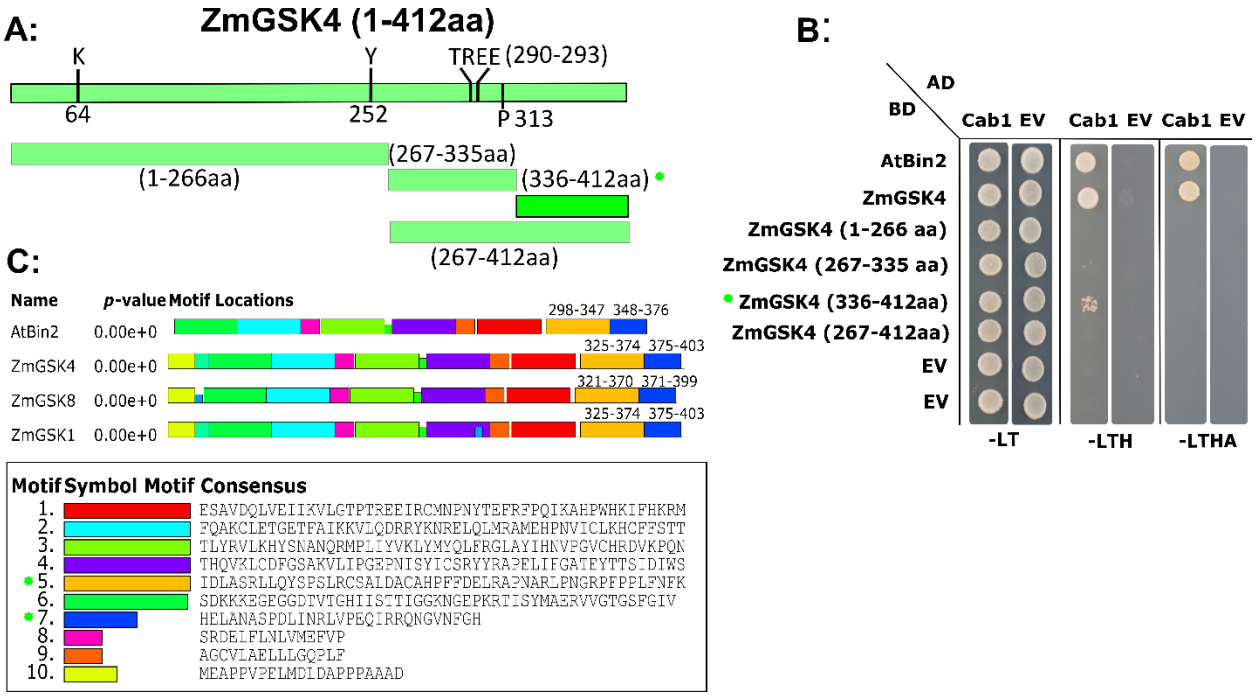

Fig 8. Cab1 targets C-terminal of ZmGSK4

a. Schematic representation of truncated ZmGSK4 in a Yeast-two-Hybrid assay. The TREE motif and Pro^{313} are aligned with AtBIN2 TREE$^{261-264}$ motif and Pro^{284} which are *bin2/dwarf12/ucu1* mutant. Phosphorylation of AtBIN2-Tyr^{200} aligned with ZmGSK4-Tyr^{252}, increases BIN2 activity, and AtBIN2-Lys^{35} is aligned with ZmGSK4-lys^{64} which is ubiquitinated with KIB1.

b. Cab1 targets C-terminal of ZmGSK4. ZmGSK4 truncated in 4 different pieces, each fragment was cloned into pGBKT7 bait vectors and transformed into the yeast strain Y187, whereas Cab1 was cloned into pGADT7 activation vector and transformed into the yeast strain AH109. Diploid yeast after mating, containing both plasmids, were dropped on selective synthetic dropout media (SD) and yeast growth was monitored 3 days after spotting. ZmGSK4 and AtBIN2 were used as positive controls. Cab1 targets C-terminal of ZmGSK4 (GalBD-ZmGSK4$_{336-412}$).

c. Cab1 targets two conserved motifs at C-terminal of AtBIN2 and ZmGSKs. Conserved motif analysis of AtBIN2, ZmGSK1, 4 and 8 amino acids sequence was performed by MEME. Motifs were designated 1–10 and distinguished with different colors. Motifs 5 and 7 (green asterisks) have most overlap with Cab1 target sites.

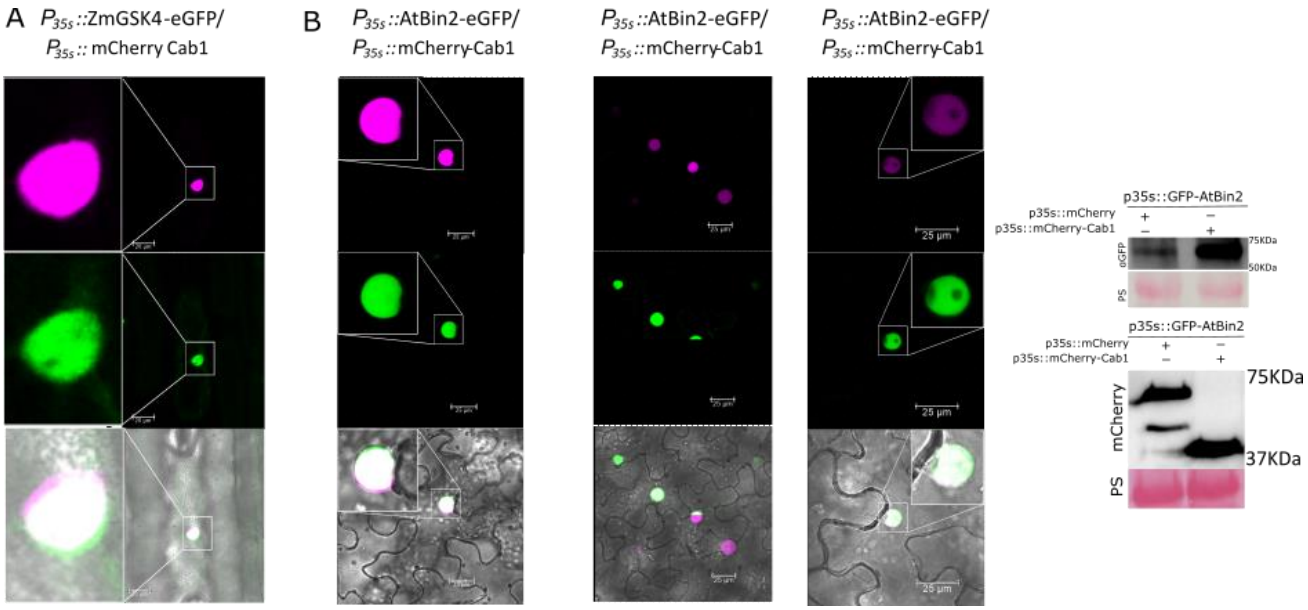

Fig S.9:

a. Cab1 relocalises ZmGSK4 from the cytosol to the nucleus. Subcellular co-localization of ZmGSK4 (P_{35S}::ZmGSK4-GFP) co-expressed with Cab1 (P_{35S}::mCherry-cab1$_{28\text{-}113}$) via biolistic bombardment in maize plant leaves was observed 1 dpi through confocal microscopy. Left panel: mCherry, Middle panel: GFP, right panel: merged mCherry and GFP. Scale bar = 25 µm.

b. Cab1 re-localizes and stabilizes AtBin2. AtBin2 re-localizes into the nucleus in the presence of Cab1 in *N. benthamiana*. Full-length AtBin2 was fused to GFP (*P_{35S}::AtBin2-GFP*) and Cab1 lacking its signal peptide was fused to mCherry (*P_{35S}::mCherry-Cab1$_{28\text{-}113}$*) transiently expressed in *N. benthamiana* leaves via *A. tumefaciens* strain GV3101. Constitutively expressed mCherry (P35S::mCherry-mCherry) was used as control for the colocalization assay. The samples were subjected for confocal-microscopy 3 dpi. Following settings were used:. mCherry panels: 552nm, laser power: 0.2, gain: 800%. Left panel GFP: (GFP: 448nm, laser power: 1.5%, gain: HyDi 15%). Left panel GFP: GFP: 448nm, laser power: 1.5%, gain: HyDi 10% (more than 10% HyDi activates microscope protection system because of overloaded signal.) Upper: mCherry fluorescence, middle panels: GFP fluorescence, Lower panel: merged mCherry and GFP fluorescence, brightfield images. Scale bar = 25 µm. The western blot was performed with GFP and mCherry antibodies. GFP antibodies present the stability of AtBin2 in presence of Cab1 in comparison with the control.

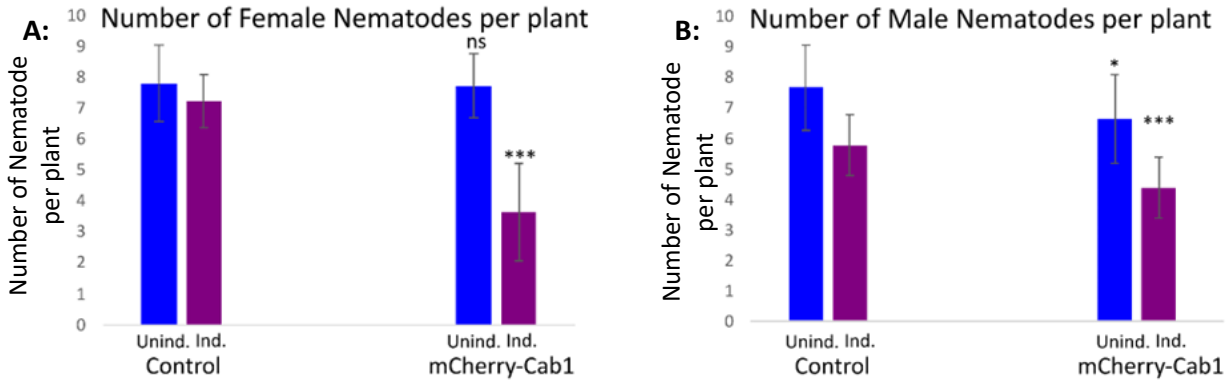

Fig S. 10: Development of *Heterodera schachtii* at Arabidopsis thaliana roots. A. Female nematodes B. Male Nematodes. The expression of Cab1 prevents the formation of *H. schachtii* female and male nematodes respectively. *A. thaliana* transgenic lines expressing Cab1 ($P_{35S\text{-}XVE}$*::mcherry-cab1*$_{28\text{-}113}$) and mCherry ($P_{35s\text{-}XVE}$*::mCherry*) were subjected to *H. schachtii* infection. The number of female nematodes was counted at 14 days post infections (dpi).

13 Publications and presentations of Pouria Bahrami

Conference Presentations/Posters

- Kishor D. Ingole, **Pouria Bahrami**, Nithya Nagarajan, & Armin Djamei. (2022, August 28). Characterization of dual functional fungal effector ApoE1 to establish biotrophy in maize. Botanik-Tagung 2022
- Nithya Nagaranjan, Kishor D. Ingole, **Pouria Bahrami**, & Armin Djamei. (2022, August 28). An experimental study on a family of effectors from Ustilago maydis in non-host model plants reveals evolutionarily conserved targets. Bontanik-Tagung 2022.
- **Pouria Bahrami**, & Armin Djamei. (2022, April 6). Screening for effectors with conserved host targets in a non-host plant. Biotrophy Workshop 2022

Highlight of Publications

- **Bahrami, P**., Ingole, K., Khan-Djamai. M., Pettkó-Szandtner. A., Prokchorchik, M., Dahale. S., deSousa Teixeira E-Silva, N., & Djamei, A. (2023) Fungal effector targets plant Shaggy-like kinases to manipulate the plant cell expansion. is in the process.
- Zare P, Shahbazifar A, Alem M, Varmaghani S, Ebrahimikatouli A, Parvareshanbar A, **Bahrami P**. 2017. Effects of coadministration of artemisinin and iron on istopathological alterations in the AGS gastric adenocarcinoma cell line. Turkish Journal of Medical Sciences 47:364-7. https://doi.org/10.3906/sag-1507-126